

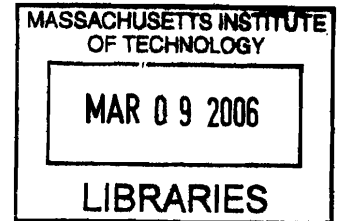
ACOUSTIC DATA COMMUNICATION SYSTEM FOR IN-PIPE WIRELESS SENSOR NETWORKS

by

George Kokossalakis

S.M. Civil and Environmental Engineering
Massachusetts Institute of Technology (2000)

Diploma of Civil Engineering
National Technical University of Athens (1998)



Submitted to the Department of Civil and Environmental Engineering
in partial fulfillment of the requirements
for the degree of

DOCTOR OF SCIENCE IN CIVIL AND ENVIRONMENTAL
ENGINEERING

at the
MASSACHUSETTS INSTITUTE OF TECHNOLOGY

February 2006

© 2006 Massachusetts Institute of Technology.

Signature of Author.....

Department of Civil and Environmental Engineering

January 15, 2006

Certified by.....

Eduardo Kausel

Professor of Civil and Environmental Engineering

Thesis Supervisor

Accepted by.....

Andrew J. Whittle

Chairman, Departmental Committee for Graduate Students

ARCHIVES

ACOUSTIC DATA COMMUNICATION SYSTEM FOR IN-PIPE WIRELESS SENSOR NETWORKS

by

George Kokossalakis

Submitted to the Department of Civil and Environmental Engineering
on January 15, 2006 in partial fulfillment of the requirements for the degree of
Doctor of Science in Civil and Environmental Engineering.

ABSTRACT

Sustainability of ageing infrastructure is one of the greatest current civil engineering challenges, especially in the case of pipelines, where no direct access is available. Being simultaneously massive and distributed, their normal operation is critical for the health and prosperity of the community. In current practice, the condition of pipelines is assessed by non-destructive inspection techniques. Nonetheless, frequent pipeline failures warrant the continuous assessment of their condition, in order to schedule the maintenance activities accordingly, and assure their safe operation. Continuous monitoring necessitates the deployment of autonomous wireless sensor networks (WSN). This thesis proposes solutions for the communication and power units of a WSN for monitoring underground water pipelines.

Regarding the communication unit, it is proposed to use the pipeline as an acoustic waveguide for the transmission of appropriately modulated acoustic waves that encapsulate the digital data, since radio frequency transmission is not feasible underground. The confined acoustic channel imposes severe distortion on the propagating signal. In order to compensate for the dispersion and ambient noise, the proposed communication system employs an elaborate set of signal processing steps, such as Reed-Solomon Encoding, Barker Code Synchronization, Adaptive Equalization, Bandpass Filtering, Stacking and application of Inverse Transfer Function techniques. The robust performance of the proposed system is evaluated and verified by means of numerical simulations and scaled laboratory experiments. The bandwidth vs. power relationship is identified as the major trade-off for its design, since the in-pipe acoustic channel is bandwidth limited, while the WSN application is power limited. Excessive bandwidth use would impose severe distortion on the propagating signal, while power limitations restrict the use of bandwidth efficient digital communication techniques.

In order to address the power availability, a miniature power harvesting system, extracting energy from the flow of water inside the pipeline, is proposed, composed of a generator and a turbine combination. A hybrid design presenting the high efficiency of Gorlov's helical turbine and the high startup torque of Savonius turbine is provided. The resulting power harvesting system is capable of sustaining a continuous 1 watt of power under normal water pipeline operating conditions.

Thesis Supervisor: Eduardo Kausel

Title: Professor of Civil and Environmental Engineering

Acknowledgements

This work would not have been accomplished, without the collaboration of many individuals.

I am first indebted to my thesis supervisor, Prof. Eduardo Kausel, who supported my work and provided superior intellectual challenges. I have learned enormously from him and gained insight to numerous problems that I have encountered throughout this challenging experience. This work would not have been accomplished without his support, without the energy that he dedicated, both as a mentor and as a friend.

I would also like to thank Prof. Andrew J. Whittle for his constant encouragement and financial support. I am also thankful to Dr. Kevin S. Amaratunga, Prof. Jerome J. Connor, and Dr. John Germaine for their advice and willingness to assist in numerous tasks that arose throughout my doctoral the educational process. I am obliged to Dr. Ruaidhri M. O'Connor for his guidance and support in both my research and personal issues over the past 3 years.

I also feel that I owe a big thank you to the administrative staff of the Department, and especially to Cynthia Stewart, Pat Dixon, Anthee Travers, Joannie McCusker, Jeanette Marchocki, Steven Rudolph, James Riefstahl and Alice Kalemkarian.

I am especially grateful to my close friends from Greece and MIT, who I will not name because I am afraid of not mentioning somebody important to me; however they are all written deeply in my heart. I would especially like to thank my friends in the US for the unforgettable experiences we have lived together, and for making my life at MIT enjoyable and my effort less tiring. I great thank you goes to my close friends in Greece for thinking of me and waiting patiently every holidays to welcome me back home.

To my parents and sister I owe the most. This work would not have been possible without their continuous support and love. This thesis is dedicated to them, who have been the main source of my strength throughout this challenging period of my life.

Finally, I would like to thank my wife Dominic, who has been continuously there for me, supporting my efforts, and helping me overpass obstacles that I wouldn't have managed to, if I were on my own.

This work has been completed under the financial support of the Cambridge-MIT Initiative (CMI) under the grant 080/P-IR FT, “New Technologies for Condition Assessment and Monitoring of Ageing Infrastructure”. I am grateful for their support throughout my doctoral studies.

To my parents and sister
who are always there for me...

Table of contents

CHAPTER 1	
INTRODUCTION.....	23
1.1 THESIS OBJECTIVES	23
1.2 MOTIVATION.....	25
1.3 PIPELINE FAILURES AND INSPECTION METHODS	28
1.4 WIRELESS SENSOR NETWORKS	32
1.5 THESIS OUTLINE	35
1.6 REFERENCES	38
CHAPTER 2	
STATE OF THE ART IN UNDERWATER ACOUSTIC COMMUNICATION ...	39
2.1 INTRODUCTION	39
2.2 OPEN SEA ACOUSTIC COMMUNICATION	40
2.2.1 <i>Signal Distortion</i>	40
2.2.2 <i>Communication techniques</i>	42
2.2.3 <i>Hardware</i>	44
2.3 OPEN SEA VS. IN-PIPE COMMUNICATION	48
2.4 IN-PIPE ACOUSTIC APPLICATIONS.....	50
2.5 REFERENCES	52
CHAPTER 3.....	
WAVE PROPAGATION IN PIPELINE WAVEGUIDES	57
3.1 INTRODUCTION	57
3.2 STATE OF THE ART FOR IN PIPE WAVE PROPAGATION	58
3.3 PIPELINE WAVEGUIDE SIMULATIONS.....	60
3.4 RIGID PIPE APPROXIMATION.....	62
3.4.1 <i>Dynamic equations for a fluid</i>	63
3.4.2 <i>Harmonic point source in an unbounded fluid medium</i>	65
3.4.3 <i>Centered line source in a rigid cylindrical pipe: wave solution</i>	67
3.4.4 <i>Pipe with rigid walls: Source expansion into modes</i>	70
3.4.5 <i>Pipe with rigid walls: Off-center point source</i>	73
3.4.6 <i>Simulations</i>	75
3.5 FLEXIBLE PIPE EMBEDDED IN SOIL.....	93
3.5.1 <i>Off-center source in a layered flexible pipe</i>	94
3.5.2 <i>Estimation of p^*</i>	95
3.5.3 <i>Fluid cylinder subjected to external pressure</i>	96
3.5.4 <i>Fluid cylinder via stiffness matrix method</i>	97
3.5.5 <i>Graf addition theorem</i>	102
3.5.6 <i>Simulations</i>	102
3.6 CONCLUSIONS	112
3.7 REFERENCES	114

CHAPTER 4	
DIGITAL COMMUNICATIONS	117
4.1 INTRODUCTION	117
4.2 DIGITAL VS. ANALOG COMMUNICATION.....	118
4.3 DIGITAL COMMUNICATION SYSTEM COMPONENTS.....	121
4.4 MATHEMATICAL MODELS FOR COMMUNICATION CHANNELS	122
4.4.1. <i>Additive White Gaussian Noise</i>	123
4.4.2. <i>Linear Time Invariant Filter</i>	124
4.4.3. <i>Linear Time Variant Filter</i>	125
4.5 DIGITAL COMMUNICATION TECHNIQUES	126
4.5.1. <i>Formatting</i>	126
4.5.2. <i>Encoding</i>	128
4.5.3. <i>Mapping & Modulation</i>	138
4.5.4. <i>Equalization</i>	148
4.5.5. <i>Synchronization</i>	155
4.6 TRADE-OFFS OF DIGITAL COMMUNICATION SYSTEMS	159
4.7 ADVANCED COMMUNICATION ISSUES.....	165
4.8 REFERENCES	167
CHAPTER 5	
PROPOSED COMMUNICATION SYSTEM.....	169
5.1 INTRODUCTION	169
5.2 OPERATIONAL LAYOUT.....	170
5.3 SOFTWARE IMPLEMENTATION.....	172
5.3.1 <i>Message Formatting</i>	172
5.3.2 <i>Encoding</i>	174
5.3.3 <i>Modulation</i>	175
5.3.4 <i>Synchronization</i>	178
5.3.5 <i>Inverse Transfer Function</i>	180
5.3.6 <i>Stacking</i>	183
5.3.7 <i>Bandpass Filtering</i>	185
5.3.8 <i>Equalization</i>	186
5.4 HARDWARE IMPLEMENTATION	187
5.4.1 <i>Microprocessor</i>	188
5.4.2 <i>Analog to Digital Converter</i>	189
5.4.3 <i>Signal Amplifier</i>	190
5.4.4 <i>Transducers</i>	190
5.4.5 <i>Power unit</i>	193
5.4.6 <i>Installation</i>	199
5.5 REFERENCES	202
CHAPTER 6	
SIMULATIONS	205
6.1 INTRODUCTION	205
6.2 MODULATION	206

6.2.1	<i>Frequency Shift Keying</i>	207
6.2.2	<i>Amplitude Shift Keying</i>	211
6.2.3	<i>Quadrature Amplitude Modulation</i>	214
6.3	ENCODING.....	217
6.4	STACKING	221
6.5	ADAPTIVE EQUALIZER	228
6.5.1	<i>Linear Equalizer</i>	229
6.5.2	<i>Decision Feedback Equalizer</i>	234
6.5.3	<i>Equalization of ASK and QAM signals</i>	236
6.5.4	<i>Effect of pipeline waveguide on equalization process</i>	240
6.5.5	<i>Equalization of higher data rate signals</i>	244
6.6	EFFECT OF AMBIENT NOISE	248
6.7	CONCLUSIONS	251
6.8	REFERENCES	255
CHAPTER 7		
LABORATORY EXPERIMENTS.....		257
7.1	INTRODUCTION	257
7.2	EXPERIMENTAL LAYOUT.....	258
7.3	HARDWARE.....	263
7.4	RESULTS	269
7.4.1	<i>Straight Pipe</i>	269
7.4.2	<i>Bent Pipe</i>	277
7.4.3	<i>Branch Pipe</i>	283
7.5	REFERENCES	290
CHAPTER 8		
CONCLUSIONS		291
8.1	CONCLUSIONS	291
8.2	FUTURE WORK.....	294

List of Figures

Figure 1.1: In-pipe acoustic data communication	24
Figure 1.2: Pipe bursts in Santa Monica and Boston [1], [2]	26
Figure 1.3: Examples of Pipeline Defects: root intrusion, and cross section blockage, [4]	29
Figure 1.4: Typical locations of fracture type of burst pipes, ([3] from Jones, 1983)	30
Figure 1.5: Acoustic Emission	32
Figure 1.6: Components of an integrated wireless sensor node	33
Figure 1.7: Typical Wireless Sensor Network Architecture	35
Figure 2.1: Volumetric absorption including all known relaxation processes, [4], [5] ...	42
Figure 2.2: Typical Transmitter – Receiver system	45
Figure 2.3: Open – Sea acoustic modem (photo courtesy of Link Quest)	47
Figure 2.4: Published experimental performance of underwater acoustic telemetry systems. The channels vary from deep and vertical to shallow and horizontal. In general, the high rate or high range results are for deep channels while the cluster of low range, low rate results are for shallow channels. Modems developed by the research community are represented with diamonds while stars denote commercially available systems. The range \times rate bound represents an estimate of the existing performance envelope. [2]	47
Figure 3.1: Modes of Propagation inside hollow fluid filled elastic cylinders: <i>Longitudinal waves (L), Helical or Torsional waves (T), and Flexural waves (F)</i> ..	58
Figure 3.2: Parametric Analyses to identify the effect of the transmission channel to the propagating signal	61
Figure 3.3: Azimuthally distributed modes of propagation Regions of uniform phase: (a) along the cross section, [31], (b) along the pipe length	63
Figure 3.4: Bessel Functions of the (a) first J_n and (b) second Y_n kind, [32]	68
Figure 3.5: Fluid filled cylinder, with source of arbitrary spatial distribution	70
Figure 3.6: Off-center source in pipe with rigid walls	73
Figure 3.7: Excitation Waveforms	77
Figure 3.8: Frequency Spectrum (a) Single squared sinusoidal pulse, (b) Tapered group of sinusoidal waves	77
Figure 3.9: Attenuation vs. Distance; Pressure Time History and Frequency Response Spectrum for $R = 0.5\text{m}$, $a = r = 0\text{m}$, $f_o = 5\text{kHz}$, and (a) $z = 10\text{m}$, (b) $z = 100\text{m}$, and (c) $z = 500\text{m}$	78
Figure 3.10: Attenuation vs. Frequency; Pressure Time History and Frequency Response Spectrum for $R = 0.5\text{m}$, $a = r = 0\text{m}$, $z = 10\text{m}$, and (a) $f_o = 1\text{kHz}$, (b) $f_o = 5\text{kHz}$, and (c) $f_o = 20\text{kHz}$	79
Figure 3.11: Transfer Function for a pipeline with $R = 0.5\text{m}$, at a distance $z = 10\text{m}$, for the $n = 0$ solution containing the first 50 modes	80
Figure 3.12: Transfer Function for a pipeline with $R = 1\text{m}$, at a distance $z = 10\text{m}$, for the $n = 0$ solution containing the first 50 modes	81
Figure 3.13: Dispersion Curves for $n = 0$ and (a) $R = 0.15\text{m}$, (b) $R = 0.5\text{m}$ and (c) $R = 1\text{m}$	83
Figure 3.14: Dispersion Curves for $R = 0.15\text{m}$	84

Figure 3.15: Effect of pipeline radius; Pressure Time Histories for $z = 10\text{m}$, $a = r = R$, $f_o = 5\text{kHz}$ and (a) $R = 0.15\text{m}$, (b) $R = 0.5\text{m}$ and (c) $R = 1\text{m}$	85
Figure 3.16: Effect of pipeline radius; Pressure Time Histories for $z = 10\text{m}$, $a = r = R$, $f_o = 5\text{kHz}$ and (a) $R = 0.15\text{m}$, (b) $R = 0.5\text{m}$ and (c) $R = 1\text{m}$ [Close up of Figure 3.15]	85
Figure 3.17: Pipe Radius vs. modes of propagation; Pressure Time Histories for $z = 10\text{m}$, $a = r = R$, $f_o = 1.5\text{kHz}$ and (a) $R = 0.15\text{m}$, (b) $R = 0.5\text{m}$ and (c) $R = 1\text{m}$	86
Figure 3.18: Effect of damping; Pressure Time Histories for $z = 10\text{m}$, $R = 0.5\text{m}$, $a = r = R$, $f_o = 5\text{kHz}$, and (a) $\xi = 0.5\%$, (b) $\xi = 1\%$ and (c) $\xi = 5\%$	88
Figure 3.19: Pressure Time History of the direct and scattered signals arriving at the receiver for $f_o = 1.5\text{kHz}$, and $R = 0.5\text{m}$, $z = 10\text{m}$, $a = r = R$, (a) $z_s = 5\text{m}$, and (b) $z_s = 1\text{m}$ or 9m	90
Figure 3.20: Pressure Time History of the direct and scattered signals arriving at the receiver for $f_o = 5\text{kHz}$, and $R = 0.5\text{m}$, $z = 10\text{m}$, $a = r = R$, (a) $z_s = 5\text{m}$, and (b) $z_s = 1\text{m}$ or 9m	91
Figure 3.21: Pressure Time History of the direct and scattered signals arriving at the receiver for $f_o = 20\text{kHz}$, and $R = 0.5\text{m}$, $z = 10\text{m}$, $a = r = R$, (a) $z_s = 5\text{m}$, and (b) $z_s = 1\text{m}$ or 9m	92
Figure 3.22: Flexural modes, [34]	94
Figure 3.23: Two stage solution for flexible pipe embedded in soil (a) Source and inward pressure p^* , (b) Outward traction p^*	95
Figure 3.24: Graf addition theorem	102
Figure 3.25: Attenuation vs. Distance; Pressure Time History and Frequency Response Spectrum for $R = 0.5\text{m}$, $a = r = R$, $f_o = 1\text{kHz}$, $C_s = 0.2\text{ km/sec}$, $t = 2\text{cm}$, and (a) $z = 10\text{m}$, (b) $z = 100\text{m}$	104
Figure 3.26: Pressure Time History and Frequency Response Spectrum for the tapered sinusoidal waveform excitation and $R = 0.5\text{m}$, $a = r = R$, $z = 10\text{m}$, $f_o = 1.5\text{ kHz}$, $C_s = 0.2\text{ km/sec}$, and $t = 2\text{cm}$	105
Figure 3.27: Attenuation vs. Frequency; Pressure Time History and Frequency Response Spectrum for $R = 0.5\text{m}$, $a = r = R$, $z = 10\text{m}$, $C_s = 0.2\text{ km/sec}$, $t = 2\text{cm}$, and (a) $f_o = 2\text{kHz}$, (b) $f_o = 5\text{kHz}$ and (c) $f_o = 20\text{kHz}$	106
Figure 3.28: Pressure Time History and Frequency Response Spectrum for $z = 10\text{m}$, $f_o = 1\text{ kHz}$, $a = r = R$, $C_s = 0.2\text{ km/sec}$, and (a) $R = 0.15\text{m}$, and (b) $R = 1\text{m}$	107
Figure 3.29: Effect of soil stiffness; Pressure Time History and Frequency Response Spectrum for $z = 10\text{m}$, $f_o = 1\text{ kHz}$, $R = 0.5\text{m}$, $a = r = R$, $t = 2\text{cm}$, and soil acoustic wave velocity (a) $C_s = 0$ (No soil), and (b) $C_s = 2\text{ km/sec}$	109
Figure 3.30: Radiation Damping (Pressure Time History for $n = 0$, $z = 10\text{m}$, $f_o = 1\text{ kHz}$, $R = a = r = 0.5\text{m}$, and $C_s = 0, 0.2$, and 2 km/sec)	110
Figure 3.31: Effect of pipeline thickness; Pressure Time History for $z = 10\text{m}$, $f_o = 1\text{ kHz}$, $R = 0.5\text{m}$, $a = r = R$, $C_s = 0.2\text{ km/sec}$ and pipe wall thickness (a) $t = 5\text{mm}$, and (b) $t = 10\text{cm}$	111
Figure 3.32: Effect of pipeline material; Pressure Time History and Frequency Response Spectrum for PVC pipe with $z = 10\text{m}$, $f_o = 1\text{ kHz}$, $R = 0.5\text{m}$, $a = r = R$, $C_s = 0.2\text{ km/sec}$	112
Figure 4.1: Morse code, [1]	118
Figure 4.2: Signal distortion and recognition	119

Figure 4.3: Traditional components of a digital communication system, [2]	122
Figure 4.4: Additive Noise Model	123
Figure 4.5: Linear time invariant filter model.....	125
Figure 4.6: Linear time variant filter model.....	125
Figure 4.7: Common Signal Processing Steps of a Digital Communication System	126
Figure 4.8: 5-Bit Baudot Code, [1]	127
Figure 4.9: 7-Bit American Standard Code for Information Interchange (ASCII), [4] .	127
Figure 4.10: Linear Block Codes	134
Figure 4.11: Pulse coded modulation waveforms, [4]	141
Figure 4.12: ASK signal constellation	143
Figure 4.13: ASK waveform.....	144
Figure 4.14: PSK Signal Constellations.....	145
Figure 4.15: PSK waveform.....	145
Figure 4.16: QAM signal constellations	146
Figure 4.17: QAM waveforms	146
Figure 4.18: FSK representation in the frequency plane	147
Figure 4.19: FSK waveform.....	147
Figure 4.20: Linear Adaptive Equalizer.....	150
Figure 4.21: Transversal filter detail.....	150
Figure 4.22: Decision Feedback Equalizer	151
Figure 4.23: Phase Locked Loop	156
Figure 4.24: Bit error probability P_B versus Signal to noise ratio per bit E_b/N_0 for coherently detected M -ary signaling: (a) orthogonal signaling, (b) Multiple phase signaling, [4]	161
Figure 4.25: Bandwidth efficiency η_o in bit/s/Hz as a function of SNR per bit, for constant symbol error probability of 10^{-5} , [3].	163
Figure 4.26: Bandwidth of digital data, [4]. (a) Half Power, (b) Noise equivalent, (c) Null to Null, (d) 99% of Power, (e) Bounded Power Spectral Density at 35 and 50 dB.	164
Figure 5.1: Operational diagram of proposed digital communication system.....	170
Figure 5.2: Transmitter and receiver hardware diagram.....	171
Figure 5.3: 7-Bit American Standard Code for Information Interchange (ASCII), [1] .	173
Figure 5.4: Bandwidth efficiency η_o in bit/s/Hz as a function of SNR per bit, for constant symbol error probability of 10^{-5} , [2]	177
Figure 5.5: Example of signal with Barker Code illustrating silent time τ	179
Figure 5.6: Azimuthally distributed modes of propagation Regions of uniform phase along the cross section for the first mode of each of the first 4 orders	184
Figure 5.7: Beam Patterns (a) Omnidirectional, (b) Hemispherical, (c) Toroidal, and (d) Conical, [9].	192
Figure 5.8: Volumetric absorption including all known relaxation processes, [12]	195
Figure 5.9: Power harvesting system from the flow of water inside the pipeline.....	197
Figure 5.10: (a) Gorlov's Helical Turbine, (b) Savonius Turbine, [17], (c) Hybrid Design	198
Figure 5.11: Examples of Pipeline Robot Configurations, [18]	200
Figure 6.1: Amplitude and Frequency Response of Transmitted Signal for FSK modulation at data rates (a) 1kbps, (b) 4kbps and (c) 7kbps	208

Figure 6.2: Pressure Time History and Frequency Response of Received Signal from a pipeline waveguide with $R = a = r = 0.5\text{m}$, $z = 10\text{m}$ for FSK modulation at data rates (a) 1kbps, (b) 4kbps and (c) 7kbps	209
Figure 6.3: Synchronization with Barker Code, Matched Filter Response (a) Theoretical, and (b) Actual.....	210
Figure 6.4: Amplitude and Frequency Response of Transmitted Signal for ASK modulation at data rates (a) 1kbps, (b) 4kbps and (c) 7kbps	212
Figure 6.5: Pressure Time History and Frequency Response of Received Signal from a pipeline waveguide with $R = a = r = 0.5\text{m}$, $z = 10\text{m}$ for ASK modulation at data rates (a) 1kbps, (b) 4kbps and (c) 7kbps	213
Figure 6.6: Signal Constellations for ASK modulated signals (a) 1kbps, (b) 4kbps, and (c) 7kbps.....	214
Figure 6.7: Amplitude and Phase of Transmitted Signal for QAM at data rates (a) 1kbps, (b) 4kbps, and (c) 7kbps.....	215
Figure 6.8: Pressure Time History and Signal Constellation of Received Signal from a pipeline waveguide with $R = a = r = 0.5\text{m}$, $z = 10\text{m}$ for QAM at data rates (a) 1kbps, (b) 4kbps, and (c) 7kbps	216
Figure 6.9: Amplitude and Frequency Spectrum of Transmitted signals for FSK modulation of encoded messages at data rates (a) 1kbps, (b) 4kbps, and (c) 7kbps.	219
Figure 6.10: Pressure Time History and Frequency Response of Received Signal from a pipeline waveguide with $R = a = r = 0.5\text{m}$, $z = 10\text{m}$ for FSK modulation of encoded messages at data rates (a) 1kbps, (b) 4kbps, and (c) 7kbps	220
Figure 6.11: Pressure Time History and Frequency Response of Received Signal at the bottom of a pipeline waveguide with $R = a = r = 0.5\text{m}$, $z = 10\text{m}$ for FSK modulation of encoded messages at data rates (a) 1kbps, (b) 4kbps and (c) 7kbps.....	222
Figure 6.12: Stacked Signal by addition of received signals at crown and bottom of pipe. Pressure Time History and Frequency Response for FSK modulation at data rates (a) 1kbps, (b) 4kbps and (c) 7kbps.....	223
Figure 6.13: Stacked Signal by subtraction of received signals at crown and bottom of pipe. Pressure Time History and Frequency Response for FSK modulation at data rates (a) 1kbps, (b) 4kbps and (c) 7kbps	223
Figure 6.14: Transfer Functions of the first four orders of modes for a pipeline waveguide with $R = 0.5\text{m}$ and $z = 10\text{m}$	226
Figure 6.15: Pressure Time Histories and Frequency Response of FSK modulated signal at 0.4kbps data rate for a pipeline waveguide with $R = a = r = 0.5\text{m}$, $z = 10\text{m}$ (a) Transmitted signal, (b) Received signal at the crown, and (c) Stacked signal generated by addition of top and bottom recorded signals	228
Figure 6.16: Example Pressure time history and Frequency response of (a) inadequate length and (b) poorly trained Linear Adaptive Equalizer using the LMS filter tap weight adaptation algorithm for FSK modulated signals at 1kbps data rate	231
Figure 6.17: Pressure time history and Frequency response of Linear Equalizer using the LMS filter tap weight adaptation algorithm for FSK modulated at data rates (a) 1kbps, (b) 4kbps and (c) 7kbps	232

Figure 6.18: Pressure time history and Frequency response of Linear Equalizer using the RLS filter tap weight adaptation algorithm for FSK modulated signals at data rates (a) 1kbps, (b) 4kbps and (c) 7kbps.....	233
Figure 6.19: Pressure time history and Frequency response of DFE using the LMS filter tap weight adaptation algorithm for FSK modulated signals at data rates (a) 1kbps, (b) 4kbps and (c) 7kbps.....	235
Figure 6.20: Pressure time history and Frequency response of DFE using the RLS filter tap weight adaptation algorithm for FSK modulated signals at data rates (a) 1kbps, (b) 4kbps and (c) 7kbps.....	235
Figure 6.21: Pressure time history, Frequency Response, and Signal Constellation of DFE using the LMS filter tap weight adaptation algorithm for ASK modulated signals at data rates (a) 1kbps, (b) 4kbps, and (c) 7kbps	237
Figure 6.22: Pressure Time History and Signal Constellation of received and equalized signals with DFE using the LMS filter tap weight adaptation algorithm for QAM modulated signals at data rates (a) 1kbps, (b) 4kbps, and (c) 7kbps.....	239
Figure 6.23: Pressure Time History and Frequency Response of Received Signal for FSK modulation at 4kbps data rate for propagation distance $z = 10\text{m}$ and pipeline radius (a) $R = 0.15\text{m}$, and (b) $R = 1\text{m}$	241
Figure 6.24: Pressure time history and Frequency response of DFE using the LMS filter tap weight adaptation algorithm for FSK modulated signals at 4kbps data rate, for a propagation distance of $z = 10\text{m}$ in a pipe with radius (a) $R = 0.15\text{m}$ and (b) $R = 1\text{m}$	242
Figure 6.25: Pressure Time History and Frequency Response of Received Signal for FSK modulation at 4kbps data rate for pipeline radius $R = 0.5\text{m}$ and propagation distance (a) $z = 100\text{m}$, and (b) $z = 500\text{m}$	243
Figure 6.26: Pressure time history and Frequency response of DFE using the LMS filter tap weight adaptation algorithm for FSK modulated signals at 4kbps data rate inside a $R = 0.5\text{m}$ pipeline for a propagation distance of (a) $z = 100\text{m}$, and (b) $z = 500\text{m}$	244
Figure 6.27: Formatting and encoding of textual message	245
Figure 6.28: Amplitude and Phase of Transmitted Signal for QAM at data rates (a) 12kbps, and (b) 21kbps	246
Figure 6.29: Pressure Time History and Signal Constellation of Received Signal and equalized signals with DFE using the RLS adaptation algorithm for QAM at data rates (a) 12kbps, and (b) 21kbps inside a pipeline waveguide with $R = a = r = 0.5\text{m}$, $z = 10\text{m}$	247
Figure 6.30: Effect of Ambient noise on transmitted signal; Pressure Time History and Frequency response for FSK modulated signal at 4kbps data rate for SNR equal to (a) 10dB, (b) 2dB, and (c) 0dB	249
Figure 6.31: Effect of Ambient noise on transmitted signal; Pressure Time History and Frequency response for FSK modulated signal at 4kbps data rate for SNR equal to (a) 10dB, (b) 2dB, and (c) 0dB	250
Figure 7.1: Laboratory Experiment Pipeline layout (a) Straight, (b) Bend, (c) Branch	259
Figure 7.2: Simulated Pressure Time Histories single pulse transmitted inside a (a) 4" diameter, 10m long PVC pipe, and (b) 1m diameter, 100m long cast iron pipe. ..	262
Figure 7.3: Schematic Diagram of Laboratory Experiment Hardware Configuration ..	263

Figure 7.4: (a) Speaker and (b) Microphone used as transmitter and receiver and corresponding frequency response, [1]	265
Figure 7.5: Speaker Amplifier	266
Figure 7.6: Microphone supporting circuit and preamplifier.....	267
Figure 7.7: Pressure Time History and Frequency Response of Laboratory Experiment for 30 ft propagation distance in straight pipe of FSK modulated signals at data rates (a) 1kbps, (b) 4kbps, and (c) 7kbps	270
Figure 7.8: Transfer Functions of the 30 feet straight pipe laboratory experiment for the first 9 orders of modes	271
Figure 7.9: Pressure Time History and Frequency Response of Stacked signal generated by subtraction of the crown and bottom recordings for the 7kbps FSK modulated signal in a 30ft straight pipe	272
Figure 7.10: Pressure Time History and Frequency Response of equalized signal with a DFE utilizing the RLS adaptation algorithm for FSK modulated signals at data rates (a) 1kbps, (b) 4kbps, and (c) 7kbps.....	273
Figure 7.11: Pressure Time History and Frequency Response of 7kbps FSK transmitted signal for simulated laboratory experiment of air filled 30 feet long and 0.05m in radius PVC pipe	274
Figure 7.12: Pressure Time History and Frequency Response of received and DFE equalized FSK 7kbps signal for propagation distance 10 feet	275
Figure 7.13: Pressure Time History and Frequency Response of (a) received, (b) stacked by subtraction, and (c) DFE equalized, 7kbps ASK modulated signal for 30 ft propagation distance in straight pipe	276
Figure 7.14: Pressure Time History and Signal Constellation of (a) received, (b) stacked by subtraction, and (c) DFE equalized, 7kbps QAM modulated signal for 30 ft propagation distance in straight pipe	277
Figure 7.15: Pressure Time History and Frequency Response of a 30ft bent pipe Laboratory Experiment for FSK modulated signals at data rates (a) 1kbps, (b) 4kbps, and (c) 7kbps	278
Figure 7.16: Qualitative explanation of transmission loss near to the frequency at which the wavelength equals twice the pipe diameter, [2]	279
Figure 7.17: Pressure Time History and Frequency Response of Stacked signal generated by subtraction of the crown and bottom recordings for the 7kbps FSK modulated signal propagating inside a 30ft bend pipe.....	280
Figure 7.18: Pressure Time History and Frequency Response of equalized signal with a DFE utilizing the RLS adaptation algorithm for FSK modulated signals at data rates (a) 1kbps, (b) 4kbps, and (c) 7kbps.....	281
Figure 7.19: Pressure Time History and Frequency Response of (a) received, and (b) DFE equalized, 7kbps ASK modulated signal for 30 ft propagation distance in a bent pipe	282
Figure 7.20: Pressure Time History and Signal Constellation of (a) received, and (b) DFE equalized, 7kbps QAM modulated signal for 30 ft propagation distance in a bent pipe	282
Figure 7.21: Signal energy distribution at branch location	283

Figure 7.22: Pressure Time History and Frequency Response of Laboratory Experiment for 30 ft propagation distance in branched pipe of FSK modulated signals at data rates (a) 1kbps, (b) 4kbps, and (c) 7kbps	284
Figure 7.23: Pressure Time History and Frequency Response of branch pipe received signal from 30ft branched pipe Laboratory Experiment for FSK modulated signals at data rates (a) 1kbps, (b) 4kbps, and (c) 7kbps.....	285
Figure 7.24: Pressure Time History and Frequency Response of Stacked signal generated by subtraction of the crown and bottom recordings for the 7kbps FSK modulated signal in a 30ft branched pipe	287
Figure 7.25: Pressure Time History and Frequency Response of equalized signal with a DFE utilizing the RLS adaptation algorithm for FSK modulated signals at data rates (a) 1kbps, (b) 4kbps, and (c) 7kbps.....	288
Figure 7.26: Pressure Time History and Frequency Response of (a) received, (b) stacked by subtraction, and (c) DFE equalized, 7kbps ASK modulated signal for 30 ft propagation distance in a branched pipe	288
Figure 7.27: Pressure Time History and Signal Constellation of (a) received, (b) stacked by subtraction, and (c) DFE equalized, 7kbps QAM modulated signal for 30 ft propagation distance in a branched pipe	289

List of Tables

Table 4.1: Barker Codes.....	159
Table 5.1: Barker Codes.....	180
Table 6.1: Error Performance before and after decoding of Crown, Bottom and Stacked signals for FSK modulation	224
Table 6.2: Bit error rates following the signal processing blocks of the receiver.....	253
Table 7.1: Acoustic wave velocity and density of Water, Cast Iron, Air, and PVC.....	261

Chapter 1

Introduction

1.1 Thesis Objectives

Digital communication systems are nowadays used in every aspect of human life and operations. Cell phones, television broadcasts, global positioning systems, internet, to name a few, are examples of applications employing digital communication techniques. In essence, any operation requiring data exchange of some sort utilizes digital systems, due to their inherent reliability and effectiveness. Digital data can be reproduced accurately very easily even after severe distortion while there exist an abundance of error correction algorithms that preserve the robustness of the communication system even under extreme events. In parallel with the emergence of digital communication systems, monitoring is currently a very active area with an enormous number of potential applications, ranging from wildlife to instrumentation and operation to infrastructure monitoring. Especially the latter one has become the center of attention in many due to sustainability and homeland security concerns.

Within the context of monitoring infrastructure, the scope of this thesis is to implement and evaluate an acoustic digital data communication system for use with in-pipe wireless sensor networks. The term wireless at this point it is used to express a tetherless connection rather than the commonly used radio frequency communication. The proposed communication system uses appropriately modulated acoustic waves, in the place of electromagnetic waves, since pipelines are typically laid underground and radio frequency transmission is not feasible.

More explicitly, the objective of this research work is to prototype the communication unit of a monitoring sensor system, as shown in Figure 1.6. The proposed communication system is based on the exchange of acoustic signals between stationary nodes in a sensor network, through the water flowing in the pipeline. The pipe will be used as an acoustic wave guide, while underwater acoustic transducers will both generate

and record appropriately formed and modulated acoustic signals to carry data, see Figure 1.1. Once generated, these waves will propagate through the water inside the pipe and can be detected by a receiver at the remote location. The target distance of this data communication system is in the order of 300 to 500 m, while the bit rate is on the order of 1kbps.

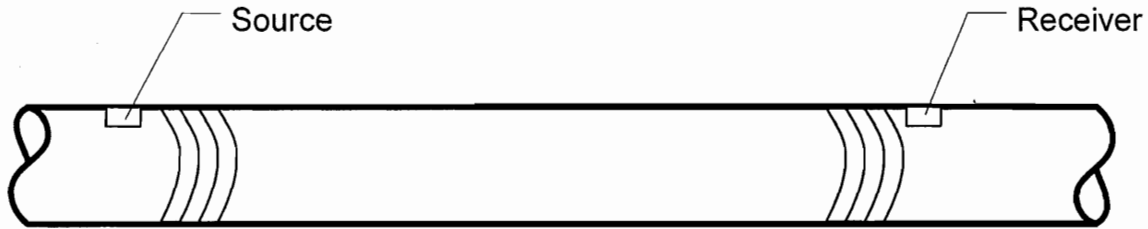


Figure 1.1: In-pipe acoustic data communication

During propagation the acoustic wave undergoes several distorting phenomena, which alter its shape, amplitude, frequency or phase characteristics. Two are the major signal distortion mechanisms of the in-pipe waveguide, namely ambient noise and dispersion. Ambient noise refers to the addition of a random signal of specific mean value and variance. Dispersion corresponds to a number of phenomena, such as multipath propagation, that cause signal reverberation and time spreading, as well as phase and frequency shift. The delayed arrivals of the propagating signal may overlap destructively causing severe signal attenuation, or signal fading. Channels presenting such behavior are referred to as *fading channels*.

In such a confined environment, as the inside of a pipeline, high dispersion and attenuation of the signal is anticipated, mainly because high frequency signals will excite many modes of vibration, which successively propagate at different speeds. Furthermore, there is loss of signal into the surrounding medium as well as reverberation of waves at points of discontinuity, such as pipe joints and bends. Thus, in order to achieve reliable transmission, the data communication system should employ dispersion compensation and error correction algorithms. Ideally, such a system should operate under the additional restriction of limited power supply.

Under the aforementioned considerations along with any additional environmental limitations and digital communication technique restrictions the current thesis constitutes

essentially a feasibility analysis on the idea of acoustic communication using a water pipeline as the transmission channel. The conclusion of the research is expected to propose and evaluate the performance of a communication system that addresses all the issues mentioned above and discussed in detail in the Chapters to follow. It will be seen that the successful completion of this research work involves resolution of several conflicting issues.

1.2 Motivation

The basic concepts related to the motivation supporting the objectives of this thesis can be expressed in four basic steps; (a) the primal problem that needs to be addressed is pipeline monitoring, (b) the proposed solution is to deploy wireless sensors in a network arrangement inside the pipelines, (c) the problem in deploying wireless sensor networks is that wireless communication in terms of radio frequency is not feasible underground, while the availability and long term sustainability of power is scarce, (d) this thesis addresses these two problems with emphasis on the former one. Four major questions directly arise; why study pipeline problems, why use monitoring; why install sensors inside the pipeline, and why do we need wireless communication. Justification to these questions is provided in the following paragraphs.

Why pipelines?

One of the greatest challenges that the science of civil engineering is facing nowadays is to preserve the safe operation of ageing infrastructure. This challenge is further aggravated for underground networks such as pipelines, where no direct access is feasible. Being simultaneously massive and distributed, their normal operation is critical for the health and prosperity of the community, while providing water, oil, gas, and steam supply, as well as sewage removal, they affect the functioning of whole cities.

The vast majority of this infrastructure was constructed more than 50 years ago, when both the long-term performance of the materials used was hardly known, and the methods applied were not technologically advanced enough, to ensure material production and on site construction uniformity. As a result, not only nowadays is there

clear evidence that this infrastructure is highly deteriorated – since pipe bursts are frequent – but also the fragility of old pipelines constitutes a major problem in congested urban environments. This is supported by the recent pipeline bursts in Santa Monica and Boston presented in Figure 1.2.

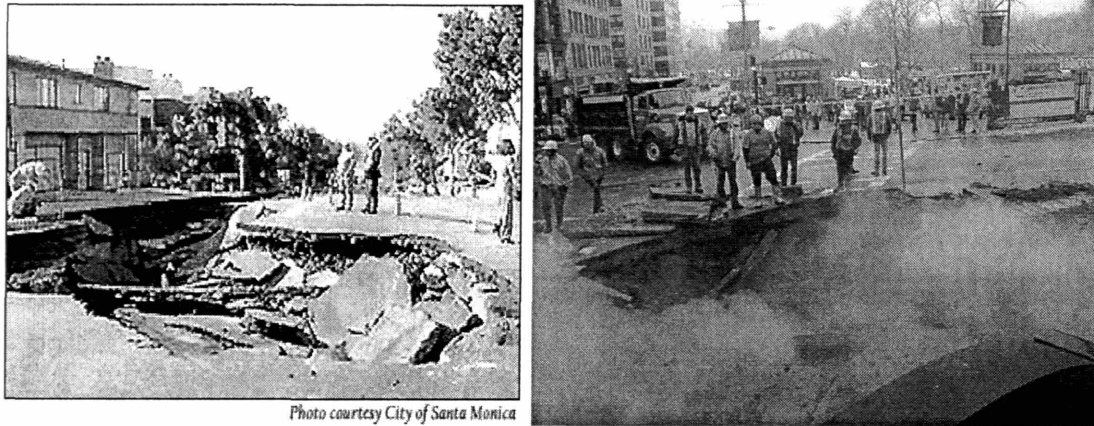


Figure 1.2: Pipe bursts in Santa Monica and Boston [1], [2]

Due to the nature of this infrastructure, it is practically impossible to monitor its current state in detail. Nonetheless, the financial and the societal cost of associated failures is usually enormous: floods, large surface settlements, waste water leakage, cease of clean water supply, even loss of human life are only some of their catastrophic consequences. Even further, the recent terrorist attacks indicate the potential of using these facilities as means for mass destruction.

The proposed wireless sensor monitoring system will be deployed to fresh water pipelines; despite their critical importance for the public health and quality of life, fresh water networks are among the oldest infrastructures currently in use, with very frequent failures and enormous associated replacement and maintenance cost. Based on this reasoning water pipelines were selected among other infrastructure for the deployment of the proposed wireless sensor network. However, the outcome of this thesis can be projected and extended to applications related to other pipeline networks.

Why monitoring?

The quick answer to this question is that continuous monitoring of water pipeline networks is necessary because inspection is not enough. All of the aforementioned issues suggest that it is critical for these networks to be continuously assessed, to predict their long term behavior, to extend their remaining life, to schedule the maintenance activities accordingly, and assure their safe operation. In current practice, the condition of pipelines is assessed by inspection techniques, as discussed in a subsequent paragraph. Nonetheless, the processes, events or conditions that lead to catastrophic failures of pipelines frequently occur in between two scheduled inspections, rendering the constant monitoring of critical pipelines necessary. This monitoring capability can be provided through careful selection of the system installation combined with the recent advances in wireless sensing, which leads to the two final questions.

Why inside?

The installation of monitoring system inside the pipeline provides a number of advantages. First of all the proximity of the sensors to the failure, or failure prone, location of the pipe provides enhanced detection capabilities, since the received signals are distorted less by the propagation path. More explicitly, the monitoring system is expected to record acoustic, pressure, optical, pH and so forth data and decide on the presence of a potential failure event. The proximity of the sensors to the failure area guaranties smaller propagation distances of the recorded parameters, which consequently means less interaction with the surrounding media resulting in clean received signals. The less disturbed signals indicate the increased event detection resolution of the monitoring system.

The proposed installation of the monitoring system inside the pipeline is also not restricted by landscape limitations. External placement of the monitoring system requires the presence of access points, with sufficient space for the installation of the system, as well as sufficient clearance for the insertion of sensors that require contact with the water. While water pipelines are laid mainly under roads, they may also encounter buildings, other utilities, or locations of interest where it is impossible to access the external surface of the pipe by excavating. Elimination of the use of access points allows installation of

the monitoring systems anywhere it is necessary regardless of landscape restrictions. In addition, elimination of the use of access points eliminates excavation and pipe drilling operations resulting in significant reduction of the total monitoring cost.

Why wireless?

One of the objectives of this work is to prototype components for wireless sensing, currently one of the most active research areas with exponential market growth potentials in the near future. The wireless sensor connectivity makes the initial installation and deployment of the network easier, due to its inherent ad hoc properties. The sensors can be located anywhere in the pipeline without any prior installation specific study, while the interconnectivity with the neighboring sensors is automatic. Moreover, in conjunction with the aforementioned internal location of the monitoring system, wireless communication enables the installation of additional sensors inside the pipeline network anywhere it is required, such as critical, failure prone areas or locations of increased importance. The denser deployment of sensor nodes provides higher resolution and therefore increased reliability of the monitoring system. In case the data exchange among the sensor nodes is achieved through wired connections, such ad hoc deployment is impossible, while a wire failure results in failure of the whole monitoring system. Wireless connectivity provides some level of redundancy of the communication system, since single sensor node failures do not result in failure of the complete system, while communication can be maintained through several transmission paths.

1.3 Pipeline failures and Inspection methods

The urban underground terrain is congested with several complex networks of pipelines serving the fresh water, gas and steam supply, sewage removal, and so forth. The increasing frequency of pipe failures indicates the high level of deterioration of the underground pipeline network infrastructure. As indicated in the literature, [3], there exists no single mechanism of failure. In pipe water temperature and internal pressure variations, traffic loading, frost heaving, nearby construction, expansive soils, obstacles, and intrusion of tree roots are some of the failure mechanisms commonly reported during

inspections or following pipeline bursts. Figure 1.3 illustrates root intrusions and cross section blockage identified during regular inspections as examples of pipeline defects. All of the aforementioned failure mechanisms affect the structural integrity of the pipeline which eventually leads to failure. In addition, the affect of the failure mechanism can be aggravated by the presence of corrosion or defects at the pipe wall. The corrosion mechanism of the pipe wall is usually material dependent, with cast iron pipes suffering mostly from graphitization, while pre-cast concrete pipes suffering from wire oxidization and breakage. On the other hand defects include manufacturing or installation imperfections such as slag voids or sand inclusions, and uneven bedding or pipe misalignment, respectively.

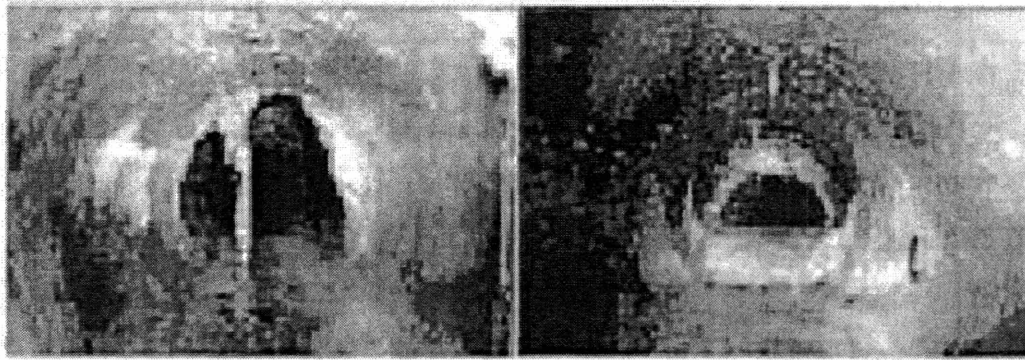
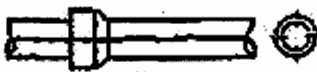
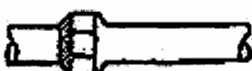
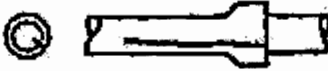

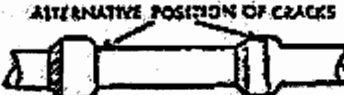






Figure 1.3: Examples of Pipeline Defects: root intrusion, and cross section blockage, [4]

At this point it is necessary to define pipeline failure, since it can be segregated into several levels from an operational to a catastrophic point of view. With respect to the former, failure is defined as insufficient or ceased fluid supply inside the pipe. Such conditions can be generated by obstacles and leak points, which obstruct or divert the normal flow inside the pipe. While obstacles can be composed by roots intrusions or residue deposits, leaks are initiated by holes or cracks at the pipe wall or joints and potentially lead to major events such as bursts. Such events are considered at the other end of the failure spectrum, since they correspond to localized catastrophic failure of the pipe, disruption of the normal operation of significant portion of the pipeline network and frequently severe damage to nearby properties. A list of typical failure mechanisms and crack patterns leading to catastrophic failure of pipelines is provided in Figure 1.4.

Type of failure	Appearance	Cause	Preventive measures
(a) Overload fracture		Excessive vertical load or inadequate bedding	Higher bedding class, or stronger pipe, or concrete surround
(b) Burst socket		Differential thermal or moisture expansion of joining mortar	Resilient joining material which does not cause excessive radial pressure on the socket
(c) Distortion fracture		Differential heating or cooling or moisture content	Protection of uncovered pipes against sun or cold night (or drying wind, with concrete pipes)
(d) Beam fractures		Uneven resistance of foundation, or soil movement, or differential settlement	Flexible joints and uniform hardness of foundation
(e) Pull fractures		Thermal or drying shrinkage of pipe or site concrete, drying shrinkage of clay soil	Flexible telescopic joints and gaps in site concrete at pipe joints
(f) Shear fractures		Differential settlement of wall relative to pipe efflux vena	Flexible joints at least at A and B and making AB not more than 5 ft.
(g) Boreing fracture		Hard spots in pipe bed	Elimination of hard spots
(h) Thrust fracture		Restricted thermal or moisture expansion of pipe or compression due to subsidence	Flexible telescopic joints which do not cause excessive radial pressure on the sockets. Spigot end not hard up in socket
(i) Leverage fracture		Excessive angular displacement	Avoidance of excessive slew when laying

Types of failure b, d, e and f may occur with rigid (e.g. cement mortar) joints.
 Type h may occur with flexible (e.g. rubber ring) joints.
 The other failures are uninfluenced by type of joint.

Figure 1.4: Typical locations of fracture type of burst pipes, ([3] from Jones, 1983)

Leaks are usually identified by customer feedback, periodical inspections and surface occurrence of water. However, only large leaks can get detected, while there is a large number of leaks that remain unnoticed for an extended period of time causing potentially severe environmental damage and resulting in significant cost in resources.

Moreover, even when a leak is identified, locating the exact leak point involves usually a painstaking process, especially in large diameter pipelines with low pressure, and low noise frequency. Moreover, identifying and locating leaks in rural area pipelines becomes increasingly complicated due to the remote locations, great lengths and uneven terrain they are laid, while their exact position is sometimes uncertain.

There exist several studies that attempt to establish a policy and provide a systematic method for the assessment of pipelines, [5]. However, currently utility companies and the pipeline industry carry out sporadic inspections in order to assess and maintain their pipeline networks. The inspection methods currently employed to detect pipeline defects such as cracks and obstacles, are essentially non destructive evaluation techniques adapted specifically for the type and material of the investigated pipeline. Such methods include acoustic emission, flow monitoring, ground penetrating radar, hydrogen gas tracing, and pressure transients identification for identifying leak locations, impact echo, visual inspection, laser profilometry, thermal imaging, eddy current and ultrasound techniques for corrosion and crack detection.

Figure 1.5 illustrates the operation of the acoustic emission method extensively used for locating leaks in water pipelines. According to this technique a pair of hydrophones installed in the pipeline is passively listening for sounds emitted from crack generation and leak orifices. Cross correlation of the recorded signals provides useful data regarding the presence and location of the leak, i.e. the distance from each hydrophone. However, large leaks or low pressure pipelines may emit sounds of very low amplitude, which diffuses within the ambient noise level, reducing consequently the effectiveness of this method. Even though acoustic emission is cited here due to its extensive applicability to water pipelines, further discussion of the aforementioned inspection methods is beyond the scope of this text. Moreover, the acoustic communication system proposed in this thesis provides the potential of applying the acoustic emission method continuously with no additional hardware requirements.

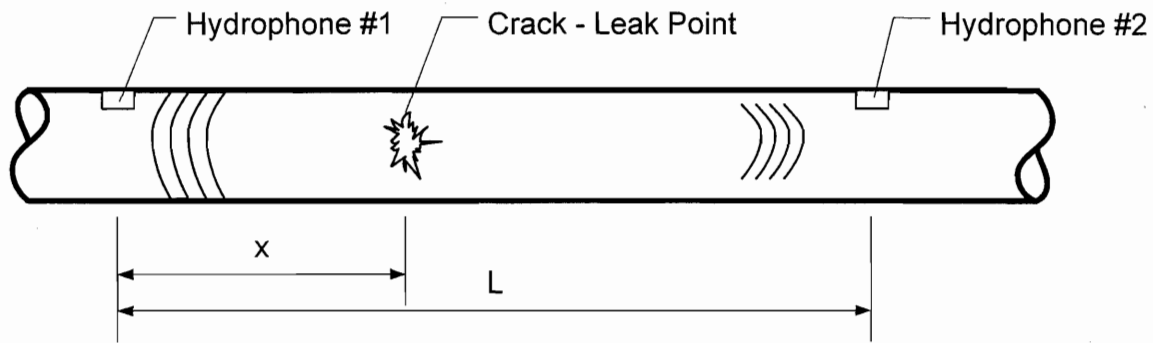


Figure 1.5: Acoustic Emission

Even though there exist a large number of techniques to identify and locate cracks corrosion points and leaks that potentially lead to pipeline failures, they all correspond to inspection techniques frequently requiring interruption of the normal operation of the pipeline while they are very demanding in human resources. The two latter characteristics increase significantly their application cost. The intermittent nature of inspection methods prevents the early detection of failure events, which usually occur in between of two scheduled inspections, indicating the necessity for the implementation of a continuous and automated monitoring system, such as the one introduced in this research study.

1.4 *Wireless sensor networks*

“Sensors will be to this decade what microprocessors were to the 1980’s and the Internet was to the 1990’s” says Paul Saffo of the Institute for the Future. In the past, engineers and scientists built mathematical models to estimate the behavior of processes, by approximating or estimating their response under various conditions, usually resulting in inaccuracies, errors or very conservative designs. With the use of sensors in the information age, we are capable of identifying the exact response of these processes and extract very accurate conclusions. Combining sensors with the recent advances of wireless networking enabled the design and deployment of wireless sensor networks for a very diverse variety of environments and uses. Harbor Research Inc. (www.harborresearch.com) predicts an exponential growth of the market over the next few years. In terms of dollars, Venture Development Corp. (www.vdc-corp.com) forecasts that the market of wireless sensor networks for monitoring and control in North

America will grow from \$235.5 million in 2003 to more than \$750 million by 2006. The recent growth of wireless sensing is justified by its major advantages over wired solutions, such as decreased implementation cost, ease of installation, and increased flexibility. Furthermore, the potential of deploying wireless sensor networks for applications with no wired alternative, such as covering dangerous areas or unwired facilities, is another major advantage. The capabilities of wireless sensors consist of distributed sensing and processing of the information by many independent sensor units. All the sensor units compose a network that assess the condition of the area, process, or infrastructure under monitoring, and decide on the required action.

Any sensor system is composed by four interconnected modules, Figure 1.6. Apart from the sensor devices (i.e. the component *Sensors*), the system comprises a processing, a power and a communication unit. These four individual components are briefly described in the ensuing:

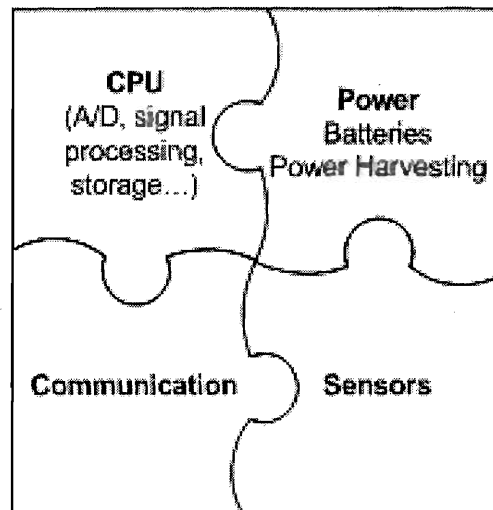


Figure 1.6: Components of an integrated wireless sensor node

- (i) The sensor part comprises the sensors and actuators required by the specific application, and the analog signal conditioning unit (amplifiers or analog filters).
- (ii) The processing section is responsible for handling the analog to digital conversion of the information, and the digital signal processing and storage of

sensor inputs. Moreover, it is capable to decide on potential action, or communication with other sensor systems in the network or the central base station.

- (iii) The power module provides the power supply that is necessary for the operation of all the components. This power is stored in a battery or capacitor. The sensor system however, is usually required to operate for long periods of time, and despite its power efficiency and minimal energy requirements, the replacement of batteries is often necessary due to their finite capacity. Including a power harvesting system in the power unit is an alternative to battery replacement, and the surrounding environment of the wireless sensor network has frequently sufficient amounts of energy for its operation, in the form of light, flow, vibration, temperature and so on. A power harvesting system will capture adequate quantities of this energy and convert it to electrical, resulting in the recharge of the energy storage component of the sensor system.
- (iv) Finally, the communication unit is responsible for the transmission and reception of data from neighboring sensor modules. The typical mean of communication for wireless sensors is radio frequency signals. However, the notion of wireless can easily be extended to everything that lacks the wired connection. Therefore, depending on the environment, other wireless connections may be used, such as acoustic, vibration, ultrasound, bubbles, and so forth.

These sensor nodes are usually arranged in a network pattern, within which the data gets transmitted from sensor node to sensor node sometimes with the assistance of data repeaters, towards a centralized base station as shown in Figure 1.7. Data is processed both locally as well as at the base station. It is very frequent to employ centralized nodes with increased duties of cross correlating data from several nodes for robust event identification. The processing capabilities of each node allow the reduction of data volume transmitted resulting in more power efficient operation schemes, since usually the transmitter consumes the most power. The complete concept of sensor nodes architecture is linked inherently to power efficient methods, employing low power

components and processing algorithms. The reduction of the total power consumption extends the uninterrupted, and without human intervention, service life of the sensor node. An extensive list of references is provided in [6]-[9].

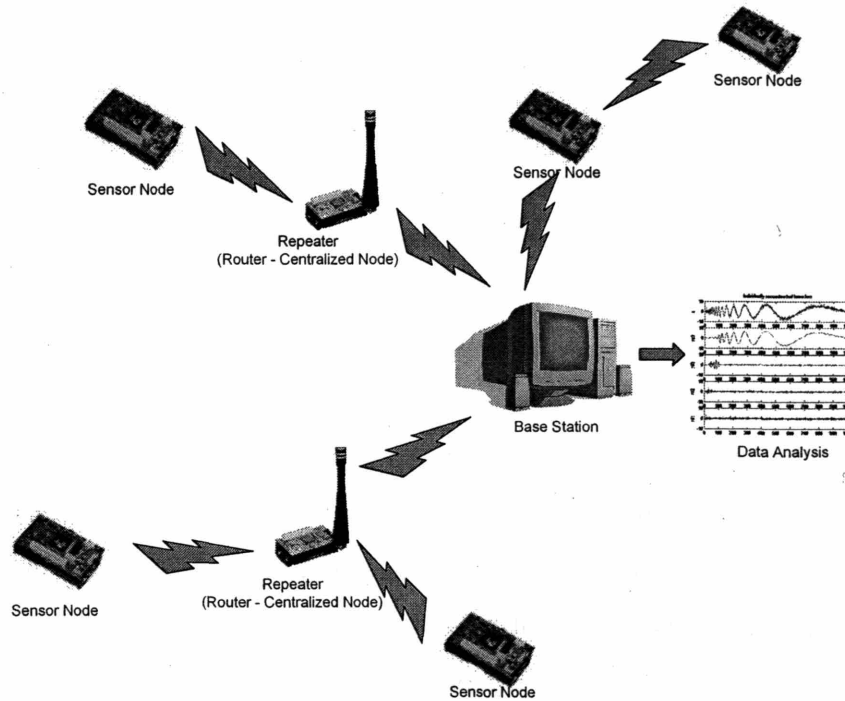


Figure 1.7: Typical Wireless Sensor Network Architecture

1.5 Thesis Outline

This thesis builds step by step the concepts required for the implementation and evaluation of a digital communication system for the in-pipe wireless sensor networks. An effort to provide a consistent notation throughout the text is made, which can be summarized as follows; *italic* formatting is used to denote *scalars* in equations or within the text as well as it is generally used to provide *emphasis*, or provide designation at a *definition* or a *concept*; **vectors** are denoted with bold formatting, while **matrices** are denoted with bold and underlined formatting; finally the hat pointer $\hat{}$ above a specific quantity indicates that the value is estimated.

The systematic approach for the implementation of the in-pipe acoustic communication system reflects the outline of this thesis, thus including step by step analysis of the in-pipe waveguide, the digital communication system as well as their interaction. Following the introduction of Chapter 1, Chapter 2 presents the state of the art of underwater communication systems, mainly developed for ocean applications, along with the restrictions imposed by the confined pipeline environment. Thereafter, in-pipe wave propagation is studied in Chapter 3, which presents the theoretical development and parametric analysis of the pipeline waveguide with the assistance of computerized simulations. The effect of the geometry, materials, environment, and signal characteristics are examined as a first step to identify potential obstacles to the reliable transmission of digital data associated with the channel imposed signal distortion. Chapter 4 serves as an introduction to digital communication systems. It presents a brief description of the available signal processing, error correction and dispersion compensation techniques, along with their restrictions and limitations associated with the implementation of the proposed in-pipe communication system, which is presented in Chapter 5. In this chapter the issues introduced in the preceding chapters are addressed one by one justifying the selection of the proposed digital communication components. This section presents both the software and hardware required for the implementation of the communication system, and provides guidelines for the installation and material selection of the components. Chapter 6 evaluates the performance of the communication system introduced in Chapter 5, through a series of computerized simulations. Gradual introduction of each of the signal processing techniques implemented assesses their effectiveness in performing their intended task, i.e. eliminating part of the signal distortion imposed by a specific phenomenon. Finally, Chapter 7 verifies the performance of the acoustic communication system initially identified in Chapter 6 with the assistance of laboratory experiments, specifically scaled to represent accurately the field conditions. Furthermore, the effect of pipe bends and branches is studied, while it introduces all the parameters examined in Chapters 3 and 6.

The objective of this text is not to provide an exhaustive analysis of the aforementioned topics but to introduce a non expert reader into these concepts and allow

him/her to understand the discussions related to this research. References are provided along with each topic introduced in the present work for further study.

With this research study, the design and deployment of a wireless sensor network to fresh water pipelines is illustrated, yet the same components can be readily applied for the continuous monitoring of other facilities: the wireless monitoring and controlling of buildings, bridges, tunnels, containers, environmental parameters, processes, events, traffic are only some examples where the proposed robust generic wireless sensor platform is applicable. Beyond ageing infrastructure monitoring, wireless sensor networks can be also used as an invaluable assistant to homeland security, facilitating the detection of biological agents, explosive or radioactive materials, tracking packages, etc. The outcome of this research work proves that it is possible to deploy wireless sensor networks even at areas where radio frequency communication is not feasible.

1.6 References

- [1]. Ocean Park Gazette, issue of January 3rd 2003, Web reference:
http://www.oceanparkgazette.org/03jan/sinkhole_jan1.htm
- [2]. Pictures are property of OrnothLand website
<http://users.rcn.com/ornoth/scrapbook.html>
- [3]. O'Shea P.J., "Failure Mechanisms for Small Diameter Cast Iron Water Pipes", Doctor of Philosophy Thesis, Department of Civil and Environmental Engineering, University of Southampton, 2000.
- [4]. Photos are courtesy of Everest VIT Ltd., <http://www.everestvit.com/>
- [5]. Farley M. and Trow S., "Losses in Water Distribution Networks: A Practitioner's Guide to Assessment, Monitoring and Control", IWA Publishing, London, UK, 2003.
- [6]. Mini R.A.F., Webpage, "Sensor Networks", Electronic Reference Oct. 2005,
<http://www.research.rutgers.edu/~mini/sensornetworks.html>
- [7]. Lebeck A.R. Webpage, "Distributed Sensor Networks Reading List", Electronic reference Oct. 2005, <http://www.cs.duke.edu/~alvy/courses/sensors/Papers.html>
- [8]. Jain R. Webpage, "Sensor Networks: References", Electronic reference Oct. 2005, http://www.cse.wustl.edu/~jain/refs/sns_refs.htm
- [9]. Zhou, Y., Webpage, "References on Wireless Sensor Networks", Electronic reference Oct. 2005, <http://appsrv.cse.cuhk.edu.hk/~yfzhou/sensor.html>

Chapter 2

State of the Art in Underwater Acoustic Communication

2.1 Introduction

Over the past decades underwater communication has evolved into a very active research area since it facilitates the needs of many military or more recently commercial operations. Applications that require underwater communication extend, but are not restricted, to communication with submarines, communication between divers, command of autonomous underwater vehicles (AUV), animal tracking, sea bed exploration, pollution monitoring, remote control of off-shore equipment, data collection from deep sea sensors, and so on. These applications of underwater communication rely mostly on the transmission of acoustic waves. The potential of using other types of waves, such as optical or electromagnetic waves, has also been explored, but their applicability is limited because they are only capable of propagating short distances in water due to their very high rates of absorption in this medium. Indeed, the attenuation of electromagnetic waves is on the order of $\sim 45\sqrt{f}$ dB per kilometer, with f being the frequency in Hertz. Thus, such waves require large antennae and high power transmitters. Still, even with the use of high power transmitters, the usable frequency range is constrained by the absorption factor, which limits the practical bit rate that can be achieved. On the other hand, optical waves are not nearly as much affected by absorption as they are by scattering. To minimize the latter, researchers have employed narrow optical beams from green and blue lasers because these exhibit the lowest rates of absorption in water, and offer a potential of enormous data throughput. Nonetheless, these attempts are currently limited to short transmission distances of at most 200m under ideal conditions.

In contrast to electromagnetic and optical waves, the susceptibility of acoustic waves to absorption and scattering by water is some three orders of magnitude smaller. The use of underwater acoustic waves was recognized very early as a means of communication and detection. Leonardo da Vinci wrote in 1490: “If you cause your ship

to stop, and place the head of a long tube in the water and place the outer extremity to your ear, you will hear ships at a great distance from you” [1]. In the early 1900’s acoustic echoes were used as means to determine the distance between objects in the water. The first successful implementation of an underwater acoustic communication system was an underwater telephone developed in 1945 by the Naval Underwater Sound Laboratory for communication with submarines. Nowadays, several military, commercial and research implementations exist that are capable of achieving high data rates at considerable range.

2.2 *Open Sea Acoustic Communication*

Research and development on underwater acoustic communication has almost exclusively focused to open-sea applications. In addition, the majority, if not all of commercial products are developed to facilitate open-sea operations. The performance requirements of current applications continue to grow steadily as their scope broadens and new needs emerge. The same driving forces that contributed to the evolution of digital communications in the areas of high data rate links, real time data transmission, bidirectional communication, multiple access carriers, and wireless networks, have also extended to underwater applications. However, the underwater acoustic channel is band limited and highly reverberant, which poses formidable obstacles to reliable, high speed digital communications, [2], [3]. Moreover, the channel characteristics vary with time and are highly dependent on the location of the transmitter and receiver. In that respect, open sea acoustic channels are characterized as horizontal or vertical and as shallow or deep sea.

2.2.1 *Signal Distortion*

The two major factors affecting the distortion of an acoustic signal in water are the attenuation and reverberation. Attenuation is the reduction of the signal’s magnitude due to energy redistribution along the path between the transmission and the reception points. At this stage, attenuation needs to be defined in contrast to absorption. “Absorption refers to any large number of processes that take energy from a wave and transform it to some other form, such as heat. Attenuation refers to processes of wave

diminution that also follow the exponential law, but which reorders the wave energy rather than transforms it”, [4]. However, these terms have been used interchangeably by researchers including all physical phenomena associated with them. In general, the larger the distance, the more the attenuation of the signal, and therefore the more the impact of the environmental noise resulting in decrease of the signal to noise ratio (SNR). The usual remedy to attenuation is to increase the power of the transmitted signal.

Reverberation, on the other hand, is the distortion of the signal due to scattering and multipath propagation. It is a function of several environmental and signal parameters, such as size, shape and material of the transmission medium, boundaries and discontinuities of the acoustic waveguide, wavelength of the transmitted signal etc. The two principal mechanisms of multipath formation are reflection from boundaries and ray bending. In shallow and/or horizontal channels, reflection from boundaries such as the sea surface or the bottom becomes the dominant effect. In deep long range channels ray bending from changes in acoustic wave velocity is the governing reason for distortion. It becomes apparent that reverberation is a more complex phenomenon than attenuation, resulting in time spreading, amplitude and phase distortion, and shifting of the frequency content of the wave. In a digital communication system, reverberation causes intersymbol interference, i.e. overlap of adjacent transmitted bits of information. Unlike attenuation, increasing the transmitted signal's power increases proportionally the reverberation related noise, not affecting the signal to noise ratio of the received signal. Several actions are required to decrease the effect of reverberation on the signal, such as beam-steering, focusing, or phase correction with adaptive equalizers. Careful selection of the transmitted signal is required, in terms of frequency content, as well as beam-forming.

Along with the reverberation requirements, the frequency content of the signal is also controlled by the required bit rate and the desirable range of the application, which are inversely proportional to each other, see Figure 2.4. A rule of thumb frequently used to estimate an upper bound to the frequency with respect to range is provided by the absorption relation for sonar applications. This relation is $\alpha(f) \times r = 10dB$, where $\alpha(f)$ is an absorption coefficient that is controlled by the frequency of the transmitted wave, the salinity, temperature and pressure of the water and r is the range. A typical graph that

provides values for α is shown in Figure 2.1. These factors essentially limit the available bandwidth for any communication application.

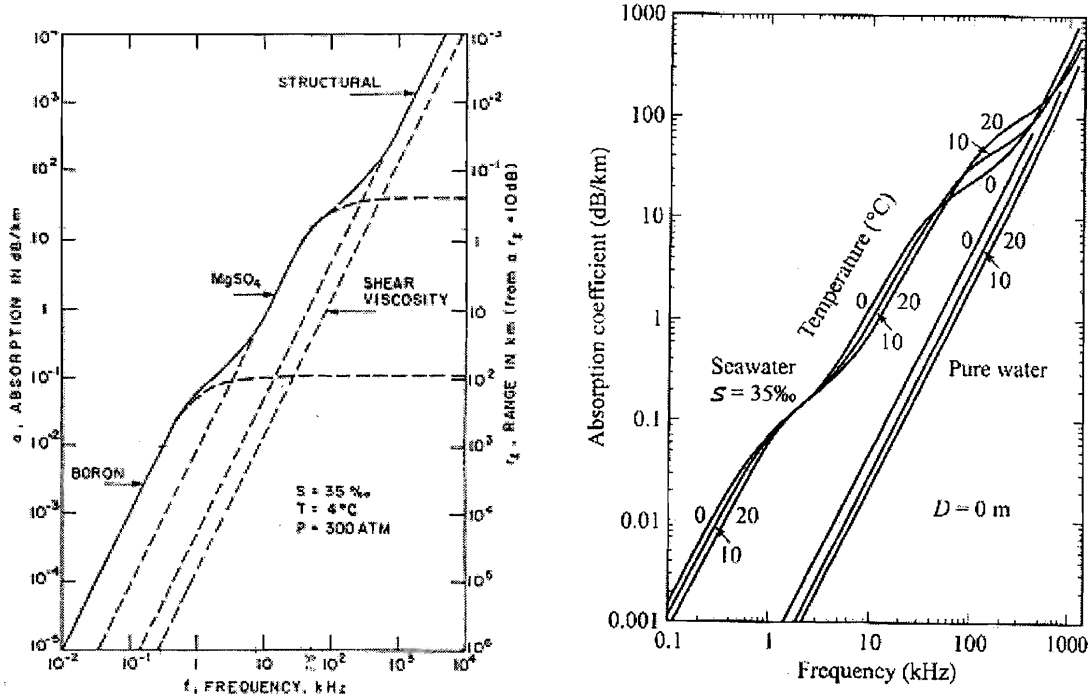


Figure 2.1: Volumetric absorption including all known relaxation processes, [4], [5]

2.2.2 Communication techniques

Very early implementations of underwater acoustic communication devices were based on analog systems, being essentially sophisticated loudspeakers, [2] with minimal compensation capabilities for the distortion and noise introduced to the propagating signal. The evolution of microprocessors and radio frequency communications brought into the limelight the use of digital systems for underwater applications. Digital processing allows the use of distortion compensation and error correction algorithms, resulting in more reliable communication. Due to the inherently distorting character of the underwater acoustic channel, frequency shift keyed (FSK) modulation of the digitally encoded data was initially used. FSK modulation provided for many years a viable solution for underwater digital communication, since it allows the use of simple error correction algorithms and enables reliable signal transmission in an incoherent manner, thus eliminating the propagation of errors in the subsequent symbols of the signal.

However, this simplicity and robustness comes with the penalty of poor bandwidth efficiency. Further discussion on digital communication techniques is provided in Chapter 4.

The aforementioned demand of current applications for increased data throughput, as well as the band-limited nature of the underwater acoustic channel, mandated the use of coherent modulation methods which are more bandwidth efficient. The research community has recently turned its attention to phase shift keying (PSK) and quadrature amplitude modulation (QAM), along with their extensions to multiple dimensions and channels, as the modulation methods of the encoded digital signal, in order to achieve better bandwidth efficiency [3], [6], and [7]. However, the applicability of these coherent modulation methods for long transmission ranges requires complicated signal compensation and extensive error correction algorithms, [8], since they are more prone to errors than the incoherent modulation methods because of phase instabilities in the channel and the relative motion of the transmitter-receiver system.

Probably multipath propagation of the transmitted wave is the most important signal distortion phenomenon in underwater acoustic communications. For this reason, specialized tools have been developed to resolve or suppress the effects of multipath propagation, mainly by adjusting the signal formation in the software level or with the hardware implementation of transmitting and/or receiving arrays. Most solutions are based on the idea of transmitting a narrow beam in order to achieve minimum interaction with the boundaries and create a single path of wave propagation. For this reason, many implementations have introduced long transmitting arrays that are capable of beamforming the transmitted signal and directing it to a specific target. Within the context of generating highly directive signals, the use of parametric sources have been proposed [9], [10], and [11]. Parametric sources use a high primary frequency signal and are capable of transforming a region of water into a large low frequency source, resembling an array. The main advantage, especially with respect to transmitting arrays, is that the source is smaller in size. However, they require significant amount of power to operate. One disadvantage of all techniques that generate narrow beams is the introduction of pointing errors, especially in the case of moving targets. For this reason several researchers have proposed the use of receiving arrays to suppress multipath [12].

These receivers are capable of separating the signals arriving from different directions and selecting the arrival of the main signal. Such systems have been used successfully for short ranges, while they are not effective for long ranges since the angular resolution of the various arrivals becomes very small.

Spread spectrum techniques have been proposed recently to resolve the effect of multipath propagation of the transmitted signal, [13]-[16]. According to this technique, the symbols to be transmitted are multiplied by a numerical sequence, preserving the effective data rate but spreading at the same time the used bandwidth. The result of this method is that sequential symbols are transmitted in different parts of the bandwidth, eliminating as much as possible the issue of overlapping received symbols.

Finally, digital communication techniques are very frequently employed to resolve signal distortion such as adaptive equalization, encoding, phase lock loops etc. Further analysis of digital communication systems is beyond the scope of this chapter, since the focus at this point is on underwater acoustic communications. More extended discussion of digital communication techniques and error correction algorithms will be provided in chapter 4.

2.2.3 Hardware

The successful implementation of an underwater communication system not only depends on a robust communication protocol and error correction algorithm, but also is heavily dependent on the appropriate design of the pertinent hardware. The hardware of primary importance includes hydrophones (for receiving sound), projectors (for transmitting sound) or transducers (for both receiving and transmitting), along with preamplifier or power amplifier units to drive the receiver or transmitter respectively. These devices can be set alone or laid in an array configuration as mentioned above. The hardware configuration of the communication system is completed by the supporting electronic circuit, in which the software of the communication protocol is embedded, along with an analog to digital converter for the receiver, or a digital to analog converter for the transmitter side, and of course a power supply. A typical transmitter – receiver system is presented in Figure 2.2.

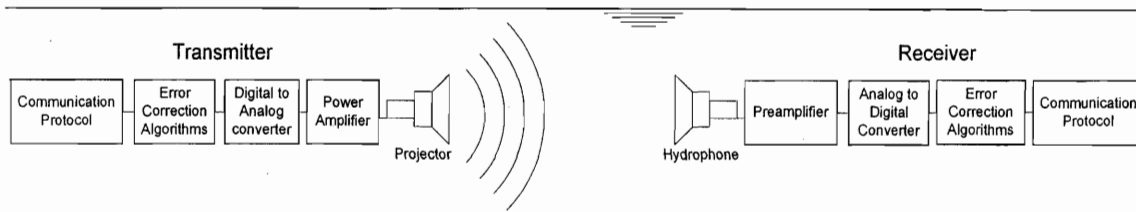


Figure 2.2: Typical Transmitter – Receiver system

At this stage, the devices capable of transmitting and/or receiving acoustic signals, will be referred to as transducers. There is a large number of parameters, such as resonant frequency, efficient bandwidth, beam pattern, beam width, directivity, transmitting power, receiving sensitivity, and so on, that needs to be defined in order to select an appropriate transducer. Moreover, depending on the application parameters such as size, weight, operational depth, service life, material and so on may become of critical importance. In what follows only a brief discussion of the most important factors from the in-pipe telemetry application point of view will be provided.

Due to the bandlimited nature of the underwater acoustic channel, the efficient bandwidth range is probably the most critical characteristic of an underwater acoustic transducer. Recall that the frequency content of the transmitted signal affects tremendously the bitrate, range and the quality of the received signal. Therefore, a transducer with an appropriate efficient transmitting and/or receiving frequency range is required for the robust generation of the acoustic signal. Beyond this range, any transmitted or recorded signal is subject to random nonlinearities, which affect significantly the quality of the communication link.

Several underwater acoustic communication implementations require the use of a narrow-beam acoustic signal, which is generated with the introduction of an appropriate set of transducers usually coordinated in an array pattern. These transducers have special construction, size and shape in order to generate beams of specific pattern and beamwidth. For example, spherical transducers provide an omnidirectional pattern, whereas others are capable of generating elliptical, toroidal, or conical patterns, and so on. The beamwidth is defined as the width of the main lobe in degrees, and it is usually measured between the half power points where the power has dropped 3dB. The

capability of steering the main lobe to a specific direction may also be of importance for some applications. Beam steering is achieved by application of proper phase or time delays between signals driven by the transducer array.

Since attenuation is a critical parameter affecting the quality and range of the propagating signal, the transmitting power of the projector and the receiving sensitivity of the hydrophone emerge as significant factors of the communication system. The higher the transmitting power capabilities of the projector the further a robust signal will propagate, while the greater the receiving sensitivity of the hydrophone, the better becomes the reception of a significantly attenuated signal. However, there exist several applications where power resources are limited, such as a wireless sensor network or an autonomous underwater vehicle, imposing therefore restrictions on the available power for the transmitter. Furthermore, in cases where reverberation is the main factor of the signal distortion, such as inside an in-pipe acoustic channel, increasing the power will not improve the quality of the reception, since the signal pressure level and reverberation increase proportionally.

The transducer materials can become of major importance in hostile environments or where health considerations are of primal importance. In the first case, the transducer must be durable enough to sustain the corrosive environment whereas in the second case the transducer's material must be biocompatible with the surrounding materials and live organisms. Guidelines for designing and specifying underwater transducers including a large number of the aforementioned parameters can be found in [17] and [18].

The combination of a transducer with an appropriate communication protocol and the supporting hardware constitutes an *Acoustic Modem*. These devices are capable of transforming digital data into acoustic signals which are transmitted to the ocean and vice versa. There exist several research attempts or commercially available acoustic modems that are able to achieve respectable bit rates at significant distances in the ocean, [19]-[24], Figure 2.3.

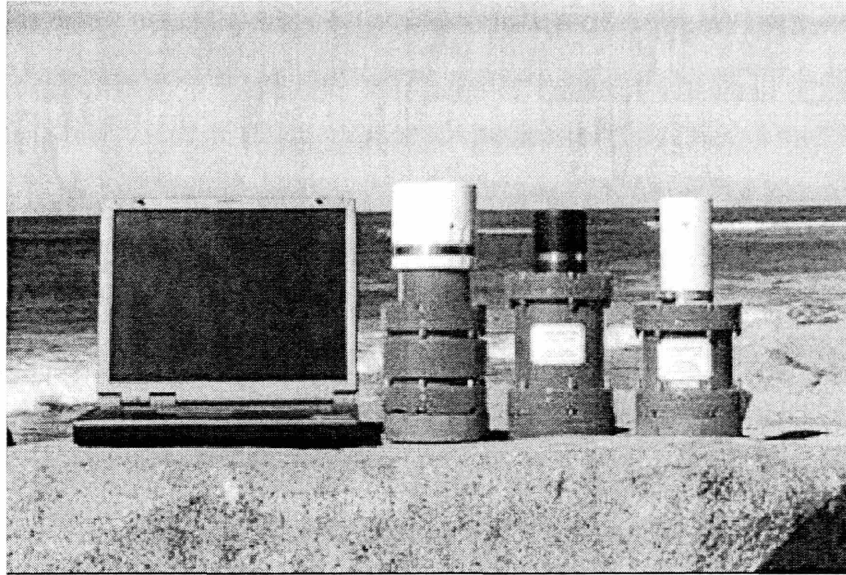


Figure 2.3: Open – Sea acoustic modem (photo courtesy of Link Quest)

The commercial acoustic modems are capable of transmitting and receiving signals from moving targets, such as ships, submarines, autonomous vehicles, etc. at rates that reach 19.2 kbps at several kilometers range, whereas there exist research attempts up to 500kbps. However, it has been shown that the range is inversely proportional to the available bit-rate, see Figure 2.4.

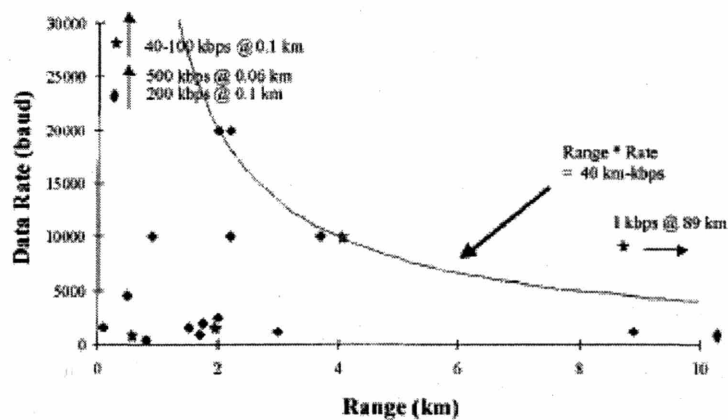


Figure 2.4: Published experimental performance of underwater acoustic telemetry systems. The channels vary from deep and vertical to shallow and horizontal. In general, the high rate or high range results are for deep channels while the cluster of low range, low rate results are for shallow channels. Modems developed by the research community are represented with diamonds while stars denote commercially available systems. The range \times rate bound represents an estimate of the existing performance envelope. [2]

2.3 *Open sea vs. In-pipe communication*

Despite the extensive research in open sea underwater applications, there exists minimal research on in-pipe acoustic communication systems. The acoustic communication systems, examined in the preceding paragraph, are developed mainly for ocean applications. Nevertheless, most of them are large in size and very expensive. On the other hand, the point of interest in this research is to deploy a wireless sensor network inside pipelines, which translates into small and inexpensive devices. This imposes several constraints to the design of the communication system.

In contrast to long range open sea acoustic communications, where attenuation is the primary cause of signal degradation, for in-pipe acoustic applications reverberation is the most important signal distortion factor. The confined space of the pipeline imposes severe multipath propagation and time spread, as well as phase and frequency dispersion on the propagating wave, see Chapter 3 and [25]. Whereas in long range open sea communication ray theory is usually sufficient for the description of the acoustic channel, the simulation of the in-pipe waveguide requires very sophisticated techniques, as it will be shown in the next chapter. As alluded to in a preceding paragraph, the acoustic channels in the ocean are characterized with respect to the location of the transmitter and receiver as horizontal or vertical and as deep or shallow. Such standardization does not exist for in-pipe acoustic channels, since parameters such as pipe material, and geometry, presence of joints, shafts, curves, and branches affect tremendously the properties of the pipeline waveguide.

The list of all aforementioned factors significantly affects the performance of the in-pipe communication system. A simple example that proves the aforementioned statement is the rule of thumb that provides the upper limit of the signal frequency with respect to the transmission range. From Figure 2.1 and assuming a maximum transmission range of 500m the maximum frequency that can be used for a sonar application is around 80 kHz. Consider also that signal attenuation is controlled by a number of factors such as salinity, temperature, pressure, hardness, and particle content of the water. While in the above calculation typical values of these factors are considered for the pipeline environment, these factors increase the attenuation and scattering of the propagating wave in the ocean. As it will be shown in a following chapter, this rule of

thumb overestimates by approximately a factor of 10 the maximum frequency that can be used at an in-pipe acoustic communication system.

On the other hand, time variation of environmental variables, which is significant in the ocean, is minimal in the pipeline system. Waves, fish, ships, temperature and so on are constantly changing the characteristics of the open sea acoustic channel, while for the in-pipe acoustic channel probably only daily or seasonal variations of temperature may slightly affect the system.

Furthermore, acoustic communication over a wireless sensor network installed in a pipeline is simplified with respect to an open sea system, since it operates with stationary targets in space. In open sea applications the communication link is usually implemented between moving devices such as ships, submarines, autonomous underwater vehicles, divers and so on. In such systems it is required to compensate for Doppler spreading [2], or in other words frequency dispersion and time selective fading.

The notion of wireless sensing is connected with low power consumption, whereas most of the current acoustic modems are operating at the 100 or even 1000 watt scale. Inside a pipeline, the power resources are limited, and therefore it is necessary to implement an energy efficient communication system. Since pipelines are usually buried underground the wireless sensor nodes will not be accessible for battery replacement and maintenance, constituting mandatory the presence of a constant power supply. A potential source of energy could be the flow of water inside the pipeline. In such case the power harvesting system would be comprised of a small generator connected to a propeller or turbine driven by the water flow, as discussed in Chapter 5. However, the capacity of such a system is restricted to the energy potential in the flow, while the undisturbed operation of the pipeline needs to be considered at the same time, limiting the size of the turbine used.

Water pipeline networks supply potable water to communities. As a consequence health considerations are far more stringent in such systems than in the ocean. Any devices installed inside a pipeline must be rigorously tested for compatibility with the environment and must be safe for the drinking water. These devices may not interact in any way, i.e. electrostatically, chemically, and so forth, with materials present in the

environment, and may not disturb the biofilm, a thin biological layer present on the inside of all fresh water pipelines.

2.4 *In-Pipe Acoustic Applications*

In pipe acoustics have been studied extensively for inspection purposes, such as leak detection. Acoustic emission is a well established non destructive evaluation technique for assessing the condition of pipelines. In this technique, a set of acoustic sensors are passively “listening” for sounds emitted by the structure of interest, related to release or dissipation of energy from specific locations in the structure. For a pipe such sounds are related to crack formation and to water leaking from cracks. An elaborate in-pipe wave propagation study can be found in [25]-[29] as well as in Chapter 3.

Underground exploration with boreholes is another application that requires extensive analysis of acoustics within and around cylindrical shafts embedded in the ground, [30]-[34]. Acoustic signals sent among various boreholes are used in the oil industry, geophysics, geology and earthquake engineering for underground exploration.

The first communication attempt through a cylindrical borehole was implemented in oil well drills. During drilling, operators need to know the location, the orientation and the conditions in the area of the drill head as well as other factors such as the presence of oil. One way communication is achieved by sending bubbles in the slurry surrounding the drill head. Buoyancy drives the bubbles at the surface at a certain rate defining the binary data. However, the data rate achieved is very low, on the order of 1 bit per second. In addition there is not potential for communication from the surface to the drill head.

A more sophisticated attempt for oil drill communication is presented in [35]-[39]. According to this “Acoustic telemetry system” extensional stress waves are transmitted through the drill pipe. These waves are generated and captured with the use of piezoelectric films. The achieved data rate without compression is up to 10 baud at a range of 10,000 feet. Since this system is based on the propagation of extensional stress waves, a significant factor of signal loss in this system is reflections at the joints of the drill pipe and the repeaters of the system. Elaborate analysis of the wave impedance of

the drill pipe had to be completed and the impedance of the repeaters had to be matched to the one of the joints for the successful implementation of this communication method.

An acoustic telemetry system for communication with an autonomous robot in water pipelines is presented in [40]-[43]. According to this system acoustic waves in the ultrasonic range are sent through the water between the robot and a base station. Unfortunately, the only published experimental results are limited to successful communication in a range of 4m inside a 400mm diameter pipeline. The potential of the system, according to the authors, is a communication link at a distance of 500m inside a 1m diameter pipe at a maximum data rate of 9.6kbps.

2.5 References

- [1]. *Notebooks of Leonardo da Vinci*. Edward MacCurdy, ed., New York, George Braziller, 1954.
- [2]. Kilfoyle D. B., and Baggeroer A. B., "The State of the Art in Underwater Acoustic Telemetry", *IEEE Journal of Oceanic Engineering*, pp. 4-27, Vol. 25, No. 1, January 2000.
- [3]. Stojanovic M., "High speed underwater acoustic communications", in *Underwater Acoustic Digital Signal Processing and Communication Systems*, edited by Istepanian R.S.H. and Stojanovic M., Kluwer Academic Publishers, pp. 1-35, 2002.
- [4]. Dyer I. "Fundamentals and Applications of Underwater Sound", *13.851 Lecture notes*, Department of Ocean Engineering, Massachusetts Institute of Technology.
- [5]. François R.E, and Garrison G.R., "Sound absorption based on ocean measurements: Part II. Boric acid contribution and equation for total absorption", *Journal of Acoustical Society of America*, Vol. 72, pp. 1879-1890, 1982.
- [6]. Stojanovic M., "Recent Advances in High-Speed Underwater Acoustic Communications", *Journal of Oceanic Engineering*, Vol. 21, No. 2, pp. 125-136, April 1996.
- [7]. Stojanovic M., Catipovic A., and Proakis J.G., "Phase coherent digital communications for underwater acoustic channels", *IEEE Journal of Oceanic Engineering*, Vol. 19, pp. 100-111, January 1994.
- [8]. Stojanovic M., "Underwater Acoustic Communications", *Proc. IEEE Electro International*, pp. 435-440, Boston, June 1995.
- [9]. Coates R. and Kopp L., "The use of parametric transducers for underwater acoustic communication: Project PARACOM", *Proc. European Conference on Underwater Acoustic*, pp. 96-99, Weydert, M. Editor, Brussels, Belgium, 1992.
- [10]. Coates R., Zheng M., and Wange L., "'Bass 300 PARACOM': A 'model' underwater parametric communication system", *IEEE Journal of Oceanic Engineering*, Vol. 21, pp. 225-232, 1996.
- [11]. Loubet G., Vial F., Essebar A., Kopp L., and Cano D., "Parametric transmission of wide-band signals", *Proceedings of Oceans '96*, Ft. Lauderdale, FL, 1996.

- [12]. Howe G.S., Tarbit P.S.D, Hinton O.R, Sharif B.S., and Adams A.E., "Sub-sea acoustic remote communication utilizing an adaptive receiving beamformer for multipath suppression", *Proceedings of Oceans '94*, Brest, France, 1994.
- [13]. Fischer J.H., Bennett K.R., Reible S.A., Cafarella J.H., and Yao I., "A high data rate, underwater acoustic data communications transceiver", *Proceedings of Oceans '92*, Newport, RI, 1992.
- [14]. Ritcey J.A., and Griep K.R., "Code shift keyed spread spectrum for ocean acoustic telemetry", *Proceedings of Oceans '95*, San Diego, CA, 1995.
- [15]. Loubet G., Capellano V., and Filipiak R., "Underwater spread-spectrum communications", *Proceedings of Oceans '97*, Halifax, Nova Scotia, Canada, 1997.
- [16]. Boulanger C., Loubet G., and Lequepeys J.R., "Spreading sequences for underwater multiple access communications", *Proceedings of Oceans '98*, Nice, France, 1998.
- [17]. Kuntsal E, and Bunker W.A, "Guidelines for specifying underwater electroacoustic transducers", *Proceedings of UDT '92 Conference*, London, England, June 1992. (See also revised version at <http://www.itc-transducers.com/pdf/guidespec.pdf>)
- [18]. Coates R.F.W., "The design of transducers and arrays for underwater data transmission", *IEEE journal of Oceanic Engineering*, Vol. 16, No. 1, pp. 123-135, January, 1991.
- [19]. Yu X., "Wireline quality underwater wireless communication using high speed acoustic modems", *Proceedings of Oceans '00*, Providence, RI, 2000.
- [20]. Herold D., and Johnson M., "A compact underwater acoustic modem", *Proceedings of the 1994 Symposium on Autonomous Underwater Vehicle Technology*, Cambridge, MA, 1994.
- [21]. DSP-Comm website, electronic reference July 2005, <http://www.dspcomm.com/index.htm>
- [22]. Applied Acoustics Engineering website, electronic reference, July 2005, http://www.appliedacoustics.com/mainframe/acoustic_telemetry/acoustic_telemetry.htm
- [23]. Benthos Inc. website, electronic reference, July 2005, <http://www.benthos.com/>
- [24]. Catipovic J., Brady D., and Etchemendy S., "Development of underwater acoustic modems and networks", *Oceanography*, Vol. 6, No. 3, April, 1994.

- [25]. Long R.S., Cawley P., and Lowe M.J.S., "Acoustic wave propagation in buried iron water pipes", *Proc. Royal Society London: Mathematical, Physical and Engineering Sciences*, Vol. 459, pp. 1749-2770, September, 2003.
- [26]. Long, R., Lowe, M.J.S. and Cawley, P., "Axisymmetric modes that propagate in buried iron water pipes", *Review of Progress in Quantitative Non-Destructive Evaluation*, Vol. 22, Thompson D.O. and Chimenti D.E. (eds), American Institute of Physics, pp1201-1208, 2003.
- [27]. Long, R., Lowe, M.J.S. and Cawley, P., "Attenuation characteristics of the fundamental modes that propagate in buried iron water pipes", *Ultrasonics*, Vol. 41, pp509-519, 2003.
- [28]. Long, R., Vine, K., Lowe, M.J.S. and Cawley, P., "The effect of soil properties on acoustic wave propagation in buried iron water pipes", *Review of Progress in Quantitative Non-Destructive Evaluation*, Vol. 21, Thompson D.O. and Chimenti D.E. (eds), American Institute of Physics, pp. 1310-1317, 2002. Similar paper also in *Proceedings of 8th Euro Non-Destructive Testing Conference*, Barcelona, June 17-21, 2002.
- [29]. Demma, A., Cawley, P., Lowe, M.J.S., Roosenbrand, A.G. and Pavlakovic, B., "The reflection of guided waves from notches in pipes: a guide for interpreting corrosion measurements", *NDT&E International*, Vol. 37, pp 167-180, 2004.
- [30]. Cheng C.H., and Toksöz M.N., "Elastic wave propagation in a fluid filled borehole and synthetic acoustic logs", *Geophysics*, Vol. 46, No. 7, pp 1042-1053, July, 1981.
- [31]. Tubman K.M., Cheng C.H., and Toksöz M.N., "Synthetic full waveform acoustic logs in cased boreholes", *Geophysics*, Vol. 49, No 7, pp 1051-1059, July, 1984.
- [32]. Tubman K.M., Cheng C.H., Cole S.P., and Toksöz M.N., "Synthetic full waveform acoustic logs in cased boreholes, II Poorly bonded casing", *Geophysics*, Vol. 51, No. 4, pp 902-913, April, 1986.
- [33]. Kurkjian A.L., and Chang S.K., "Acoustic multipole sources in fluid filled boreholes", *Geophysics*, Vol. 51, No. 1, pp. 148-163, January, 1986.
- [34]. Poletto F., Carcione J.M., Lovo M., and Miranda F., "Acoustic velocity of seismic-while-drilling (SWD) borehole guided waves", *Geophysics*, Vol. 67, No. 3, pp. 921-927, May-June, 2002.
- [35]. Drumheller D.S., "Acoustical Properties of Drill Strings," *Journal of the Acoustical Society of America*, Vol. 85, No. 3, pp. 1048-1064, March, 1989.

- [36]. Drumheller D.S., "Extensional Stress Waves in One-Dimensional Elastic Waveguides", *Journal of the Acoustical Society of America*, Vol. 92, No. 6, pp. 3389-3402, December, 1992.
- [37]. Drumheller D.S., "Attenuation of Sound Waves in Drill Strings", *Journal of the Acoustical Society of America*, Vol. 94, No. 4, pp. 2387-2396, October, 1993.
- [38]. Drumheller D.S., and Knudsen S.D., "The Propagation of Sound Waves in Drill Strings", *Journal of the Acoustical Society of America*, Vol. 97, No. 4, pp. 2116-2125, April, 1995.
- [39]. Drumheller D.S., and Knudsen S.D., "Wave impedances of drill strings and other periodic media", *Journal of the Acoustical Society of America*, Vol. 112, No. 6, December, 2002.
- [40]. Li Y., Harrold S.O., and Yeung L.F., "Ultrasonic data communication along large diameter water filled pipes", *Proceedings of the 2nd IEEE Conference on Mechatronics and Machine Vision in Practice*, pp. 239-244, Hong Kong, September, 1995.
- [41]. Li Y., Harrold S.O., and Yeung L.F., "Experimental study on ultrasonic signal transmission within the water filled pipes", *Mechatronics and Machine Vision in Practice*, pp. 93-98, Australia, September, 1997.
- [42]. Li Y., Harrold S.O., and Yeung L.F., "Model-based simulation for ultrasonic communication channel inside pipeline", *In Proceedings of International Conference on Signal Processing Applications and Technology*, pp. 1163-1167, 2000.
- [43]. Bin L., Harrold S.O., Bradbeer R., and Yeung L.F., "An Underwater Acoustic Digital Communication Link", *in Mechatronics and Machine Vision*, Billingsley J. (Ed), Research Studies Press, UK, pp 275-282, 2000.

Chapter 3

Wave Propagation in pipeline waveguides

3.1 Introduction

This aim of this chapter is to provide the basic understanding of wave propagation inside a pipeline waveguide. Such knowledge allows the reader to recognize the dispersive nature of the pipeline transmission channel and appreciate the difficulties behind the implementation of an in-pipe acoustic communication system. Chapter 2 emphasized on the increased complexity of wave propagation inside pipelines in comparison to open sea acoustic channels. The interaction of the wave with the pipe wall and surrounding soil results in extensive multipath propagation and reverberation of the transmitted signal. While in long range open sea communication ray theory is usually sufficient to describe the acoustic channel, for the pipeline waveguide it is required to apply modal superposition including an ample number of types and modes of propagation.

To achieve a sufficient level of understanding of the channel physics, this chapter presents examples of simple pulses propagating in a simulated channel. Sensitivity analysis with respect to propagation distance, pipeline diameter, surrounding soil properties, damping, pipe wall thickness, frequency spectrum of wave, position of transmitter and receiver, and so forth, provide useful insight on the effect of the channel on the propagating wave. These results will assist in the efficient design the transmitted signal generated by the digital communication system, utilizing the favorable properties while minimizing at the same time the distorting effect of the transmission channel. The *rigid pipe approximation* and the *flexible pipe embedded in soil* are the two major categories of the provided simulations. In all cases, the pipe is completely filled with water, with an approximated acoustic wave velocity of 1500 m/sec. The mathematical representation of each simulation is presented in advance of the presentation of the case results, but first the main facts regarding in-pipe acoustics are discussed.

3.2 State of the Art for in pipe wave propagation

In-pipe acoustics was initially studied for the interests of musical instruments such as the pipe organ. Early studies of acoustics from both a theoretical as well as application specific point of view include [1]-[9]. In the recent years, motivation for studying pipe acoustics arises from the need to provide practical solutions to a broad range of problems in engineering and geophysics, such as noise and vibration restriction in ventilation shafts, pipeline monitoring, underground exploration with boreholes, and so forth.

Most theoretical analyses of wave propagation decompose the wave into various forms of propagation, called *modes*. There are three major types of wave that propagate inside hollow, fluid-filled, elastic cylinders, namely the *Longitudinal waves* (L), the *Helical or Torsional waves* (T), and the *Flexural waves* (F), see [10] and Figure 3.1.

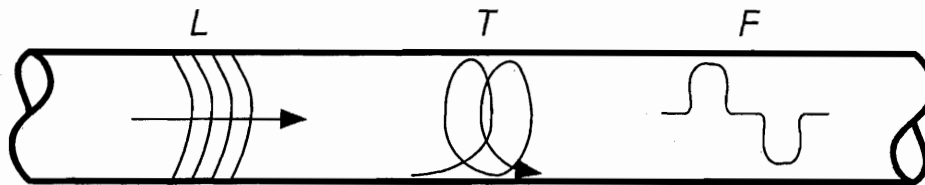


Figure 3.1: Modes of Propagation inside hollow fluid filled elastic cylinders: *Longitudinal waves* (L), *Helical or Torsional waves* (T), and *Flexural waves* (F)

The modes –types– of waves are further decomposed into levels of modes (m) and orders (n), indicating the shape of the wave as well as its frequency content. The fundamental mode corresponds to waves that travel in the axial direction and have wavefronts with uniform phase across the cylinder cross section. Such a mode corresponds to $m = n = 0$. In addition to the fundamental wave, there exist waves that reflect back and forth from the cylinder walls or diverge from the straight propagation direction as they travel along, and for which the pressure distribution is not uniform across the cylinder. All modes except the fundamental mode are found to be dispersive. A medium in which the wave velocity is frequency dependent is called a *dispersive medium*. A pipe with elastic walls is a dispersive medium for longitudinal acoustic waves. Hence, waves of arbitrary shape will not maintain their shape as they travel along the interior of the tube, since different modes, or equally different frequencies, travel with

diverse velocities. In general it can be said that higher modes contain the higher frequencies. To invert this statement, a signal with a higher frequency spectrum excites higher modes of wave propagation. According to this statement, for every mode a frequency can be found below which it does not get excited, the so called *cut-off frequency*. It is implied that higher modes have higher corresponding cut-off frequencies, while, a signal with a finite frequency spectrum excites a finite number of modes. The lower the frequency of the signal, the smaller the number of modes excited, whereas the modes with higher cut-off frequencies generate wave fields that decay exponentially with distance from the source, called *evanescent waves*. It has also been proven, and will be verified in what follows, that even when they get excited, higher modes attenuate faster with respect to propagation distance, allowing only the few first modes to be detected at great distances from the signal source, [11]-[14].

The wave energy radiation to the environment is mainly controlled by the acoustic wave velocities of the surrounding media as well as the material of the cylinder, [15]-[17]. This radiation is accounted for the rapid decay of the signal with distance as well as leads to multipath propagation, since waves propagate not only inside the cylinder waveguide, but also at the cylinder's wall and the surrounding media. Reflections of waves from all the possible transmission paths overlap at any point of interest resulting into a highly distorted received signal.

The presence of obstacles, particles and changes in geometry, such as pipe joints, bends and branches, is another major source of distortion of the propagating signal, [18] – [19]. The wave reflections from obstacles scatter to the environment, consequently diffusing significantly the wave energy and increasing once more multipath propagation. The acoustic impedances of the joints of an oil drill pipe have been investigated to match the impedance of signal transmitters in order to reduce reflections of waves that travel along the pipe wall, used for a data telemetry system in oil wells, [20]-[24].

Apart from the aforementioned applications of musical instruments, pipeline inspection, underground exploration and oil well drill telemetry, in pipe acoustics have been studied for communication systems in water pipelines, [25]-[29], which is the main focus of this research. However, most of these applications involve transmission of waves with medium to low frequency content, consequently exciting only a few modes. A

digital communication system frequently requires the transmission of high frequency signals in order to achieve data rate mandated by the application. These signals are modulated appropriately to encapsulate the digital data, resulting in the creation of complicated waveforms, as it will be presented in Chapter 4. Such signals suffer from significant dispersion in phase, amplitude and frequency when presented to the pipeline waveguide. In order to achieve reliable transmission and efficiently utilize the available bandwidth, comprehensive understanding of the physics of the in-pipe acoustic channel is required. An attempt to acquire this knowledge is presented in the subsequent sections.

3.3 Pipeline Waveguide Simulations

In order to understand the physics of wave propagation inside pipelines, it is necessary to simulate the environment and experiment with its behavior. The dispersive character of the pipeline waveguide is observed with the assistance of single pulses and waveforms of certain frequency spectrum, which are introduced to it. These waves after propagating through the pipe are recorded at certain distances along its length with several receivers arranged at various points across the pipe cross section. These recordings facilitate the study of the distortion of the pulses in amplitude, phase and frequency as well as the effect of multiple arrivals, materials and geometries.

The computer simulations included here are focused in wave propagation on water-filled cast iron pipe. However, the method and the results can be projected to represent other fluid and pipeline material combinations. In what follows four case studies are examined, as illustrated in Figure 3.2. First of all, in order to isolate the effect of the geometry of the pipeline waveguide, the waves are allowed to propagate only inside the pipe by assigning it to be rigid. In this case the pipe material and the properties of the surrounding soil are not important, since the wave gets completely reflected at the pipe wall. The simulations identify the pipeline acting as a lowpass filter on the propagating signal. This fact was implied in the preceding paragraph, during the discussion that the higher modes, which contain the higher frequencies, attenuate faster with distance. The various modes of propagation inside the pipeline are identified in sequence. The effect of multipath propagation inside the pipe is studied and the channel

is characterized as dispersive and fading, introducing overlap, frequently destructive, among the arriving signals. The final simulation using the rigid pipe assumption, examines the signal distortion under the presence of obstacles and joints that act as scatterers.

The investigation of parameters that affect the signal propagation at a pipeline waveguide is completed with the introduction of a flexible pipe embedded in soil. At this stage the wave does not only propagate inside the fluid, but also on the pipe wall and the surrounding soil. Therefore, the signal energy distribution among the water, pipe wall and surrounding soil can be considered as a function of the pipe material and thickness, as well as soil stiffness, or alternatively the soil acoustic wave velocity. The radiation of acoustic waves from the water to the environment results in the introduction of additional signal transmission paths, aggravating the phenomenon of multipath propagation.

For all the aforementioned cases of rigid and flexible pipeline simulations, parametric analyses were implemented with respect to a number of variables, such as the distance between the source and the target, radius of the pipeline, the radial location of the source and the receiver, the frequency content of the signal, and so forth.

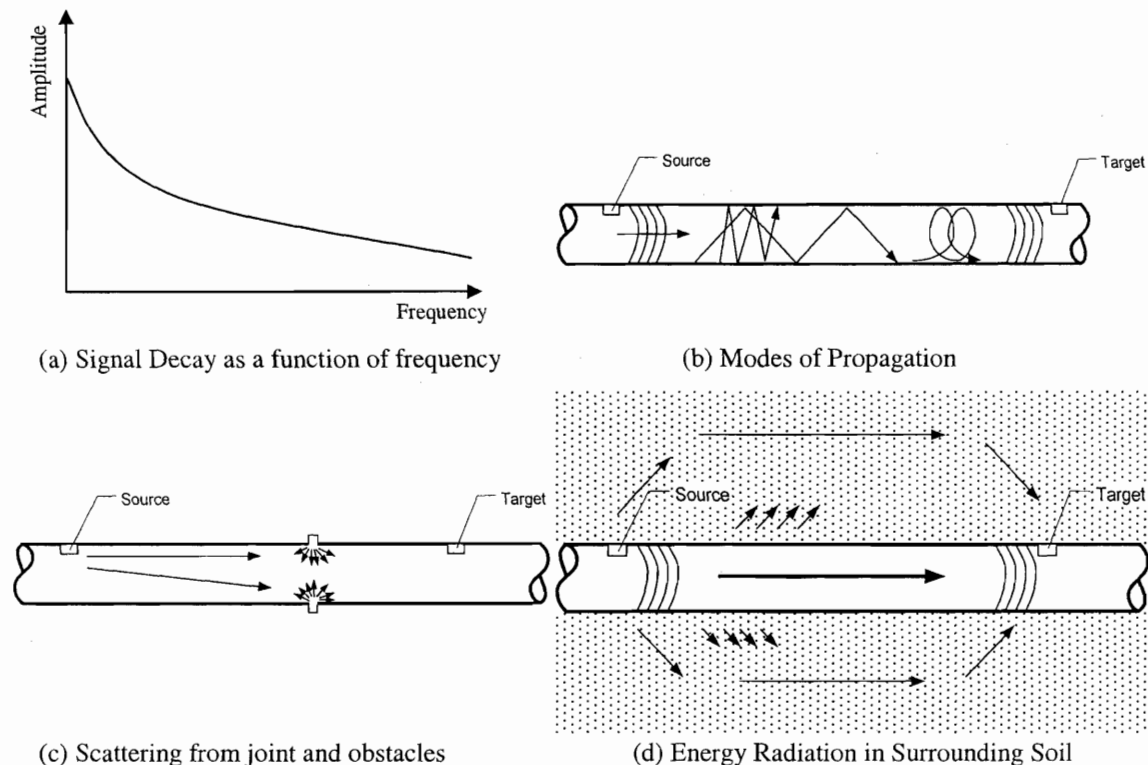


Figure 3.2: Parametric Analyses to identify the effect of the transmission channel to the propagating signal

Each of the subsequent sections provides analysis of the mathematical background on which the simulation codes were based, followed by the corresponding results. The main wave propagation theoretical development and code implementation are due to Kausel, [30].

3.4 *Rigid Pipe Approximation*

According to what is mentioned above, when a signal is presented in a fluid filled cylinder embedded in another medium, the wave follows several paths along the length of the cylinder, through the fluid as well as the cylinder wall and the surrounding media. The combined effect on the signal of all these transmission paths, including the random interactions and overlaps, results in a very complicated waveform received at the point of interest. The first step in order to understand the effect of the in-pipe waveguide on the propagating signal, the transmission channel comprised from the fluid inside the pipe should be isolated. The value of such results is significant, since a majority of the signal energy is actually propagating within the pipe, as will be shown from the flexible pipe simulations towards the end of the chapter. The basic assumption for the implementation of the current solution is to consider the pipe infinitely rigid, or in other words that the pipe wall cannot undergo radial displacements. More specifically, for the case of water pipelines, the commonly used pipe materials are cast iron, steel and concrete. It is understood that the stiffness contrast between the water and the pipe wall is significant, since the bulk modulus of steel and concrete is 160 GPa and 25 GPa respectively, while that of water is only 2.2 GPa. For reference the remaining material properties of interest for the water filled cast iron pipe currently considered are provided here; the density of iron is 7874 kg/m^3 and the acoustic wave velocity is 5100 m/sec, while the corresponding values for water are 1000 kg/m^3 and 1500 m/sec, respectively, which further emphasize their impedance contrast. The pressure caused by acoustic waves is generally much smaller than the static pressure in the water, resulting into small displacements with respect to the dimensions of the pipe. Hence, it can be safely assumed that the propagation of a sound wave through the pipeline waveguide is not going to generate fluid separation from the pipe wall. The interface of the pipe wall and the water will

present compatibility in radial displacements and equilibrium of stresses, two relations that act as boundary conditions in the mathematical formulation of the simulation described below.

According to this analysis, only modes propagating inside and without affecting the shape of the pipe are involved. As such are the longitudinal modes, the phase of which is azimuthally distributed as illustrated in Figure 3.3.

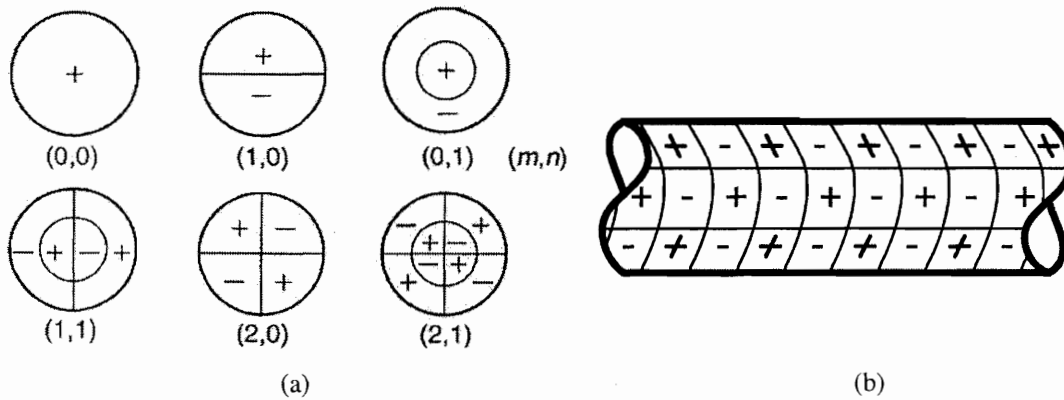


Figure 3.3: Azimuthally distributed modes of propagation
Regions of uniform phase: (a) along the cross section, [31], (b) along the pipe length

Mode m corresponds to changes in phase along the circumference, with mode 0 having uniform phase, mode 1 separating into semicircles, mode 2 separating into quadrants, and so forth. On the other hand, order n corresponds into change of phase along the radius of the pipe, with order 0 indicating no change of phase, order 1 corresponding to one change of phase along the radius, and so on. It becomes apparent that the mode $(0,0)$ corresponds to the fundamental mode, which exhibits uniform phase throughout the whole cross section of the pipe.

3.4.1. Dynamic equations for a fluid

The basic governing equations of motion are presented in this section in order to provide the mathematical basis for further development specialized for the in-pipe waveguide.

A waveform \mathbf{x} which varies with time t is described in space as projections x , y , and z on the three unit vectors \hat{i} , \hat{j} , and \hat{k} as

$$\mathbf{x} = x(t)\hat{i} + y\hat{j} + z\hat{k} \quad (3.1)$$

The velocity and acceleration of the wave are given by

$$\mathbf{v} = \frac{d\mathbf{x}}{dt} = \frac{dx}{dt}\hat{i} + \frac{dy}{dt}\hat{j} + \frac{dz}{dt}\hat{k} = \mathbf{v}(\mathbf{x}, t) \quad (3.2)$$

$$\mathbf{a} = \frac{d\mathbf{v}}{dt} = \frac{\partial \mathbf{v}}{\partial x} \frac{dx}{dt} + \frac{\partial \mathbf{v}}{\partial y} \frac{dy}{dt} + \frac{\partial \mathbf{v}}{\partial z} \frac{dz}{dt} + \frac{\partial \mathbf{v}}{\partial t} = \frac{\partial \mathbf{v}}{\partial t} + \mathbf{v} \cdot \nabla \mathbf{v} = \frac{\partial \mathbf{v}}{\partial t} + \frac{1}{2} \nabla v^2 \quad \text{with } v^2 = \mathbf{v} \cdot \mathbf{v} \quad (3.3)$$

The fundamental laws of physics are given for this fluid for reference:

Conservation of mass:

$$\frac{\partial \rho}{\partial t} = -\nabla \cdot \rho \mathbf{v} \quad (3.4)$$

Newton's 2nd law:

$$\frac{\partial \mathbf{v}}{\partial t} + \frac{1}{2} \nabla v^2 + g \nabla z = -\frac{1}{\rho} \nabla p \quad (3.5)$$

Adiabatic state equation:

$$p = p_0 + \Delta p \left. \frac{\partial p}{\partial p} \right|_{S=\text{const}} + \dots = p_0 + c^2 \Delta p \quad (3.6)$$

where ρ is the density, p is the pressure and g is the acceleration of gravity.

The homogeneous linear equation of motion is

$$\rho \nabla \cdot \frac{\partial}{\partial t} \Delta p - \frac{1}{\rho} \frac{\partial^2 p}{\partial z^2} = 0 \quad (3.7)$$

If ρ is approximately constant, then the wave equation is written as

$$\nabla^2 p = \frac{1}{c^2} \frac{\partial^2 p}{\partial t^2} \quad (3.8)$$

or in terms of potentials

$$\nabla^2 \phi = \frac{1}{c^2} \frac{\partial^2 \phi}{\partial t^2} \quad (3.9)$$

with c the acoustic wave velocity of the fluid. The velocity potential is written as:

$$\dot{\mathbf{u}} = \frac{\partial \mathbf{u}}{\partial t} = \nabla \phi \quad (3.10)$$

or in radial terms, where r is the distance from the origin

$$\dot{u}_r = \frac{\partial u_r}{\partial t} = \frac{\partial \phi}{\partial r} \quad (3.11)$$

The pressure is finally expressed as

$$\frac{\partial p}{\partial t} = -K \nabla^2 \phi \quad (3.12)$$

or otherwise

$$p = -\rho \frac{\partial \phi}{\partial t} \quad (3.13)$$

Under the presence of a source f , the wave equation (3.9) is

$$\nabla^2 \phi - \frac{1}{c^2} \frac{\partial^2 \phi}{\partial t^2} = f(\mathbf{x}, t) \quad (3.14)$$

where $f(\mathbf{x}, t)$ can be considered as volume injection per unit time and volume in [l/s].

3.4.2. Harmonic point source in an unbounded fluid medium

Consider a spherical cavity of radius a in an unbounded fluid medium that is subjected to a pulsating pressure p . Taking into consideration the spherical symmetry of this problem, the equation of motion for the velocity potential reduces to

$$\frac{\partial^2 \phi}{\partial r^2} + \frac{2}{r} \frac{\partial \phi}{\partial r} + k^2 \phi = 0 \quad (3.15)$$

for $r \geq a$ with the wavenumber $k = \omega/c$ for the frequency ω and the distance $r = \sqrt{x^2 + y^2 + z^2}$. Its solution can be written as

$$\phi(r) = A \frac{e^{-ikr}}{r} + B \frac{e^{+ikr}}{r} \quad (3.16)$$

To satisfy radiation conditions at infinity with an exponential term of the form e^{iax} , we must have $B = 0$. Hence from (3.11) the velocity potential is

$$\dot{u}_r = \frac{\partial \phi}{\partial r} = -\frac{A}{r^2} (1 + ikr) e^{-ikr} \quad (3.17)$$

If the normal velocity at the boundary of the cavity is prescribed, then

$$\dot{u}_r|_{r=a} = V(\omega) = -\frac{A}{a^2}(1+ika)e^{-ika} \quad (3.18)$$

so

$$A = -a^2 V(\omega) \frac{e^{ika}}{(1+ika)} \quad (3.19)$$

and

$$\phi(r) = -a^2 V(\omega) \frac{e^{ika}}{(1+ika)} \frac{e^{-ikr}}{r} \quad (3.20)$$

The source strength is defined as the rate of volume injection in $[m^3/s]$

$$S(\omega) = 4\pi a^2 V(\omega) \quad (3.21)$$

Thus equation (3.20) is written as

$$\phi(r) = -S(\omega) \frac{e^{ika}}{(1+ika)} \frac{e^{-ikr}}{4\pi r} \quad (3.22)$$

With the use of the approximation $e^{ika} \approx 1+ika$ for small values of a , in the limit of an infinitesimal cavity equation (3.22) is finally written

$$\phi(r, \omega) = -S(\omega) \frac{e^{-ikr}}{4\pi r} \quad (3.23)$$

This solution satisfies the inhomogeneous Helmholtz equation in an unbounded medium

$$\nabla^2 \phi + k^2 \phi = S(\omega) \delta(\mathbf{x}) \quad (3.24)$$

with \mathbf{x} being the position vector, while $S(\omega)$ is the rate of volume injection. This can be shown by integrating the above equation in a small sphere containing the source:

$$\iiint_{vol} (\nabla^2 \phi + k^2 \phi) dV = \iiint_{vol} S(\omega) \delta(\mathbf{x}) dV \quad (3.25)$$

The right hand side of equation (3.25) is

$$\iiint_{vol} S(\omega) \delta(\mathbf{x}) dV = S(\omega)$$

Integrating the components of the left hand side separately

$$\iiint_{vol} \nabla^2 \phi dV = \oint_{ext.area} (\nabla \phi) \cdot \hat{\mathbf{r}} dA = -S(\omega) \left[\hat{\mathbf{r}} \frac{\partial}{\partial r} \left(\frac{e^{-ikr}}{4\pi r} \right) \right] \cdot \hat{\mathbf{r}} 4\pi r^2 \Big|_{r=a} = S(\omega)(1+ika)e^{-ika}$$

Also

$$\iiint_{vol} k^2 \phi dV = -S(\omega) \int_0^a r e^{-ikr} dr = -S(\omega) (1+ikr) e^{-ikr} \Big|_0^a = S(\omega) [1 - (1+ika) e^{-ika}]$$

Addition of the two expressions above cancels the exponential terms, and we obtain the identity $S(\omega) = S(\omega)$ from equation (3.25).

3.4.3. Centered line source in a rigid cylindrical pipe: wave solution

In this section, a line source centered on the z -axis of an infinitely long cylindrical pipe of radius R and *rigid* walls is considered. The wave equation (3.14) is written

$$\nabla^2 \phi - \frac{1}{c^2} \frac{\partial^2 \phi}{\partial t^2} = \delta(\mathbf{r}) S(z, t) \quad (3.26)$$

The distance vector is expressed as $\mathbf{r} = x\hat{\mathbf{i}} + y\hat{\mathbf{j}}$, the source term $S(z, t)$ is arbitrary, and $\delta(\mathbf{r}) = \delta(r)/2\pi r$ with $r = \sqrt{x^2 + y^2}$. The problem discussed in the preceding paragraph of a cylindrical cavity of small radius a subjected to forced vibrations that vary harmonically in the axial direction with velocity amplitude V is closely related to the cylindrical problem considered here. It obeys the Helmholtz equation in cylindrical coordinates

$$\frac{\partial^2 \phi}{\partial r^2} + \frac{1}{r} \frac{\partial \phi}{\partial r} + (k_0^2 - k_z^2) \phi = 0 \quad (3.27)$$

with $a \leq r \leq R$, $k_0 = \omega/c$, k_z is the axial wavenumber, and $\phi = \phi(r, k_z, \omega)$. The boundary conditions are compatibility of velocities on the source surface and zero velocities on the rigid pipe wall

$$\dot{u}|_{r=a} = \frac{\partial \phi}{\partial r} \Big|_{r=a} = V(\omega) \quad (3.28)$$

$$\dot{u}_r|_{r=R} = \frac{\partial \phi}{\partial r} \Big|_{r=R} = 0 \quad (3.29)$$

Equation (3.27) is a Bessel equation, which has a Bessel function solution of the form

$$\phi = A J_0(kr) + B Y_0(kr) \quad (3.30)$$

with $k = \sqrt{k_0^2 - k_z^2}$. The shape of Bessel functions of the first, J_n , and second, Y_n , kind is presented in Figure 3.4, where n is the order of the solution.

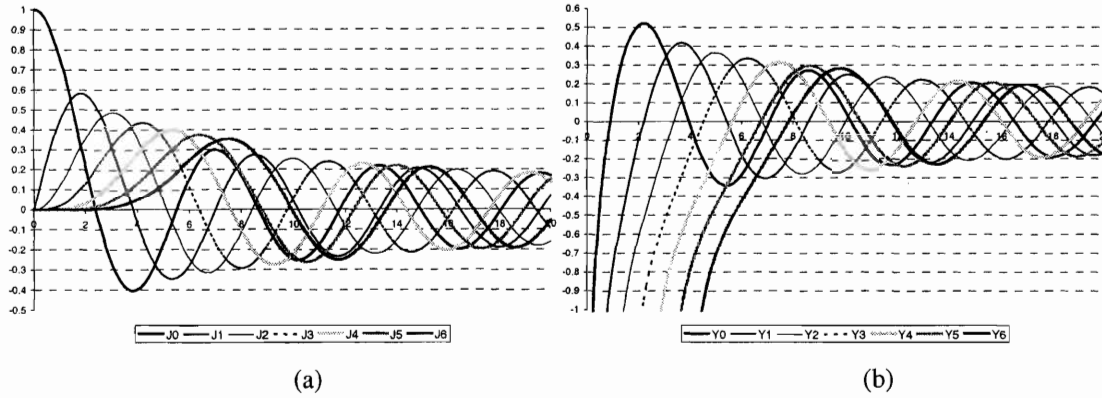


Figure 3.4: Bessel Functions of the (a) first J_n and (b) second Y_n kind, [32]

Imposing the boundary conditions on the Bessel equation, the following matrix form can be obtained

$$-k \begin{Bmatrix} J_1(ka) & Y_1(ka) \\ J_1(kR) & Y_1(kR) \end{Bmatrix} \begin{Bmatrix} A \\ B \end{Bmatrix} = \begin{Bmatrix} V \\ 0 \end{Bmatrix} \quad (3.31)$$

and solving for the two constants A and B :

$$\begin{Bmatrix} A \\ B \end{Bmatrix} = \frac{V/k}{J_1(ka)Y_1(kR) - Y_1(ka)J_1(kR)} \begin{Bmatrix} -Y_1(kR) \\ J_1(kR) \end{Bmatrix} \quad (3.32)$$

Hence, from equations (3.30) and (3.32) the solution of the wave equation takes the form:

$$\phi = \frac{-V [Y_1(kR)J_0(kr) - J_1(kR)Y_0(kr)]}{k [Y_1(kR)J_1(ka) - J_1(kR)Y_1(ka)]}$$

In the limit $a \rightarrow 0$, the Bessel functions in the denominator tend to $J_1(ka) \rightarrow 0$,

$Y_1(ka) \rightarrow -\frac{2}{\pi} / ka$, so

$$\phi \rightarrow -\frac{\pi V a}{2} \left[\frac{Y_1(kR)}{J_1(kR)} J_0(kr) - Y_0(kr) \right] \quad (3.33)$$

By choosing source strength $S(k_z, \omega) = 2\pi a V$ and taking the limit $a = 0$, the solution for a line source becomes:

$$\phi = \frac{-S(k_z, \omega)}{4} \left[\frac{Y_1(kR)}{J_1(kR)} J_0(kr) - Y_0(kr) \right] \quad (3.34)$$

Including the axis, this solution satisfies the inhomogeneous differential equation (3.26)

$$\frac{\partial^2 \phi}{\partial r^2} + \frac{1}{r} \frac{\partial \phi}{\partial r} + k^2 \phi = S(k_z, \omega) \delta(\mathbf{r}) \quad \text{with} \quad \left. \frac{\partial \phi}{\partial r} \right|_{r=R} = 0 \quad \text{as can be demonstrated by integration}$$

$$\iint_{\text{area}} \left(\frac{\partial^2 \phi}{\partial r^2} + \frac{1}{r} \frac{\partial \phi}{\partial r} + k^2 \phi \right) dA = \iint_{\text{area}} S(k_z, \omega) \delta(\mathbf{r}) dA \quad (3.35)$$

The right hand side becomes

$$\iint_{\text{area}} S(k_z, \omega) \delta(\mathbf{r}) dA = S(k_z, \omega) \iint_{\text{area}} \delta(\mathbf{r}) dA = S(k_z, \omega) \quad (3.36)$$

For the left hand side it is convenient to work in plane polar coordinates

$$\frac{\partial^2 \phi}{\partial r^2} + \frac{1}{r} \frac{\partial \phi}{\partial r} = \nabla^2 \phi$$

and by Green's theorem

$$\iint_{\text{area}} \nabla^2 \phi dA = \oint_{\text{perimeter}} (\nabla \phi) \cdot \hat{\mathbf{r}} ds = \oint_{\text{perimeter}} \frac{\partial \phi}{\partial r} ds = \left. \frac{\partial \phi}{\partial r} 2\pi r \right|_{r=R} = 0$$

which is zero because of the boundary condition at $r = R$. Also for the other term of the left hand side of (3.35)

$$\begin{aligned} k^2 \iint_{\text{area}} \phi dA &= 2\pi k^2 \int_0^R \phi r dr \\ &= 2\pi k^2 \frac{-S(k_z, \omega)}{4 J_1(kR)} \int_0^R [Y_1(kR) J_0(kr) - J_1(kR) Y_0(kr)] r dr \end{aligned}$$

But

$$\int_0^R J_0(kr) r dr = \frac{1}{k} r J_1(kr) \Big|_0^R = \frac{R}{k} J_1(kR)$$

and

$$\int_0^R Y_0(kr) r dr = \frac{1}{k} r Y_1(kr) \Big|_0^R = \frac{1}{k} \left[R Y_1(kR) + \frac{2}{\pi k} \right]$$

Hence

$$\pi k^2 \frac{-S(k_z, \omega)}{2} \left[\frac{R Y_1(kR) J_1(kR) - R J_1(kR) Y_1(kR)}{k J_1(kR)} - \frac{2}{\pi k^2} \right] = S(k_z, \omega)$$

From (3.36) and the above expression the equality is proven

$$S(k_z, \omega) = S(k_z, \omega)$$

Therefore, it has been shown that the solution found is the Fourier transform of the original problem of a line load with arbitrary source term $S(z, t)$. Hence, the solution to the original problem is

$$\phi(r, z, t) = -\frac{1}{2\pi} \int_{-\infty}^{+\infty} \frac{1}{2\pi} \int_{-\infty}^{+\infty} \frac{1}{4} S(k_z, \omega) \left[\frac{Y_1(kR)}{J_1(kR)} J_0(kr) - Y_0(kr) \right] e^{i(\omega t - k_z z)} dk_z d\omega \quad (3.37)$$

The solution found corresponds to a pressure distribution

$$p(r, z, t) = \rho \frac{1}{2\pi} \int_{-\infty}^{+\infty} \frac{1}{2\pi} \int_{-\infty}^{+\infty} \frac{1}{4} i\omega S(k_z, \omega) \left[\frac{Y_1(kR)}{J_1(kR)} J_0(kr) - Y_0(kr) \right] e^{i(\omega t - k_z z)} dk_z d\omega \quad (3.38)$$

and a radial velocity

$$\dot{u}_r(r, z, t) = -\frac{1}{2\pi} \int_{-\infty}^{+\infty} \frac{1}{2\pi} \int_{-\infty}^{+\infty} \frac{1}{4} S(k_z, \omega) k \left[\frac{Y_1(kR)}{J_1(kR)} J_1(kr) - Y_1(kr) \right] e^{i(\omega t - k_z z)} dk_z d\omega \quad (3.39)$$

In each of these expressions $k_0 = \omega/c$ and $k = \sqrt{k_0^2 - k_z^2}$, which is multi-valued.

3.4.4. Pipe with rigid walls: Source expansion into modes

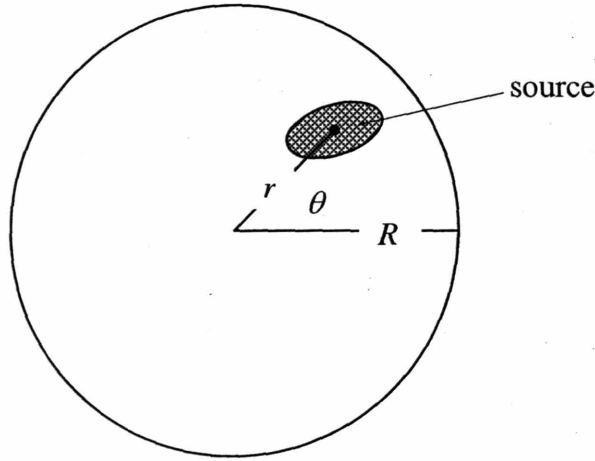


Figure 3.5: Fluid filled cylinder, with source of arbitrary spatial distribution

Let $S(r, \theta, k_z, \omega)$ be the strength of a source with arbitrary spatial distribution in r, θ and harmonic distribution in z, t . This source can be expanded in a Fourier-Bessel series of the form

$$S(r, \theta, k_z, \omega) = \sum_{n=0}^{\infty} \sum_{j=1}^{\infty} S_{nj} = \sum_{n=0}^{\infty} \sum_{j=1}^{\infty} (a_{nj} \cos n\theta + b_{nj} \sin n\theta) J_n(k_{nj}r) \quad (3.40)$$

in which the wavenumbers k_{nj} are the roots of $J'_n(k_{nj}R) = 0$, and the coefficients are to be determined. Thus, each term in the series satisfies the homogeneous Helmholtz equation in cylindrical coordinates with boundary condition $J'_n(k_{nj}R) = 0$. To obtain the coefficients a_{nj} , b_{nj} , it is necessary to multiply by an appropriate factor, integrate over the area of the circle, and use the orthogonality conditions. The coefficients a_{nj} , b_{nj} are found to be

$$a_{nj} = \frac{\int_0^R \int_0^{2\pi} S(r, \theta, \omega) \cos m\theta J_n(k_{nj}r) r dr d\theta}{\frac{\pi}{2} (1 + \delta_{0n}) R^2 J_n^2(k_{nj}R) \left[1 - \left(\frac{n}{k_{nj}R} \right)^2 \right]} \quad \text{for } \begin{matrix} n = 0, 1, 2, \dots \\ j = 1, 2, 3, \dots \end{matrix} \quad (3.41)$$

$$b_{nj} = \frac{\int_0^R \int_0^{2\pi} S(r, \theta, k_z, \omega) \sin m\theta J_n(k_{nj}r) r dr d\theta}{\frac{\pi}{2} R^2 J_n^2(k_{nj}R) \left[1 - \left(\frac{n}{k_{nj}R} \right)^2 \right]} \quad \text{for } \begin{matrix} n = 1, 2, 3, \dots \\ j = 1, 2, 3, \dots \end{matrix} \quad (3.42)$$

For reference the integrals and orthogonality conditions of the first kind Bessel functions are provided here:

$$\int_0^R J_n(\alpha r) J_n(\beta r) r dr = \frac{R [J_n(\alpha R) J'_n(\beta R) - J'_n(\alpha R) J_n(\beta R)]}{\alpha^2 - \beta^2} \quad \alpha \neq \beta \quad (3.43)$$

$$\int_0^R J_n^2(\alpha r) r dr = \frac{R^2}{2} \left\{ \left(\frac{1}{\alpha} \frac{dJ_n(\alpha r)}{dr} \right)^2 \right|_{r=R} + \left[1 - \left(\frac{n}{\alpha R} \right)^2 \right] J_n^2(\alpha R) \right\} \quad (3.44)$$

First orthogonality condition:

$$\int_0^R J_n(k_{ni}r) J_n(k_{nj}r) r dr = \frac{1}{2} R^2 \left[\frac{d}{dx} J_n(x) \right]_{x=k_{nj}R}^2 \delta_{ij} \quad (3.45)$$

Second orthogonality condition:

$$\int_0^R J_n(k'_{ni}r) J_n(k'_{nj}r) r dr = \frac{1}{2} R^2 J_n^2(k'_{ni}R) \left[1 - \left(\frac{n}{k'_{ni}R} \right)^2 \right] \delta_{ij} \quad (3.46)$$

The differential equation for waves in the pipe is then

$$\nabla^2 \phi + k^2 \phi = \sum_{n=0}^{\infty} \sum_{j=1}^{\infty} (a_{nj} \cos n\theta + b_{nj} \sin n\theta) J_n(k_{nj}r) \quad (3.47)$$

in which $k^2 = k_0^2 - k_z^2$ and $k_0 = \omega/c$. To solve this equation, ϕ is expressed in terms of a Fourier-Bessel series analogous to the expansion used for the source, namely

$$\phi(r, \theta, k_z, \omega) = \sum_{n=0}^{\infty} \sum_{j=1}^{\infty} \phi_{nj} = \sum_{n=0}^{\infty} \sum_{j=1}^{\infty} (A_{nj} \cos n\theta + B_{nj} \sin n\theta) J_n(k_{nj}r) \quad (3.48)$$

Substitution into the differential equation yields

$$\sum_{n=0}^{\infty} \sum_{j=1}^{\infty} (\nabla^2 + k^2) (A_{nj} \cos n\theta + B_{nj} \sin n\theta) J_n(k_{nj}r) = \sum_{n=0}^{\infty} \sum_{j=1}^{\infty} (a_{nj} \cos n\theta + b_{nj} \sin n\theta) J_n(k_{nj}r) \quad (3.49)$$

Clearly, if each term of the two series is equal, so are also the sums. Hence,

$$(\nabla^2 + k^2) (A_{nj} \cos n\theta + B_{nj} \sin n\theta) J_n(k_{nj}r) = (a_{nj} \cos n\theta + b_{nj} \sin n\theta) J_n(k_{nj}r) \quad (3.50)$$

This implies

$$\left\{ \left[\left(J_n'' + \frac{1}{r} J_n' + \left(k_{nj}^2 - \left(\frac{n}{r} \right)^2 \right) J_n \right) \right] + (k^2 - k_{nj}^2) J_n \right\} (A_{nj} \cos n\theta + B_{nj} \sin n\theta) = (a_{nj} \cos n\theta + b_{nj} \sin n\theta) J_n \quad (3.51)$$

The term in square brackets is zero, because it is the differential equation for $J_n(k_{nj}r)$.

Considering that $k^2 - k_{nj}^2 = k_0^2 - k_{nj}^2 - k_z^2$, then

$$A_{nj} = \frac{a_{nj}}{k_0^2 - k_{nj}^2 - k_z^2} \text{ and } B_{nj} = \frac{b_{nj}}{k_0^2 - k_{nj}^2 - k_z^2} \quad (3.52)$$

which can be written as

$$A_{nj} = \frac{-a_{nj}}{\left(k_z - \sqrt{k_0^2 - k_{nj}^2} \right) \left(k_z + \sqrt{k_0^2 - k_{nj}^2} \right)} \quad (3.53)$$

and

$$B_{nj} = \frac{-b_{nj}}{\left(k_z - \sqrt{k_0^2 - k_{nj}^2} \right) \left(k_z + \sqrt{k_0^2 - k_{nj}^2} \right)} \quad (3.54)$$

These are the only terms in the solution for ϕ that contain the axial wavenumber k_z .

Hence, for a concentrated load $\delta(z)$, the inverse Fourier transform back into the spatial domain will involve the integral

$$I_j = \frac{1}{2\pi} \int_{-\infty}^{+\infty} \frac{e^{-ik_z z} dk_z}{\left(k_z - \sqrt{k_0^2 - k_{nj}^2}\right)\left(k_z + \sqrt{k_0^2 - k_{nj}^2}\right)} \quad (3.55)$$

which can be evaluated by contour integration. This requires determining the proper location of the poles. Adding a small amount of damping, then k_0 has a small negative imaginary part, and it can be seen that the two square roots $\pm\sqrt{k_0^2 - k_{nj}^2}$ lie in the second and fourth quadrants, respectively. Now, for $z > 0$, the exponential term in the integrand is bounded in the lower half-plane, which contains only one pole, namely $\sqrt{k_0^2 - k_{nj}^2}$. Hence, a contour integration must be carried out in that plane in clockwise direction, which in turn introduces a negative sign. By similar considerations when z is negative, it is obtained

$$I_j = -2\pi i \frac{1}{2\pi} \frac{e^{-i|z|\sqrt{k_0^2 - k_{nj}^2}}}{2\sqrt{k_0^2 - k_{nj}^2}} = -\frac{i e^{-i|z|\sqrt{k_0^2 - k_{nj}^2}}}{2\sqrt{k_0^2 - k_{nj}^2}} \quad (3.56)$$

Finally, the solution in the frequency-space domain is

$$\phi(r, \theta, z, \omega) = \frac{i}{2} \sum_{n=0}^{\infty} \sum_{j=1}^{\infty} \frac{e^{-i|z|\sqrt{k_0^2 - k_{nj}^2}}}{\sqrt{k_0^2 - k_{nj}^2}} (a_{nj} \cos n\theta + b_{nj} \sin n\theta) J_n(k_{nj}r) \quad (3.57)$$

3.4.5. Pipe with rigid walls: Off-center point source

The rigid pipe simulation utilizes a point source which can be located anywhere within the cross section, Figure 3.6, at a distance a from the axis.

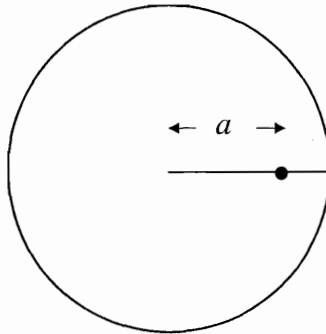


Figure 3.6: Off-center source in pipe with rigid walls

The source term is then taking the form

$$S(r, \theta, z, \omega) = \frac{1}{r} \delta(r-a) \delta(\theta) \delta(z) f(\omega) \quad (3.58)$$

which satisfies

$$\int_0^R \int_0^{2\pi} S(r, \theta, k_z, \omega) r dr d\theta = \delta(z) f(\omega) \quad (3.59)$$

In this case, from equations (3.41) and (3.42) the coefficients a_{nj} , b_{nj} are found

$$a_{nj} = \frac{J_n(k_{nj}a)}{\frac{\pi}{2}(1+\delta_{0n})R^2 J_n^2(k_{nj}R) \left[1 - \left(\frac{n}{k_{nj}R}\right)^2\right]} \quad (3.60)$$

$$b_{nj} = 0 \quad (3.61)$$

and

$$\phi(r, \theta, z, \omega) = \frac{i}{\pi R^2} f(\omega) e^{i\omega t} \sum_{n=0}^{\infty} \sum_{j=1}^{\infty} \frac{e^{-i|z|\sqrt{k_0^2 - k_{nj}^2}}}{\sqrt{k_0^2 - k_{nj}^2}} \frac{\cos n\theta J_n(k_{nj}a) J_n(k_{nj}r)}{(1+\delta_{0n}) J_n^2(k_{nj}R) \left[1 - \left(\frac{n}{k_{nj}R}\right)^2\right]} \quad (3.62)$$

In particular, for a *centered* source $a = 0$, the source term reduces to

$$S(r, \theta, z, \omega) = \frac{1}{r} \delta(r) \delta(\theta) \delta(z) f(\omega) \quad (3.63)$$

which satisfies

$$a_{0j} = \frac{1}{\pi R^2 J_0^2(k_{0j}R)}, \quad a_{n>0,j} = 0 \text{ and } b_{nj} = 0 \quad (3.64)$$

It is interesting to observe that the solution is dependent only on the $n = 0$ order solution for a point source located at the center. Finally, equation (3.62) reduces to:

$$\phi(r, \theta, z, \omega) = \frac{i}{2\pi R^2} f(\omega) e^{i\omega t} \sum_{j=1}^{\infty} \frac{e^{-i|z|\sqrt{k_0^2 - k_{nj}^2}}}{\sqrt{k_0^2 - k_{nj}^2}} \frac{J_0(k_{0j}r)}{J_0^2(k_{0j}R)} \quad (3.65)$$

resulting in a pressure field

$$p(r, \theta, z, \omega) = \frac{\rho}{2\pi R^2} \omega f(\omega) e^{i\omega t} \sum_{j=1}^{\infty} \frac{e^{-i|z|\sqrt{k_0^2 - k_{nj}^2}}}{\sqrt{k_0^2 - k_{nj}^2}} \frac{J_0(k_{0j}r)}{J_0^2(k_{0j}R)} \quad (3.66)$$

Observe that the normal modes of the pipe are given by $k_{nj} = \omega_{nj}/c = z_{nj}/R$, i.e.

$$\omega_{nj} = z_{nj} \frac{c}{R} \rightarrow k_{nj}r = z_{nj} \frac{r}{R}, \quad k_{nj}a = z_{nj} \frac{a}{R} \text{ with } J'_n(z_{nj}) = 0.$$

Equation (3.62) can be used to estimate the pressure field in a pipe with rigid walls for a point source located anywhere within the cross section. It should be noted that in this equation the forcing function $f(\omega)$ is expressed in the frequency domain. The response of the pipeline waveguide to this excitation is consequently calculated in the frequency domain. With the assistance of an inverse Fourier transform, the solution is expressed back in the time domain. Special caution should to be exercised in the selection of the number of points for the Fourier transform, which need to be sufficient to describe all the frequencies of interest. The implementation of the Fast Fourier Transform (FFT) assumes that the input signal is periodic. In case of non periodic signals, the FFT implementation converts the signal into periodic form by adding zeros at the tail and repeating itself in a periodic manner. The number of zeros needs to be adequate to allow enough time for the decay of the system response to reach zero. It is very frequently observed that the system under consideration does not have enough damping for the system response to vanish within a reasonable time. In such cases the FFT suffers from a phenomenon called *leakage* or *wrap around*, in which the remaining response of the system at the end of the one cycle appears at the beginning of the next. To avoid such phenomena, the Exponential Window Method, [33], was used, which essentially adds artificial damping to the system and forces its response to zero. This artificial damping is removed from the final result by inverting the effect of the exponential window in the last step.

3.4.6. Simulations

The controllable parameters of this experiment concern the geometry of the pipeline waveguide as well as the transmitted signal characteristics and the fluid material properties. Parameters related to the waveguide geometry are the radius of the pipe R , the distance between the source and receiver z , the radial location of the source a and the receiver r . The main adjustable characteristic of the transmitted signal in this section is the frequency spectrum, due to its significance on the signal distortion. The two distinct waveforms introduced for the current simulations are the single pulse and the tapered sinusoidal wave which are described in the next paragraph. The only variable material

properties are the ones related to the fluid contained within the pipeline. Since water is the fluid under consideration, the fluid acoustic wave velocity is 1500m/sec, the density 1000kg/m³, and the damping is ζ . Material properties are the least critical parameters for the rigid pipe approximation, since in relative terms similar, but scaled, response can be obtained from different set of parameters. The base case, around which parametric analyses are implemented, has a pipe with radius of $R = 0.5\text{m}$, distance between source and receiver $z = 10\text{m}$, radial location of source and receiver $a = r = R = 0.5\text{m}$, the transmitted signal has a central frequency of $f_o = 1\text{kHz}$, and the material damping is $\zeta = 0.1\%$. The selected radius of $R = 0.5\text{m}$ corresponds to the majority of the water transmission pipelines, which have diameters of 32'' to 42''. Other values used for the pipeline diameter are $R = 0.15\text{m}$ and 1m , representing 12'' distribution pipelines and large trunk mains, which are extra large pipelines used for transportation of water from reservoirs to the transmission stations. In order to ensure the accuracy of the modal decomposition simulation, the first 50 modes are taken into account from up to the $n = 8$ order of solutions, even though only few modes and the first 3 orders provide response of any significant magnitude. Recall that when the source, or the receiver, is located on the axis of the pipeline, only the $n = 0$ order is needed, as indicated from equation (3.64). If the source is located on the axis then the higher orders do not get excited, whereas if the receiver is located on the axis, it does not record any of the higher orders that propagate away from the centerline.

For the purposes of both the rigid and the flexible pipe simulations two waveforms are used which have a *clean*, easily recognizable shape, and a relatively narrow bandwidth with adjustable central frequency. The waveforms are a single squared sinusoidal pulse, and a tapered group of sinusoidal waves, which offers a narrower bandwidth at the expense of a more *complicated* wave than the pulse, Figure 3.7. For reference the frequency spectrum of these waveforms is presented in Figure 3.8 for a central frequency of 1 kHz.

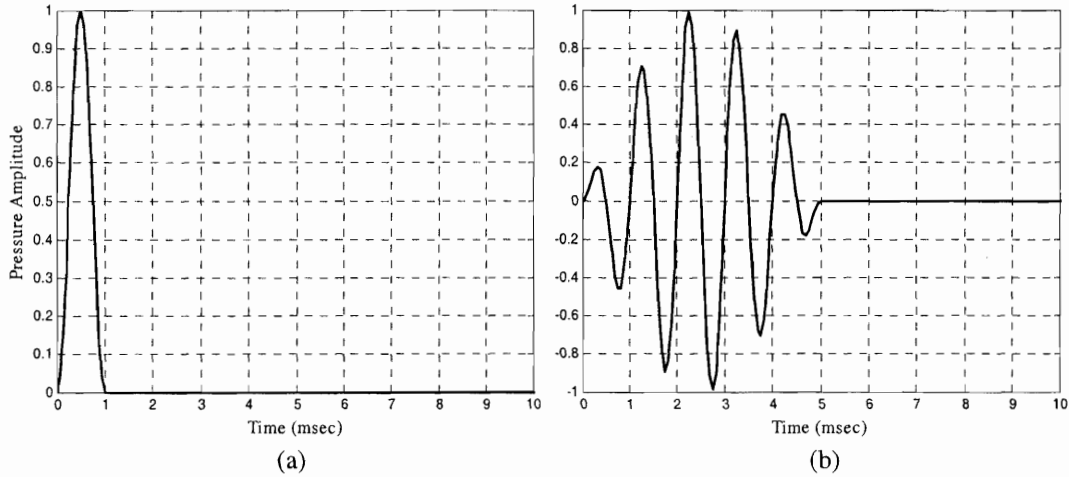


Figure 3.7: Excitation Waveforms
(a) Single squared sinusoidal pulse, (b) Tapered group of sinusoidal waves

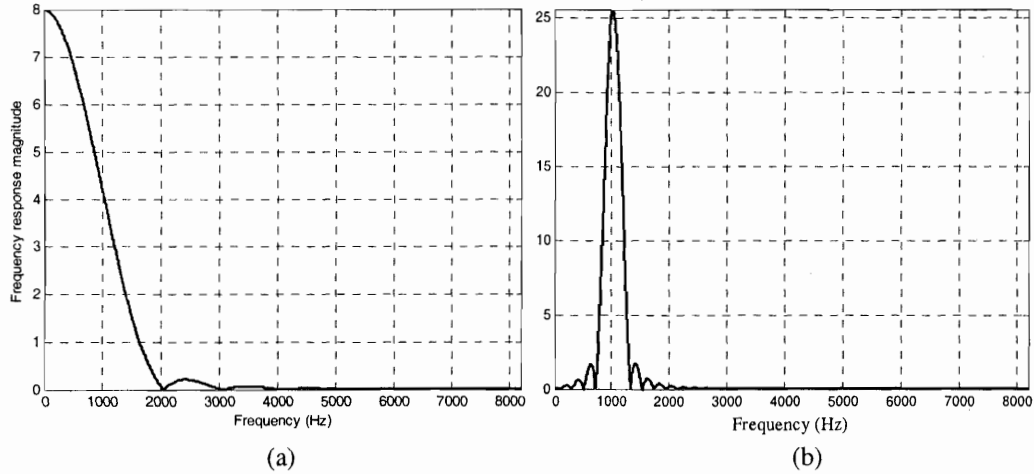


Figure 3.8: Frequency Spectrum
(a) Single squared sinusoidal pulse, (b) Tapered group of sinusoidal waves

- ***Distortion vs. Frequency and Range***

In this section the pipeline waveguide is identified acting as a lowpass filter to the propagating wave. Signal attenuation is not only controlled by the propagation distance, but also by the frequency spectrum of the wave. It is intuitively understandable that the larger the distance the more the attenuation, while the higher the frequency content the more the reverberation. The signal distortion mechanisms, attenuation and reverberation are defined in Chapter 2.

To illustrate that signal attenuation is a function of propagation distance, the pressure time history response of a tapered sinusoidal wave transmitted in a pipeline

recorded at distances $z = 10\text{m}$, 100m and 500m from the source is presented in Figure 3.9. For reference the corresponding frequency spectrum of each recording is also provided. The pipeline has radius $R = 0.5\text{m}$, while the source and receiver are located at the axis of the pipeline for simplicity. The frequency content of the transmitted signal is preserved constant with a central frequency $f_o = 5\text{ kHz}$.

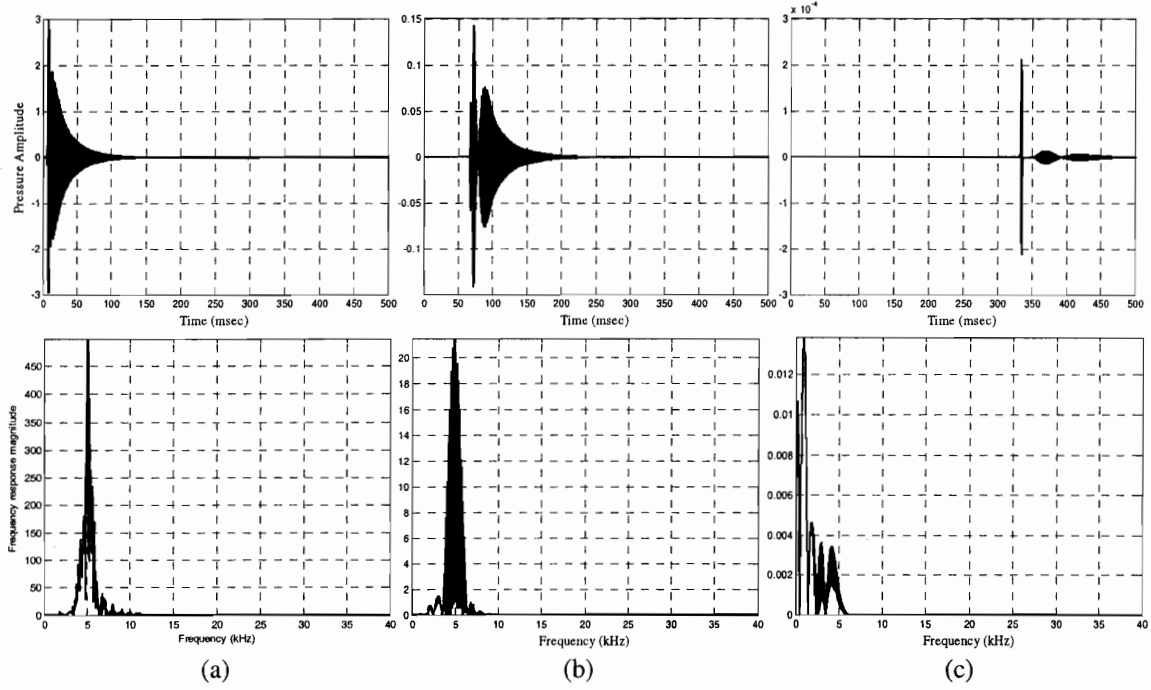


Figure 3.9: Attenuation vs. Distance; Pressure Time History and Frequency Response Spectrum for $R = 0.5\text{m}$, $a = r = 0\text{m}$, $f_o = 5\text{kHz}$, and (a) $z = 10\text{m}$, (b) $z = 100\text{m}$, and (c) $z = 500\text{m}$

The above pressure time histories illustrate the magnitude decay of the propagating wave with distance. It is also observed that following the initial signal arrival a significant tail is present in all recordings. This signal is the result of an overlap of waves propagating from different transmission paths, which have longer propagation distances than the direct one, resulting in delay at the signal arrivals. This is the first indication of the multipath propagation behavior of the in-pipe waveguide, which results in severe reverberations of the transmitted signal. It is very interesting to notice the increase with distance at the separation between the first signal arrival and the subsequent group of the signals. The separation increase indicates that the length of the multiple propagation paths increase disproportionately with respect to the direct path along the length of the pipe. It is important to comment that these reverberations correspond to the

higher modes, which describe those reflected paths. In addition to the increased separation it can be noted that the magnitude of these tails decays faster with distance with respect to the initial arrival. This observation is a first indication that the higher modes attenuate faster with distance.

The conclusion that higher modes attenuate faster with distance, can be also obtained by observing the frequency response of the signals. The second row of plots in Figure 3.9 indicates a shift into lower frequencies with propagation distance. Since the higher modes are the ones corresponding to higher frequencies, it can be safely assumed that these modes decay faster, once more proving the lowpass character of the pipeline waveguide.

To illustrate the dependency of signal attenuation with frequency Figure 3.10 provides plots of the tapered sinusoidal waveform recorded at a distance of $z = 10\text{m}$ in a pipe of $R = 0.5\text{m}$ radius, but with varying central frequency $f_o = 1\text{kHz}$, 5kHz , and 20kHz , respectively.

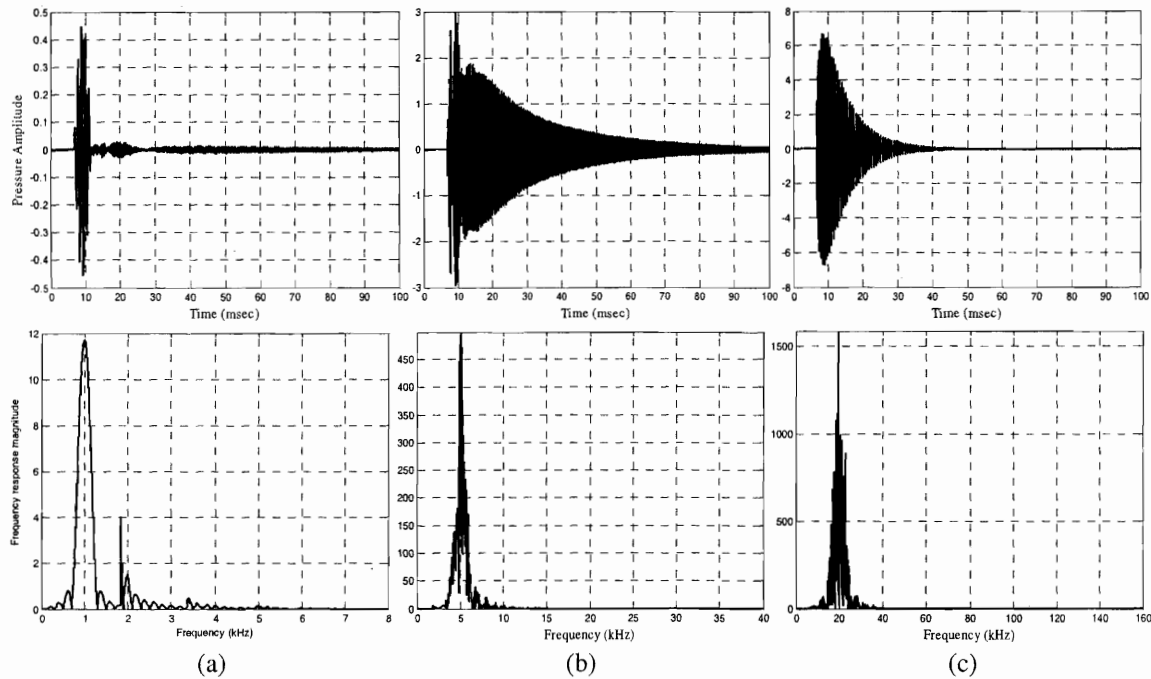


Figure 3.10: Attenuation vs. Frequency; Pressure Time History and Frequency Response Spectrum for $R = 0.5\text{m}$, $a = r = 0\text{m}$, $z = 10\text{m}$, and (a) $f_o = 1\text{kHz}$, (b) $f_o = 5\text{kHz}$, and (c) $f_o = 20\text{kHz}$

The first conclusion that can be obtained from the pressure time history plots of Figure 3.10 is that signals with higher frequency content excite an increasing number of propagation modes. As the frequency content of the transmitted signal gets higher, the magnitude of the tail of the recorded signal grows larger. According to the preceding paragraph the tail corresponds to the signal reverberation in the waveguide, represented in the simulation model from the higher modes of propagation. It can be understood that the more the excited modes, the more the observed reverberation of the wave. It is also important to notice that the relative difference of magnitude of the initial arrival from the tail of the signal diminishes in the high frequency signals, indicating the dominance of the higher modes over the fundamental for these frequencies.

The lowpass behavior of the pipeline waveguide is finally verified by observing the transfer function plot, Figure 3.11. A transfer function is defined as the response of the transmission channel in the frequency domain to the introduction of an impulse. Since the impulse is assumed to have infinite bandwidth, the transfer function indicates the response of the channel at any signal frequency. Multiplication of the frequency spectrum of any signal with the transfer function provides the response of the channel to that particular signal. If the result is transformed back to the time domain the time history response is obtained.

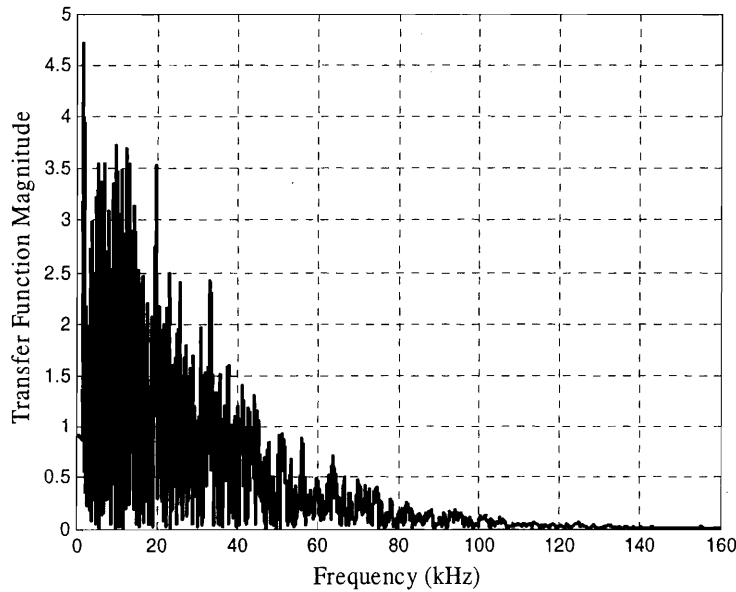


Figure 3.11: Transfer Function for a pipeline with $R = 0.5\text{m}$, at a distance $z = 10\text{m}$, for the $n = 0$ solution containing the first 50 modes

Figure 3.11 illustrates the transfer function of a pipeline with radius $R = 0.5\text{m}$, at a distance $z = 10\text{m}$, for a source and receiver located at the axis of the pipe. The decaying, with increasing frequency, shape of the transfer function indicates the lowpass nature of the pipeline channel. Moreover, the dispersive character of the channel is illustrated by the abrupt variations of the transfer function magnitude for adjacent frequencies, as illustrated nicely in Figure 3.12 which corresponds to the transfer function for a 1m radius, 10m long pipeline. High levels of attenuation and reverberation caused by increased distance and frequency content will be proven detrimental to the fidelity of the received signal as will be discussed in Chapter 6 which examines the performance of the proposed acoustic communication system.

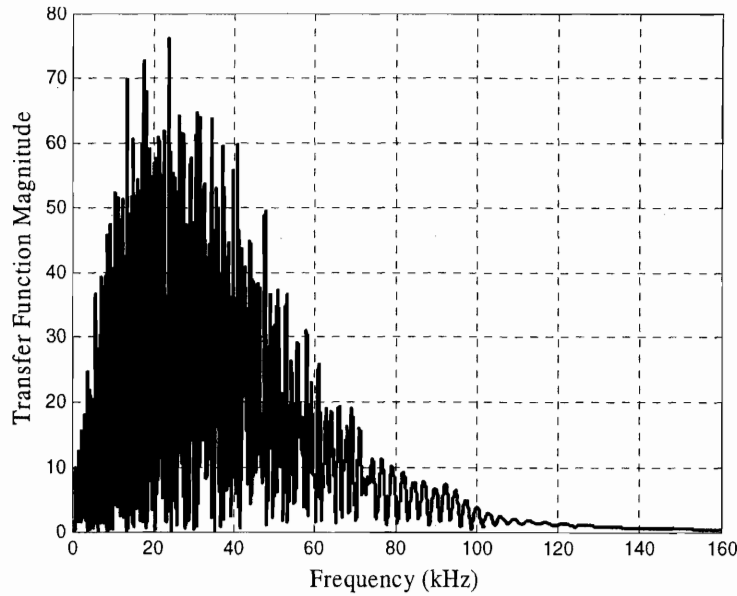


Figure 3.12: Transfer Function for a pipeline with $R = 1\text{m}$, at a distance $z = 10\text{m}$, for the $n = 0$ solution containing the first 50 modes

- ***Modes of propagation***

This section focuses on the effect of the multiple mode overlap on propagating wave emphasizing on the dispersive nature of the acoustic channel. Parametric analyses with respect to the pipeline radius, frequency of the propagating wave and damping of the acoustic waveguide system are implemented, revealing the effect of high modes. As a first step, the *dispersion* relationship for the in-pipe acoustic channel is examined, which corresponds to the association between the wavenumber k and the frequency f , and it is a

property of the type of wave, as well as the acoustic waveguide characteristics. The dispersion relationship indicates, among other things, whether the spatial form of a wave gets distorted by the propagation channel. This distortion is called *dispersion* and concerns time, frequency and phase changes of the transmitted wave. When the relationship between k and f is linear, the propagating waveform is not subjected to dispersion. From what follows, it will be found that the fundamental mode is not dispersive due to the linear correlation of k and f for the waves corresponding to this mode.

The correlation of k and f for the various modes is pictorially represented by the *dispersion curves*. Such curves present the potential non-linear behavior of the corresponding modes as well as the lowest frequency at which each mode can propagate, the *cut-off frequency*. The dispersive curves can also be very useful for the study of interaction between waves in coupled media, such as the fluid-filled pipeline waveguide system. To study the interaction of vibration waves in solids and acoustic waves in fluids the dispersion curves are plotted in a common graph. The intersections of the dispersion curves of two different types of waves indicate points with common wavenumber and frequency, usually denoted as *critical* or *lowest coincidence frequency*, and therefore common wavelength and phase speed. However, in this section the pipeline is considered rigid and the interaction of the fluid and solid is not taken into account.

The dispersion curves for the $n = 0$ order of modes are illustrated in Figure 3.13 for pipelines with radius $R = 0.15\text{m}$, $R = 0.5\text{m}$ and $R = 1\text{m}$, respectively. In each of these plots the horizontal axis corresponds to the frequency f and the vertical axis corresponds to the axial wavenumber k_z . The curves plotted represent the relationship between k_z and f for each mode in increasing order, with the leftmost corresponding to the fundamental mode. The aforementioned statement that the fundamental mode is not dispersive is illustrated here, since the leftmost dispersion curve is a straight line, indicating a linear correlation between k_z and f . The point that each curve meets the horizontal axis corresponds to the lowest frequency that this mode can get excited. Therefore, the modes that will get excited from the transmission of a specific frequency spectrum signal can be easily identified with the assistance of the dispersion curves. It is important to notice the change in density of the dispersion curves with increasing radius of the pipe, which

indicates that a signal propagating inside a large pipe excites more modes than when it propagates in a small pipe. In other words, the cut-off frequencies of the modes become smaller as the radius of the pipeline grows larger.

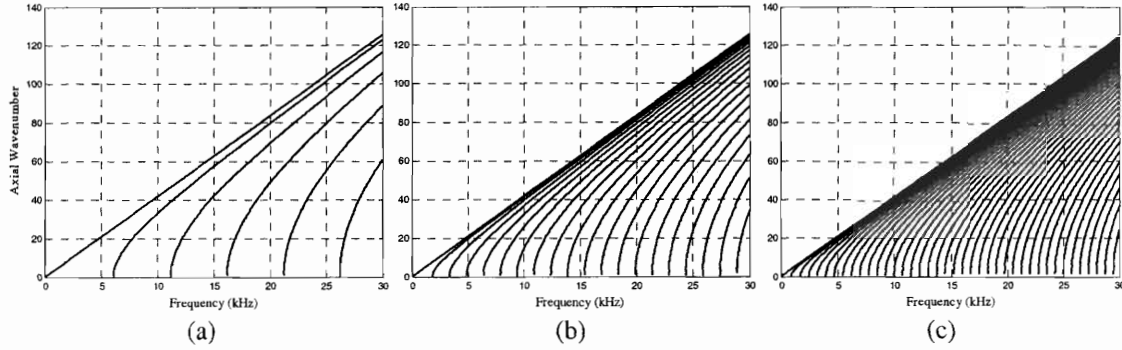


Figure 3.13: Dispersion Curves for $n = 0$ and (a) $R = 0.15\text{m}$, (b) $R = 0.5\text{m}$ and (c) $R = 1\text{m}$

The case $n = 0$ is sufficient only when waves at the axis of the pipeline are considered, i.e. the source and/or the receiver are located at the center of the pipe cross section. When waves at off-center locations are of interest, it is important to account for the $n > 0$ modes. The dispersion curves of these modes are located at the intervals among the dispersion curves discussed above, therefore indicating the increased number of modes excited at off-axis locations. Example of the complete set of dispersion curves for a pipe with radius $R = 0.15\text{m}$ is presented in Figure 3.14.

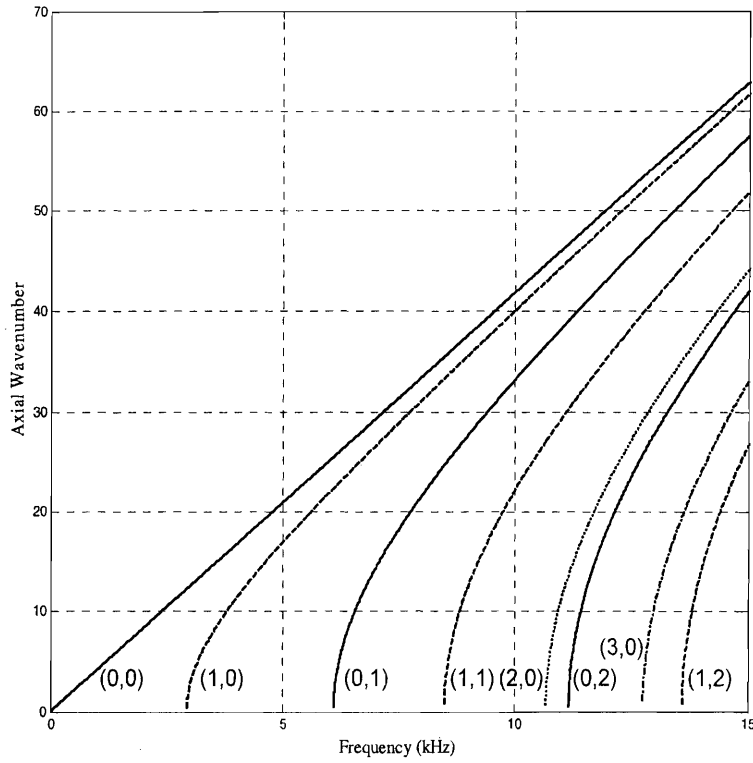


Figure 3.14: Dispersion Curves for $R = 0.15\text{m}$

Following the above discussion for the dispersion curves it is necessary to present the result of the introduction of the additional modes $n > 0$ at the propagating wave. The pressure time histories of a tapered sinusoidal wave with central frequency $f_o = 5\text{kHz}$ for the reference distance of $z = 10\text{m}$ having the both the source and the receiver located at the periphery of the pipe is presented in Figure 3.15. The three consecutive plots correspond to pipelines with radius of $R = 0.15\text{m}$, 0.5m and 1m , respectively. In these plots the effect of the higher order $n > 0$ of solutions is present and can be observed by the high levels of reverberation, apparent from the long tail signals following the initial arrival, as well as the significant signal distortion. As the dispersion curves have indicated, waves that propagate in larger pipes excite more modes, a phenomenon apparent from the highly dispersed received signal at the large pipe plots.

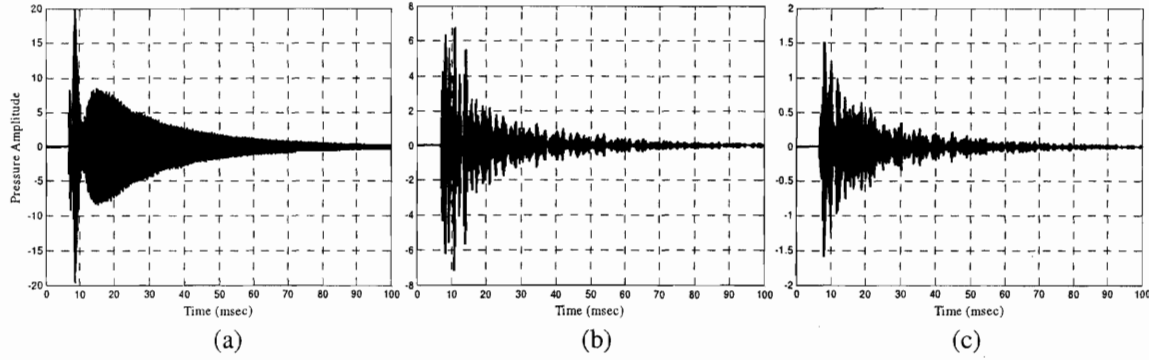


Figure 3.15: Effect of pipeline radius; Pressure Time Histories for $z = 10\text{m}$, $a = r = R$, $f_o = 5\text{kHz}$ and (a) $R = 0.15\text{m}$, (b) $R = 0.5\text{m}$ and (c) $R = 1\text{m}$

A direct comparison of Figure 3.10b with Figure 3.15b reveals the increased reverberation due to the $n > 0$ modes, since the former plot corresponds to the $n = 0$ solution and the latter includes all the significant orders n . The received signal in the second case is highly distorted, with multiple arrivals of significant magnitude, which can be detrimental for the performance of a digital communication system. A close up examination of the plots of Figure 3.15 reveals the extent of signal distortion, as shown in Figure 3.16.

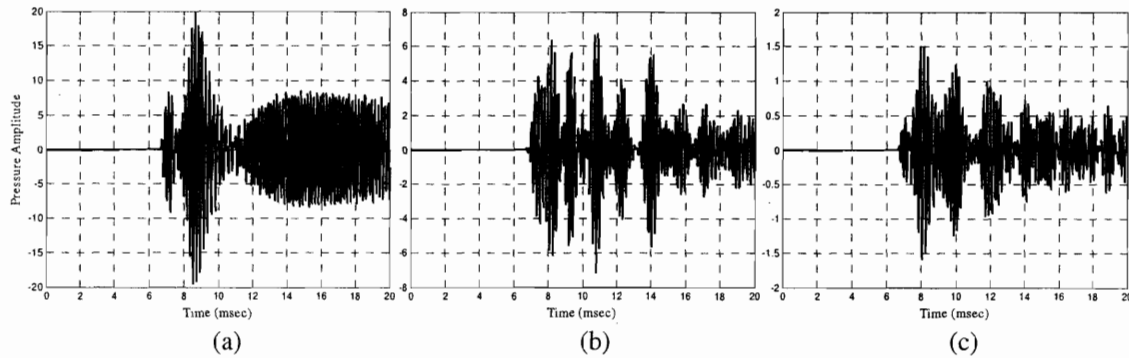


Figure 3.16: Effect of pipeline radius; Pressure Time Histories for $z = 10\text{m}$, $a = r = R$, $f_o = 5\text{kHz}$ and (a) $R = 0.15\text{m}$, (b) $R = 0.5\text{m}$ and (c) $R = 1\text{m}$ [Close up of Figure 3.15]

From the above plots can be identified that the initial arrival, which corresponds to the $n = 0$ solution, does not correspond to the maximum magnitude signal, indicating that higher order solutions are dominant at the off-center positions. Because of the increased number of modes excited at the larger pipes the initial arrival is significantly distorted due to overlaps with signals arriving from other paths. Larger pipes can also

offer longer propagation paths for the higher modes. This fact along with the increased number of modes excited, which carry higher frequencies, is the cause of the augmented separation observed between some of the delayed arrivals at the larger pipes. This phenomenon is certainly more apparent at high frequency signals, which present shorter duration in time for the same waveform, and correspond to higher modes propagating at various multipath trajectories. However, the same behavior is apparent even at lower frequency signals, when the pipe is large enough to allow for larger propagation distances. Such behavior is presented in Figure 3.17, which exhibits the pressure time histories of a pipeline system with the source and receiver at the periphery, at the reference distance of $z = 10\text{m}$, but now for an excitation with central frequency $f_o = 1.5\text{kHz}$.

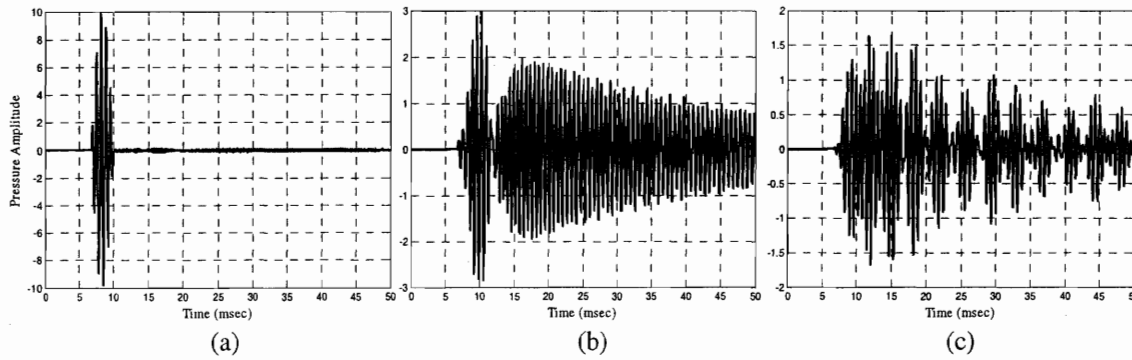


Figure 3.17: Pipe Radius vs. modes of propagation; Pressure Time Histories for $z = 10\text{m}$, $a = r = R$, $f_o = 1.5\text{kHz}$ and (a) $R = 0.15\text{m}$, (b) $R = 0.5\text{m}$ and (c) $R = 1\text{m}$

The first plot corresponds to the case of a pipeline with radius $R = 0.15\text{m}$, and presents no signal distortion as expected from the dispersion curves shown in Figure 3.14, since the frequency spectrum of the signal is below the first cut-off frequency, therefore exciting only the fundamental mode. However, when the same signal is introduced to a larger pipeline, plots (b) and (c), the received wave gets significantly distorted due to the excitation of higher modes. Once again, when the pipeline is large enough, the multiple delayed arrivals present some separation among them, as illustrated in plot (c) by the multiple distinct peaks. It is also interesting to observe from both Figure 3.15 and Figure 3.17 that the magnitude of the received signal gets smaller with

increasing the radius of the pipe, consistent with the notion of wave energy distribution in larger space, or in other words signal spreading.

In general it can be said that the higher the frequency spectrum of the signal the more modes it excites, resulting in increased reverberation. However, since high frequency signals correspond to high modes of propagation, when it is required to transmit high frequencies, it is necessary to preserve some of the higher modes and orders of solutions, specifically the ones carrying the majority of signal's energy. Recall that the $n > 0$ modes present the maximum response at the periphery of the pipeline and vanish towards the center. Since the source and the receiver of the proposed in-pipe digital communication system are located at the internal surface of the pipeline, as will be discussed in Chapter 5, it is important to identify which modes contribute the maximum energy with the least dispersion. In case more than one source or receiver is available at multiple locations, it is feasible to isolate some of the modes of interest. For example, observe from Figure 3.3 that odd orders of solutions n are 180° out of phase at opposing locations, i.e. present inverse phase sign. The idea of *stacking* signals received at opposite locations in order to isolate solutions of interest is discussed in Chapter 5, while results are presented in Chapter 6.

The amount of damping in the pipeline system is certainly an important parameter affecting the wave propagation characteristics of the channel. It is known that increasing damping suppresses the higher frequencies, [9]. Consequently, since high frequencies correspond to high modes of propagation, it can be assumed that increasing damping reduces the effect of higher modes on the propagating signal. On the other hand, increasing damping restricts the propagation distance of waves, since it can significantly reduce their magnitude, thus limiting the performance of the communication system. The level of damping used in the simulations was conservatively selected to be 0.1%. The effect of other damping ratios is illustrated in Figure 3.18, which presents the default case of a 0.5m radius pipeline, having the source and receiver located at the internal perimeter at a distance of 10m. The signal introduced to the pipeline is the tapered sinusoidal wave with central frequency of $f_o = 5\text{kHz}$ and the controlling parameter is the pipeline waveguide damping with values $\xi = 0.5\%$, 1% and 5% , respectively.

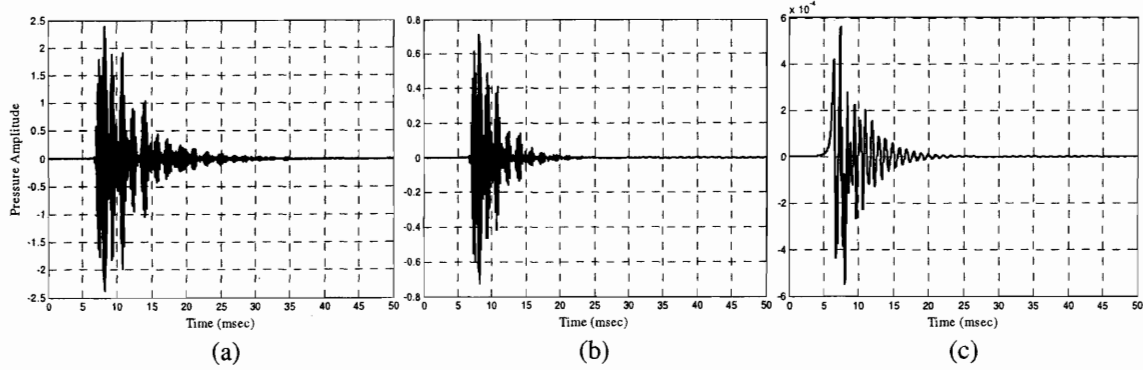


Figure 3.18: Effect of damping; Pressure Time Histories for $z = 10\text{m}$, $R = 0.5\text{m}$, $a = r = R$, $f_o = 5\text{kHz}$, and (a) $\zeta = 0.5\%$, (b) $\zeta = 1\%$ and (c) $\zeta = 5\%$

From the plots presented above it becomes apparent that the magnitude of the received waveform is significantly reduced with increased damping, especially when it is compared with Figure 3.16b. The notable reduction of the tail signal indicates the drastic decay of the higher modes and consequently the decay of the high frequency components. Even though the general shape of the received waveform is not affected, the shift towards the lower frequencies is enhanced as illustrated by the increased time spreading of the sequential pulses. In other words higher damping enhances the lowpass filtering character of the pipeline waveguide. In order to explore the dispersion characteristics of the in-pipe acoustic channel the selected damping ratio of $\zeta = 0.1\%$ is thus considered appropriate, while at the same time it provides some sense of the limiting propagation distance.

• Scattering

Geometry anomalies and features such as joints, bubbles, obstacles, and so forth that intrude the pipe act as scatterers. Any wave that reaches the location of such features is scattered in all directions introducing severe reverberations and significant energy loss of the received signal. In this section the effect of joints that are regularly spaced along the pipeline is examined. The current study of scattering effects is focused on the joints, since they are always present at regular intervals in any pipeline system, while their shape and size can be approximately estimated and hence easily modeled. Other scatterers, such as bubbles and roots, may be present in the pipeline but their geometry varies significantly and their location cannot be estimated.

For the purposes of this research, the joints are considered to be a rectangular indentation along the circumference of the pipe. In the rigid pipe code the joints are modeled as circular distributed sources, which retransmit a scaled version of whatever signal arrives at their location. The scaling factor of signal retransmission from the scatterer is assumed to be proportional to the area of the joint and is calculated as the ratio of the area of the scatterer to the total area of the pipe cross section. In the simulations presented hereafter this percentage is conservatively estimated to be 5%, which corresponds to the ratio of the areas of a pipeline with 0.5m radius and a 1.25cm deep joint. The signal arriving at the receiver is the superposition of the direct transmission according to the rigid pipe approximation and the signal radiated from the scatterer. Therefore three sets of solutions are required for the calculation of the received signal, (a) the direct transmission from the source to the receiver, (b) the transmission from the source to the location of the scatterer, and (c) the propagation of a scaled signal found at step (b) from the scatterer acting as a source to the receiver. The resulting signal is obtained by superposition of the signals calculated in steps (a) and (c).

In this section the cumulative effect of scatterers is studied for the case of the off-center source-receiver system. Scatterers are distributed near the source, near the receiver and at the mid-distance of source and receiver. Due to the Betty-Maxwell reciprocity theorem, scatterers at equal distances from the source and receiver have the same effect on the propagating wave, thus reducing the case studies to just two, the mid-distance and near the source or receiver. For the reference distance of $z = 10\text{m}$, the distance of the scatterer from the source, z_s , for the two case studies is 5m, for the mid-distance case, and 1m or 9m, for the scatterer near the source or receiver case.

In what follows, the pressure time histories for both scatterer cases are presented for transmitted tapered sinusoidal signals with central frequencies $f_o = 1.5, 5, \text{ and } 20 \text{ kHz}$ in Figure 3.19, Figure 3.20, and Figure 3.21, respectively. The left column plots correspond to the scatterer at mid-distance between the source and receiver case, $z_s = 5\text{m}$, while the right column plots correspond to the near source or receiver case, $z_s = 1\text{m}$, or 9m. The top row plots present with a solid line the direct signal transmission, identical to the discussion of the previous section, and the scattered signal arriving at the receiver

with a dotted line. The bottom row of each figure plots the cumulative effect of direct and scattered signals at the location of the receiver.

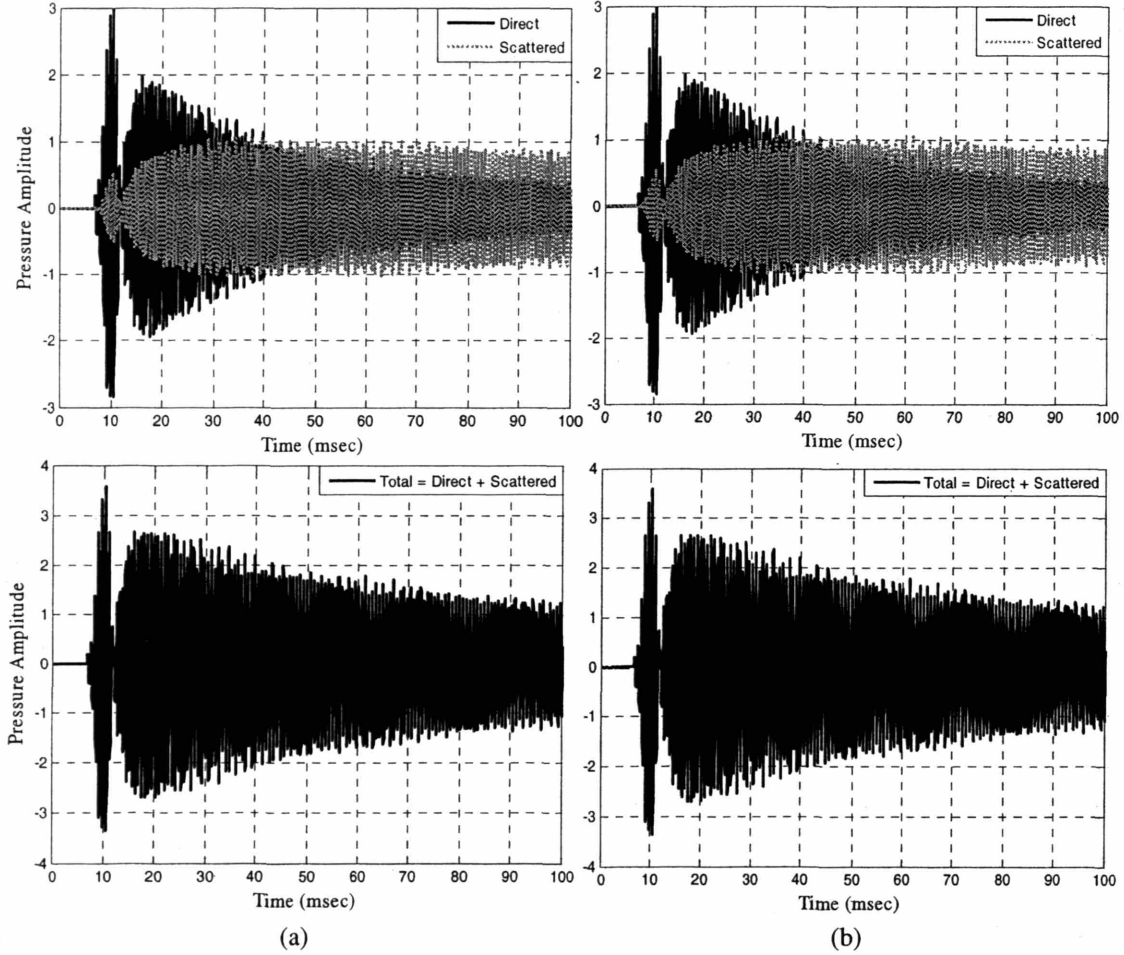


Figure 3.19: Pressure Time History of the direct and scattered signals arriving at the receiver for $f_o = 1.5\text{kHz}$, and $R = 0.5\text{m}$, $z = 10\text{m}$, $a = r = R$, (a) $z_s = 5\text{m}$, and (b) $z_s = 1\text{m}$ or 9m

The first observation from Figure 3.19, which corresponds to a low frequency transmitted waveform, $f_o = 1.5\text{kHz}$, is that the scatterer adds a significant *ringing* effect on the received signal. While the initial arrival is not significantly affected, the tail of the signal is excessively magnified in duration and amplitude. Considering a digital communication system, this additional reverberation may be limiting its data rate performance, since it would restrict the maximum length of the transmitted signal requiring long silent periods between the transmissions of the individual data packets in order to avoid overlap with this prolonged tail.

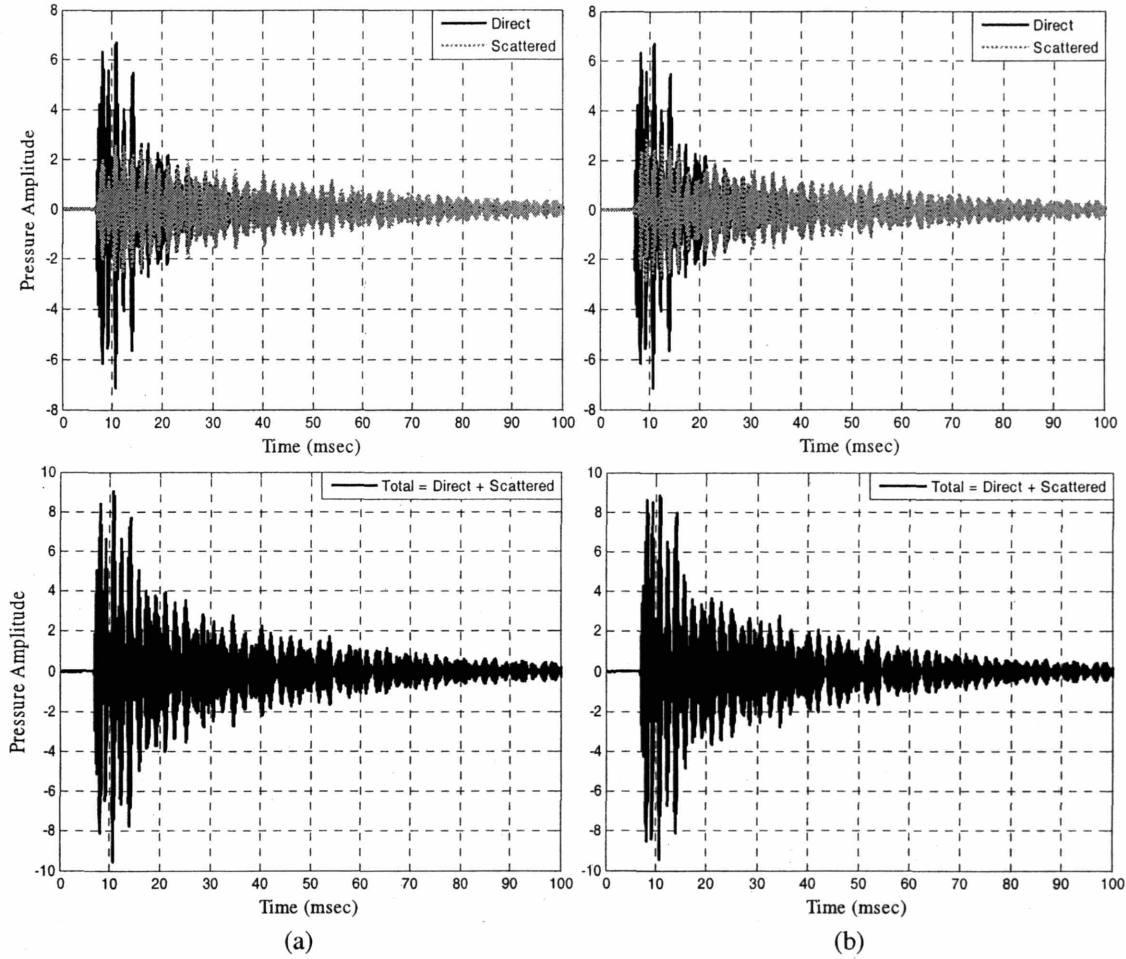


Figure 3.20: Pressure Time History of the direct and scattered signals arriving at the receiver for $f_o = 5\text{kHz}$, and $R = 0.5\text{m}$, $z = 10\text{m}$, $a = r = R$, (a) $z_s = 5\text{m}$, and (b) $z_s = 1\text{m}$ or 9m

Similar conclusions can also be extracted from Figure 3.20, which corresponds to the transmission of a tapered sinusoidal wave with a central frequency f_o of 5kHz . Due to the shorter duration of the pulse, the received signal has several distinctive peaks. This allows identifying that the scattered signal follows the directly received wave with a very small delay. It should be noted that the scatterers are located on the periphery of the pipeline where the higher order solutions $n > 0$ are dominant. These modes correspond to longer than the straight transmission paths, resulting in the observed tail signal which is essentially delayed copies of the original signal. This explains the increased magnitude of the scattered signal at the tail of the received signal, since the received scattered wave is mainly the outcome of the higher modes.

Figure 3.21 presents the received signal when a tapered sinusoidal wave with $f_o = 20\text{kHz}$ is introduced to the pipeline waveguide.

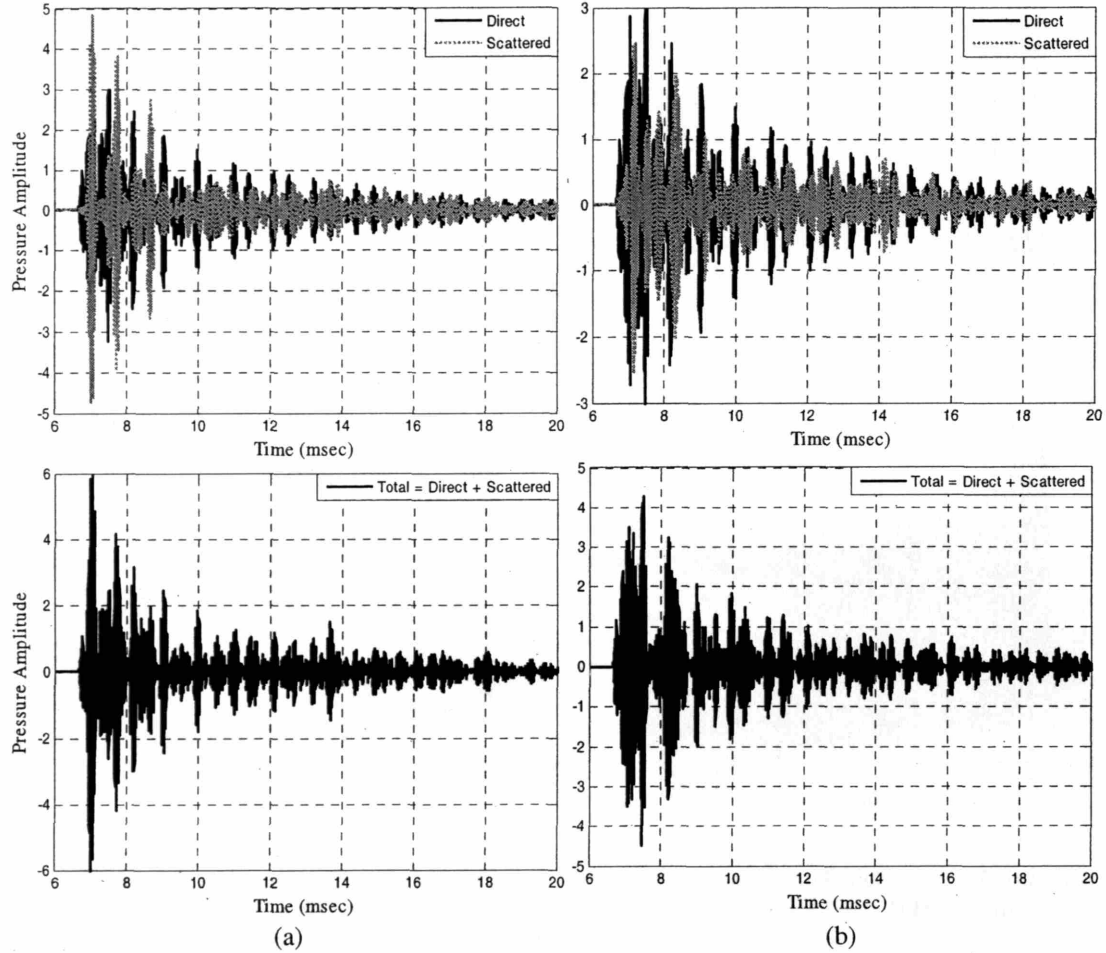


Figure 3.21: Pressure Time History of the direct and scattered signals arriving at the receiver for $f_o = 20\text{kHz}$, and $R = 0.5\text{m}$, $z = 10\text{m}$, $a = r = R$, (a) $z_s = 5\text{m}$, and (b) $z_s = 1\text{m}$ or 9m

In this figure, the response of the scatterer, located at the mid-distance between the source and receiver, presents significantly different behavior from the near the source or receiver case. The magnitude of the scattered signal for $z_s = 5\text{m}$ is larger than both the directly received signal and the scattered signal at the $z_s = 1$ or 9m case. It is important to notice that the relative magnitude of the scattered signals in both cases is much larger than the magnitude of the scattered signals at the previous frequencies. This indicates the increased importance of the higher modes excited due to the higher frequency spectrum of the transmitted signal. Following the above analysis, the effect of the enhanced

reverberation, due to scattering, on the received signal regardless of its position needs to be considered for the design of the proposed digital communication system. The system is required to transmit messages short enough and at adequately spaced intervals to avoid overlap of the main signal with the reverberant part.

3.5 *Flexible pipe embedded in soil*

In this section, an extension of the approximation of the rigid pipe is examined in order to take into account the effect of pipe stiffness and soil properties. The pipeline is no longer considered rigid, while it is embedded completely in soil, consequently allowing wave energy to be radiated to the pipe wall and the surrounding soil. It will be shown that the controlling variable of the energy distribution among the in-pipe fluid, the pipeline and the soil is their impedance contrast. For this reason, parametric analyses with respect to the pipe wall thickness and material, as well as the acoustic wave velocity of the surrounding soil are executed. The leakage of energy to the media surrounding the fluid results in faster decay of the propagating signal with respect to the rigid pipe approximation, a phenomenon frequently referred to as *radiation damping*. Portions of the transmitted signal propagate through the fluid, the pipe wall and the soil resulting in ambiguous signal arrival at the target, due to the multiple propagation paths. The acoustic wave velocity and the distance that the signal covers in each of the materials involved in these analyses is different. This results in early arrivals for short propagation distances and high acoustic wave velocities and delayed arrivals for large propagation distances and slow acoustic wave velocities. The arriving signals overlap, often destructively, resulting in a highly distorted signal of significantly reduced amplitude. The destructive overlap of the arriving signals is called *fading* and the channels presenting this behavior are called *fading channels*.

In addition to the modes propagating inside the pipe, presented in paragraph 3.4, in the flexible pipe solution one more set of modes gets excited, the flexural modes, Figure 3.22. These modes represent the response of the flexible pipe wall to the propagating signal. Figure 3.22 presents the phase on any given cross section of the first 5 mode orders. The $n = 0$ case obviously represents the fundamental mode, in which the

whole cross section has uniform phase. The rest of the modes have n number of pairs of opposing phase. Once again it becomes apparent that higher modes present higher frequencies. It will be shown that the first three modes ($n = 0, 1, 2$) are the most important ones corresponding the pipe breathing, beam bending, and pipe ovalling shapes, respectively, [34]. The $n = 0$ “breathing” mode radiates as a line monopole, the $n = 1$ “bending” mode radiates as a line dipole, the $n = 2$ “ovalling” mode radiates as a line quadrupole, and so on. The efficiency of radiation at any frequency is decreasing with the increase in the order of the equivalent source.

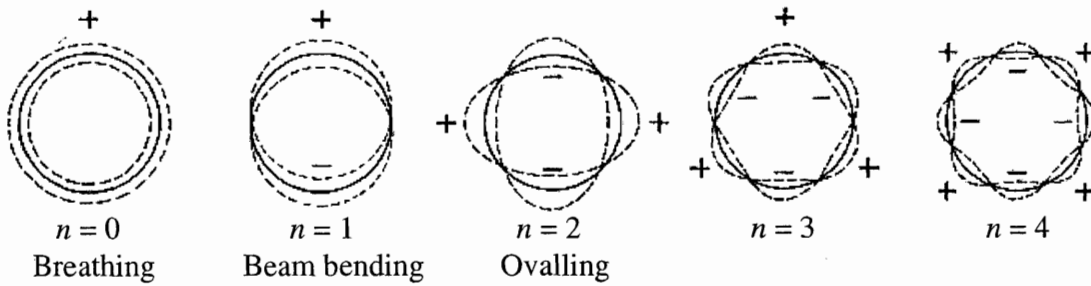


Figure 3.22: Flexural modes, [34]

The results from the aforementioned analyses, in addition to the results presented from the rigid pipe approximation, complete the understanding of the pipeline waveguide behavior required to design an efficient digital communication system. In the subsequent sections a brief description of the algorithm used to simulate the flexible pipe is presented followed by the results of the parametric analyses.

3.5.1. Off-center source in a layered flexible pipe

A two stage approach is implemented to solve the problem of wave propagation in a flexible pipe embedded in soil, as illustrated in Figure 3.23. First, a radially *inward* pressure p^* is applied to the fluid at the pipe wall interface, which matches exactly the pressure of the rigid pipe case of paragraph 3.4. The overlap of the source excitation and p^* results in a perfectly firm pipe with stationary walls. In effect, this is the same as if a radial constraint had been applied to the wall, and measured the support reaction, which equals the pressure at the wall.

Second, a radially *outward* traction p^* is applied at the pipe wall as the only source. This whole system will respond as appropriate, and by superposition with stage one, the inward and outward pressures cancel out, thus providing the final solution to the flexible pipe problem. Consequently, p^* is the effective source which must be estimated. Observe that for the interior points, the two *displacement* solutions must be overlapped, but this is not necessary for points on or beyond the wall.

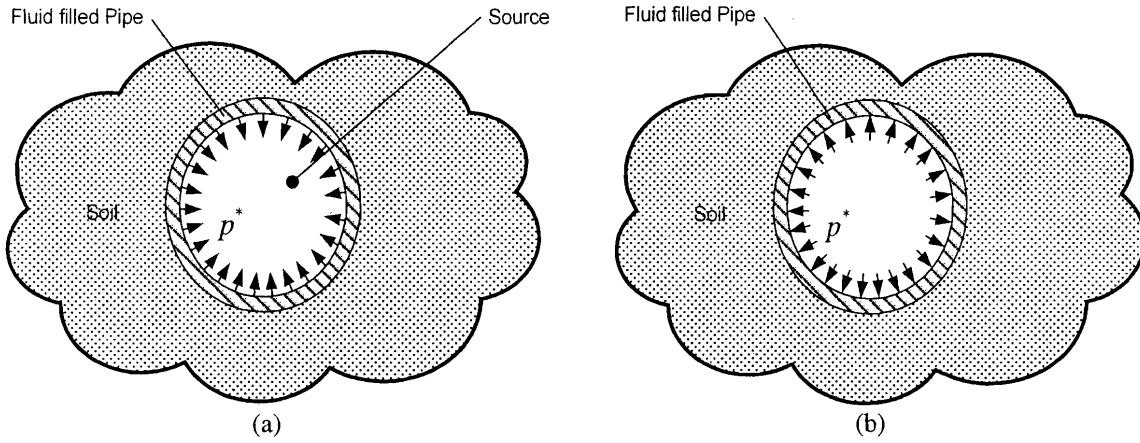


Figure 3.23: Two stage solution for flexible pipe embedded in soil
(a) Source and inward pressure p^* , (b) Outward traction p^*

3.5.2. Estimation of p^*

From equations (3.13) and (3.62), the expression in the frequency-wavenumber domain of the pressure at the pipe wall is:

$$p^* = -i\omega\rho\phi(R, \theta, \omega, k_z) = -i\omega\rho \sum_{n=0}^{\infty} \phi_n(R, \omega, k_z) \cos n\theta = \sum_{n=0}^{\infty} p_n^* \cos n\theta \quad (3.67)$$

in which

$$\phi_n = \sum_{j=1}^{\infty} \phi_{nj} = \sum_{j=1}^{\infty} A_{nj} J_n(k_{nj}R) \quad (3.68)$$

$$A_{nj} = \frac{R^2 a_{nj}}{\kappa_0^2 - \kappa_{nj}^2 - \kappa_z^2} \quad (3.69)$$

$$\kappa_0 = k_0 R, \quad \kappa_{nj} = k_{nj} R, \quad \kappa_z = k_z R \quad (3.70)$$

$$a_{nj} = \frac{2}{\pi(1+\delta_{0n})R^2} \frac{J_n(\kappa_{nj}\alpha)}{J_n^2(\kappa_{nj}) \left[1 - \left(\frac{n}{\kappa_{nj}} \right)^2 \right]}, \text{ with } \alpha = \frac{a}{R} \leq 1 \quad (3.71)$$

Hence,

$$p^* = -i\omega \rho \frac{2}{\pi} f(\omega) \sum_{n=0}^{\infty} \frac{\cos n\theta}{1+\delta_{0n}} \sum_{j=1}^{\infty} \frac{1}{\kappa_0^2 - \kappa_{nj}^2 - \kappa_z^2} \frac{J_n(\kappa_{nj}\alpha)}{J_n(\kappa_{nj}) \left[1 - \left(\frac{n}{\kappa_{nj}} \right)^2 \right]} \quad (3.72)$$

Finally, the fictitious source term is

$$p_n^* = i\omega f(\omega) \frac{\rho \frac{2}{\pi}}{1 - \frac{1}{2}\delta_{0n}} \sum_{j=1}^{\infty} \frac{1}{\kappa_{nj}^2 - \kappa_0^2 + \kappa_z^2} \frac{J_n(\kappa_{nj}\alpha)}{J_n(\kappa_{nj}) \left[1 - \left(\frac{n}{\kappa_{nj}} \right)^2 \right]} \quad (3.73)$$

3.5.3. Fluid cylinder subjected to external pressure

It remains to evaluate the motions and pressures elicited in the fluid during the second stage. Since there are in this case no sources in the fluid other than at the pipe wall, the solution for interior points is obtained from the motions at the pipe wall via analytic continuation.

Consider next a fluid cylinder of finite radius R subjected to a prescribed outward traction p^* . The Helmholtz equation in this case is

$$\nabla^2 \phi + k_0^2 \phi = 0 \quad (3.74)$$

or in full

$$\frac{\partial^2 \phi}{\partial r^2} + \frac{1}{r} \frac{\partial \phi}{\partial r} + \left(k^2 - \frac{n^2}{r^2} \right) \phi = 0, \text{ with } k = \sqrt{k_0^2 - k_z^2} \quad (3.75)$$

The n^2/r^2 term comes from the second derivative in θ . Its solution is

$$\phi = B_n J_n(kr) e^{i(\alpha x - k_z z)} \quad (3.76)$$

so from (3.11), the velocity is

$$\dot{u}_r = k B_n J'_n(kr) \quad (3.77)$$

and the corresponding pressure

$$p_r = -i\omega\rho B_n J_n(kr) \quad (3.78)$$

At the boundary $r=R$, it is obtained

$$\frac{-p_R}{\dot{u}_R} = \frac{i\omega\rho}{k} \frac{J_n(kR)}{J'_n(kR)} = K_{ni} \quad (3.79)$$

which is the impedance of the fluid cylinder as seen from the external surface. The negative sign is used for consistency of the direction of pressure calculated in this stage with radial velocity.

For $r = R$, equation (3.77) can be written as

$$k B_n = \frac{\dot{u}(k, R)}{J'_n(kR)}$$

in which $\dot{u}(k, R)$ is the radial fluid velocity at the pipe wall for the pipe in layered medium provided by the program for the fictitious source p^* , given by (3.73). Substituting kB_n in equation (3.77), it follows that

$$\dot{u}(k, r) = \dot{u}(k, R) \frac{J'_n(kr)}{J'_n(kR)} \quad (3.80)$$

and from (3.78) the pressure of the second stage is

$$p_n(k, r) = -i\omega\rho \dot{u}(k, R) \frac{J_n(kr)}{k J'_n(kR)} \quad (3.81)$$

To obtain total pressure, it suffices to overlap the pressure of the rigid pipe case with those given by the above formula.

3.5.4. Fluid cylinder via stiffness matrix method

This section elaborates on flexible pipe solution subjected to a point source, and use for this purpose the stiffness (impedance) matrix formulation, which is convenient to implement in a computational environment.

Stiffness matrix

Consider a hollow fluid cylinder bounded by inner and outer surfaces with radii r_1, r_2 , which is subjected to external, harmonic pressures p_1, p_2 with implied azimuthal

variation of order n . From previous sections it was found that the solution for the fluid potential can be written as

$$\phi_n(k, r) = AY_n(kr) + BJ_n(kr) \quad (3.82)$$

in which $k = \sqrt{k_0^2 - k_z^2}$, $k_0 = \omega/c$. For notational convenience, this equation is abbreviated simply as

$$\phi_n = AY_n + BJ_n \quad (3.83)$$

The pressure and radial velocity at the radial distance r are then

$$p = -i\omega\rho(AY_n + BJ_n) \quad (3.84)$$

and

$$\dot{u} = k(AY'_n + BJ'_n) \quad (3.85)$$

with $J'_n = dJ_n/d(kr)$ and $Y'_n = dY_n/d(kr)$. For simplicity, the following notation is used

$$J_{n1} = J_n(kr_1), \quad J_{n2} = J_n(kr_2), \quad Y_{n1} = Y_n(kr_1), \quad Y_{n2} = Y_n(kr_2) \quad (3.86)$$

The external tractions per radian are then

$$q_1 = r_1 p_1 = -i\omega\rho \begin{Bmatrix} Y_{n1} & J_{n1} \end{Bmatrix} \begin{Bmatrix} A \\ B \end{Bmatrix} \quad (3.87)$$

$$q_2 = -r_2 p_2 = i\omega\rho \begin{Bmatrix} Y_{n2} & J_{n2} \end{Bmatrix} \begin{Bmatrix} A \\ B \end{Bmatrix} \quad (3.88)$$

Hence, in a matrix form the tractions can be expressed as

$$\begin{Bmatrix} q_1 \\ q_2 \end{Bmatrix} = -i\omega\rho \begin{Bmatrix} r_1 Y_{n1} & r_1 J_{n1} \\ -r_2 Y_{n2} & -r_2 J_{n2} \end{Bmatrix} \begin{Bmatrix} A \\ B \end{Bmatrix} \quad (3.89)$$

Similarly, following equation (3.85) the velocities are

$$\begin{Bmatrix} \dot{u}_1 \\ \dot{u}_2 \end{Bmatrix} = k \begin{Bmatrix} Y'_{n1} & J'_{n1} \\ Y'_{n2} & J'_{n2} \end{Bmatrix} \begin{Bmatrix} A \\ B \end{Bmatrix} \quad (3.90)$$

Inverting equation (3.90) the constants A, B are estimated

$$\begin{Bmatrix} A \\ B \end{Bmatrix} = \frac{1}{k} \begin{Bmatrix} Y'_{n1} & J'_{n1} \\ Y'_{n2} & J'_{n2} \end{Bmatrix}^{-1} \begin{Bmatrix} \dot{u}_1 \\ \dot{u}_2 \end{Bmatrix} = \frac{1}{k(Y'_{n1} J'_{n2} - J'_{n1} Y'_{n2})} \begin{Bmatrix} J'_{n2} & -J'_{n1} \\ -Y'_{n2} & Y'_{n1} \end{Bmatrix} \begin{Bmatrix} \dot{u}_1 \\ \dot{u}_2 \end{Bmatrix} \quad (3.91)$$

Substituting the above to (3.89) gives

$$\begin{Bmatrix} q_1 \\ q_2 \end{Bmatrix} = \frac{-i\omega\rho}{k(Y'_{n1} J'_{n2} - J'_{n1} Y'_{n2})} \begin{Bmatrix} r_1 Y_{n1} & r_1 J_{n1} \\ -r_2 Y_{n2} & -r_2 J_{n2} \end{Bmatrix} \begin{Bmatrix} J'_{n2} & -J'_{n1} \\ -Y'_{n2} & Y'_{n1} \end{Bmatrix} \begin{Bmatrix} \dot{u}_1 \\ \dot{u}_2 \end{Bmatrix} \quad (3.92)$$

or more compactly

$$\mathbf{q} = \mathbf{K}\dot{\mathbf{u}} \quad (3.93)$$

in which \mathbf{K} is the stiffness matrix of the fluid layer. Its elements are

$$K_{11} = \frac{-i\omega\rho r_1 (Y_{n1} J'_{n2} - J_{n1} Y'_{n2})}{k (Y'_{n1} J'_{n2} - J'_{n1} Y'_{n2})} \quad (3.94)$$

$$K_{21} = \frac{i\omega\rho r_2 (Y_{n2} J'_{n2} - J_{n2} Y'_{n2})}{k (Y'_{n1} J'_{n2} - J'_{n1} Y'_{n2})} \quad (3.95)$$

$$K_{12} = \frac{i\omega\rho r_1 (Y_{n1} J'_{n1} - J_{n1} Y'_{n1})}{k (Y'_{n1} J'_{n2} - J'_{n1} Y'_{n2})} \quad (3.96)$$

$$K_{22} = \frac{-i\omega\rho r_2 (Y_{n2} J'_{n1} - J_{n2} Y'_{n1})}{k (Y'_{n1} J'_{n2} - J'_{n1} Y'_{n2})} \quad (3.97)$$

The stiffness matrix is symmetric, as indicated by expanding the derivatives in terms of the recursive equations and from the Wronskian property of Bessel functions, [35]. It follows that

$$\begin{aligned} r_2 (Y_{n2} J'_{n2} - J_{n2} Y'_{n2}) &= r_2 Y_{n2} \left(\frac{n}{k r_2} J_{n2} - J_{n+1,2} \right) - r_2 J_{n2} \left(\frac{n}{k r_2} Y_{n2} - Y_{n+1,2} \right) \\ &= -r_2 (J_{n+1,2} Y_{n2} - J_{n2} Y_{n+1,2}) = -r_2 \frac{2}{\pi k r_2} = -\frac{2}{\pi k} \end{aligned} \quad (3.98)$$

and by a similar expansion of the numerator in K_{12} , it is finally obtained

$$K_{12} = K_{21} = \frac{-2i\omega\rho}{\pi k^2 (Y'_{n1} J'_{n2} - J'_{n1} Y'_{n2})} \quad (3.99)$$

Static condensation

For a source placed on the inner surface, and especially in the limit of a vanishingly small cavity $r_1 \rightarrow 0$, it will be found necessary to condense out the inner degree of freedom so as to avoid both a singularity and an ambiguity in the formulation. The result is

$$K \dot{\mathbf{u}}_2 = (K_{22} - K_{21} K_{11}^{-1} K_{12}) \dot{\mathbf{u}}_2 = \mathbf{q}_2 - K_{21} K_{11}^{-1} \mathbf{q}_1 = \mathbf{q}_{eq} \quad (3.100)$$

and from the expressions in the previous section,

$$K_{21} K_{11}^{-1} = \frac{2}{\pi k r_1 (Y_{n1} J'_{n2} - J_{n1} Y'_{n2})} \quad (3.101)$$

$$K = \frac{-i\omega\rho}{k(Y'_{n1}J'_{n2} - J'_{n1}Y'_{n2})} \left[r_2(Y_{n2}J'_{n1} - J_{n2}Y'_{n1}) - \frac{4}{\pi^2 k^2 r_1(Y_{n1}J'_{n2} - J_{n1}Y'_{n2})} \right] \quad (3.102)$$

In particular, when $r_1 \rightarrow 0$, then $Y_{n1} \rightarrow \infty$, $Y'_{n1} \rightarrow \infty$, $r_1 Y_{n1} Y'_{n1} \rightarrow \infty$ and

$$K_{21} K_{11}^{-1} \rightarrow \frac{2}{\pi k J'_{n2}} \frac{1}{r_1 Y_{n1}} \quad (3.103)$$

$$K \rightarrow \frac{i\omega\rho r_2 J_{n2}}{k J'_{n2}} \quad (3.104)$$

Point source at axis

A source of the form is considered

$$\begin{aligned} q_1 &= \lim_{r_1 \rightarrow 0} r_1 p_1^* = \lim_{r_1 \rightarrow 0} r_1 \left[\frac{\rho\omega}{4} (2 - \delta_{0n}) H_n^{(2)}(kr_1) J_n(ka) \right] \\ &\rightarrow -i \frac{\rho\omega}{4} (2 - \delta_{0n}) J_n(ka) r_1 Y_{n1} \end{aligned} \quad (3.105)$$

which corresponds to a point source at $r = a$ expressed in terms of point sources on the axis via Graf's theorem, presented in paragraph 3.5.5. Hence,

$$\lim_{r_1 \rightarrow 0} K_{21} K_{11}^{-1} q_1 = -i \frac{\rho\omega}{\pi k} \frac{J_n(ka)}{J'_{n2}} \left(1 - \frac{1}{2} \delta_{0n}\right) \quad (3.106)$$

so the equivalent load (radial traction per radian) to be applied at the exterior surface is

$$q_{eq} = q_2 + i \frac{\rho\omega}{\pi k} \frac{J_n(ka)}{J'_{n2}} \left(1 - \frac{1}{2} \delta_{0n}\right) \quad (3.107)$$

Observe that if $q_{eq} = 0$, then $\dot{u}_2 = 0$, in which case there is a rigid pipe containing the fluid, and $q_2 = -r_2 p_2$ is the reaction of the rigid wall on the fluid.

Analytic continuation

From the preceding paragraph it was found that

$$\dot{u} = k \begin{Bmatrix} Y'_n & J'_n \end{Bmatrix} \begin{Bmatrix} A \\ B \end{Bmatrix} \quad (3.108)$$

and

$$p = -i\omega\rho \begin{Bmatrix} Y_n & J_n \end{Bmatrix} \begin{Bmatrix} A \\ B \end{Bmatrix} \quad (3.109)$$

in which

$$\begin{Bmatrix} A \\ B \end{Bmatrix} = \frac{1}{k(Y'_{n1} J'_{n2} - J'_{n1} Y'_{n2})} \begin{Bmatrix} J'_{n2} & -J'_{n1} \\ -Y'_{n2} & Y'_{n1} \end{Bmatrix} \begin{Bmatrix} \dot{u}_1 \\ \dot{u}_2 \end{Bmatrix} \quad (3.110)$$

or alternatively from equation (3.89)

$$\begin{aligned} \begin{Bmatrix} A \\ B \end{Bmatrix} &= \frac{1}{-i\omega\rho} \begin{Bmatrix} r_1 Y_{n1} & r_1 J_{n1} \\ -r_2 Y_{n2} & -r_2 J_{n2} \end{Bmatrix}^{-1} \begin{Bmatrix} q_1 \\ q_2 \end{Bmatrix} \\ &= \frac{1}{-i\omega\rho} \frac{1}{(Y_{n1} J_{n2} - J_{n1} Y_{n2})} \begin{Bmatrix} J_{n2} & -J_{n1} \\ -Y_{n2} & Y_{n1} \end{Bmatrix} \begin{Bmatrix} p_1 \\ p_2 \end{Bmatrix} \end{aligned} \quad (3.111)$$

Substituting equation (3.110) in (3.108) and (3.111) in (3.109), it is found

$$\dot{u}(r) = \frac{\begin{Bmatrix} Y'_n & J'_n \end{Bmatrix}}{(Y'_{n1} J'_{n2} - J'_{n1} Y'_{n2})} \begin{Bmatrix} J'_{n2} & -J'_{n1} \\ -Y'_{n2} & Y'_{n1} \end{Bmatrix} \begin{Bmatrix} \dot{u}_1 \\ \dot{u}_2 \end{Bmatrix} \quad (3.112)$$

$$p(r) = \frac{\begin{Bmatrix} Y_n & J_n \end{Bmatrix}}{(Y_{n1} J_{n2} - J_{n1} Y_{n2})} \begin{Bmatrix} J_{n2} & -J_{n1} \\ -Y_{n2} & Y_{n1} \end{Bmatrix} \begin{Bmatrix} p_1 \\ p_2 \end{Bmatrix} \quad (3.113)$$

respectively. After expansion, this gives

$$\dot{u}(r) = \frac{(Y'_n J'_{n2} - J'_n Y'_{n2}) \dot{u}_1 + (J'_n Y'_{n1} - Y'_n J'_{n1}) \dot{u}_2}{(Y'_{n1} J'_{n2} - J'_{n1} Y'_{n2})} \quad (3.114)$$

$$p(r) = \frac{(Y_n J_{n2} - J_n Y_{n2}) p_1 + (J_n Y_{n1} - Y_n J_{n1}) p_2}{Y_{n1} J_{n2} - J_{n1} Y_{n2}} \quad (3.115)$$

which express the velocity and pressure fields in the interior in terms of the fields on the boundaries. Observe that these expressions return the proper values when $r = r_1$ or $r = r_2$.

In particular, in the limit when $r_1 \rightarrow 0$ and for a point source on the axis,

$$p_1 \rightarrow -i \frac{\rho\omega}{4} (2 - \delta_{0n}) J_n(ka) Y_{n1} \quad (3.116)$$

$$p(r) = \left[-i \frac{\rho\omega}{4} (2 - \delta_{0n}) \frac{J_n(ka)}{J_{n2}} (Y_n J_{n2} - J_n Y_{n2}) + p_2 \frac{J_n(kr)}{J_{n2}} \right] \quad (3.117)$$

3.5.5. Graf addition theorem

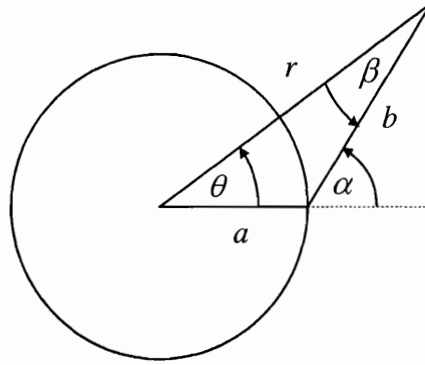


Figure 3.24: Graf addition theorem

This section presents the Graf Addition Theorem used to express a source at an arbitrary location in terms of sources at the pipeline's axis. Let $C_n(kr)$ be shorthand for any of the Bessel functions. Then, with reference to Figure 3.24, the following addition theorem holds, [35]:

$$C_m(kb) \begin{pmatrix} \cos m\beta \\ \sin m\beta \end{pmatrix} = \sum_{-\infty}^{\infty} C_{m+n}(kr) J_n(ka) \begin{pmatrix} \cos n\theta \\ \sin n\theta \end{pmatrix}, \quad r > a \quad (3.118)$$

in which $\beta = \alpha - \theta$. In particular, for integer $m=0$, $C_m = H_0^{(2)}(kb)$, $\cos m\beta = \cos 0 = 1$

$$H_0^{(2)}(kb) = \sum_{-\infty}^{\infty} H_n^{(2)}(kr) J_n(ka) \cos n\theta \quad (3.119)$$

But

$$H_{-n}^{(2)} = (-1)^n H_n^{(2)} \text{ and } J_{-n} = (-1)^n J_n \quad (3.120)$$

so

$$H_{-n}^{(2)} J_{-n} = H_n^{(2)} J_n \quad (3.121)$$

It follows that

$$H_0^{(2)}(kb) = H_0^{(2)}(kr) J_0(ka) + 2 \sum_{n=1}^{\infty} H_n^{(2)}(kr) J_n(ka) \cos n\theta \quad (3.122)$$

3.5.6. Simulations

According to the flexible pipe solution, not only the geometry of the pipeline and the characteristics of the transmitted signal are controlled, but also the surrounding soil

properties and the pipeline stiffness are parameters to the problem. The reference case has the same geometry as the rigid pipe approximation concerning a pipe with radius $R = 0.5\text{m}$, a source and receiver located at the periphery of the pipe separated with a distance $z = 10\text{m}$, while the damping of the system is $\xi = 0.1\%$. The excitations used are the single squared pulse and the tapered sinusoidal wave, similar to those of the rigid pipe solution. However, the novelty of this section is the adjustable surrounding soil acoustic wave velocity, which by default is set to $C_s = 0.2\text{km/sec}$, and the pipeline thickness, of which the default value is $t = 2\text{cm}$. The selected value of $C_s = 0.2\text{km/sec}$ corresponds to a relatively soft soil frequently encountered in the top soil layers where most pipelines are located. The acoustic wave velocity of the surrounding soil controls the impedance contrast among the three materials, water, cast iron, and soil, which as it will be shown, is responsible for the wave energy distribution among them. The pipeline thickness, on the other hand, provides a factor for adjusting the pipe wall stiffness, once more affecting the energy trapped in the water, and its interaction with the pipe wall. Similar to the rigid pipe approximation, the first $n = 8$ orders of solutions are considered in the results with the 50 first modes taken into account for each order.

In what follows, parametric analyses regarding the distance between the source and the receiver, the frequency content, and the pipe radius will be presented in order to provide a relative sense of the role of the flexible pipe and the soft surrounding soil in comparison with the rigid pipe approximation. Thereafter, results of varying soil properties and pipe wall thickness will be presented, which is the main focus of this section. Due to the increased complexity of the phenomena associated with the flexible pipe solutions, the single pulse waveform will be the main excitation presented in this section. Results with the tapered sinusoidal wave excitation will be presented at points of interest for comparison with the rigid pipe approximation.

- ***Distance***

In order to illustrate the effect of propagation distance on a wave transmitted inside a flexible pipeline, Figure 3.25 presents the pressure time histories for distances $z = 10\text{m}$ and 100m . The transmitted signal is a single squared pulse with duration $t_d = 1\text{msec}$ corresponding to a central frequency of 1 kHz , the pipeline has radius

$R = 0.5\text{m}$, with the source and the receiver located at the internal perimeter of the pipe. The acoustic wave velocity of the soil is $C_s = 0.2 \text{ km/sec}$ and the pipeline thickness $t = 2\text{cm}$. The frequency spectrum of the received waveforms is also provided for reference. It becomes directly apparent that the pipeline waveguide acts as a lowpass filter on the propagating signal. Such information becomes available not only by observing the frequency spectrum of the received signals, but also by noticing the increasing time spread of the pulse with distance and the reduction of the ripples following the main pulse. The lowpass characteristics are even more pronounced than the rigid pipe approximation, as presented in paragraph 3.4.6.

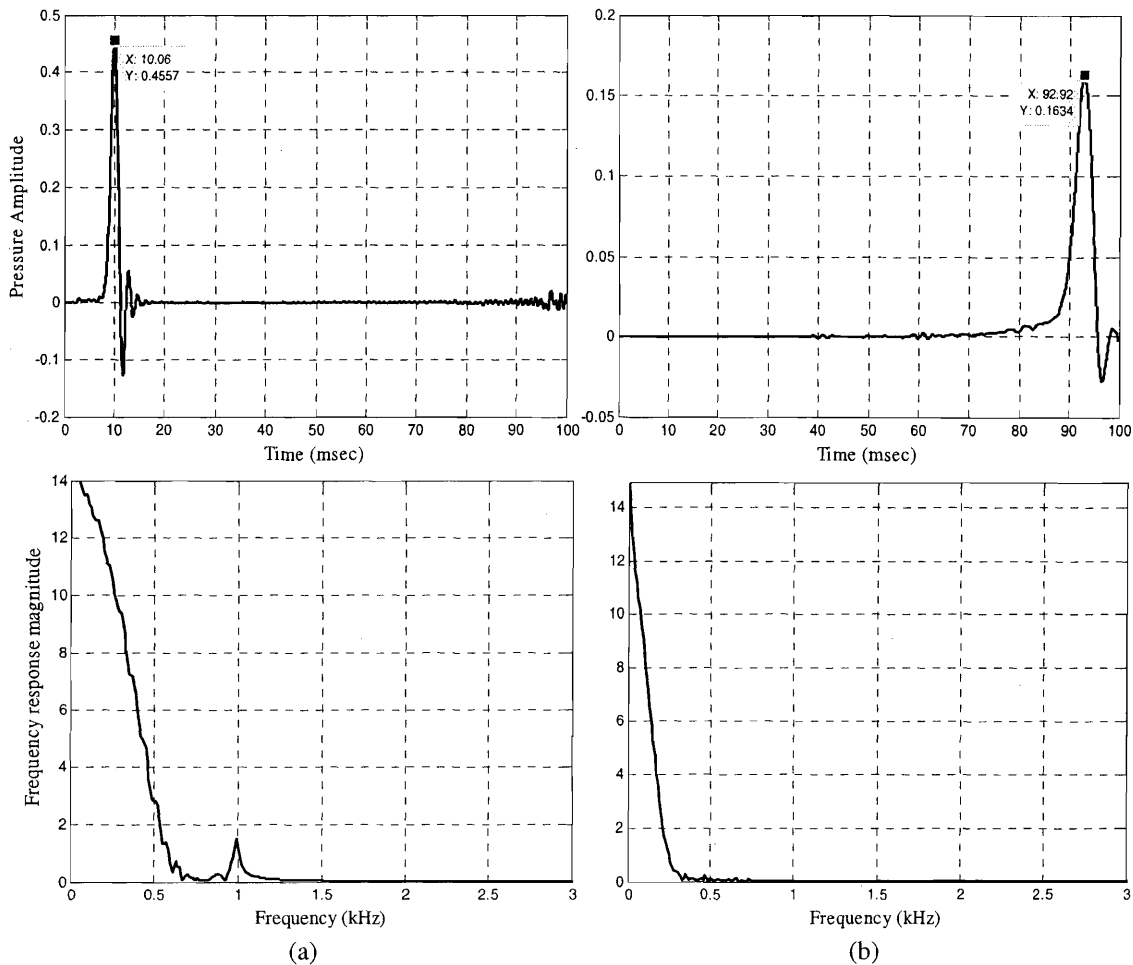


Figure 3.25: Attenuation vs. Distance; Pressure Time History and Frequency Response Spectrum for $R = 0.5\text{m}$, $a = r = R$, $f_o = 1\text{kHz}$, $C_s = 0.2 \text{ km/sec}$, $t = 2\text{cm}$, and (a) $z = 10\text{m}$, (b) $z = 100\text{m}$

One interesting observation is that the flexible pipe system has a slower acoustic wave velocity than each of the materials constituting the waveguide. More specifically from the $z = 10\text{m}$ plot the effective acoustic wave velocity is $C_{eff} = 10\text{m} / 10.26\text{msec} = 0.97\text{km/sec}$, while from the $z = 100\text{m}$ plot $C_{eff} = 100\text{m} / 92.92\text{msec} = 1.076\text{km/sec}$. In the literature, [36], an analytical far field approximation of the acoustic velocity of a wave propagating in a hollow fluid filled thin-walled tube is found to be equal to:

$$C_r = \left[\rho \left(\frac{1}{B} + \frac{1}{Et/2b} \right) \right]^{-1/2} \quad (3.123)$$

where ρ is the fluid's density, B is the fluid's bulk modulus, E is the Young's modulus of the tube, b is the internal radius, and h is the thickness of the tube wall. Substituting for the water filled cast iron pipe of the system under consideration with $\rho = 1 \text{ ton/m}^3$, $B = 2.25\text{GPa}$, $E = 91 \text{ GPa}$, $b = 0.50\text{m}$, and $t = 0.02\text{m}$ the acoustic wave velocity is found to be in agreement with the simulation results equal to $C_r = 1\text{km/sec}$.

For reference, Figure 3.26 presents the pressure time history response and the frequency spectrum for a tapered sinusoidal wave excitation for a pipeline system identical to the above and for a propagation distance of $z = 10\text{m}$. It is interesting to notice in this plot the absence of the extended tail signal received in Figure 3.17b and the concentration of the distortion around the initial arrival. The absence of a tail signal can be explained mainly due to the radiation of the energy into the surrounding soil, as will be discussed later in this section.

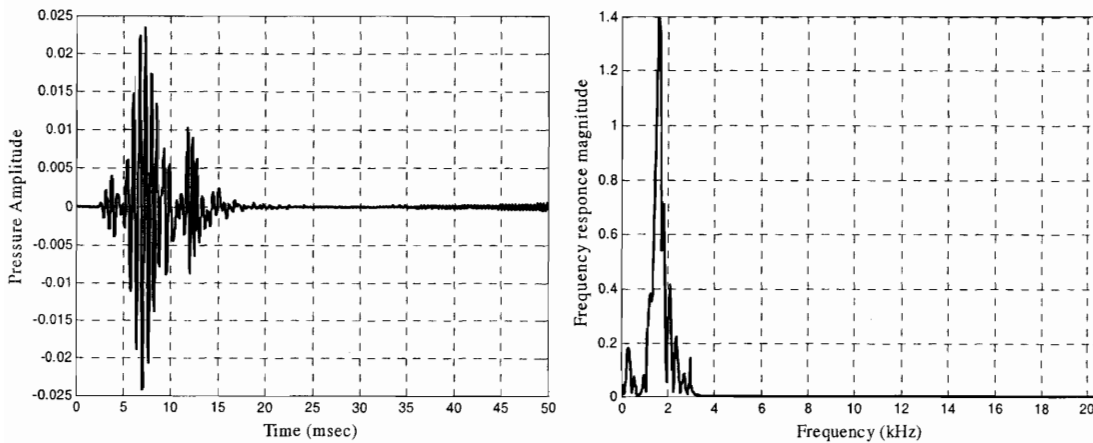


Figure 3.26: Pressure Time History and Frequency Response Spectrum for the tapered sinusoidal waveform excitation and $R = 0.5\text{m}$, $a = r = R$, $z = 10\text{m}$, $f_o = 1.5 \text{ kHz}$, $C_s = 0.2 \text{ km/sec}$, and $t = 2\text{cm}$

- **Frequency content**

Figure 3.27 presents the pressure time histories and the corresponding frequency spectra of the response of the transmission channel introduced with pulses of various durations. The plots illustrate the channel's response to pulses with durations $t_d = 0.5\text{msec}$, 0.2msec , and 0.05msec , which correspond to central frequencies of $f_o = 2\text{kHz}$, 5kHz and 20kHz respectively. The increased reverberation of the higher frequency spectrum pulses becomes directly apparent, in accordance with the behavior identified from the rigid pipe approximation. The presence of the flexible pipe and the surrounding soil introduces more transmission paths for the signals to propagate. The plots reveal signals arriving earlier than the main pulse, probably from propagation through the pipe wall, which has acoustic wave velocity of 5100m/sec in contrast with the water's 1500m/sec . Significant delayed arrivals are observed for a long period of time, implying signals that propagate through longer transmission paths, possibly including reflections through the surrounding soil and the pipe wall.

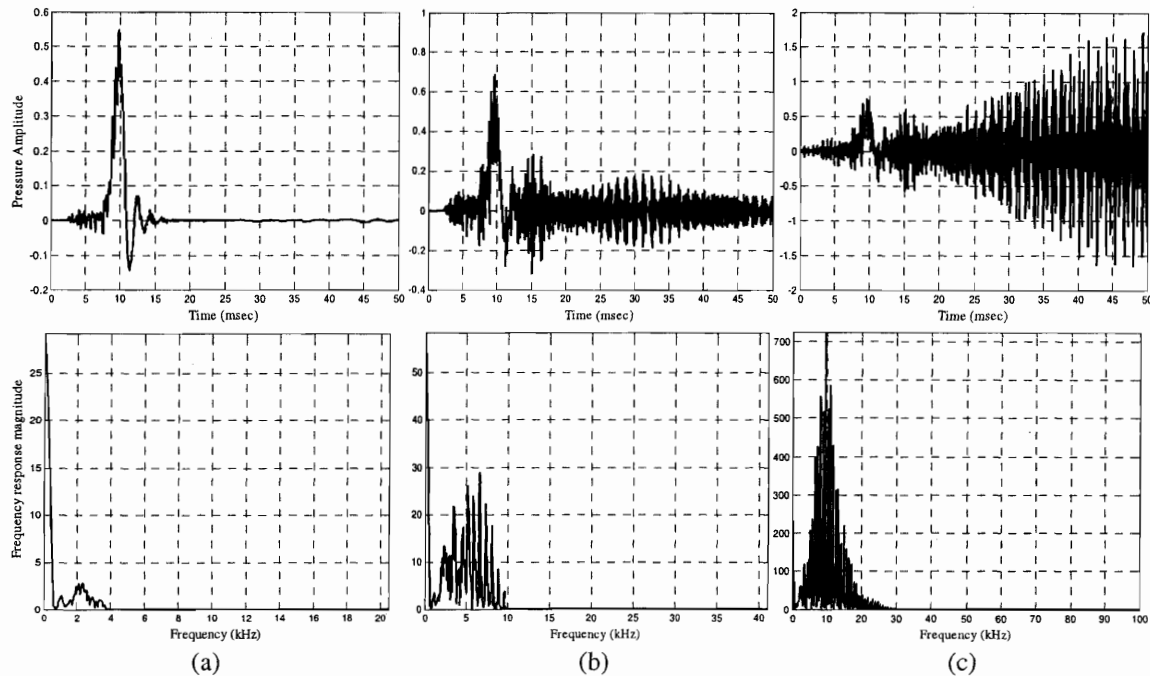


Figure 3.27: Attenuation vs. Frequency; Pressure Time History and Frequency Response Spectrum for $R = 0.5\text{m}$, $a = r = R$, $z = 10\text{m}$, $C_s = 0.2\text{ km/sec}$, $t = 2\text{cm}$, and (a) $f_o = 2\text{kHz}$, (b) $f_o = 5\text{kHz}$ and (c) $f_o = 20\text{kHz}$

• Pipe Radius

This section examines the effect of pipe radius on the propagating signal. The $R = 0.5\text{m}$ case was presented in Figure 3.25a, while the $R = 0.15\text{m}$ and $R = 1\text{m}$ cases are presented in Figure 3.28. The remaining parameters are held constant with the transmitter and receiver located at the internal perimeter of the pipe at a distance of $z = 10\text{m}$, the excitation is a squared single pulse with central frequency of $f_o = 1\text{kHz}$, and the acoustic wave velocity of the surrounding soil is $C_s = 0.2\text{km/sec}$. Finally, the thickness of the pipe wall has been adjusted proportionally to the radius used starting from $t = 2\text{cm}$ for $R = 0.5\text{m}$.

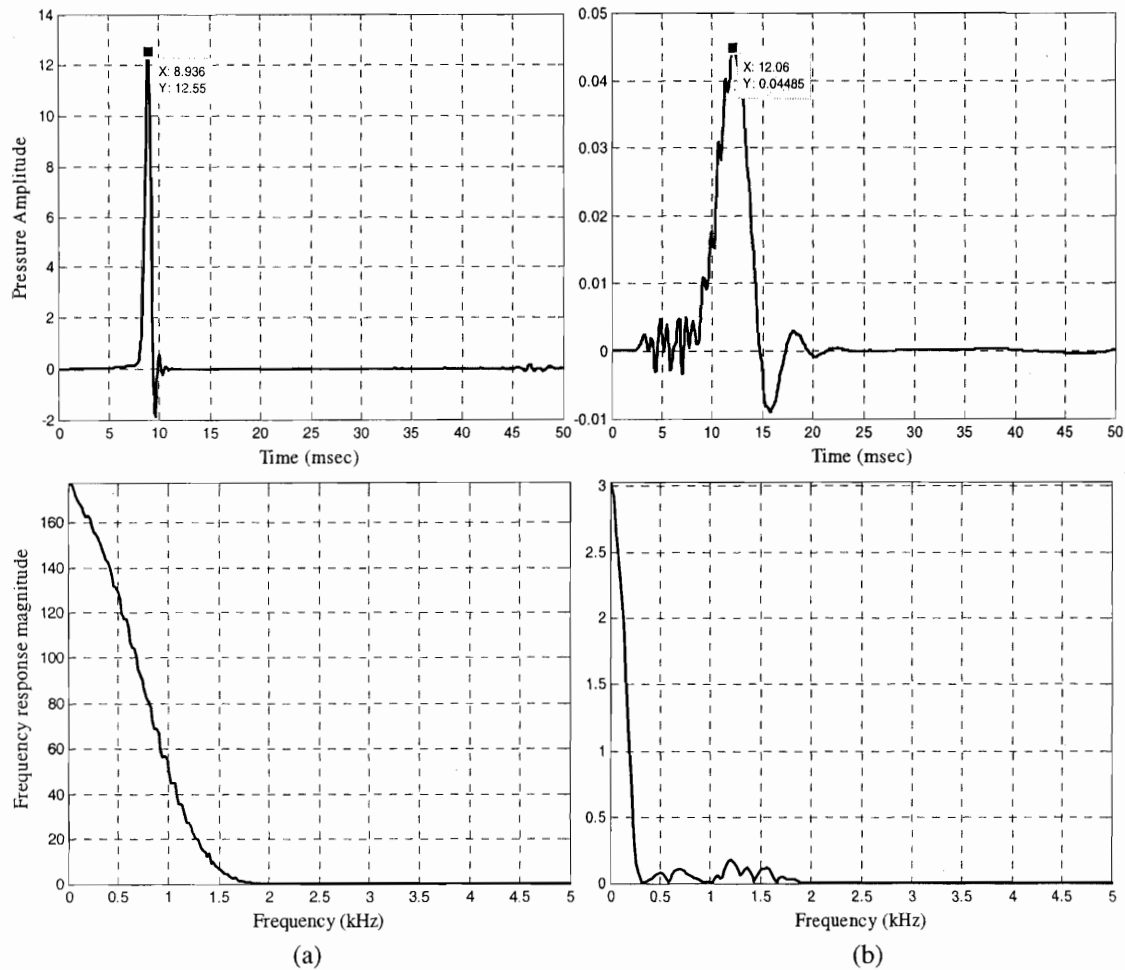


Figure 3.28: Pressure Time History and Frequency Response Spectrum for $z = 10\text{m}$, $f_o = 1\text{ kHz}$, $a = r = R$, $C_s = 0.2\text{ km/sec}$, and (a) $R = 0.15\text{m}$, and (b) $R = 1\text{m}$

A remarkable first observation is that the lowpass filtering character of the pipeline waveguide is enhanced with the increase of the pipe radius. Even though larger pipelines excite a large number of high order modes, $n > 0$, the frequency content of the signal drops significantly. The main reason for this phenomenon is the reduction of stiffness of the pipe wall with increasing radius, allowing more high frequency signals to radiate to the surrounding media. This phenomenon will become apparent also in the following sections where the soil properties and the pipe wall thickness will be the adjustable parameters. The presence of the higher modes in the larger pipes is revealed from the high frequency ripples preceding and following the main received pulse. Finally, the energy of the received signal, revealed by the area under the main pulse, is significantly reduced in larger pipelines as expected, due to energy spread over a larger volume, and the aforementioned radiation of energy into the surrounding media. This section concludes the parametric analyses regarding variables also examined at the rigid pipe approximation. The following sections examine properties related to the pipeline itself and the surrounding soil, and more specifically, the pipe wall thickness and the soil acoustic wave velocity.

- ***Soil Properties***

The effect of the soil hardness is examined in this paragraph. The hardness of the pipeline surrounding media is important since it affects the stiffness of the pipeline waveguide system. An indicator of the material hardness is the acoustic wave velocity, which is used in this section as an adjustable parameter. The default value of the acoustic wave velocity $C_s = 0.2$ km/sec used in the simulations up to this point corresponds to a soft soil frequently found in the upper soil layers, where the pipelines are usually located. Extreme cases are considered in both directions for the acoustic wave velocity parameter, using values $C_s = 0$ km/sec, and $C_s = 2$ km/sec. The first one, $C_s = 0$ km/sec, corresponds to no soil surrounding the pipeline, as if the pipe were located in free space and therefore there were no support of the pipe wall from other media, which results in the minimum stiffness case. The latter case, $C_s = 2$ km/sec, corresponds to a pipeline laid in a very hard soil, or even soft rock, resulting in a significantly stiff pipe configuration. Figure 3.29

presents the results for the two extreme cases, whereas for comparison Figure 3.25a is considered for the case $C_s = 0.2$ km/sec.

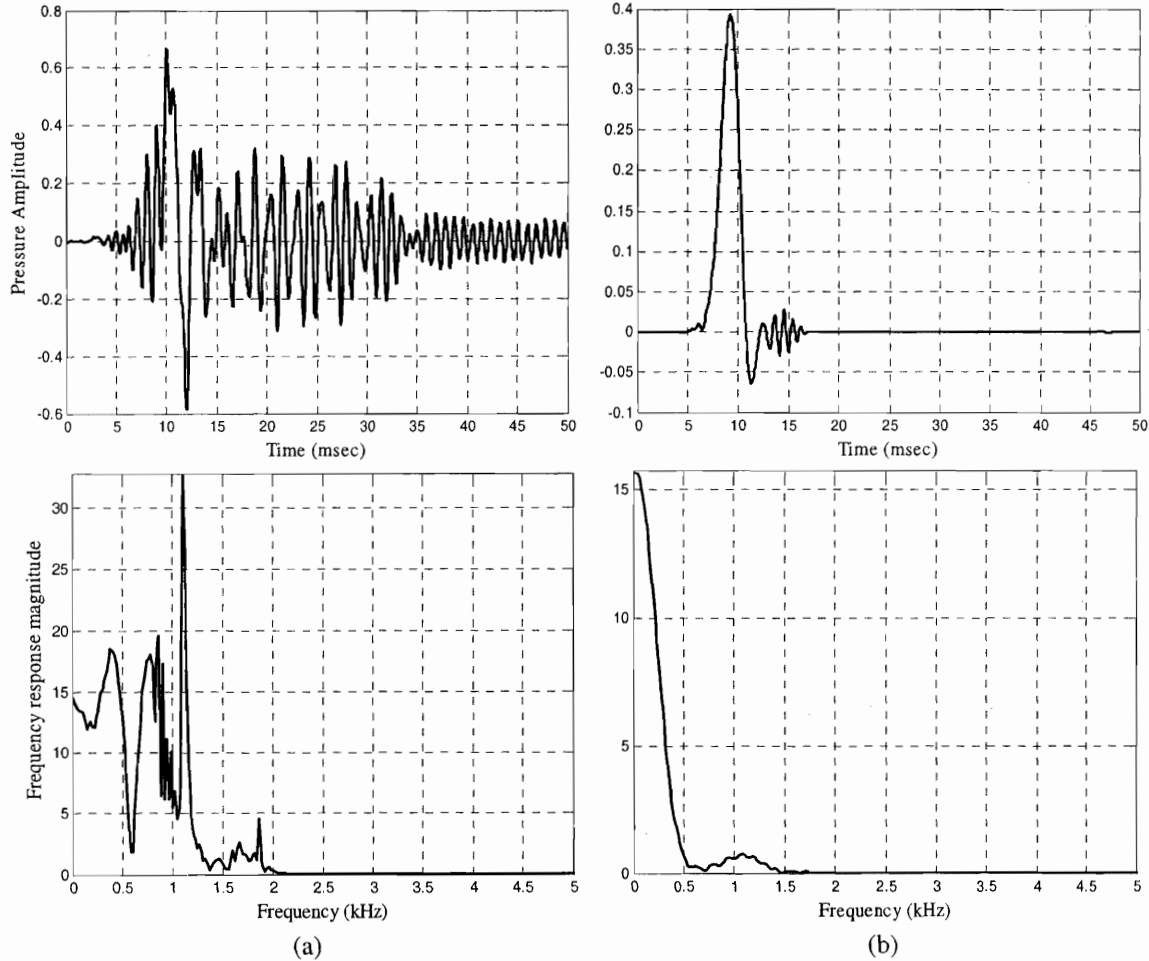


Figure 3.29: Effect of soil stiffness; Pressure Time History and Frequency Response Spectrum for $z = 10$ m, $f_o = 1$ kHz, $R = 0.5$ m, $a = r = R$, $t = 2$ cm, and soil acoustic wave velocity (a) $C_s = 0$ (No soil), and (b) $C_s = 2$ km/sec

The effect of the soil stiffness is directly evident from the presented results. The pipe in free space plot indicates the presence of significant ringing around the main pulse. On the other hand, the observed ringing is minimal in the hard soil case, which is an indication that the ringing energy has radiated to the surrounding soil. This theory is supported by the fact that the soft soil case presents the minimum ripples. The impedance contrast of the soft soil with the pipe wall allows the most radiation of energy away from the waveguide, thus reducing significantly the energy of the received signal. The hard soil offers some stiffness to the pipeline, which allows confining the energy in the

transmission channel. Alternatively, the hard soil can be considered as an intermediate step between the soft soil and the rigid pipe solution, as indicated by the received signals presented and the resulting stiffness of the acoustic waveguide. The loss of energy from the transmission channel into the surrounding media is frequently referred to as *radiation damping*, since it results in significant decay of the signal with time resembling to systems with increased damping. Figure 3.30 illustrates this point by plotting the results for the first order of solutions, $n = 0$, presenting at the same time the relative energy distribution among the channel materials.

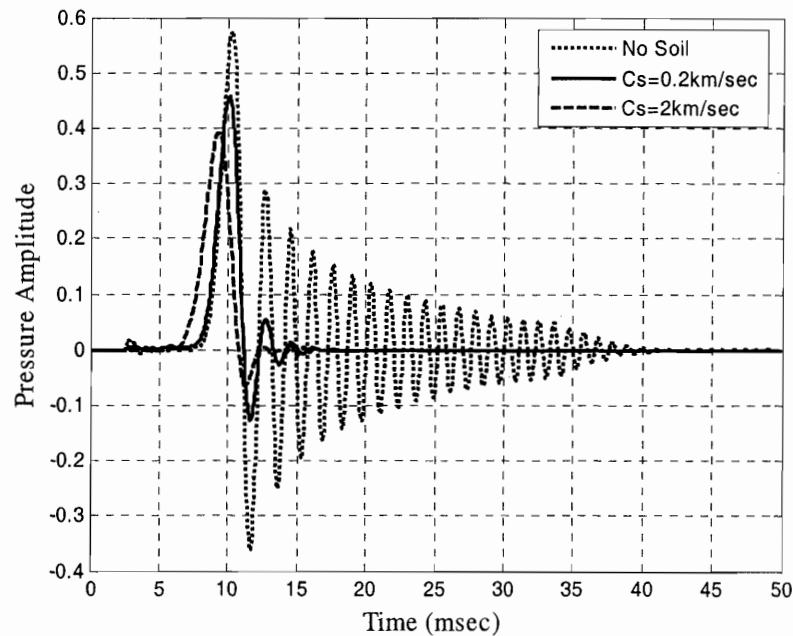


Figure 3.30: Radiation Damping
(Pressure Time History for $n = 0$, $z = 10\text{m}$, $f_o = 1\text{ kHz}$, $R = a = r = 0.5\text{m}$, and $C_s = 0, 0.2$, and 2 km/sec)

- **Pipe Stiffness**

Following the results where the waveguide stiffness is controlled by the soil hardness, this section examines the effect of the stiffness of the pipe itself. The adjustable parameter at this stage is the pipe wall thickness, as a measure of controlling the pipeline stiffness. Figure 3.31 presents results for very thin pipe wall $t = 5\text{mm}$ to very thick pipe wall $t = 10\text{cm}$. The thin pipe wall case generates a transmission channel with very small stiffness. In sequence, the signal energy radiates tremendously to the environment, especially the high frequency signal components, as indicated by Figure 3.31a in which

the recorded signal is mainly the result of the $n = 0$ order of modes and essentially no high frequencies are present. On the other hand, the thick pipe wall creates a very stiff waveguide, resulting in the entrapment of the high frequency vibrations observed around the main pulse. Once again, the thick pipe case can be considered as an intermediate stage between the default flexible pipe case studied in the above sections and the rigid pipe approximation.

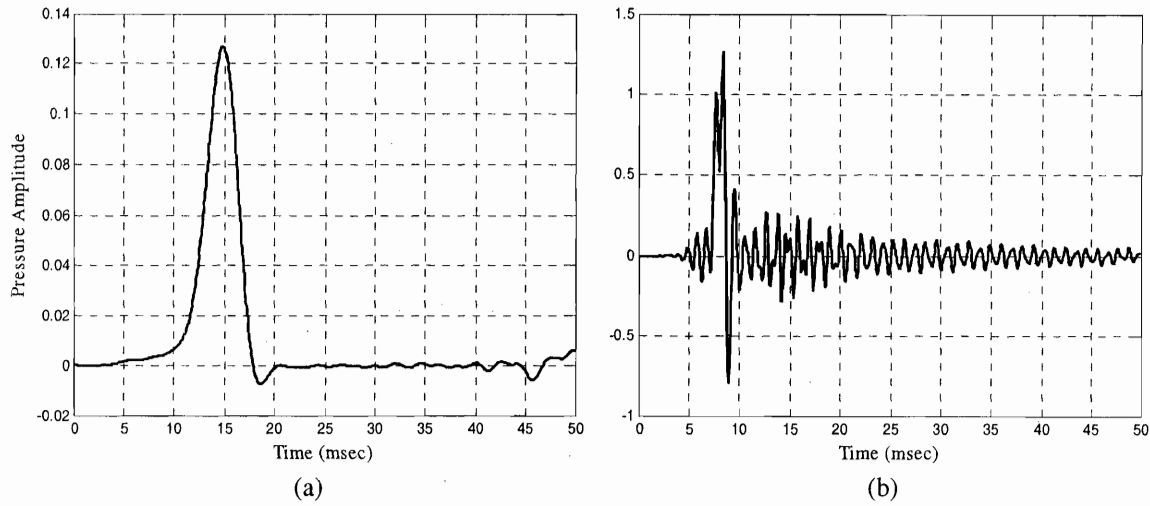


Figure 3.31: Effect of pipeline thickness; Pressure Time History for $z = 10\text{m}$, $f_o = 1\text{ kHz}$, $R = 0.5\text{m}$, $a = r = R$, $C_s = 0.2\text{ km/sec}$ and pipe wall thickness (a) $t = 5\text{mm}$, and (b) $t = 10\text{cm}$

• Pipe Material

Finally, this section examines the effect of the pipeline material in the propagation of acoustic waves. Even though most of the water pipeline networks consist of cast iron pipes, other materials have also been used such as concrete, steel and PVC. Since concrete is a heterogeneous material, it is not trivial to model it for acoustic wave propagation purposes. Moreover, the increased stiffness of concrete pipes, which usually have thick pipe walls, and steel pipes, which are harder than cast iron, allow to estimate their behavior as a projection of the characteristics observed in the preceding cases. In this section, the cast iron pipe will be replaced with a PVC pipe, which has density $\rho = 1400\text{ton/m}^3$, acoustic wave velocity $C_{PVC} = 1580\text{m/sec}$, and Young's Modulus $E_{PVC} = 1500\text{GPa}$. The remaining parameters have the default values of the previous analyses.

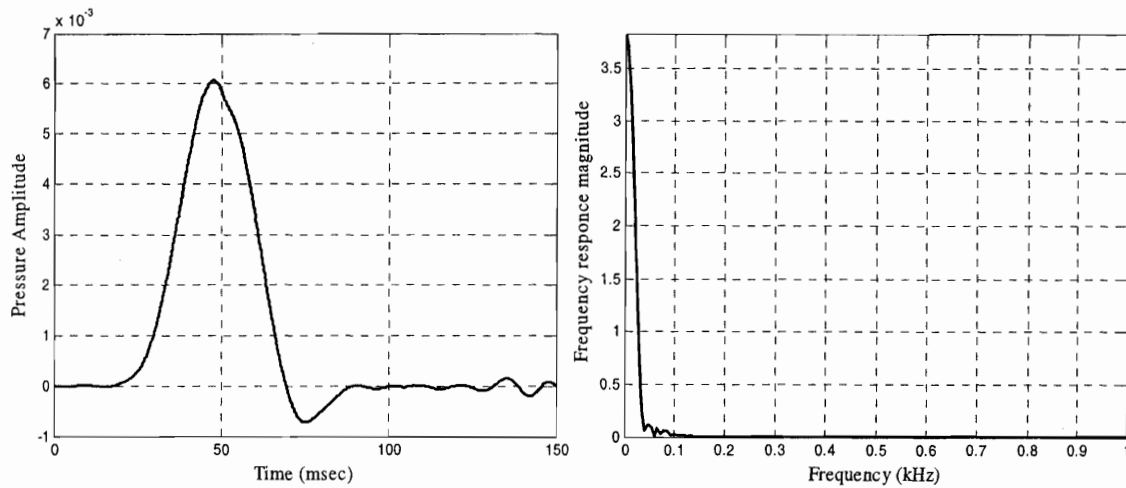


Figure 3.32: Effect of pipeline material; Pressure Time History and Frequency Response Spectrum for PVC pipe with $z = 10\text{m}$, $f_o = 1\text{ kHz}$, $R = 0.5\text{m}$, $a = r = R$, $C_s = 0.2\text{ km/sec}$

The above plots reveal the significant lowpass filter character of the PVC pipe. The PVC waveguide strongly shifts the frequency content of the propagating signal towards the origin, while at the same time its magnitude drops dramatically. This is an indication that the damping of the transmission channel is very high, mostly due to radiation of energy into the surrounding soil. However, the recorded signal is the result mainly of the fundamental mode, and therefore presents minimal dispersion. A successful digital communication system operating in such an environment should employ a sensitive receiver in combination with an amplifier in order to be able to record the transmitted signal, while it should compensate for the frequency shift in order to decode the encapsulated data.

3.6 Conclusions

This chapter examined the effect of the pipeline waveguide on a propagating signal as well as the interaction of the waveguide with the surrounding media. The behavior of the channel was studied with respect to a number of parameters, initially for a simple rigid pipe approximation and thereafter for the complete model of flexible pipe embedded in soil. The initial study allowed identifying the propagation characteristics of a hollow fluid filled cylinder, while the second set of simulations focused on the interaction of the surrounding soil and pipe wall with the propagating signal. From the

complete set of results it was identified that the distortion of the recorded signal is the outcome of a complex interaction of all parameters involved. Key findings include that high frequency signals excite more modes of propagation resulting in severe reverberation. The number of the excited modes of propagation is also a function of the pipe radius, with larger pipes introducing more modes for lower frequencies. The pipeline waveguide on the other hand acts as a lowpass filter on the propagating signal, resulting in frequency shifts on the recorded wave, especially for long propagation distances, and low stiffness acoustic channels. The previous statement implies that the higher modes, carrying the high frequency content signals, attenuate faster than the lower modes. However, due to multipath propagation and severe attenuation the fidelity of the received signal degrades significantly with distance. For the implementation of a reliable digital communication system it is important to identify the modes with the highest energy concentrated at the frequency spectrum, i.e. bandwidth, of the transmitted signal, with the simultaneous minimum resulting dispersion. This can be achieved by identifying the transfer functions for each order of modes after a thorough examination of the transmission channel. Further analysis of the behavior of the pipeline waveguide will be provided in Chapter 6, where simulations of actual digital signals with specific characteristics will be introduced to the computational models introduced in this chapter, and in Chapter 7, where experimental results are presented.

3.7 References

- [1]. Mersenne M., "Harmonie Universelle: The books on Instruments", Initially published in Paris at 1636, Translated by R.E. Chapman, *The Hague*, M. Nijhoff, 1957.
- [2]. J. Tyndall, "Sound", *Longmans*, 5th ed., London, Green, 1893.
- [3]. Rayleigh J.W.S., "The theory of Sound", *Dover Publications*, Reprint of 2nd ed. 1894, New York, 1945.
- [4]. Stone W. H., "Elementary lessons on sound", *Macmillan*, London, 1891.
- [5]. Lamb H., "The Dynamical theory of Sound", *Dover Publications*, Reprint of the 2nd ed. 1925, New York, 1960.
- [6]. Crandall I.B., "Theory of vibrating systems and sound", *Van Nostrand*, New York, 1926.
- [7]. Morse P.M., "Vibration and Sound", *McGraw-Hill*, 2nd ed., New York, 1948.
- [8]. Olson H.F., "Music, Physics and Engineering", *Dover Publications*, 2nd ed., New York, 1967.
- [9]. Morse P.M., and Ingard K.U., "Theoretical Acoustics", *McGraw Hill*, Princeton, New Jersey, 1968.
- [10]. Silk M., and Bainton K., "The propagation in metal tubing of ultrasonic wave modes equivalent to Lamb waves", *Ultrasonics*, Vol. 17, No. 1, pp. 11-19, January, 1979.
- [11]. Rama Rao V.N., and Vandiver J.K., "Acoustics of fluid-filled boreholes with pipe", *Journal of Acoustical Society of America*, Vol. 105, No. 6, pp. 3057-3066, 1999.
- [12]. Aristegui C., Lowe M.J.S., and Cawley P., "Guided waves in fluid-filled pipes surrounded by different fluids", *Ultrasonics*, Vol. 39, pp. 367-375, 2001.
- [13]. Long, R., Lowe, M.J.S. and Cawley, P., "Axisymmetric modes that propagate in buried iron water pipes", *Review of Progress in Quantitative Non-Destructive Evaluation*, Vol. 22, Thompson D.O. and Chimenti D.E. (eds), American Institute of Physics, pp1201-1208, 2003.

- [14]. Long, R., Lowe, M.J.S. and Cawley, P., "Attenuation characteristics of the fundamental modes that propagate in buried iron water pipes", *Ultrasonics*, Vol. 41, pp. 509-519, 2003.
- [15]. C.R. Fuller, F.J. Fahy, "Characteristics of wave propagation and energy distributions in cylindrical elastic shells filled with fluid", *Journal of Sound and Vibration*, Vol. 81, pp. 501-518, 1982.
- [16]. Long, R., Vine, K., Lowe, M.J.S. and Cawley, P., "The effect of soil properties on acoustic wave propagation in buried iron water pipes", *Review of Progress in Quantitative Non-Destructive Evaluation*, Vol. 21, Thompson D.O. and Chimenti D.E. (eds), American Institute of Physics, pp. 1310-1317, 2002. Similar paper also in *Proceedings of 8th Euro Non-Destructive Testing Conference*, Barcelona, June 17-21, 2002.
- [17]. Cheng C.H., and Toksöz M.N., "Elastic wave propagation in a fluid filled borehole and synthetic acoustic logs", *Geophysics*, Vol. 46, No. 7, pp 1042-1053, July, 1981.
- [18]. Demma, A., Cawley, P., Lowe, M.J.S., Roosenbrand, A.G. and Pavlakovic, B., "The reflection of guided waves from notches in pipes: a guide for interpreting corrosion measurements", *NDT&E International*, Vol. 37, pp 167-180, 2004.
- [19]. Tubman K.M., Cheng C.H., Cole S.P., and Toksöz M.N., "Synthetic full waveform acoustic logs in cased boreholes, II Poorly bonded casing", *Geophysics*, Vol. 51, No. 4, pp 902-913, April, 1986.
- [20]. Drumheller D.S., "Acoustical Properties of Drill Strings," *Journal of the Acoustical Society of America*, Vol. 85, No. 3, pp. 1048-1064, March, 1989.
- [21]. Drumheller D.S., "Extensional Stress Waves in One-Dimensional Elastic Waveguides", *Journal of the Acoustical Society of America*, Vol. 92, No. 6, pp. 3389-3402, December, 1992.
- [22]. Drumheller D.S., "Attenuation of Sound Waves in Drill Strings", *Journal of the Acoustical Society of America*, Vol. 94, No. 4, pp. 2387-2396, October, 1993.
- [23]. Drumheller D.S., and Knudsen S.D., "The Propagation of Sound Waves in Drill Strings", *Journal of the Acoustical Society of America*, Vol. 97, No. 4, pp. 2116-2125, April, 1995.
- [24]. Drumheller D.S., and Knudsen S.D., "Wave impedances of drill strings and other periodic media", *Journal of the Acoustical Society of America*, Vol. 112, No. 6, December, 2002.

- [25]. Havlena V., "Communication for water distribution networks", *US Patent Office*, Patent no. US 6,626,042 B2, September 30th, 2003.
- [26]. Li Y., Harrold S.O., and Yeung L.F., "Ultrasonic data communication along large diameter water filled pipes", *Proceedings of the 2nd IEEE Conference on Mechatronics and Machine Vision in Practice*, pp. 239-244, Hong Kong, September, 1995.
- [27]. Li Y., Harrold S.O., and Yeung L.F., "Experimental study on ultrasonic signal transmission within the water filled pipes", *Mechatronics and Machine Vision in Practice*, pp. 93-98, Australia, September, 1997.
- [28]. Li Y., Harrold S.O., and Yeung L.F., "Model-based simulation for ultrasonic communication channel inside pipeline", In *Proceedings of International Conference on Signal Processing Applications and Technology*, pp. 1163-1167, 2000.
- [29]. Bin L., Harrold S.O., Bradbeer R., and Yeung L.F., "An Underwater Acoustic Digital Communication Link", in *Mechatronics and Machine Vision*, Billingsley J. (Ed), Research Studies Press, UK, pp 275-282, 2000.
- [30]. Kausel E., "Compendium of Fundamental Solutions in Elastodynamics", *Cambridge University Press*, 2005, in print.
- [31]. Fahy F., "Foundations of Engineering Acoustics", *Academic Press*, London, UK, 2001.
- [32]. Kondis A., "Acoustical wave propagation in buried water filled pipes", Master of Science Thesis, Department of Civil and Environmental Engineering, Massachusetts Institute of Technology, January, 2005.
- [33]. Kausel E., Roësset J.M., "Frequency domain analysis of undamped systems", *Journal of Engineering Mechanics*, Vol. 118, No. 4, pp. 721-734, April, 1992.
- [34]. Fahy F., "Sound and Structural Vibration: Radiation, Transmission and Response", *Academic Press*, London, UK, 1985.
- [35]. Abramovitz M, and Stegun I.A., "Handbook of Mathematical Functions, with Formulas, Graphs and Mathematical Tables", *Dover Publications*, 9th printing of the original 1965 edition, New York, 1965.
- [36]. White J.E., "Underground sound, Application of Seismic Waves", *Elsevier*, Amsterdam, The Netherlands, 1983.

Chapter 4

Digital Communications

4.1 Introduction

The evolution of society mandated the use of devices that would allow exchange of data and communication of people at remote locations. These communication systems are capable of transferring data reliably over long distances and enable, apart from voice and video transfer, remote control of devices, telemetry, navigation aids for ships and airplanes, and so on.

Communication systems can be categorized into two very broad groups with respect to the type of data they handle, namely analog or digital. The term *data* here implies any type of information that must be transmitted, from sound, voice and video to numbers and records. Analog systems are capable of processing and transmitting analog data, i.e. continuous waveforms with infinite number of shapes. In digital systems on the other hand, data is digitized, i.e. discrete in time, and can form into a finite number of states from a finite number of characters.

From a historical perspective an interesting fact is that the first electrical communication system was digital. The telegraph, invented by Gauss and Weber in 1833, was used by Samuel Morse in 1837 to send digital signals. The messages were encoded into binary form using dots and dashes, groups of which were representing letters from the English alphabet, the well known “Morse Code”, illustrated in Figure 4.1. This code uses variable length codewords separated by a brief silent time between the transmission of each one. The most commonly used letters are represented by the smaller sequences.

A	.-	N	-.	0	-----
B	-...	O	---	1
C	-.-.	P	---.	2-
D	-. .	Q	---.	3-
E	.	R	...	4-
F	...	S	...	5
G	...	T	-	6	-----
H	U	...	7	-----
I	..	V-	8	-----
J-	W	...	9	-----
K	-. -	X	---.	,	----- (comma)
L	Y	---.	.	----- (period)
M	--	Z	?

Figure 4.1: Morse code, [1]

There exist several fundamental quantities and concepts that must be defined before proceeding to the analysis of a digital communication system (DCS). The dashes and dots of the “Morse Code” correspond to the bits of a current DCS. A bit is the fundamental information unit for all digital systems, which is represented in binary form by zeroes and ones. A sequence of bits is called a *bit stream*. Similar to the “Morse Code”, where the groups of dashes and dots represent letters, in current DCS, groups of bits are representing *symbols*. Symbol is a group of k bits which are considered as a unit. The number of available symbols M , or in other words the size of the alphabet, is $M = 2^k$, where k is the number of bits included in the symbol. The rate at which the bits are transmitted through the communication system is called the *data rate*, which is measured in bits per second (bits/s) and is given by $R = k/T = (1/T)\log_2 M$ bits/s, where k bits identify a symbol from an $M = 2^k$ symbol alphabet and T is the k -bit symbol duration.

4.2 Digital vs. Analog Communication

Most communication systems nowadays follow the trend of digital implementation, a selection justified by a direct comparison between analog and digital systems. The key feature of a digital communication system is that it deals with a finite set of discrete messages, in contrast to an analog communication system in which messages are defined on a continuum. The objective at the digital receiver is not to reproduce the transmitted waveform with precision, but rather to identify from the

distorted received signal which of the predetermined finite set of waveforms was sent by the transmitter.

The main advantage of digital communication is the easy identification and regeneration of distorted data. When a signal propagates through any transmission channel, it gets noisy and distorted, as illustrated in Figure 4.2. However, the distorted signal can be easily matched to one of the predetermined states and regenerated to its original form.



Figure 4.2: Signal distortion and recognition

However, this is not true for analog signals since there are no predetermined shapes that are generated and therefore expected by the receiver. A distorted signal cannot be recovered completely and this affects the quality of the transmitted data. Only when the transmitted signals have a predetermined frequency range, filtering can be applied to reduce the effect of the ambient noise added to the signal.

By contrast, there exist numerous signal processing techniques for digital signals that allow distortion compensation and error correction, resulting in more reliable communication. These techniques can be embedded into microchips that handle the recognition and regeneration of the data efficiently, allowing easy and flexible implementation of the signal processing algorithms. These digital circuits are in general more reliable and less expensive than analog circuits. Processing of digital data is further assisted by the packetized transmission of data, i.e. clusters of data that are sent as a group at the same time. Digital circuits are capable to buffer these data packets for review and further processing, if required.

However, the use of packets for digital data transmission requires synchronization of the transmitter and receiver. The receiver has to collect the packets in the correct order, appoint the packet numbers and check if all the packets were received, and decide if they

were or not received correctly. The whole procedure of synchronization, buffering, processing and correcting the data is frequently a very resource intensive process. In addition, the digital signals present non-graceful degradation, meaning that when the signal to noise ratio (SNR) falls below a certain point, the performance of the communication system drops from very good to very poor.

Signal to noise ratio, defined as S/N , is a quantity mainly used to represent the quality of analog signals. The numerator represents the average power of the received signal S and the denominator is the average electrical noise power N observed in that signal. However, in digital communications the *signal to noise per bit* ratio, E_b/N_0 , is used, where E_b is the bit energy and N_0 is the noise power spectral density. The bit energy E_b can be described as noise power S times the bit time $T_b = (1/R_b)$, where R_b is the bit rate, while the noise power spectral density N_0 can be described as noise power N divided by bandwidth W , as presented in equation (4.1):

$$\frac{E_b}{N_0} = \frac{S T_b}{N/W} = \frac{S/R_b}{N/W} = \frac{S}{N} \left(\frac{W}{R} \right) \quad (4.1)$$

It becomes apparent that E_b/N_0 is just a version of the S/N that has been normalized by the bandwidth and the bit rate. It is important to notice that E_b/N_0 is an energy comparison and not a power comparison as the analog S/R is. The selection of E_b/N_0 as a quality measure for digital signals is justified due to the characterization of the digital signals as energy signals. An *energy signal* is defined as a signal that has zero average power and a finite energy, in contrast with a *power signal* that has finite average power and infinite energy. An analog signal is a continuous signal in time and is frequently characterized as power signal, since it can be considered having infinitely long waveform resulting in carrying infinite amount of energy. Therefore, the comparison of signal and noise is a comparison of average powers, i.e. average rates of delivering the energy. On the other hand, a digital signal is transmitted by using finite duration waveforms. These waveforms have finite energy and zero average power, resulting in the characterization of digital signals as energy signals. In addition, it is important to notice that the E_b/N_0 is a comparison of the corresponding signal and noise energies *per bit*. Each transmitted waveform corresponds to different amounts of data in terms of bits (contains different number of bits), depending on the modulation method used, as

described in paragraph 4.5.3. To compare the performance of different systems utilizing different modulation methods, it is important to decompose the signal to noise ratio requirement into a ratio corresponding to each separate bit.

Finally, the differences between analog and digital systems are extended on the performance measures. While performance in digital communication is usually evaluated by the probability of incorrectly detecting a digit, bit or symbol, in analog communication performance is evaluated with fidelity criteria, such as signal to noise ratio, percent distortion, expected mean square error between transmitted and received waveforms, and so on.

4.3 *Digital Communication System Components*

Three main objects are present in any communication implementation: a transmitter to send the signals, a communication channel to carry the signals and a receiver to collect the transmitted signals. To send a signal through a transmission medium, it is necessary to convert it to a set of waveforms that encapsulate the digital data. Depending on the transmission channel the output of a transmitter can be either in pulse shape, resembling to digital data, or an analog wave modulated appropriately to encapsulate the digital data. The structure of the transmitter and receiver may vary from simple to very complex and consist of several elaborate signal processing steps, which depend on the channel imposed signal distortion, and the need to provide reliable communication. However, there are only two essential steps, namely the mapping and the modulation of the signal, illustrated in Figure 4.3. *Mapping* is the process of converting the digital message into a sequence of pulses. Mapping is also frequently referred to as *pulse modulation* or *baseband modulation*, since it generates waveforms that have frequency spectra from DC to some specific finite frequency. Filtering is frequently used at this step to limit the frequency range used. There are some applications where pulse modulation is adequate to transmit the digital signal, such as fiber optic channels. However, for the majority of the communication systems, the modulation step is required. *Modulation*, frequently referred to as *bandpass modulation*, is the process of generating a signal with a specific frequency spectrum capable of carrying the pulse

modulated signal. The pulse modulated signal is enclosed within this generated signal in the form of predefined variations from a wave that has specific amplitude, frequency and phase characteristics. More detailed analysis will be provided in paragraph 4.5.3.

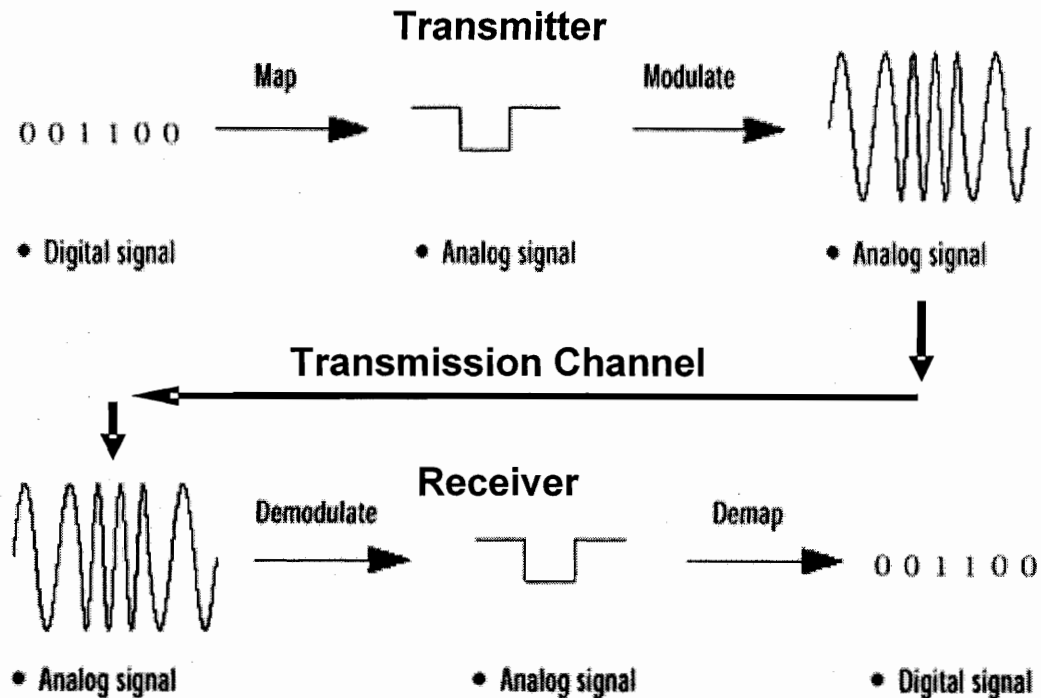


Figure 4.3: Traditional components of a digital communication system, [2]

The modulated signal propagates through the transmission channel and is recorded by the receiver. The signal processing steps executed at the receiver are essentially reversing the ones implemented at the transmitter. Detailed analysis of the various elements that compose the transmitter and receiver is provided in paragraph 4.5.

4.4 Mathematical models for communication channels

To facilitate the design of a digital communication system, its operation is frequently simulated using mathematical models of the transmission channel. Such models attempt to capture the most important characteristics of the channel. The simulations lead to more efficient and reliable designs for the transmitter and receiver, adjusted to deal with the limitations and make use of the good properties of the channel.

Depending on the application, a large variety of transmission media have been used for the propagation of the digital signals, such as the air, water, wires, optical fibers, and so on, varying the nature and efficient frequency range of the transmitted waves. Despite the fact that each combination of transmission medium and propagating wave presents different characteristics, they all have several common properties, such as all physical channels must obey wave propagation principles. To simulate these channels, several models have been proposed in the literature [3], from very simple to very complex. However, the most frequently used ones are the simplest models, since the uncertainty is very large due to the variability and unpredictability of the transmission path, which renders the elaborate models not practical for general use. In the following paragraphs, the three dominant and most general models are summarized. Frequently, the more elaborate models are refinements of these models that capture the special characteristics of a specific channel.

4.4.1. Additive White Gaussian Noise

The additive noise model of a communication channel is the simplest and probably the most powerful simulation technique. The applicability of the model is so broad that it has been incorporated even in the most elaborate communication channel models. According to this model, the received signal $y(t)$ is the superposition of the transmitted signal $x(t)$ and a random noise signal $n(t)$, as illustrated in Figure 4.4.

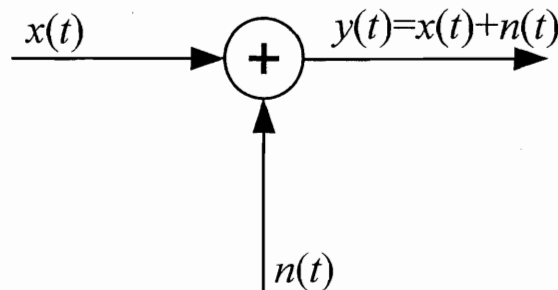


Figure 4.4: Additive Noise Model

The noise considered in this model refers to the total effect of several noise sources, such as the electrical circuit components, electromagnetic interference, ambient

noise, and so on. This noise is considered to follow a zero mean Gaussian distribution, according to the *central limit theorem*. According to this theorem, the probability distribution of the sum of j statistically independent and identically distributed random variables, with finite mean and variance values, approaches the Gaussian distribution as $j \rightarrow \infty$. Therefore, even though individual noise mechanisms might have other than Gaussian distribution, the cumulative effect of these mechanisms will tend toward the Gaussian distribution.

The noise considered in this model is also characterized as white, meaning that the power spectral density is the same for all frequencies of interest in most communication systems. It is apparent that there exists no globally white noise, or in other words there exists no noise that has the same amount of power for all frequencies. However, as long as the bandwidth of noise is significantly larger than that of the communication system, the noise can be considered to have an infinite bandwidth. Due to the “whiteness” of the noise, it can be shown that its individual samples are uncorrelated. It is important to observe at this point that, since the samples of noise are uncorrelated and follow the Gaussian distribution, they are also independent. The importance of this statement is that the noise affects each transmitted symbol independently.

The model resulting from this analysis is usually referred to as *Additive White Gaussian Noise* (AWGN) channel. An extension of this model includes the attenuation α of the channel as a percentage of the transmitted signal:

$$y(t) = \alpha \cdot x(t) + n(t) \quad (4.2)$$

4.4.2. Linear Time Invariant Filter

Most physical transmission channels impose distortion on the propagating wave. This distortion is frequently simulated mathematically with the use of a linear filter, $h(t)$, which attempts to encapsulate the characteristics of the channel. The result of the effect of the channel on the transmitted signal $x(t)$ is calculated as the convolution of the impulse response of the filter $h(t)$ with the transmitted signal $x(t)$. In most cases, additive white Gaussian noise is included in the model for better representation of the physical

channel. A pictorial representation of the Linear Time Invariant Filter model is provided in Figure 4.5.

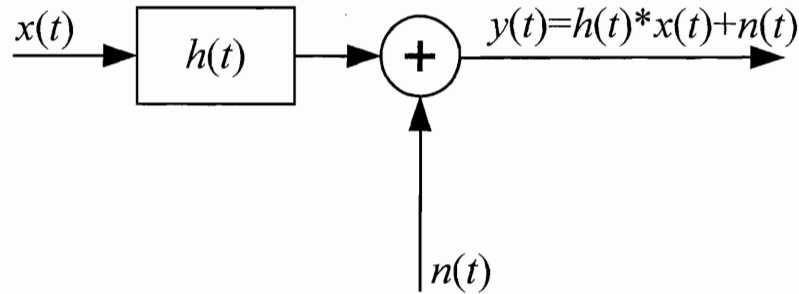


Figure 4.5: Linear time invariant filter model

4.4.3. Linear Time Variant Filter

Most physical channels present characteristics that vary with time, such as long range high altitude radio, underwater channels and so on. In these channels environmental conditions, such as temperature, interference from hovering or swimming objects and particles change their characteristics with time, mandating the use of time variant mathematical models for the simulation of their effect. For this reason, linear time variant filters $h(t, \tau)$ are employed to simulate the effect of the channel. The resulting signal $y(t)$ is calculated as the convolution of the transmitted signal $x(t)$ and the impulse response of the linear time variant filter $h(t, \tau)$, as illustrated in Figure 4.6. White Gaussian noise is frequently added to complete the effect of the channel. Here $h(t, \tau)$ is the response of the channel as time t for an impulse applied at time $t - \tau$, where the variable τ provide the time variance of the channel.

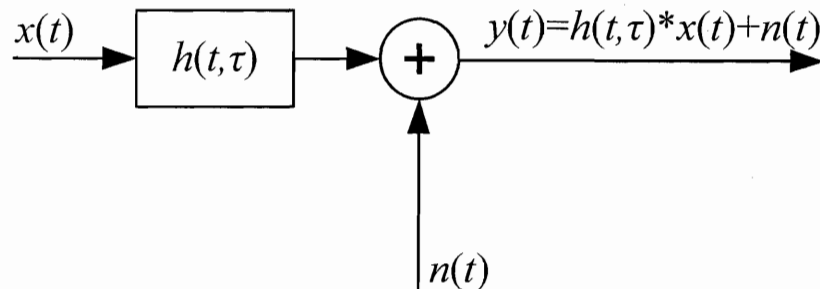


Figure 4.6: Linear time variant filter model

4.5 Digital Communication Techniques

In paragraph 4.3 the fundamental steps of a digital communication system were presented. However, depending on the severity of the channel imposed distortion of the received signal, a digital communication system may be composed of several signal processing steps, which aim to correct this distortion. A typical set of transmitter and receiver signal processing blocks is presented in Figure 4.7. In the following paragraphs a brief analysis of each component will be presented.

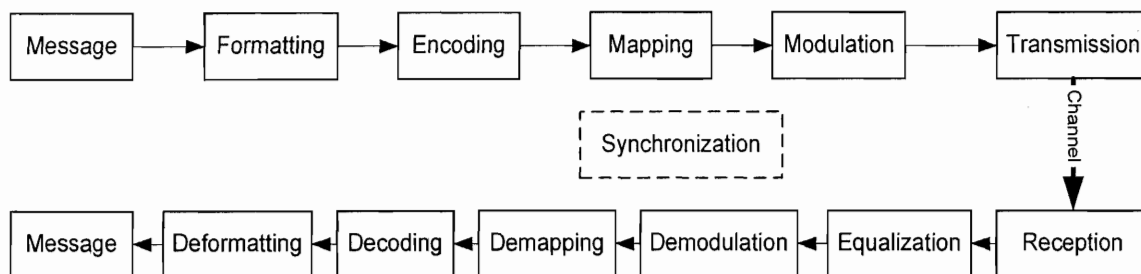


Figure 4.7: Common Signal Processing Steps of a Digital Communication System

4.5.1. Formatting

Formatting is the process of converting the message that needs to be transmitted in a form appropriate for digital processing. Thus, it is the first step in a digital communication system, where the text or numbers in the message are usually transformed into a stream of binary bits with the assistance of a standard coding format. The first formatting code was the Morse code, presented in Figure 4.1, while the first fixed length binary code for processing textual data was the Baudot code, illustrated in Figure 4.8, which was introduced in 1874 for use in the printing telegraph.

Binary value	Letters	Figures	Binary value	Letters	Figures
00011	A	-	10111	Q	1
11001	B	?	01010	R	4
01110	C	:	00101	S	BELL
01001	D	\$	10000	T	5
00001	E	3	00111	U	7
01101	F	!	11110	V	;
11010	G	&	10011	W	2
10100	H	STOP	11101	X	/
00110	I	8	10101	Y	6
01011	J	'	10001	Z	"
01111	K	(00000	n/a	n/a
10010	L)	01000	CR	CR
11100	M	.	00010	LF	LF
01100	N	,	00100	SP	SP
11000	O	9	11111	LTRS	LTRS
10110	P	0	11011	FIGS	FIGS

Figure 4.8: 5-Bit Baudot Code, [1]

Nowadays, there exist several coding formats that are used in digital communications, such as American Standard Code for Information Interchange (ASCII), the Extended Binary Coded Decimal Interchange Code (EBCDIC), Baudot, and Hollerith, to name a few. The most commonly used is the 7-bit ASCII code capable of describing 128 different characters, see Figure 4.9, whereas the EBCDIC is extensively used by IBM systems. The formatting process is essentially reversed at the final signal processing step of the receiver, in order to recover the original message.

Bits	5	0	1	0	1	0	1	0	1
	6	0	0	1	1	0	0	1	1
1 2 3 4	7	0	0	0	0	1	1	1	1
0 0 0 0	NUL	DLE	SP	0	@	P	'	p	
1 0 0 0	SOH	DC1	!	1	A	Q	a	q	
0 1 0 0	STX	DC2	"	2	B	R	b	r	
1 1 0 0	ETX	DC3	#	3	C	S	c	s	
0 0 1 0	EOT	DC4	\$	4	D	T	d	t	
1 0 1 0	ENQ	NAK	%	5	E	U	e	u	
0 1 1 0	ACK	SYN	&	6	F	V	f	v	
1 1 1 0	BEL	ETB	'	7	G	W	g	w	
0 0 0 1	BS	CAN	(8	H	X	h	x	
1 0 0 1	HT	EM)	9	I	Y	i	y	
0 1 0 1	LF	SUB	*	:	J	Z	j	z	
1 1 0 1	VT	ESC	+	;	K	[k	{	
0 0 1 1	FF	FS	,	<	L	\	l		
1 0 1 1	CR	GS	-	=	M]	m	}	
0 1 1 1	SO	RS	.	>	N	^	n	~	
1 1 1 1	SI	US	/	?	O	_	o	DEL	

NUL	Null, or all zeros	DC1	Device control 1
SOH	Start of heading	DC2	Device control 2
STX	Start of text	DC3	Device control 3
ETX	End of text	DC4	Device control 4
EOT	End of transmission	NAK	Negative acknowledge
ENQ	Enquiry	SYN	Synchronous idle
ACK	Acknowledge	ETB	End of transmission
BEL	Bell, or alarm	CAN	Cancel
BS	Backspace	EM	End of medium
HT	Horizontal tabulation	SUB	Substitute
LF	Line feed	ESC	Escape
VT	Vertical tabulation	FS	File separator
FF	Form feed	GS	Group separator
CR	Carriage return	RS	Record separator
SO	Shift out	US	Unit separator
SI	Shift in	SP	Space
DLE	Data link escape	DEL	Delete

Figure 4.9: 7-Bit American Standard Code for Information Interchange (ASCII), [4]

The process of converting the output of a digital or analog source into a sequence of binary digits is called *source encoding*. Analog signals are frequently converted into digital form so as to be processed and transmitted more efficiently. For this reason, the analog signal must be sampled at an appropriate rate. The sampling frequency must be at least twice the maximum frequency represented by the analog signal according to the *Nyquist theorem*. Signals sampled below the Nyquist frequency are subject to *aliasing*, which is an effect that causes different continuous signals to become indistinguishable. Digital representation of analog signals is outside the scope of this research.

4.5.2. *Encoding*

Since the communication channel distorts the propagating signal, it is possible that one or more bits may be identified incorrectly by the receiver. In anticipation of faulty transmission, digital communication systems employ an encoding scheme to identify and potentially correct any erroneous transmitted bits. The purpose of the encoder is to add some redundant bits in the transmitted signals that would allow the receiver to identify these erroneous bits and possibly correct them. There exist several categories of encoders, which, according to the complexity of the algorithm, allow identifying if there is an error at the received signal, where is the error at the received signal, and even to correct this error. The two main categories of error control codes are the *Block*, and *Convolutional* codes. This section is mainly focused on linear block codes and more specifically on *Reed-Solomon* codes, since they are used in the proposed system, due to simple implementation, low computational complexity and robustness. The three essential elements that describe any block codes are: the number of information input bits k , the number of encoded output bits n , and a generator matrix or polynomial. In what follows a brief description of the linear block codes is presented.

According to the linear block code algorithm, a specific number of bits are added in a block of k bits of the original signal, forming a new extended series of bits, the *code words*. A block code consists of a collection of such code words with fixed length n , which corresponds to the number of included elements. In a binary block code of length n there are 2^n possible code words. From these 2^n code words the $M = 2^k$ may be selected to form a code ($k < n$). Therefore, a block of k information bits is mapped into a code word

of length n , selected from the set of $M = 2^k$ code words. The resulting block code is referred to as (n,k) code and the ratio $k/n = R$ is the ratio of the code. The elements of a code word are selected from an alphabet of q symbols. The $q = 2$ case corresponds to a binary code and the elements of the code words are bits 0 and 1. In the non-binary case where the number of symbols corresponds to a power of 2, $q = 2^b$, where b is a positive integer, each symbol has an equivalent binary representation consisting of b bits. In this case, a non-binary code of length N can be represented with a binary code of length $n = bN$. Another important parameter of a code word is its *weight*, which corresponds to the number of nonzero elements that it contains. Each code word in a block code has its own weight and the collection of all the weights compose the weight distribution of the code. The apparent categorization emerges at this point, which separates the codes into *fixed weight* codes, when all the code words have the same weight, and *variable weight* codes.

The encoding and decoding signal processing steps involve addition and multiplication operations performed on the code words. These operations are performed according to the conventions of the algebraic field to which the elements of the used alphabet belong to. These fields are comprised from a limited, finite, number of elements q and are generally called *Galois fields*, $GF(q)$. In order to construct a $GF(q)$, q must be a prime number or a power of a prime, $q = p^m$, integer number larger than 1. The arithmetic operations of this field are defined as modulo q . If $q = p^m$, where p is a prime number and m is any positive integer, it is possible to extend the field $GF(p)$ to the field $GF(p^m)$, where the addition and multiplication operations are based on modulo p arithmetic. The basic properties for these arithmetic operations for a Galois Field F are described as follows:

Addition

1. *Closed* $a, b \in F \Rightarrow a + b \in F$
2. *Associative* $a, b, c \in F \Rightarrow (a + b) + c = a + (b + c)$
3. *Commutative* $a + b = b + a$
4. *The set F contains a zero element:* $a + 0 = a, \forall a \in F$

5. Every element in F has its own negative element, i.e. the negative element of a is $-a$ and it holds that $a + (-a) = 0$

Multiplication

1. Closed $a, b \in F \Rightarrow a \cdot b \in F$
2. Associative $a, b, c \in F \Rightarrow (a \cdot b) \cdot c = a \cdot (b \cdot c)$
3. Commutative $a \cdot b = b \cdot a$
4. Distributive over addition $(a + b) \cdot c = a \cdot c + b \cdot c$
5. The set F contains an identity element: $a \cdot (1) = a, \forall a \in F$
6. Every element of F , except zero, has an inverse, $a \cdot a^{-1} = 1$

An important parameter of a block code is the distance among the various code words, frequently referred to as *Hamming distance*. If C_i and C_j are two code words of a (n,k) block code, the distance d_{ij} , is the number of corresponding elements in which they differ. The Hamming distance satisfies the condition $0 \leq d_{ij} \leq n$, whereas of importance is the minimum distance among all the code words, denoted d_{min} . Since the Hamming distance is a measure of the separation between pairs of code words, it is related to the cross correlation coefficient between corresponding pairs of waveforms generated from the code words. It can be understood that it is desirable to maximize the minimum distance of the code words in order to increase their separation and be able to distinguish as much as possible the different transmitted waveforms, or in other words reduce their detection ambiguity. The block code is linear if and only if $a_1C_i + a_2C_j$ is also a code word, where a_1 and a_2 are any two elements from the alphabet. This definition implies that a linear code must contain the all-zero element code word, since for any code word C_i it holds that $C_i = C_i + C_0$, where C_0 represents the zero code word. However the zero code word has zero weight, as a consequence of which it is concluded that a constant weight code is always non-linear. The weight of the code word is very important because the distance between two code words of the same code is simply the weight of the code word formed from the difference of the two code words, which in the current case is also a code word since the code is considered linear. Therefore, the weight distribution of a linear block code completely characterizes the distance properties of the code.

Furthermore, excluding the weight of the all-zero element code word, the minimum distance is equal to the weight of the code word with the smaller weight.

The aforementioned code words are generated by simply multiplying blocks of information with the generator matrix of the code. On the receiver side, the recorded code words are multiplied with a parity check matrix to detect any potential errors, and the initial multiplication is reversed to reveal the original information block. This brief description of the complete encoding process is described in more detail in what follows.

Assume that $x_{m1}, x_{m2}, \dots, x_{mk}$ are a block of k information bits to be encoded into the code word C_m with n elements $c_{m1}, c_{m2}, \dots, c_{mn}$. In a linear block code the encoding operation is represented by a set of n equations of the form:

$$c_{mj} = x_{m1}g_{1j} + x_{m2}g_{2j} + \dots + x_{mk}g_{kj}, \text{ where } j = 1, 2, \dots, n \quad (4.3)$$

The g_{ij} represent elements of the generator of the code, which for the binary case take the values 0 or 1. It is frequently convenient to describe the complete operation in vector form as follows:

$$X_m = [x_{m1} \quad x_{m2} \quad \dots \quad x_{mk}] \quad (4.4)$$

$$C_m = [c_{m1} \quad c_{m2} \quad \dots \quad c_{mn}] \quad (4.5)$$

$$C_m = X_m \underline{G} \quad (4.6)$$

where \underline{G} is a $k \times n$ matrix which contains all the elements of the generator of the code, hence called the *generator matrix*:

$$\underline{G} = \begin{bmatrix} g_{11} & g_{12} & \dots & g_{1n} \\ g_{21} & g_{22} & \dots & g_{2n} \\ \vdots & \vdots & \ddots & \vdots \\ g_{k1} & g_{k2} & \dots & g_{kn} \end{bmatrix} \quad (4.7)$$

It can be shown that the linear (n,k) code with 2^k code words is a subspace of dimension k . As a consequence, the rows of the generator matrix \underline{G} must be linearly independent, meaning that they span a subspace of k dimensions, or in other words the rows constitute a basis of the code. The basis vectors of this space are not unique, having as a consequence that the generator matrix \underline{G} is not unique. Moreover, since k is the dimension of the subspace considered, the rank of \underline{G} is also k .

To simplify the implementation, a *systematic code* is desired, having code words with the first k information symbols unchanged followed by $n - k$ check symbols. The generator matrix then takes the form:

$$\underline{G} = [\underline{I}_k | \underline{P}] = \begin{bmatrix} 1 & 0 & \dots & 0 & p_{11} & p_{12} & \dots & p_{1n-k} \\ 0 & 1 & \dots & 0 & p_{21} & p_{22} & \dots & p_{2n-k} \\ \vdots & \vdots & \ddots & \vdots & \vdots & \vdots & \ddots & \vdots \\ 0 & 0 & \dots & 1 & p_{k1} & p_{k2} & \dots & p_{kn-k} \end{bmatrix} \quad (4.8)$$

where \underline{I}_k is the $k \times k$ identity matrix and \underline{P} is a $k \times (n - k)$ matrix that determines the $n - k$ redundant bits or *check parity bits*. A non-systematic code can be transformed into a systematic one by elementary row and column operations on the generator matrix. The non-systematic linear code and the resulting systematic code are frequently called *equivalent codes*.

Associated with any linear (n, k) code is the dual code of dimension $n - k$. The dual code is a linear $(n, n - k)$ code with 2^{n-k} code vectors, which corresponds to the null space of the (n, k) code. The generator matrix for the dual code, \underline{H} , consists of $n - k$ linearly independent code vectors selected from the null space. Any code word C_m of the (n, k) code is orthogonal to any code word in the dual code. Hence, any code word of the (n, k) code is orthogonal to every row of matrix \underline{H} :

$$C_m \underline{H}^T = \underline{0} \quad (4.9)$$

where $\underline{0}$ is an all zero row vector with $n - k$ elements. Since equation (4.9) holds for every code word C_m of the (n, k) code, it follows due to (4.6) that

$$\underline{G} \underline{H}^T = \underline{0} \quad (4.10)$$

where $\underline{0}$ is a $k \times (n - k)$ zero matrix. If the code is systematic, from equation (4.10) the matrix \underline{H} takes the form:

$$\underline{H} = [-\underline{P}^T | \underline{I}_{n-k}] \quad (4.11)$$

The negative sign in equation (4.11) may be dropped when binary codes are considered, since modulo-2 subtraction is equivalent to modulo-2 addition.

The matrix \underline{H} , called *parity check matrix*, is used to assist the error control algorithm at the decoding process. During this process the block of n bits recorded by the receiver need to be associated with a transmitted code word from the set of $M = 2^k$

possible code words. The code word that presents the shortest Hamming distance to the received block of bits is selected. Assuming that Y represents the block of the n received bits and C_m is the actual transmitted code word, Y takes the form:

$$Y = C_m + E \quad (4.12)$$

where E is the corresponding error vector, which is the zero vector if the received bits contain no errors. The *Syndrome of the Error Pattern* is defined as:

$$Y \underline{H}^T = (C_m + E) \underline{H}^T = C_m \underline{H}^T + E \underline{H}^T = 0 + E \underline{H}^T = E \underline{H}^T = S \quad (4.13)$$

The $(n - k)$ sized vector S has components that are zero for all parity check equations that are satisfied and nonzero for those not satisfied. Therefore, S contains a pattern of failures in the parity checks. It is important to recognize that the syndrome is a characteristic of the error pattern and not of the transmitted code word. Furthermore, the use of syndrome cannot correct all potential errors, since there exist 2^n potential error patterns and only 2^{n-k} syndromes, having as a consequence that different error patterns may result in the same syndrome. All the potential combinations of transmitted code words along with the corresponding errors are presented in an array of the form:

$$\begin{array}{ccccc} 0 & C_2 & C_3 & \dots & C_{2^k} \\ E_2 & C_2 + E_2 & C_3 + E_2 & \dots & C_{2^k} + E_2 \\ E_3 & C_2 + E_3 & C_3 + E_3 & \dots & C_{2^k} + E_3 \\ \vdots & \vdots & \vdots & \ddots & \vdots \\ E_{2^{n-k}} & C_2 + E_{2^{n-k}} & C_3 + E_{2^{n-k}} & \dots & C_{2^k} + E_{2^{n-k}} \end{array} \quad (4.14)$$

This array is called *standard array* and is constructed by distributing at the columns all the potential code words and at the rows all the potential error patterns. It is considered that the C_1 corresponds to the all zero code word and E_1 corresponds to the all zero error pattern. It can be seen from equation (4.13) that all potential combinations at each row of the standard array have the same syndrome, since S depends only on the error pattern. The first column of the standard array represents the minimum weight error pattern. For received block of bits Y , the syndrome calculated according to equation (4.13) as $S = Y \underline{H}^T$ is associated to the most likely error vector from the first column of the standard array, E_m . The estimated transmitted code word is recovered from the received signal then:

$$\hat{C}_m = Y + E_m \quad (4.15)$$

It is important to note that the properties of the parity check matrix \underline{H} define an upper limit on the minimum distance that can be achieved by a linear block code (n,k) . The product $C_m \underline{H}^T$ with $C_m \neq \mathbf{0}$ represents a linear combination of the n columns of \underline{H} . Since $C_m \underline{H}^T = \mathbf{0}$, the columns of \underline{H} are linearly dependent. The minimum weight code word C_{min} , should also satisfy the condition $C_{min} \underline{H}^T = \mathbf{0}$. Since minimum weight corresponds to minimum distance, it follows that d_{min} number of the columns of \underline{H} are linearly dependent, or in other words there are no more than $d_{min} - 1$ linearly independent columns of \underline{H} . Since the rank of \underline{H} is at most $n - k$, it follows that $n - k \geq d_{min} - 1$. Therefore, the upper bound of the minimum distance is

$$d_{min} \leq n - k + 1 \quad (4.16)$$

The aforementioned procedures correspond to a general description of all the linear error control block codes. There exist several variations and subcategories of the linear block codes, each one employing different code word generators to produce a set of code words with specific properties. A diagram of the categorization of the linear block codes is presented in Figure 4.10.

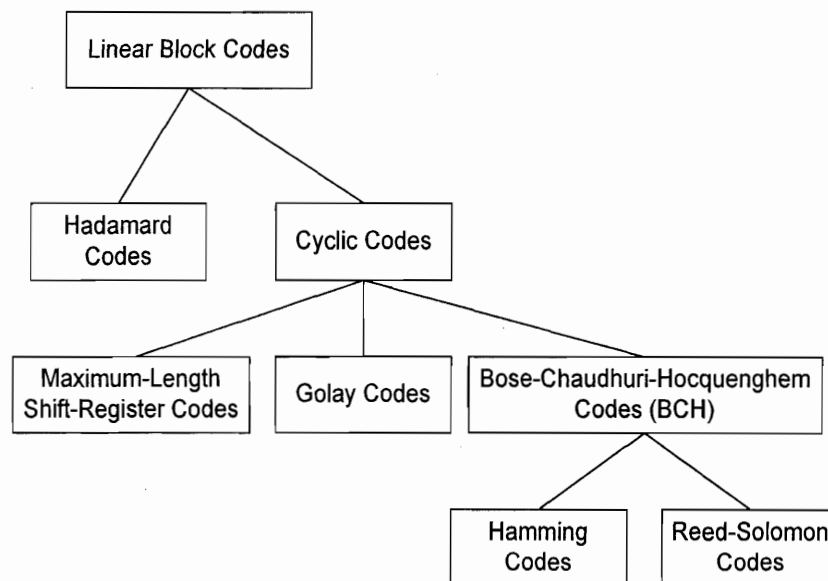


Figure 4.10: Linear Block Codes

A *Hadamard code* is obtained by selecting as code words the rows of a Hadamard matrix. A Hadamard matrix \underline{M} is an $n \times n$ matrix of zeros and ones with the property that

any row differs from any other row in exactly $\frac{1}{2}n$ positions, where n is an even integer.

One row of the matrix contains all zeros, and the others contain $\frac{1}{2}n$ zeros and $\frac{1}{2}n$ ones.

Cyclic codes are a subset class of linear codes that satisfy a cyclic shift property. If $C = [c_1, c_2, \dots, c_n]$ is a code word of a cyclic code, then $[c_n, c_1, c_2, \dots, c_{n-1}]$ obtained by a cyclic shift of the elements of C , is also a code word. As a consequence of the cyclic property, the codes possess a considerable amount of structure, which can be exploited in the encoding and decoding process. When dealing with cyclic codes it is convenient to associate with a code word $C = [c_{n-1}, c_{n-2}, \dots, c_1, c_0]$ a polynomial $C(p)$ of degree $\leq n - 1$, defined as

$$C(p) = c_{n-1}p^{n-1} + c_{n-2}p^{n-2} + \dots + c_1p + c_0 \quad (4.17)$$

For a binary code each of the coefficients of the polynomial are either zero or one. It is possible to create a cyclic linear block code by using a *generator polynomial*, $g(p)$, of degree $n - k$, and has the form:

$$g(p) = p^{n-k} + g_{n-k-1}p^{n-k-1} + \dots + g_1p + 1 \quad (4.18)$$

The generator matrix can be constructed from the generator polynomial by assigning the coefficients of the polynomial at the corresponding positions denoted by the power of the polynomial for the first row and cycling around all the possible combinations for the rest of the rows.

The *Golay code* is a (23,12) code, with $d_{min} = 7$, described by a generator polynomial of the form $g(p) = p^{11} + p^9 + p^7 + p^6 + p^5 + p + 1$.

The *Maximum length shift register codes* are a class of cyclic codes with $(n,k) = (2^m - 1, m)$, where m is a positive integer.

The *Bose-Chaudhuri-Hocquenghem (BCH) codes* comprise a large class of cyclic codes that in the binary form are constructed according to the parameters $n = 2^m - 1$, $n - k \leq mt$ and $d_{min} = 2t + 1$.

The *Hamming codes* are a class of codes with the property that $(n,k) = (2^m - 1, 2^m - 1 - m)$, where m is any positive integer. The parity matrix of a binary Hamming code consists of $n = 2^m - 1$ columns, having all possible binary vectors with $n - k = m$ elements, except the all zero vector. An important property is that no two

columns of the parity matrix are linearly dependent. However, for $m > 1$, it is possible to find three columns that add to zero, limiting the minimum distance $d_{min} = 3$.

Finally, the *Reed-Solomon Codes* are a very powerful non-binary linear block error control codes very frequently used in digital communication systems. Assuming that the code words are selected from an alphabet of $q = 2^k$ symbols, such that k information bits are mapped into one of the q symbols, the length of the code is denoted by

$N = q - 1 = 2^k - 1$, and the number of information symbols encoded into a block of N symbols is denoted by $K = 1, 2, 3, \dots, N$. The minimum distance among the code words is $D_{min} = N - K + 1$, which corresponds to the maximum value for D_{min} that can be achieved according to (4.16), and the rate of the code is $R = K / N$. The generator polynomial of the Reed-Solomon codes is:

$$G(p) = (p - a)(p - a^2) \dots (p - a^{N-K})$$

where the term a is the N th root of 1, i.e. $a^N = 1$ in $GF(q)$, and $a^i \neq 1$ for $1 \leq i \leq N - 1$.

The weight distribution of the Reed-Solomon codes is provided by:

$$A_i = \binom{N}{i} (q-1) \sum_{j=0}^{i-D_{min}} (-1)^j \binom{i-1}{j} q^{i-j-D_{min}} \quad \text{with } i \geq D_{min} \quad (4.19)$$

The Reed-Solomon code is guaranteed to correct up to

$$t = \frac{1}{2}(D_{min} - 1) = \frac{1}{2}(N - K) \quad (4.20)$$

symbol errors. Finally, the symbol error correcting probability is given by:

$$P_E \approx \frac{1}{2^k - 1} \sum_{j=t+1}^{2^k-1} j \binom{2^k-1}{j} P_s^j (1 - P_s)^{2^k-1-j} \quad (4.21)$$

where P_s is the symbol error probability.

Due to the great minimum distance characteristics and the efficient algorithms that exist for the implementation of large codes, the Reed-Solomon codes are capable of correcting not only isolated erroneous symbols, but also bursts of errors. Moreover, the implementation of the generator matrix guarantees the correction of symbols up the value t defined in equation (4.20). It becomes apparent that the Reed-Solomon codes are more efficient when the subtraction of $N - K$ provides an even number.

A convolutional code is generated by passing the information sequence to be transmitted through a linear finite state shift register. A convolutional code is described by three parameters, n , k , and K , where k is the number of data bits to be encoded, n is the length of the encoded message, which it does not correspond to a code word, and K is the constraint length representing the number of k bit series in the encoding shift register, memory of the encoder. An important distinctive characteristic of the convolutional codes with respect to block codes is that the encoder has memory, meaning that the series of n bits generated by the convolutional encoding procedure is not only a function of the input k information bits, but is also a function of the previous $K - 1$ input k bit series. In order to control the complexity of a convolutional code the n and k are usually small integers and K is varied to control the capabilities of the code. A special powerful subcategory of the convolutional codes is the *Turbo Codes*, which are essentially two or more parallel concatenated convolutional codes. In this way it is possible to achieve the error correction capability of much longer codes by using small, relatively simple, convolutional codes. For further discussion and detailed description of the block and the convolutional codes the reader should refer to [3] and [4].

The selection and use of an encoding algorithm requires the balance of quite a few parameters, since encoding introduces several trade-offs. First of all, the fact that encoding adds redundant bits to the transmitted message means that either the effective bit rate will be lower, or additional bandwidth will be required to preserve the same bit rate. In accordance with the above, the encoding algorithm provides better performance at lower signal power levels, or E_b / N_0 , at the cost of additional bandwidth. There exist channels where the additional bandwidth will result in a great penalty in the digital performance of the communication systems, i.e. channels in the bandwidth limited region, as described in paragraph 4.6. It becomes apparent that the limitations of the application in bit rate and available power, as well as the limitations of the channel in terms of bandwidth dictate the selection of the parameters of the encoding algorithm. In cases of very demanding applications for high rate real-time communication in bandwidth limited channels, the use of *Trellis Coded Modulation* error control technique may be appropriate, since it does not require higher bandwidth or increased bit rates at the expense of limited error correction capabilities and increased computational

complexity. It must be understood that the error correcting capability of all the codes is limited, usually intimately related to the code rate. If the number of errors in the received signal exceeds the error correcting capability of the code, it is not necessary that the decoded signal will contain fewer errors than the received signal. In cases with excessive received errors, i.e. very low E_b / N_0 , digital communication systems using encoding algorithms have presented worse performance than ones without error correction, due to the embedded redundant symbols. In other words the longer transmitted sequences result in increased number of errors. Turbo codes have been proven to present better performance than other error correcting algorithms in cases of low E_b / N_0 .

4.5.3. Mapping & Modulation

In order to transmit the data over a physical channel it is necessary to convert it to a waveform shape that can be easily realized with the use of antennae and is compatible with the characteristics of the channel. In real life systems, direct transmission of digital bits is not feasible since the communication is implemented with signals of some short, electrical, optical, acoustical, and so on. The *mapping* process is responsible for converting the digital information into analog pulse shaped waveforms. Mapping is also frequently referred to as *pulse modulation* or *baseband modulation*, since it generates waveforms that have frequency spectra from DC to some specific finite frequency. However, most physical channels mandate the use of waveforms of certain structure, with limited amplitude and bandwidth, to match the channel's characteristics. Moreover, the transmission of pulse signals with physical systems, such as antennae, would require very large structures and is not efficient for long ranges. Finally, due to the increasingly demanding modern applications, the high required data rates, and the simultaneous transmission at the same channel, usually denoted as *multiple access*, are not realizable with pulse waveform signals. Such tasks are implemented by using sinusoid waves, modulated accordingly from the pulse shaped waveform, called *carrier waves*.

In modern digital communication systems, the steps of mapping and modulation are frequently combined into a single step. In a broad sense, the process of mapping and modulation is performed by taking blocks of $k = \log_2 M$ binary digits at a time from the information sequence and selecting one of $M = 2^k$ deterministic, finite energy waveforms

$\{s_m(t), m = 1, 2, \dots, M\}$ for transmission over the channel. When the mapping from the digital sequence to analog waveforms is performed under the constraint that a waveform transmitted at any time interval depends on one or more previously transmitted waveforms, the modulator is said to have *memory*. On the other hand, when mapping from the data sequence to waveforms is performed without any constraint from previously transmitted waveforms, i.e. the transmitted waveform depends only on the data sequence under consideration, the modulator is called *memoryless*. This section is focused to memoryless procedures, since they were selected to be used for the proposed system, due to potential carryon errors at the demodulation process.

In digital communications, the terms *demodulation* and *detection* are often used interchangeable, although demodulation emphasizes waveform recovery and detection entails the process of symbol decision. When the receiver exploits knowledge of the carrier's phase to detect the signals, the process is called *coherent detection*, whereas in the opposite case the process is called *non-coherent detection*. In ideal coherent detection, the receiver has a prototype of all possible arriving signals. These prototype waveforms attempt to duplicate the transmitted signal set in every respect, including phase. The receiver is then said to be *phase locked* to the incoming signal. During demodulation, the receiver correlates the incoming signal with each of its prototype replicas and decides on the best match. Non-coherent demodulation refers to systems that employ demodulators designed to operate without knowledge of the absolute value of the incoming signal's phase, eliminating the need for phase estimation existing in coherent systems. The advantage of non-coherent over coherent systems is reduced complexity at the cost of increased error probability. However, in transmission channels that significantly affect the phase of the propagating signal coherent receivers suffer from incorrect estimation of the phase of the signal, resulting in significant loss of performance.

Baseband Modulation

The most basic and straightforward conversion of digital data to analog signal is achieved with pulse modulation. When pulse modulation is applied in binary symbols, the resulting waveform is called *pulse code modulation* (PCM) waveform. When pulse modulation is applied to non-binary symbols, the resulting waveform is called *M*-ary

pulse modulation waveform, of which there exist several types, such as *pulse amplitude modulation* (PAM), *pulse position modulation* (PPM), and *pulse duration modulation* (PDM) or *pulse width modulation* (PWM). Even though the title of each method is almost self explanatory, analysis of these methods is beyond the scope of this text. Figure 4.11 provides a pictorial view of the various forms of pulse coded modulation. The pulse coded modulation is the most frequently used baseband modulation type. It is separated into four major categories, namely non-return to zero (NRZ), return to zero (RZ), phase encoded, and multilevel binary. The NRZ group is the most commonly used PCM waveform. According to the NRZ-L, for *level*, which is extensively used in digital logic circuits, a binary one is represented by one level and a binary zero is represented by another level. There is a change in level whenever the data change from a one to zero and vice versa. With NRZ-M, for *mark*, a change in level happens only when a binary one is represented and no change in level happens for a zero. Complementary to NRZ-M is the NRZ-S, for *space*, case. The return-to-zero (RZ) waveforms are consisted from the unipolar-RZ, bipolar-RZ, and RZ-AMI, for *alternate mark inversion*. This category of PCM is frequently used in communication systems involving magnetic recording. Their main characteristic is that the pulse always returns to zero after taking its corresponding value. In unipolar-RZ, a one is represented by a half-bit wide pulse and a zero is represented by the absence of the pulse, in contrast with bipolar-RZ where the ones and zeros are represented by opposite level half-bit wide pulses. The RZ-AMI is a signaling scheme used in telephone systems, where the ones are represented by equal amplitude alternating pulses and zeros are represented by the absence of pulses. The phase encoded group has four variations, the bi-phase level (bi- ϕ -L), bi-phase mark (bi- ϕ -M), the bi-phase space (bi- ϕ -S), and the delay modulation. According to bi- ϕ -L, a half-bit wide pulse positioned during the first half of the bit interval represents a one, and positioned at the second half of the bit interval represents a zero. With bi- ϕ -M and bi- ϕ -S, similarly to the NRZ case, the half-bit wide pulse happens only when a one or zero appears respectively and no change happens otherwise. With delay modulation, a change in level happens at the middle of the bit interval only when there is a change in the bit sequence from a zero to one and at the end of the bit interval when there is a change from one to zero. No change in level happens for consecutive bits of the same value. According to the

dicode-NRZ the one to zero or zero to one data transition changes the pulse polarity, while without data transition the zero level is sent. Finally, with the dicode-RZ the one to zero and zero to one transition produces half duration polarity change, where otherwise the zero level is sent.

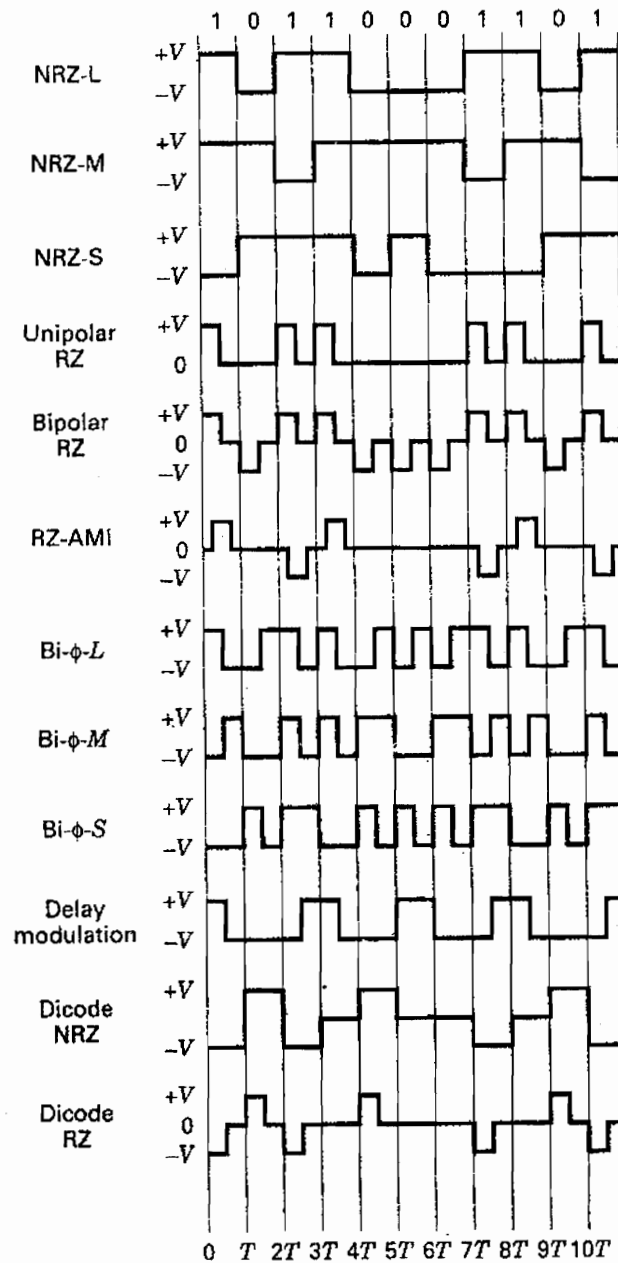


Figure 4.11: Pulse coded modulation waveforms, [4]

The special characteristics of each one of the pulse code modulation methods define the suitability for their use at digital communication systems. For example, modulation schemes which eliminate the use of DC signals are suitable for applications with little sensitivity to low frequency signals, such as magnetic recording systems. Applications requiring rigorous synchronization may benefit from methods like bi- ϕ -L that includes a transition at the middle of every bit transmitted. Other schemes provide inherently error detection, data compression capabilities, or immunity to noise due to their structure, such as the NRZ waveforms.

Bandpass Modulation

Bandpass modulation is the process where the amplitude, frequency or phase of a sinusoidal wave, or a combination of them, is varied in accordance with the information to be transmitted. The general form of the carrier wave is:

$$s(t) = a(t) \cos[\omega_c t + \phi(t)] \quad (4.22)$$

The signal $a(t)$ corresponds to the amplitude of the signal, ω_c is the angular frequency, and $\phi(t)$ is the phase of the carrier wave. Depending on the type of modulation method, the flow of information symbols controls the value of $a(t)$ or $\phi(t)$. Thus, amplitude modulation adjusts the value of $a(t)$ while phase and frequency modulation methods control the instantaneous phase $\omega_c t + \phi(t)$ and the instantaneous frequency $\omega(t) = \omega_c + d\phi(t)/dt$ of the signal respectively. The frequency in hertz f_c is very often used instead of the angular frequency ω_c , with $\omega_c = 2\pi f_c$.

Amplitude shift keying (ASK) is the modulation method where the amplitude $a(t)$ is adjusted to describe the information data. The phase term $\phi(t)$ is constant and can be considered equal to zero. The signal waveform (4.22) is written as:

$$s_m(t) = A_m g(t) \cos(2\pi f_c t) \quad (4.23)$$

with $m = 1, 2, \dots, M$ and $0 \leq t \leq T$ and where A_m denote the set of M possible amplitudes corresponding to the $M = 2^k$ possible k bit blocks of symbols. The signal amplitudes A_m take the discrete values:

$$A_m = (2m - 1 - M)d \quad (4.24)$$

where $2d$ is the distance between adjacent signal amplitudes. The waveform $g(t)$ is a real valued signal pulse whose shape influences the spectrum of the transmitted signal. The time $T = k/R$ is the symbol interval, where $T_b = 1/R$ is the bit interval. The symbol interval is the reciprocal of the symbol rate, which corresponds to the rate at which changes occur in the amplitude of the carrier to reflect the transmission of new information. In the special case of $M = 2$, corresponding to binary modulation, ASK waveforms have the special property that $s_1(t) = -s_2(t)$, thus the two signals have the same energy and a cross correlation coefficient of -1 , which characterizes them as *antipodal* signals.

The mapping of k information bits to the $M = 2^k$ possible signal amplitudes is most frequently implemented with the assistance of the *Gray encoding*, according to which adjacent signal amplitudes differ by one binary digit, as illustrated in Figure 4.12. This bit assignment is very effective, since most likely errors caused by noise involve erroneous selection of adjacent amplitude to the transmitted signal amplitude. With gray encoding, such a case, results in only one bit error in the k -bit sequence. A representative ASK waveform is presented in Figure 4.13.

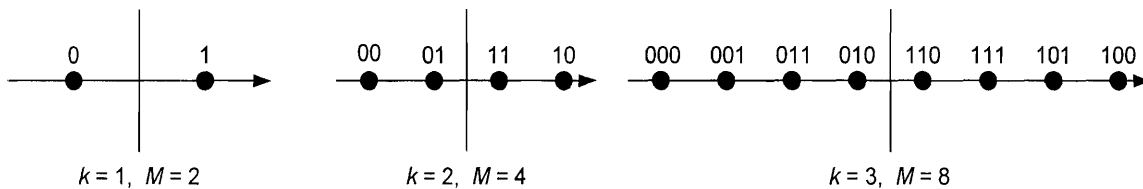


Figure 4.12: ASK signal constellation

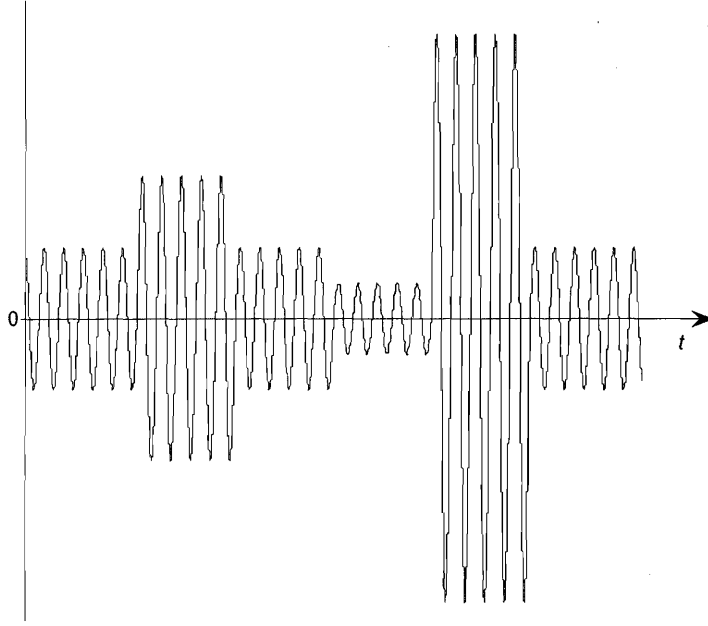


Figure 4.13: ASK waveform

Phase shift keying (PSK) is the modulation method according to which the phase of the signal is adjusted with the introduction of every new information symbol. The signal waveform (4.22) is written as:

$$s_m(t) = g(t) \cos \left[2\pi f_c t + \frac{2\pi}{M}(m-1) \right] \quad (4.25)$$

with $m = 1, 2, \dots, M$ and $0 \leq t \leq T$ and where $g(t)$ is the signal pulse shape and $\phi(t) = 2\pi(m-1)/M$ are the M possible phase states of the carrier that convey the transmitted information. The signal constellations for PSK waveforms for $M = 2, 4$, and 8 are presented in Figure 4.14. It is interesting to notice that for the binary case, $M = 2$, the PSK signal constellation is identical to the binary ASK. A representative PSK waveform is presented in Figure 4.15.

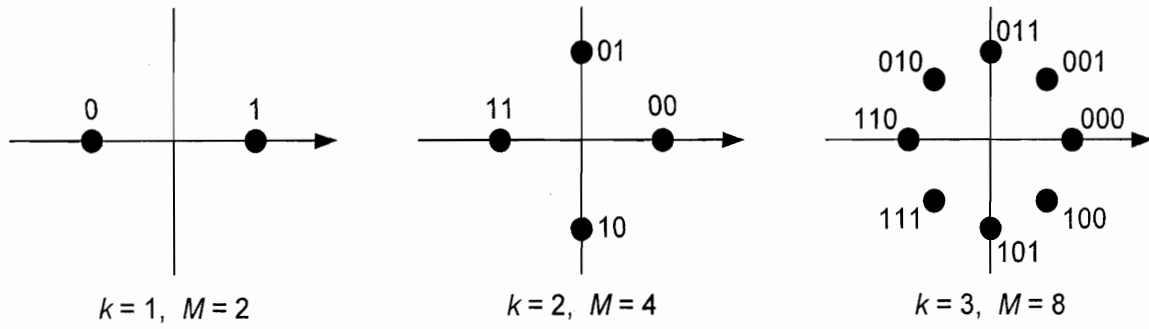


Figure 4.14: PSK Signal Constellations

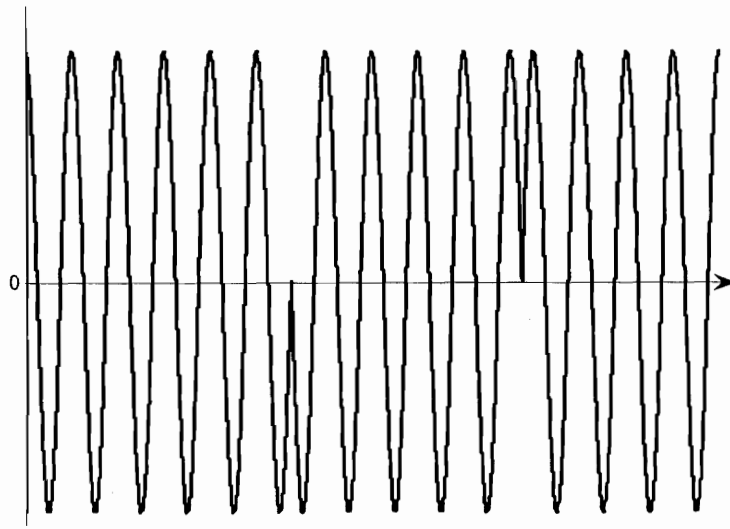


Figure 4.15: PSK waveform

In *Quadrature amplitude modulation* (QAM) both the amplitude and phase of the transmitted signal are adjusted to carry the digital information, resulting essentially in double the bandwidth efficiency. According to this method, two separate k bit symbols are transmitted on two quadrature carriers $\cos(2\pi f_c t)$ and $\sin(2\pi f_c t)$. The corresponding waveform is written as:

$$s_m(t) = A_{mc} g(t) \cos(2\pi f_c t) - A_{ms} g(t) \sin(2\pi f_c t) \quad (4.26)$$

with $m = 1, 2, \dots, M$ and $0 \leq t \leq T$ and where A_{mc} and A_{ms} are the information bearing signal amplitudes of the quadrature carriers and the $g(t)$ is the signal pulse shape. Alternatively QAM waveforms can be expressed as:

$$s_m(t) = V_m g(t) \cos(2\pi f_c t + \phi_m) \quad (4.27)$$

where $V_m = \sqrt{A_{mc}^2 + A_{ms}^2}$ and $\phi_m = \tan^{-1}(A_{ms} / A_{mc})$. It becomes apparent that QAM waveforms may be viewed as combined amplitude and phase modulation. The signal constellations for QAM waveforms for $M = 4, 8$, and 16 are presented in Figure 4.16. It is interesting to notice that QAM is not limited to the same M for phase and amplitude. Any combination of M_1 -ary ASK and M_2 -ary PSK is acceptable to generate and $M = M_1 M_2$ combined signal constellation. For $M_1 = 2^n$ and $M_2 = 2^k$, the resulting modulation scheme is capable of transmitting $n + k = \log_2 M_1 M_2$ binary digits occurring at a symbol rate $R / (n + k)$. A representative QAM waveform is presented in Figure 4.17.

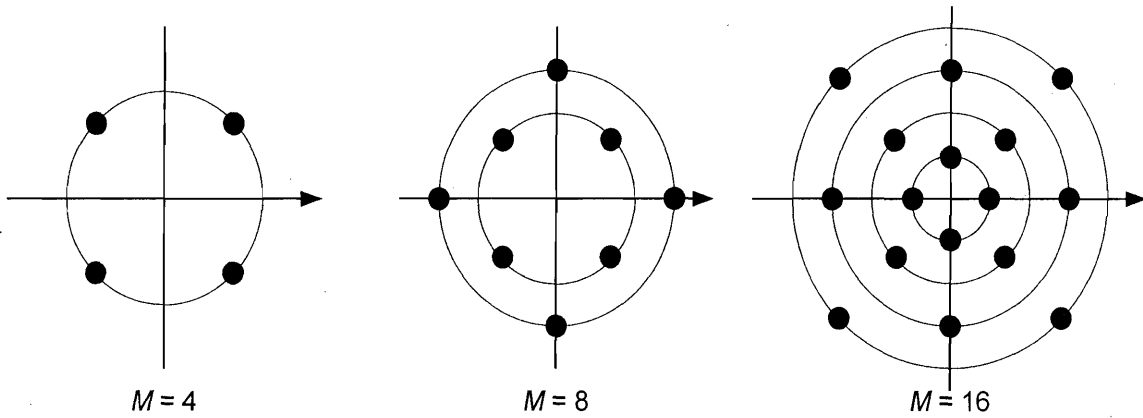


Figure 4.16: QAM signal constellations

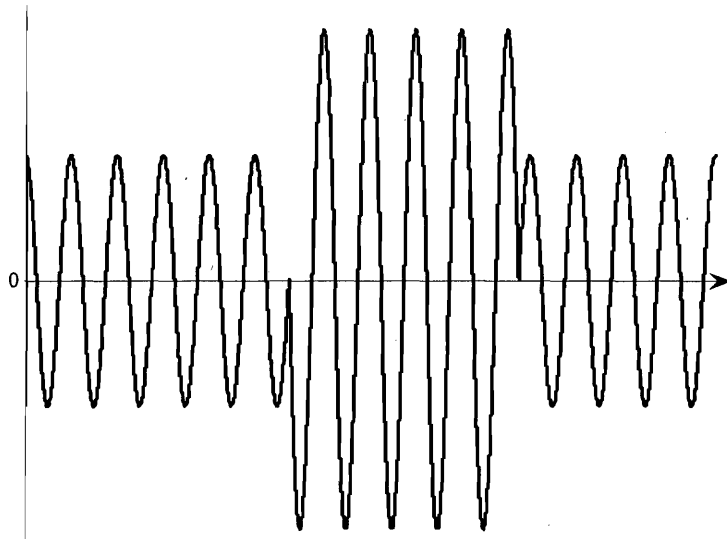


Figure 4.17: QAM waveforms

Finally, in *Frequency shift keying* (FSK) the varying parameter that encapsulates the digital information is the frequency of the carrier wave. FSK constructs M equal energy orthogonal signal waveforms which are represented as:

$$s_m(t) = A \cos[2\pi f_c t + 2\pi m \Delta f t] \quad (4.28)$$

with $m = 1, 2, \dots, M$ and $0 \leq t \leq T$ and where A is the constant amplitude term and Δf is the frequency variation term which indicates the frequency separation among the adjacent signals. In order to preserve the orthogonality of the waveforms, the minimum frequency separation Δf should be $1/2T$.

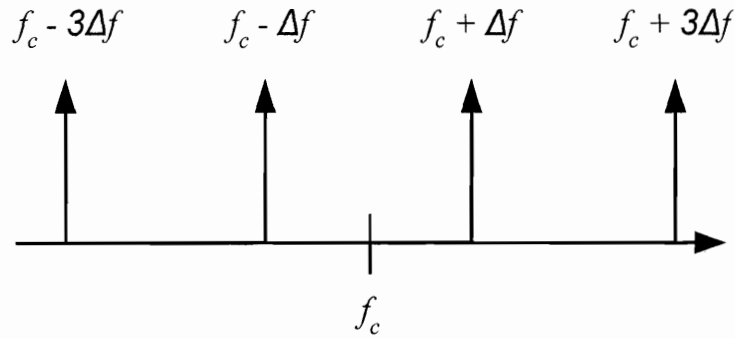


Figure 4.18: FSK representation in the frequency plane

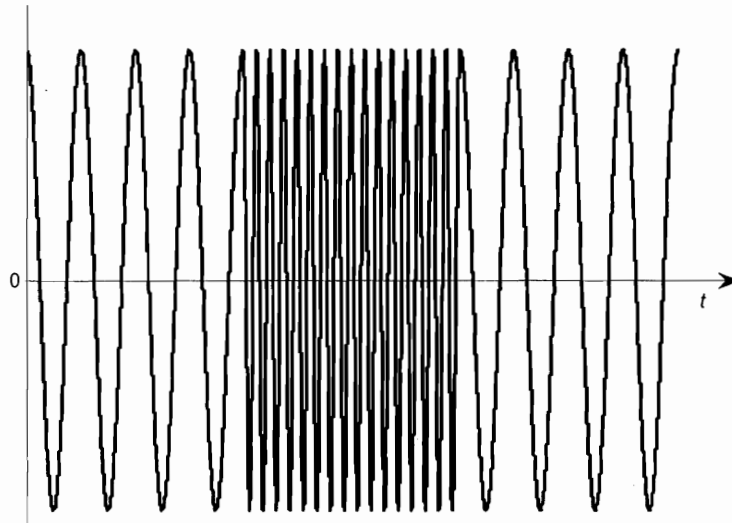


Figure 4.19: FSK waveform

Regardless of the employed modulation method, band pass filtering is very frequently applied during the modulation and demodulation processes. At the transmitter

side the objective of filtering is to limit the frequency spectrum of the generated signals only at the bandwidth region around the carrier frequency, which is usually selected to be in the favorable range according to the attenuation and dispersion properties of the channel. At the receiver side, filtering allows the demodulator to consider only the waveforms that correspond to the transmitted frequency range, while eliminating the ambient noise.

4.5.4. Equalization

Most physical communication channels introduce phase, amplitude and frequency distortion to the propagating signal as a result of multipath propagation, reverberation, scattering and time variations. It is required to remove this distortion in order to improve the error performance of the demodulator in detecting the encapsulated information in the carrier signal. The process of removing amplitude and phase distortion from multipath propagating waves is called *equalization*. In a broad sense, any filtering attempt to reduce intersymbol interference can be referred to as equalization. Such a component is not always present in digital communication systems, however it is necessary for signals propagating in multipath environments.

Signal multipath occurs when the transmitted signal arrives at the receiver via multiple propagation paths of various lengths, consequently introducing different delays. These propagation paths are generated due to reflections from interfering objects, variable ray patterns and so forth. In a digital communication system, multipath propagation results in intersymbol interference due to the multiple time spread and delayed arriving signals that overlap with each other. Moreover, these signals may add destructively, resulting in a phenomenon called *signal fading*. A channel that presents this kind of behavior is consequently called *fading channel*.

Several algorithms have been proposed in the literature to achieve signal equalization. The Maximum Likelihood Sequence Estimator (MLSE) is an equalizer based on the Viterbi algorithm and has the optimum probability error. However, its computational complexity, which grows exponentially with the length of the channel time dispersion, makes its use prohibitively expensive for practical use. Other algorithms, with reduced computational complexity with respect to MLSE, are based on the use of linear

filters with adjustable coefficients, and are usually referred to as *linear equalizers*. This idea is also extended to equalizers that use previously detected symbols to suppress intersymbol interference in the detection of the current symbol, the so called *decision feedback equalizers* (DFE). The latter two equalizers will be described in this section, since they present interesting characteristics applicable to the digital communication system considered in this research.

In most cases, due to the a priori unknown channel characteristics, as well as the uncertainty and time variability of the channel properties, equalizers with adjustable response are frequently required. These equalizers employ algorithms that automatically adjust their properties to the channel's response, and are referred to in the literature as *adaptive equalizers*. Both linear and decision feedback equalizers may employ adaptive algorithms for the real time adjustment of their properties.

The linear adaptive equalizer employs a linear transversal filter, the coefficients of which are adjusted in real time according to the response of the channel by an adaptive weight control algorithm, as illustrated in Figure 4.20. The transversal filter is a finite impulse response filter consisted from three basic elements, a unit delay element, a multiplier, and an adder, see Figure 4.21. The number of delay elements, $M - 1$, used in the filter determines the finite duration of its impulse response, frequently referred to as *filter order*. The delay elements, usually illustrated by z^{-1} , operate on the input $u(n)$ resulting in output $u(n-1)$. The multiplier is then multiplying each input with a corresponding filter coefficient $\hat{w}_k(n)$, the so called *tap weight*, with $k = 0, 1, 2, \dots, M - 1$. The sum of all the weighted inputs represents the output of the filter, $y(n)$. At the next time step $n + 1$, the filter tap weights are adjusted to their improved values $\hat{w}_k(n+1)$. The output of the filter $y(n)$ is presented to the demodulator, which detects the corresponding symbols $\hat{d}(n)$. The error of the equalization $e(n)$ is determined by comparing the detection result along with the output of the filter. This calculated error and the current sequence of data inputs is finally presented to the adaptive weight control algorithm in order to calculate the new improved tap weights for the next time step $\hat{w}_k(n+1)$. The procedure for the adjustment of the filter tap weights is initialized with the use of a reference signal with an a priori known response $d(n)$, in order to train the

algorithm to the channel properties. The length of this training signal must be at least as large as the length of the equalizer so that the spectrum of the transmitted signal adequately covers the bandwidth of the channel being equalized. The hat pointer $\hat{\cdot}$ at the demodulator output and at the tap weight coefficients indicates that these values are estimated.

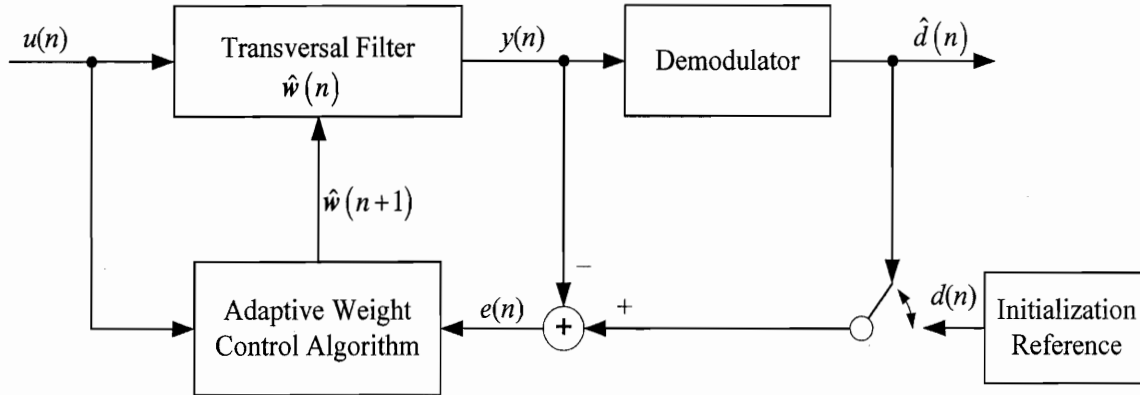


Figure 4.20: Linear Adaptive Equalizer

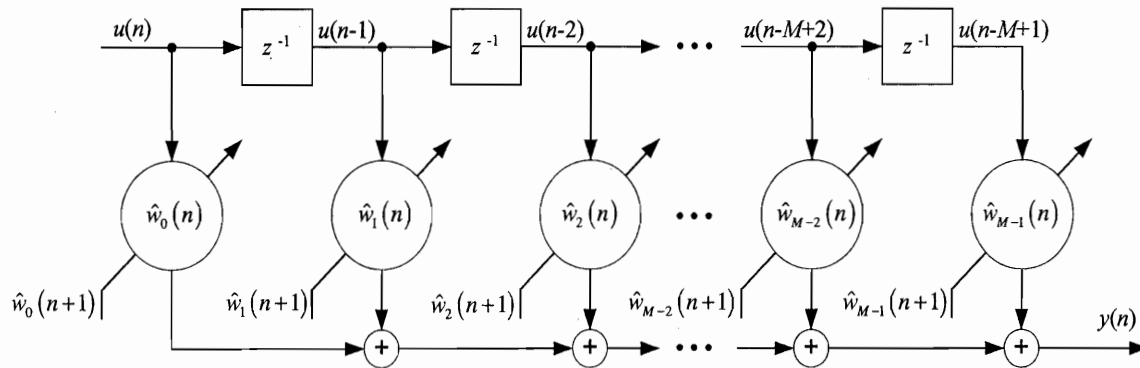


Figure 4.21: Transversal filter detail

The basic limitation of the linear adaptive equalizer is that it performs poorly on channels having spectral nulls. A powerful variation of the linear equalizer is the decision feedback equalizer in which the transversal filter is divided in a feedforward \hat{w}_{FF} and a feedback \hat{w}_{FB} component, as illustrated in Figure 4.22. According to this equalizer the demodulator is presented with the equalized inputs of both the incoming data $u(n)$ and the

last decision made by the demodulator $\hat{d}(n)$. Functionally, the feedback filter is used to remove that part of intersymbol interference from the present estimate caused by previously detected symbols, or in other words the feedback filter is subtracting the distortion on a current pulse that was caused by previous pulses. However, the performance of a decision feedback equalizer is affected by the occasional incorrect decisions made by the detector, which then propagate in the feedback section. The superiority in performance of the decision feedback equalizer over the linear equalizer has been proven in literature [3] and will be verified during the simulations and experiments conducted for the purposes of this research.

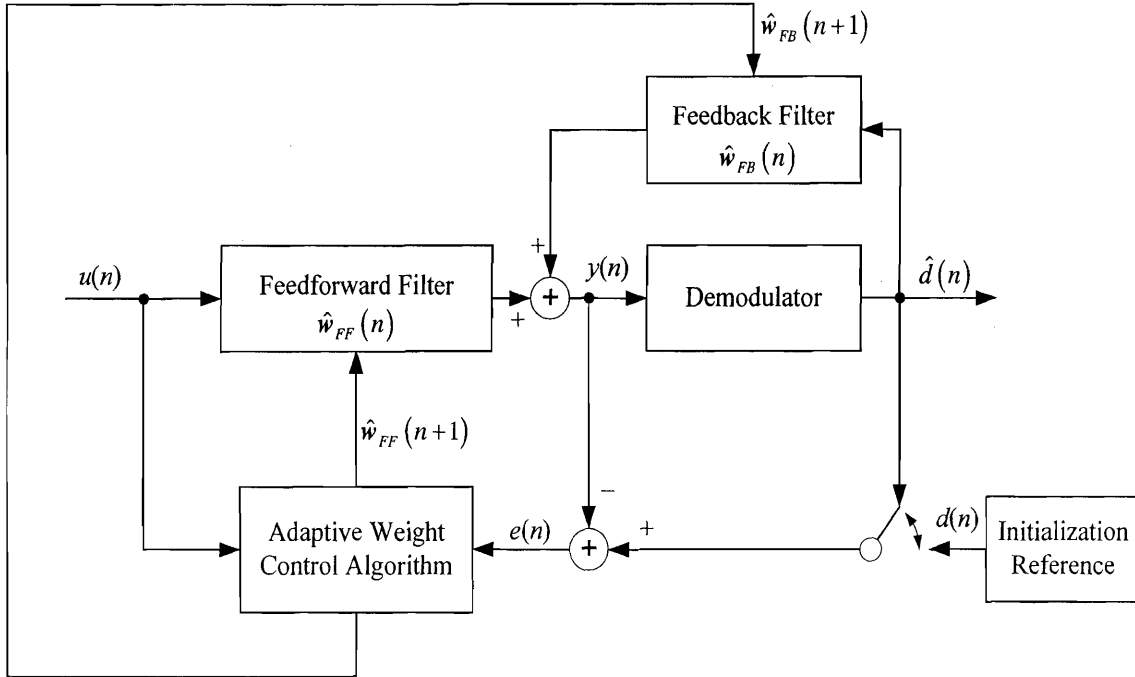


Figure 4.22: Decision Feedback Equalizer

In the above discussion the structure of adaptive equalizers is presented. The adaptive weight control algorithm remains to be examined. Two performance measures that have been used to optimize the coefficients of the filter are the peak distortion criterion and the mean square error criterion. The peak distortion is simply defined as the worst case intersymbol interference at the output of the equalizer. Adaptivity is achieved by employing the *zero forcing algorithm*, which enforces the equalizer response to be an

impulse only when the accurate symbol is achieved and zero at all other times, by cross correlating the error in the detected symbol with the desired symbol solution. This algorithm provides high gain at certain frequencies where the channel has the most attenuation. Therefore, in channels which a lowpass character, it would provide a highpass equalizer, which would cause an unintentional increase in the noise level. Hence, zero forcing equalizers are not suitable for receivers in noisy environments.

Due to the aforementioned characteristic of the zero forcing algorithms, most implementations of adaptive equalizers are employing algorithms minimizing the mean square error. The fundamental and most frequently used algorithm is the *Least Mean Square* (LMS) error algorithm. According to this method, the sum of weighted error squares is minimized to achieve an optimum solution, where the error is defined as the difference between the desired response and the actual filter output. The LMS algorithm is an important member of the *stochastic gradient algorithms* family. The term stochastic gradient is intended to distinguish the LMS algorithm from the method of steepest decent, which uses a deterministic gradient in a recursive computation. A significant feature of the LMS algorithm is its simplicity, while it eliminates matrix inversions and measurement of correlation functions. The algorithm is initialized with an initial selection of the tap weight coefficients w_k for the transversal filter. In case an appropriate value for the tap weights is not available, all w_k can be set to zero for the first time step, $\hat{\mathbf{w}}(0) = \mathbf{0}$. At every time step n , a $M \times 1$ tap input vector is presented to the filter and the adaptive algorithm,

$$\mathbf{u}(n) = [u(n), u(n-1), \dots, u(n-M+1)]^T \quad (4.29)$$

where M is the number of taps, i.e. the length of the filter. Given the tap weights at time n , $\hat{\mathbf{w}}(n)$, the objective is to calculate the tap weights at the next time step $\hat{\mathbf{w}}(n+1)$. The estimation error from the detector is

$$e(n) = d(n) - \hat{\mathbf{w}}(n)\mathbf{u}(n) \quad (4.30)$$

where $d(n)$ is the output of the demodulator. The tap weights for time step $n+1$ are then

$$\hat{\mathbf{w}}(n+1) = \hat{\mathbf{w}}(n) + \mu \mathbf{u}^T(n) e(n) \quad (4.31)$$

μ is the step size parameter with $0 < \mu < \frac{2}{M S_{\max}}$ and governs the convergence of the algorithm. S_{\max} is the maximum value of the power spectral density of the tap inputs $\mathbf{u}(n)$. The step size parameter needs to be small enough in order to reduce the mean square error but needs to be large enough to bring the equalizer coefficients in the vicinity of the optimum solution. Since μ is usually small, the vector $\mu \mathbf{u} \mathbf{u}^T(n) e(n)$ reduces to a minuscule quantity, which in a digital communication system may end up smaller than one half of the least significant bit. The LMS algorithm is appropriate for tracking slowly time varying channel characteristics, since there is always a lag between the channel change and its response due to the estimation of gradient vectors. When the time variations of the channel characteristics occur rapidly, the lag error will dominate the performance of the adaptive equalizer, even with the largest possible value of the step size parameter μ . In such channels the LMS algorithm is inappropriate and the equalizer must employ more complex algorithms such as the Recursive Least Squares to obtain faster convergence and tracking. The major advantage of the LMS algorithm is its computational simplicity. However, the price paid for simplicity is slow convergence, due to the fact that only a single adjustable parameter exists in the whole algorithm, the step size μ . Several variations of the LMS algorithm have been proposed in literature attempting to improve the performance of the original algorithm, such as the signed LMS, normalized LMS, and Variable Step LMS, [5].

The Recursive Least Squares (RLS) algorithms are capable of faster convergence, since they minimize the quadratic performance index, whereas the LMS algorithms minimize the expected value of the squared error. The rate of convergence is typically an order of magnitude faster than that of the simple LMS algorithm. However, this performance advantage is achieved at the expense of the increased computational complexity of the RLS algorithm. The algorithm is initialized by setting the tap weights $\hat{\mathbf{w}}(0) = \mathbf{0}$ and $\mathbf{P}(0) = \delta^{-1} \mathbf{I}$ where \mathbf{P} is an $M \times M$ matrix called *inverse correlation matrix* and δ is a *regularization parameter*. The parameter δ should be assigned a small value for high signal to noise ratio and large value for low signal to noise ratio, [5]. The time varying gain vector $\mathbf{k}(n)$ is computed as:

$$\mathbf{k}(n) = \frac{\underline{\mathbf{P}}(n-1)\mathbf{u}(n)}{\lambda + \mathbf{u}^T(n)\underline{\mathbf{P}}(n-1)\mathbf{u}(n)} \quad (4.32)$$

where λ is a positive constant with $0 < \lambda \leq 1$ called the *exponential weighting factor* or *forgetting factor*. This weighting factor is usually less than, but close to unity, where the inverse of $1 - \lambda$ represents a measure of the memory of the algorithm. The special case $\lambda = 1$ corresponds to infinite memory.

The a priori estimation error $\xi(n)$ is calculated from the tap weights of the previous time step as:

$$\xi(n) = d(n) - \hat{\mathbf{w}}(n-1)\mathbf{u}(n) \quad (4.33)$$

The a priori estimation error $\xi(n)$ is in general different from the a posteriori estimation error $e(n)$ of the LMS algorithm, which involves the current least squares estimate of the tap weight vector available at time n . The $\xi(n)$ can be considered as tentative value of $e(n)$ before updating the tap weight vector.

The updated weights for the n time step are finally calculated

$$\hat{\mathbf{w}}(n) = \hat{\mathbf{w}}(n-1) + \mathbf{k}(n)\xi(n) \quad (4.34)$$

At the next time step the updated inverse correlation matrix $\underline{\mathbf{P}}$ is required, which is provided by the *Riccati equation* of the RLS algorithm:

$$\underline{\mathbf{P}}(n) = \lambda^{-1}\underline{\mathbf{P}}(n-1) - \lambda^{-1}\mathbf{k}(n)\mathbf{u}^T(n)\underline{\mathbf{P}}(n-1) \quad (4.35)$$

The major drawback of the RLS algorithm is its computational complexity, which makes its use prohibitive for large equalization structures. The RLS algorithm requires $4M^2 + 4M + 2$ calculations, whereas the LMS algorithm requires $2M + 1$ multiplications and $2M$ additions. Apart from its complexity, another drawback of the RLS algorithm is its sensitivity to round-off errors that accumulate due to the recursive computations. Moreover, its performance is frequently heavily dependent of the correct selection of the regularization parameter δ and the exponential weighting factor λ . However, the RLS algorithm provides faster convergence than the LMS algorithm, even though the latter is capable of computing more steps in the same time frame. Detailed analysis of adaptive equalization as well as the LMS, RLS and other adaptive algorithms can be found in [3] and [5].

4.5.5. Synchronization

Synchronization is a fundamental element embedded in all communication systems. Most components of the communication system require and assume some sort of synchronization in order to operate. The synchronization step is illustrated with a floating box in Figure 4.7, since it may be applied at various steps of the communication system depending on the parameters that need to be synchronized and the method used. The most common synchronization tasks can be separated into three distinct groups, namely *phase and frequency*, *symbol* and *frame synchronization*.

Digital communication systems that employ coherent modulation techniques at the receiver are required to have knowledge of the absolute phase of the transmitted signal in order to demodulate it correctly. The phase of the carrier signal can be estimated by the use of a pilot signal and a local oscillator, or alternatively, by enclosing the phase information in the carrier signal, i.e. the so called *suppressed carrier*. Phase and frequency synchronization is frequently referred to in literature also as *carrier synchronization*.

According to the first method, an unmodulated carrier component is transmitted along with the information bearing signal. The receiver reproduces a replica of the carrier signal with the assistance of a *phased locked loop* (PLL), illustrated in Figure 4.23. Phase locked loops are servo-control loops, whose controlled parameter is the phase of a locally generated replica $x(t)$ of the incoming carrier signal $r(t)$. The three major components of a phase locked loop are the phase detector, a loop filter and a voltage controlled oscillator. The phase detector is a device that produces a measure of difference in phase, $e(t)$, between the incoming signal and the local copy. The phase error between the incoming signal and the local copy are introduced to a loop filter, which adjusts the response of the PLL. The PLL is designed to have a narrow bandwidth so that it is not significantly affected by the presence of frequency components and noise from the information bearing signal. However, the narrower the bandwidth, the smaller the capability of the PLL to track rapid phase shifts. The voltage controlled oscillator provides the local replica of the signal, and adjusts its output frequency according to the input voltage level.

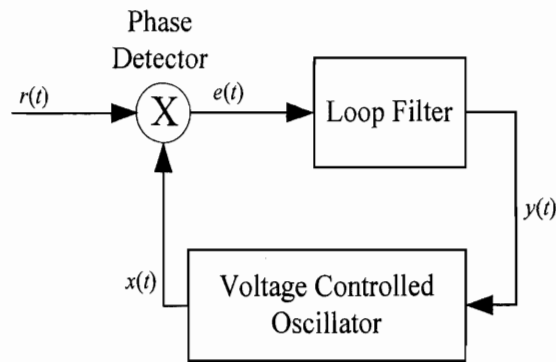


Figure 4.23: Phase Locked Loop

A very widely used technique for carrier synchronization is to modulate the signal accordingly in order to enclose the phase information. This approach has the advantage over the aforementioned method that the total transmitter power is allocated to the transmission of the information bearing signal. According to this method, the effect of modulation on the carrier signal are removed and the absolute phase is estimated. There exist several methods to remove and track the phase from a suppressed carrier signal such as the Squaring loop, Costas loop, and so forth, the description of which exceeds the scope of this text. Carrier synchronization is not required when the communication system employs non-coherent modulation techniques, with the aforementioned penalty of increased bit error probability with respect to coherent modulation.

Directing the focus of the synchronization discussion from the signal to the symbol level, the receiver should have accurate knowledge of when an incoming symbol started and when it stopped. This knowledge is required in order to know the proper symbol integration interval, the interval over which energy is integrated prior to making symbol decisions. Clearly if the receiver integrates over an interval of an inappropriate length, or over an interval that spans two symbols, the ability to make accurate symbol decisions will be degraded. Therefore, in order to acquire the transmitted symbols the demodulator needs to be sampled periodically at the symbol rate. To perform this periodic sampling, a clock signal is required at the receiver. The process of extracting this clock signal at the receiver is called *symbol synchronization*, and can be accomplished in several ways.

In some systems both the transmitter and receiver are synchronized to a master clock, which provides a very precise timing signal. In this case, the receiver estimates and compensates for the relative time delay between the transmitted and received signals. This method has been used successfully in radio communication systems, where the transmitter and receiver are synchronized with the assistance of a master radio station or a global positioning system (GPS) signal.

Other synchronization methods employ the transmission of the clock frequency at a separate signal along with the information signal. The receiver extracts the clock frequency using a narrowband filter tuned to the transmitted clock frequency, similar to the aforementioned phased locked loop. The major disadvantage of this method is that the clock signal allocates a small portion of the transmitter power and the available channel bandwidth. To overcome this disadvantage, there exist methods that extract the clock signal directly from the received data signal employing maximum likelihood timing estimators arranged in open and closed loops. The estimation of carrier phase and symbol timing can be accomplished jointly with a common synchronization algorithm. Further information and detailed analysis of the phased lock loops, suppressed carrier method, and symbol synchronization can be found in [3] and [4].

Most digital data communication systems use some sort of frame structure in order to group and transmit data. Examples of such organization are the blocks of vertical and horizontal lines in digital television transmission, the chunks of 8 bit bytes used to describe computer data, the code words of error block codes, the time windows in Time Division Multiple Access methods, and so forth. *Frame synchronization* is the process that allows the receiver to separate and process independently these blocks of data. To accomplish frame synchronization the transmitter introduces a special marker at the beginning of each separate data block or at frequent predetermined time intervals. The frequency and pattern of this marker is a priori known to the receiver. The marker can be a synchronization codeword consisted of a single bit or a sequence of bits, the presence of which can be easily recognized by the receiver by cross correlation of the incoming data signal with the locally stored marker pattern. Synchronization is achieved when the correlation coefficients are high, whereas at all other times the correlation of the incoming signal with the marker pattern is very low. Since this synchronization method

introduces a series of bits ahead of the data blocks, the effective data rate is decreased, or alternatively higher bandwidth is required to preserve the same data rate. The effective data rate is further decreased when a time delay is required for the identification process of the synchronization codeword as well as from the use of relatively long codewords. Longer codewords may need to be employed to reduce the presence of correlation sidelobes and enhance the absolute value of the main correlation lobe indicating its precise position in time.

Two complementary probabilities characterize the performance of a system using synchronization codewords, namely the *missed detection* and the *false alarm* probabilities. The probabilities of both are desired to be low. However, to decrease the probability of a missed codeword the system may allow recognition from less than perfect matches from the correlation algorithm, which may thus lead to a false alarm. On the other hand, if the false alarm probability must be decreased, only perfect correlations are recognized as codeword matches, which may lead to missed codewords. The probability of a miss P_m for an N -bit codeword where k or fewer errors are accepted is provided by:

$$P_m = \sum_{j=k+1}^N \binom{N}{j} p^j (1-p)^{N-j} \quad (4.36)$$

where p is the probability of a bit error. The probability of a false alarm P_{FA} generated by N bits of random data is given by:

$$P_{FA} = \sum_{j=0}^k \frac{\binom{N}{j}}{2^N} \quad (4.37)$$

It can be seen that for small p , P_m will decrease exponentially with increasing k , whereas P_{FA} will increase exponentially. The probabilities P_m and P_{FA} can be improved by using longer codewords, i.e. larger N .

A well known class of appropriate synchronization sequences is Barker codes, [6]. Their primary property is that when the synchronization word is introduced to a matched filter, the highest peaks of the correlation sidelobes will be equal to unity whereas the value of the main lobe is equal to the length of the code. Unfortunately, there

is no constructive method of finding Barker codes, only 10 of which are known up to a length of 13 bits, presented in Table 4.1.

Length	Code	Sidelobe level (dB)
2	+1, -1 or +1, +1	- 6.0
3	+1, +1, -1	- 9.5
4	+1, +1, -1, +1 or +1, +1, +1, -1	-12.0
5	+1, +1, +1, -1, +1	-14.0
7	+1, +1, +1, -1, -1, +1, -1	-16.9
11	+1, +1, +1, -1, -1, -1, +1, -1, -1, +1, -1	-20.8
13	+1, +1, +1, +1, +1, -1, -1, +1, +1, -1, +1, -1, +1	-22.3

Table 4.1: Barker Codes

A synchronization code can also be composed using the *synchronous idle* (SYN) character or by the *end of transmission* (ETB) character of the ASCII code, presented in Figure 4.9. Other sets of codes suitable for synchronization purposes are the Newman and Hofman, Maury-Styles, Turyn, and Linder codes, which include much longer synchronization sequences thus improving the aforementioned error probabilities, [7] – [10].

4.6 Trade-offs of Digital Communication Systems

Due to the higher performance demanding nature of current applications and the distorting characteristics of the transmission channels, several compromises are required at the design level of a digital communication system. The perfect communication system would require simultaneously maximizing the transmission bit rate R , minimizing the bit error probability P_B , minimizing the required power, minimizing the required bandwidth W , minimizing system complexity, computational load, cost, and so forth. However, most of these goals are conflicting with each other and therefore trade offs in the various performance characteristics of the communication system are required.

The most fundamental communications trade off is the adjustment of the error performance versus the bandwidth performance of the system. This trade off is presented in the *error probability performance curves*, illustrated in Figure 4.24 for the cases of coherent detection of orthogonal and multi-phase signaling. In these figures, each curve presents the probability of bit error P_B at any given signal to noise ratio per bit E_b/N_o for modulators using alphabets of $M = 2^k$ symbols. For a given system information rate, each curve can be associated with a different fixed minimum required bandwidth. The closer the curve to the origin, the more bandwidth it requires. Figure 4.24a illustrates the potential bit error improvement for orthogonal signaling with increasing k . In other words, for modulation methods using orthogonal signal sets, such as FSK, increasing the size of symbol set results in improving the bit error probability or in reducing the required E_b/N_o at the expense of additional bandwidth. On the other hand, Figure 4.24b illustrates the bit error probability increase with increase of k , for multi-phase modulation. For non orthogonal signaling methods, such as M -ary PSK, increasing the size of the symbol set results in reduction of the required bandwidth at the expense of the bit error probability, or otherwise increased E_b/N_o is required. These trade offs are indicated on the plots of Figure 4.24 with the straight arrowed lines. Line 1 represents the trade off between P_B and E_b/N_o for fixed bandwidth. Line 2 is the trade off between P_B and bandwidth for a fixed E_b/N_o . Finally, line 3 corresponds to the compromise of bandwidth for E_b/N_o , for a fixed P_B .

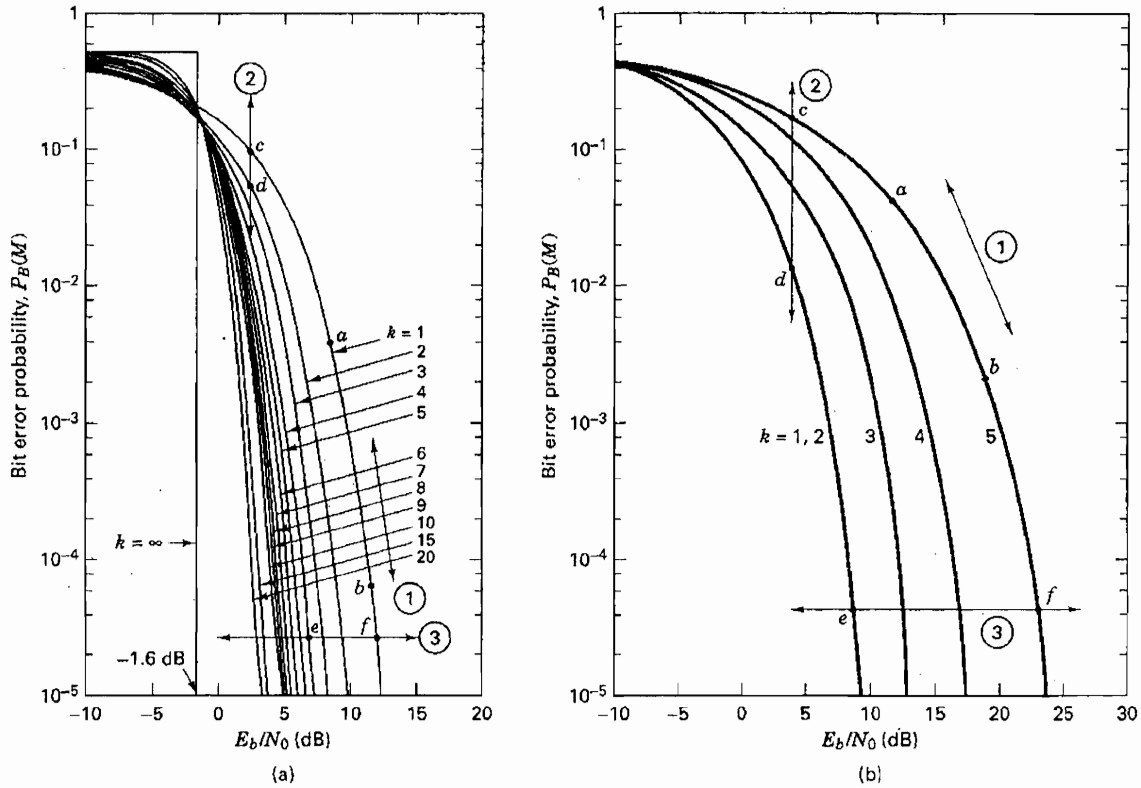


Figure 4.24: Bit error probability P_B versus Signal to noise ratio per bit E_b/N_0 for coherently detected M -ary signaling: (a) orthogonal signaling, (b) Multiple phase signaling, [4]

In Figure 4.24a the ideal communication system curve is represented with the leftmost bilinear line, theoretically achieved for orthogonal signaling when $k = \infty$. This curve corresponds to the *Shannon limit* that represents the threshold of E_b/N_0 below which the system cannot establish reliable communication. For all values of E_b/N_0 above the Shannon limit of -1.6dB the bit error probability is zero, whereas below the limit the probability goes directly to the worst case value, which for the binary case is 0.5.

An interesting point arising from the above discussion is that for orthogonal signaling the larger the symbol length the lower the power requirement E_b/N_0 . However, it should be noted that the total power required for the transmission of each symbol is larger, or in other words the signal to noise ratio demand for each symbol transmitted is greater for larger k . This power demand gets smaller for increasing k only when it is normalized with the number of bits included in each symbol, meaning signal to noise ratio per bit E_b/N_0 . It is also important to notice that an incorrectly received symbol may

correspond to just a single incorrectly received bit, making significant the distinction between the symbol error probability P_E and the bit error probability P_B .

The major trade off between the bandwidth efficiency and the required power of a communication system should be emphasized, as an extension to the above discussion regarding the required power. Real transmission channels have a specific data rate capacity that restricts the available useable bandwidth. Exceeding this capacity results into significant detection errors at the received signal. Furthermore, for a specific power level there is a limited amount of bitrate that can be extracted from a particular bandwidth. This tradeoff between the bandwidth efficiency and the required power is described by the *Shannon Theorem* and illustrated in Figure 4.25. According to this theorem the ratio of channel capacity C over bandwidth W is given by

$$\frac{C}{W} = \log_2 \left(1 + \frac{C E_b}{W N_o} \right) \quad (4.38)$$

Figure 4.25 provide plots of the bandwidth efficiency, i.e. bitrate over bandwidth, versus the required power per bit, E_b/N_o , for various modulation methods and signaling sizes corresponding to a symbol error probability of 10^{-5} . The leftmost curve corresponds to the limiting case where the bitrate R is equal to the capacity C of the channel, $C = R$. The area on the left of the $C = R$ curve is the unattainable region, where the bit error probability can be arbitrarily large. All practical communication systems lie somewhere on the right of the $C = R$ curve, where two distinct behaviors can be recognized.

Communication systems using M -ary orthogonal signaling yield to the $R/W \leq 1$ region. In this region, increasing M results in decreasing the ratio R/W , due to an increase in the required bandwidth W . At the same time, the power requirement E_b/N_o decreases. Hence, a system operating with $R/W \leq 1$ is appropriate for power-limited channels as the modulation uses excessive bandwidth but may operate at lower power levels.

On the other hand, in the case of PAM, QAM, and PSK modulation methods, increasing M results in higher bandwidth efficiency, at the expense of higher power requirement. Therefore, systems operating in the $R/W > 1$ region suitable for bandwidth-limited channels as they use bandwidth efficiently but require excessive power.

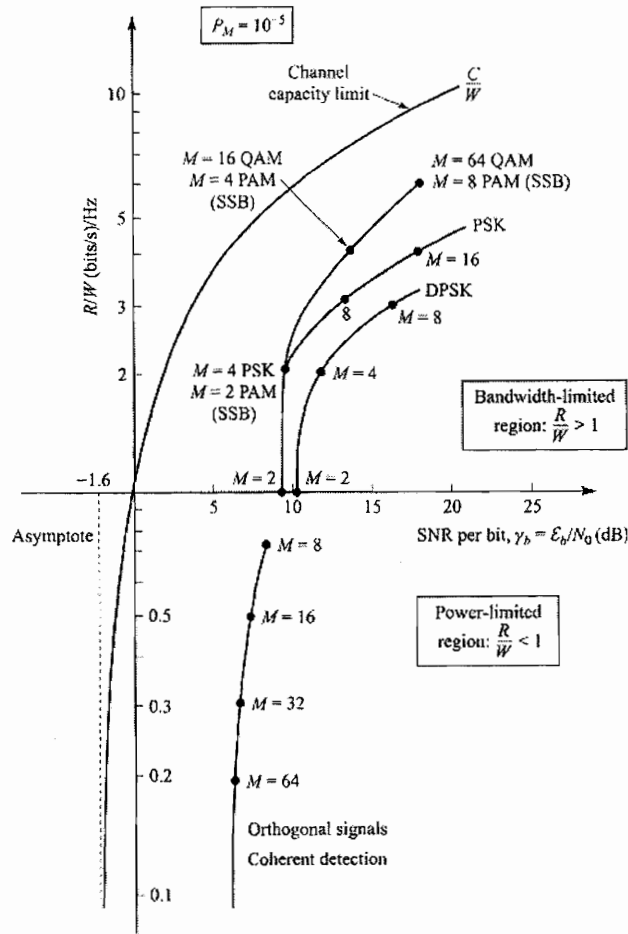


Figure 4.25: Bandwidth efficiency η_0 in bit/s/Hz as a function of SNR per bit, for constant symbol error probability of 10^{-5} , [3].

Several of the theorems and techniques presented in this section are based on the assumption of strictly bandlimited signals, which means that no power is allowed outside the defined band. However, such signals are not realizable since they require infinite duration waveforms. On the other hand, finite duration waveforms have infinite bandwidth, meaning they present some power at all frequencies. Therefore, the term bandwidth must be defined in a *relaxed* form with respect of the signals used. There exist several definitions of bandwidth generated for use to various applications. The single sided power spectral density of a single finite duration pulse follows the general analytical form of the square of a *sinc* function

$$G(f) = T \left[\frac{\sin \pi(f - f_c)T}{\pi(f - f_c)T} \right]^2 \quad (4.39)$$

where f_c is the carrier wave frequency and T is the pulse duration. The power spectral density is plotted in Figure 4.26, which also indicates according to [4] the various definitions of bandwidth.

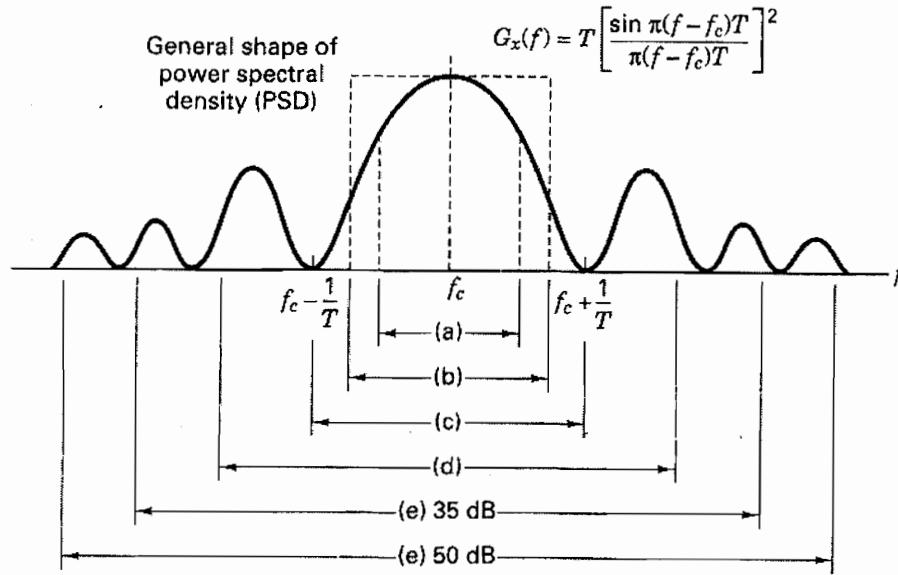


Figure 4.26: Bandwidth of digital data, [4].

(a) Half Power, (b) Noise equivalent, (c) Null to Null, (d) 99% of Power, (e) Bounded Power Spectral Density at 35 and 50 dB.

The bandwidth definitions are as follows:

- (a) *Half Power Bandwidth* is the interval between frequencies at which $G(f)$ has dropped to half power or equivalently 3dB below the peak value.
- (b) *Noise Equivalent Bandwidth* W_N of a signal is defined by the relationship $W_N = P/G_{\max}(f)$, where P is the total signal power over all frequencies and $G_{\max}(f)$ is the value at the center of the band assuming it is the maximum over all frequencies. W_N was originally conceived to permit rapid computation of the output noise power from an amplifier with a wideband noise input.
- (c) *Null to Null Bandwidth* corresponds to the width of the main spectral lobe, where the most signal power is contained. Even though it is a widespread

bandwidth definition within the digital communications community, it lacks general applicability because several modulation formats do not generate signals with well defined spectral lobes.

- (d) *Fractional Power Containment Bandwidth* is adopted by the Federal Communications Commission (FCC Rules and Regulations Section 2.202), and represents the band that leaves exactly 0.5% of the signal power beyond the upper and lower bound respectively, leaving consequently the 99% of the signal power within the occupied band.
- (e) *Bounded Spectral Density* defines bandwidth as the region that leaves outside any frequencies that have power spectral density below a certain threshold from the maximum power. Typical values for this threshold are 35dB and 50dB.

4.7 Advanced Communication Issues

In the previous paragraphs, the components and theory behind a simple digital communication system were discussed, assuming single point to point communication. However, modern applications frequently require more complex architectures with bidirectional or multiple point communications, multiple user access of the same transmission channel and so forth. Every additional feature that the communication system is required to provide is translated into more complex transmitter and receiver architectures, with supplementary components to facilitate the new needs. For example, multiple user access of the same transmission channel requires signal processing steps, such as *multiplexing*, which would allow separation of the individual transmitted signals. To avoid signal collisions, methods such as *Code Division Multiple Access* (CDMA), *Time Division Multiple Access* (TDMA) or *Frequency Division Multiple Access* (FDMA) are required. These methods utilize the channel separating the signals by encoding, time frame or individual frequency of each user respectively. As the number of users increase and the potential data connections grows among the users, the necessity to employ a communication protocol, which will handle the transmission and redirection of data, becomes apparent. There exist several communication protocols which are capable of

packetizing, routing, and receiving the data, as well as confirming the integrity of the received packets and requesting retransmission in case of an erroneous packet or absent piece from the packet sequence. Other potentially required steps may include encryption of sensitive digital data, which increases the complexity of the transmitter and receiver substantially according to the protection level. Communication protocols constitute the backbone of current communication networks. The analysis of such advanced digital communication issues are beyond the scope of this text. For further information the reader should refer to specialized books such as [11] and [12].

4.8 References

- [1]. Searle S.J. (Web Master, TRON Web), "A Brief History of Character Codes in North America, Europe, and East Asia", Electronic reference, Aug. 2005, <http://tronweb.super-nova.co.jp/characcodehist.html>
- [2]. "Communications Toolbox, for use with MATLAB", User's Guide, Version 3, The Mathworks, 2004.
- [3]. Proakis J.G., "Digital Communications", *McGraw Hill*, 4th Edition, Boston, MA, 2001.
- [4]. Sklar B., "Digital Communications: Fundamentals and Applications", *Prentice-Hall*, 2nd Edition, Upper Saddle River, NJ, 2001.
- [5]. Haykin S.S., "Adaptive Filter Theory", *Prentice-Hall*, 4th Edition, Upper Saddle River, NJ, 2002.
- [6]. Barker, R.H., "Group Synchronization of Binary Digital Systems", *Communication Theory*, W. Jackson ed., Academic Press Inc., New York, 1953.
- [7]. Öberg T., "Modulation, Detection and Coding", *John Wiley and Sons*, West Sussex, England, 2002.
- [8]. Spilker J.J., "Digital Communications by Satellite", *Prentice Hall*, Englewood Cliffs, N.J., 1977.
- [9]. Newman F., and Hofman L., "New Pulse Sequences with Desirable Correlation Properties", *Proceedings of National Telemetry Conference*, pp. 272-282, 1971.
- [10]. Wu W.W., "Elements of Digital Satellite Communications", Vol. 1, *Computer Science Press*, Rockville, MD, 1984.
- [11]. Bertsekas D., and Gallager R., "Data Networks", *Prentice-Hall*, 2nd Edition, Upper Saddle River, NJ, 1992.
- [12]. Peterson L.L., and Davie B.S., "Computer Networks", *Morgan Kaufmann Publishers, An Imprint of Elsevier Science*, San Francisco, CA, 2003.

Chapter 5

Proposed Communication System

5.1 *Introduction*

Within the context of this thesis and the restrictions imposed by the in-pipe acoustic channel and the digital communication technology, this chapter proposes a solution to the telemetry system of an in-pipe wireless sensor network. Recall that the scope of this thesis is to explore the feasibility of acoustic data communication inside pipelines, for use with wireless sensor networks. The previous chapters provided the required background to understand the characteristics and acknowledge the limitations of the in-pipe acoustic channel as well as recognize the extent of the capabilities of digital communication systems. In what follows the details of the in-pipe acoustic communication system are provided along with discussions regarding the remedies or trade-offs for the imposed limitations.

First of all, the objectives of this research should be precisely defined; the implementation of a compact, power efficient data communication system that will operate inside a water pipeline and is capable of transmitting data at rates in the order of several kilo-bits per second (kbps) at a distance of several hundred meters. The system needs to be small enough to fit in the cross section of the pipeline and not to obstruct its normal operation. The notion of power efficiency is connected with the use of the system at a wireless sensor network, which by default implies low energy consumption devices, since the available power resources are limited, while unattended long term operation of the system is required. The distance among the sensors is mandated by the required resolution of the pipeline monitoring system. It can be safely assumed that the most distant sensors will be placed in the order of hundreds of meters to a kilometer. In locations of critical importance, the spacing among the sensors may be required to be in the order of tens of meters, in order to provide more accurate and reliable failure identification or even prediction. Since most smart sensor systems are nowadays capable

of local data processing, there is no need to continuously transmit the monitored parameters, which decreases dramatically the data transmission requirement. The wireless sensor node is essential to send only alerts of identified events, or crucial parts of the monitored data for cross correlation with data from other sensor nodes. This decreased data transmission duty cycle reduces significantly the power requirement of the sensor node, since not only continuous operation of the communication module is not necessary, but also allows to use power efficient communication schemes with low data rate requirements, thus justifying the selection of several kbps throughput as adequate for the proposed system. Finally, due to environmental constraints, the materials selected for the implementation of the communication system need to be compatible with the materials of the pipeline and comply with all the health standards for potable water supply. All the aforementioned issues in relation with the communication system, and along with suggested solutions, are discussed in detail in what follows.

5.2 Operational Layout

The implementation of the digital communication system can be separated into two major categories, the software and the hardware. These two levels of implementation are essentially the signal processing steps and the devices that generate or receive the actual acoustic signal, respectively. The operational diagram of the signal processing steps for the transmitter and receiver is illustrated in Figure 5.1.

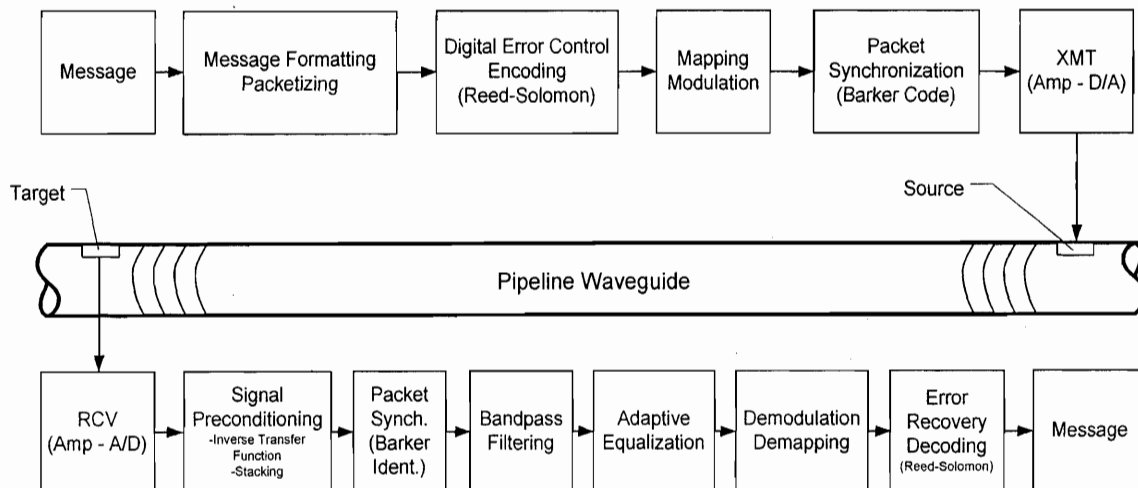


Figure 5.1: Operational diagram of proposed digital communication system

The above figure constitutes the core of the proposed digital communication system and includes all the signal processing steps required to compensate for all potential distortion mechanisms imposed to the propagating signal by the acoustic waveguide. Essentially, the signal processing steps applied at the transmitter are inverted at the receiver. The receiver also includes signal processing steps that attempt to reverse the effect of the pipeline waveguide on the propagating wave. From a hardware point of view, the transmitter and receiver signal processing steps can be incorporated in micro-processing units capable of implementing all the mathematical computations. The actual transmitting and receiving devices, denoted by XMT and RCV in Figure 5.1 respectively, are realized in the hardware level as an assortment of electronic circuits and devices. A simple organizational hardware diagram describing the transmitter and receiver is presented in Figure 5.2. In this figure the presence of a power supply is implied but not shown. According to this diagram, the outcome of the digital signal processing steps at the transmitter is introduced to a digital to analog converter, which transforms the discrete time signal to a continuous waveform. This waveform is amplified appropriately and radiated in the transmission medium, in this case the water, with the assistance of a transducer, which acts as a source. At the receiver side, a transducer, acting as a receiver, captures the transmitted waves and after a pre-amplification stage, the received waveform is converted to a discrete time signal with the assistance of an analog to digital converter. The pre-amplification stage is necessary in order to adjust the magnitude of the received waveform to fit the operating range of the analog to digital converter

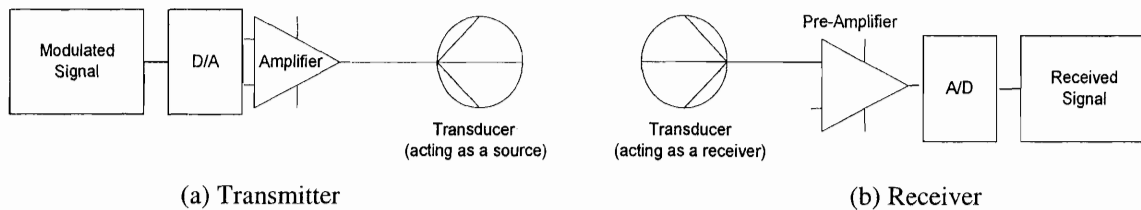


Figure 5.2: Transmitter and receiver hardware diagram

The following paragraphs analyze each of the components in both the software and the hardware level, justifying at the same time the selection among the various alternatives.

5.3 *Software Implementation*

Most signal processing steps executed at the transmitter or receiver of a digital communication system are implemented at the software level. This statement is true for all the transformations executed on digital signals, or in other words, signals that are discrete in time. The analog to digital conversion and vice versa, as well as the signal amplification, mentioned in the preceding paragraph are usually implemented at the hardware level. Minor filtering is also sometimes applied at the hardware level, limited however to the stages where the signal is still analog. This section focuses on the digital signal processing steps of the proposed data communication system, as they are presented in Figure 5.1, in conjunction with the material presented in Chapter 4.

Since the scope is to assess the feasibility of an in-pipe acoustic communication system, it is necessary to use techniques that allow isolating as many parameters as possible. Even though higher complexity methods are also introduced, most proposed techniques utilize the simpler, more basic, and robust methods, frequently at the expense of bit rate performance.

5.3.1 *Message Formatting*

The first step in the sequence of processing steps of a digital signal is the transformation of the actual message that must be transmitted in a form appropriate for processing. The alphanumeric message is converted into a stream of binary bits with the assistance of the 7-bit American Standard Code for Information Interchange (ASCII) code. This code is capable of representing 128 different characters, adequate for the description of virtually any message, allowing at the same time the introduction of several textual and device control special characters, as shown in Figure 5.3. The implementation of the ASCII code is straightforward, since it simply replaces each character with a string of seven binary bits.

Bits				5	0	1	0	1	0	1	0	1
1	2	3	4	6	0	0	1	1	0	0	1	1
0	0	0	0	7	0	0	0	0	1	1	1	1
0	0	0	0	NUL	DLE	SP	0	@	P	'	p	
1	0	0	0	SOH	DC1	!	1	A	Q	a	q	
0	1	0	0	STX	DC2	"	2	B	R	b	r	
1	1	0	0	ETX	DC3	#	3	C	S	c	s	
0	0	1	0	EOT	DC4	\$	4	D	T	d	t	
1	0	1	0	ENQ	NAK	%	5	E	U	e	u	
0	1	1	0	ACK	SYN	&	6	F	V	f	v	
1	1	1	0	BEL	ETB	'	7	G	W	g	w	
0	0	0	1	BS	CAN	(8	H	X	h	x	
1	0	0	1	HT	EM)	9	I	Y	i	y	
0	1	0	1	LF	SUB	*	:	J	Z	j	z	
1	1	0	1	VT	ESC	+	;	K	[k	{	
0	0	1	1	FF	FS	,	<	L	\	l		
1	0	1	1	CR	GS	-	=	M]	m	}	
0	1	1	1	SO	RS	.	>	N	^	n	~	
1	1	1	1	SI	US	/	?	O	-	o	DEL	

NUL	Null, or all zeros	DC1	Device control 1
SOH	Start of heading	DC2	Device control 2
STX	Start of text	DC3	Device control 3
ETX	End of text	DC4	Device control 4
EOT	End of transmission	NAK	Negative acknowledge
ENQ	Enquiry	SYN	Synchronous idle
ACK	Acknowledge	ETB	End of transmission
BEL	Bell, or alarm	CAN	Cancel
BS	Backspace	EM	End of medium
HT	Horizontal tabulation	SUB	Substitute
LF	Line feed	ESC	Escape
VT	Vertical tabulation	FS	File separator
FF	Form feed	GS	Group separator
CR	Carriage return	RS	Record separator
SO	Shift out	US	Unit separator
SI	Shift in	SP	Space
DLE	Data link escape	DEL	Delete

Figure 5.3: 7-Bit American Standard Code for Information Interchange (ASCII), [1]

Following the conversion of the textual message to binary bits, the stream of bits is separated into standard length packets. The generation of these packets is necessary to limit the duration of the transmitted waveforms and to format the bit stream into blocks appropriate for the remaining digital signal processing steps. In the experiments and simulations completed within the scope of this research, the package length used varied from 42 to 140 bits, even though larger packages can be considered.

At this point, the choice of a binary representation of the digital alphabet is implied and should be noted, since it affects the design of the remaining components. The binary representation indicates that the signal symbols in the *alphabet* can take only two distinct forms, 0 and 1. This selection is preserved across all the signal processing steps, resulting into binary modulation, as it will be shown in a later paragraph. Alternatively, the signal can be represented with an alphabet with more than two symbols. However, the ambiguity during the detection process among the various states of the signal transformation increases with increasing number of different symbols. Since, only two states exist in a binary representation, the maximum error rate is 50%, which can be achieved even with no information of the incoming data, while the distance between the two representations is maximum, resulting in decreased detection error rates.

5.3.2 Encoding

Encoding is the process of adding redundant bits to the signal prepared for transmission, which allows the receiver to detect and potentially correct any erroneously received parts of the signal. In practice the encoder transforms the incoming stream of bits into a predefined set of codewords. Therefore, any variation of the received signal from the prespecified set indicates an error, while correction is achieved by selecting a closely matching codeword. The encoding algorithm used is the Reed Solomon code, described in paragraph 4.5.2, due to its powerful attributes for detecting and correcting erroneous bits or streams of bits. The codewords generated by the Reed Solomon code present the maximum available distance among them in the detection space, enabling the algorithm to correct the maximum number of errors that can be achieved for the introduced level of redundancy. The algorithm is guaranteed to correct up to $t = \frac{1}{2}(N - K)$ errors, where N is the length of the code and K is the number of information symbols encoded into a block of N symbols. The length of the code is equal to $N = q - 1 = 2^k - 1$, with q the number of symbols in the alphabet and k the information bits mapped into each of the q symbols. For the binary case considered here, $k = 1$ and $q = 2$, corresponding to one bit mapped into each information unit and two being the total number of available symbols, 0 and 1, respectively. The length of the codewords used is $N = 15$, while each one contains $K = 7$ bits of information. Thus the resulting code is capable of correcting $t = \frac{1}{2}(15 - 7) = 4$ incorrectly received bits in each codeword.

Considering the small number of bits present in each packet, this error correcting capability is considered adequate, since each of the ASCII transformed characters is encoded separately. It is important to understand that increasing the redundancy of the encoding algorithm, i.e. increasing the ratio of the length of the codeword over the number of bits represented, results in decreasing the effective bit-rate of the system, since it uses significant part of the available bandwidth to transmit the redundant bits. The selected codeword length is a trade-off between the error control algorithm capability and the bit-rate performance of the communication system, especially considering the limited available bandwidth of the in-pipe transmission channel. In addition, the generation of large codewords should be avoided, because it increases the complexity of the algorithm,

consequently requiring more powerful processing units, with increased demand in memory and power consumption.

5.3.3 Modulation

The combination of Mapping and Modulation processes is responsible for converting the digital data into a set of waveforms appropriate for transmission into physical media. As mentioned in paragraph 4.5.3, most modern digital communication systems execute both operations in the same processing step. According to this step, a block of k binary digits is selected at a time from an information sequence and is represented by one of $M = 2^k$ deterministic, finite energy waveforms. Each of these selected blocks represents a specific symbol from the alphabet used. For the digital communication system considered here, there exist only two symbols equal to the bits 0 and 1. Therefore, $k = 1$ bit is the length of each selected block and $M = 2$ are the corresponding waveforms.

When the mapping of the digital sequence to analog waveforms is performed under the constraint that a waveform transmitted at any time interval depends on one or more previously transmitted waveforms, the modulator is said to have *memory*. On the other hand, when mapping from the sequence to waveforms is performed without any constraint on previously transmitted waveforms, the transmitted waveform depends only on the selected block, the modulator is called *memoryless*. The communication system implemented utilizes memoryless procedures, due to their immunity to potential carryon errors at the demodulation process. More explicitly, when a modulator has memory, erroneously detected signals at the receiver side may affect the integrity of signals received in the future, resulting in errors at their demodulation process.

In digital communications the terms *demodulation* and *detection* are often used interchangeably, although demodulation emphasizes waveform recovery and detection entails the process of symbol decision. When, in order to demodulate the signal, the receiver requires knowledge of the absolute phase of the carrier signal, the process is called *coherent detection*, whereas in the opposite case the process is called *non-coherent detection*. Coherent receivers preserve copies of all possible arriving waveforms and match them with the incoming signal. However, this process requires estimation of the

absolute phase of the received signal, which may potentially lead to errors, especially in dispersive channels which affect the phase characteristics of the propagating wave. On the other hand non-coherent detectors don't require knowledge of the absolute phase of the incoming signal, thus reducing the complexity of the receiver and potential phase estimation errors, at the cost of increased error probability for identical signal to noise ratio signals. In this research, non-coherent detectors are mainly used, due to their reduced complexity and elimination of phase estimation. However, some modulation methods such as phase shift keying and quadrature amplitude modulation, require coherent detection due to its superior performance.

Modulation is the process where the amplitude, phase or frequency of a sinusoidal wave, or a combination of them, is varied in accordance with the information to be transmitted. In digital communications, this variance of the parameters of the signal corresponds to different symbols of the selected alphabet. When only one parameter of the carrier signal is adjusted, amplitude, phase or frequency, each of the generated symbols corresponds to a different value of the adjustable parameter. Thus the modulation methods in digital communications are denoted as the name of the adjustable parameter with the ending *shift keying*, indicating that the method generates the modulated wave by shifting among several predefined keys, i.e. states, of the carrier wave. The widely known nomenclature *Amplitude Modulation*, *Frequency Modulation* and so forth, is used for modulation of analog signals.

Due to the binary representation of the signals used in the communication system considered in this thesis, only two values for each adjustable parameter are required for each modulation method. In that respect, the modulation methods examined in this research are the binary *Frequency Shift Keying*, (FSK), the binary *Amplitude Shift Keying*, (ASK), or the equivalent binary *Phase Shift Keying*, (PSK), and the *Quadrature Amplitude Modulation*, (QAM). The FSK is used as the method of reference, due to its simplicity and robustness, however, at the cost of low bandwidth efficiency. Detailed description of each modulation method is provided in paragraph 4.5.3. It should be noted that for QAM the number of available waveform states $M = 4$, as a result of the combination of two states for amplitude and two states for phase modulation.

For every modulation method, the frequency of the carrier signal is varied from 3 kHz to 63 kHz, with a bandwidth from 2 kHz to 20 kHz, achieving bit rates of 1kbps to 21kbps. These values reveal a bandwidth efficiency of 0.5 to 1.05 bps/Hz as calculated by the ratio of the bit rate over the bandwidth used, with the lower value corresponding to FSK and the higher value corresponding to QAM. Figure 5.4 presents the bandwidth efficiency as a function of the signal to noise ratio per information bit for a constant symbol error probability of 10^{-5} . On this plot the area that corresponds to the current implementations of the in-pipe digital communication system is indicated.

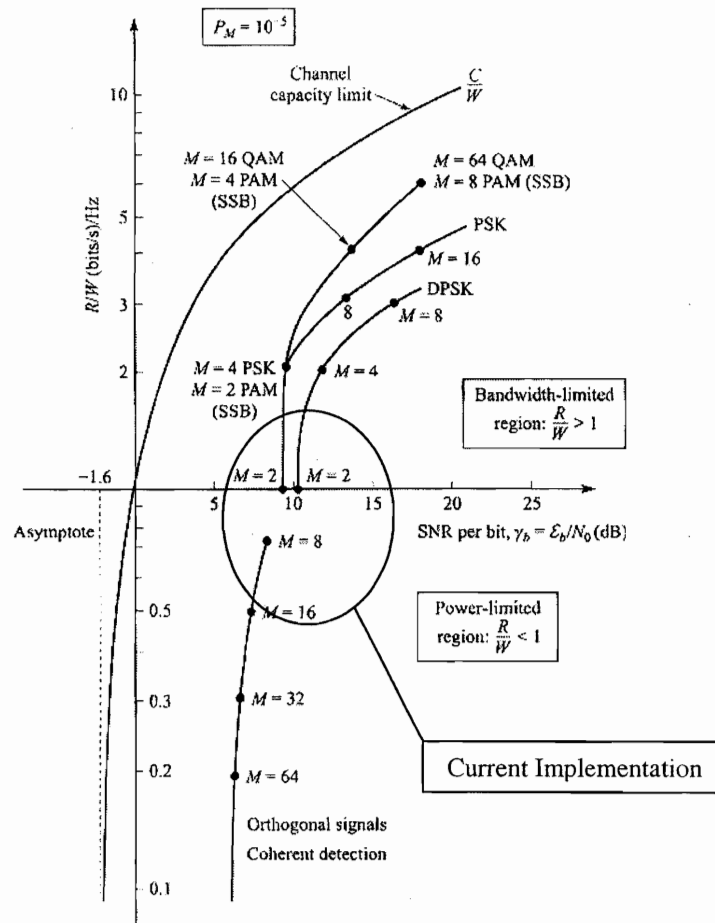


Figure 5.4: Bandwidth efficiency η_0 in bit/s/Hz as a function of SNR per bit, for constant symbol error probability of 10^{-5} , [2]

Three regions can be identified on this plot. The region on the left of the channel capacity limit curve, defined by the Shannon Theorem, see paragraph 4.6, is the

unattainable region, where the error rate of a system operating in this region cannot be predicted or corrected. On the right of the channel capacity limit curve and above the horizontal axis, is the bandwidth limited region, and below the axis is the power limited region. Recall from Chapter 4 that a system operating in the bandwidth limited region requires excessive amounts of power in order to increase the bandwidth efficiency, whereas a system operating in the power limited region requires excessive amounts of bandwidth in order to lower the required signal power. Therefore, the bandwidth limited region is suitable for bandwidth efficient methods such as PSK and QAM, while the power limited region is suitable for power efficient methods such as FSK with orthogonal signaling. At this point, it is important to realize that in a confined environment, such as the inside of a pipeline, the capacity is significantly reduced with respect to the open sea channels, due to the increased levels of reverberation as well as environmental noise. The trade-off between power and bandwidth for an in-pipe communication system becomes clear at this point, since the channel is bandwidth limited but the application is power limited. Using excessive bandwidth to reduce power is not feasible since it would increase the distortion impact on the signal. On the other hand, it is not possible to increase power to control the bandwidth, since the available power is restricted to that of a potential power harvesting system. This justifies the selection of the modulation schemes to lie near the horizontal axis of Figure 5.4, as a compromise between bandwidth and power.

5.3.4 Synchronization

The synchronization block of this communication system corresponds to frame synchronization, presented in paragraph 4.5.5. Phase, frequency and symbol synchronization are inherently included in the proposed system due to the modulation techniques used and the structure of the formatted message. Synchronization is achieved by including a *Barker Code* [3] before each packet or group of packets prepared for transmission. The Barker code corresponds essentially to a waveform with very good autocorrelation properties. The cross correlation of a signal, which includes a Barker code, with another signal including the same code, results in a distinctive peak, with

magnitude equal to the length of the included code, at the time step where the codes coincide, whereas the correlation sidelobes are equal to unity.

According to the proposed scheme, the receiver preserves a copy of the transmitted Barker Code and correlates it with the incoming signal. The highest value of the correlation corresponds to the instant of the Barker Code, allowing the receiver to establish an absolute time stamp. The synchronization code is introduced ahead of the modulated signal, allowing for some prespecified silent time τ between the code and the signal, as illustrated in Figure 5.5. The silent time is necessary to allow for the decay of the reverberations introduced by the Barker code and in order to present minimal interaction or overlap with the actual message. Moreover, this time can be used for the calculation of the correlation coefficients and thus detection of the barker code time stamp, in order to prepare the receiver for the demodulation of the recorded signal. The information bearing message is the signal received exactly time τ following the detection of a Barker Code.

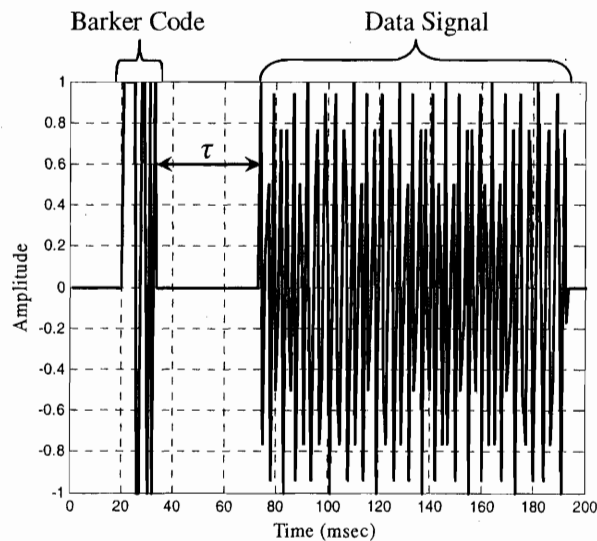


Figure 5.5: Example of signal with Barker Code illustrating silent time τ

Unfortunately, there is no constructive method of finding Barker codes, and only 10 of which are known up to a length of 13 bits. This longest available code is used in the proposed communication system, followed by silent time τ equal to 8-50msec, depending

on the carrier frequency. A complete list of the Barker Codes is provided in Table 5.1 for reference.

Length	Code	Sidelobe level (dB)
2	+1, -1 or +1, +1	- 6.0
3	+1, +1, -1	- 9.5
4	+1, +1, -1, +1 or +1, +1, +1, -1	-12.0
5	+1, +1, +1, -1, +1	-14.0
7	+1, +1, +1, -1, -1, +1, -1	-16.9
11	+1, +1, +1, -1, -1, -1, +1, -1, -1, +1, -1	-20.8
13	+1, +1, +1, +1, +1, -1, -1, +1, +1, -1, +1, -1, +1	-22.3

Table 5.1: Barker Codes

5.3.5 Inverse Transfer Function

In case the recorded signal is expected to be severely distorted, the preconditioning block is introduced to the receiver in order to prepare the signal for the remaining signal processing steps. The scope of the preconditioning block is to remove some of the channel imposed distortion and enhance the characteristics of the transmitted signal, even before any other type of filtering or identification of the Barker Code is applied. The signal enhancement is achieved by reversing the effect of the transmission channel by applying an *Inverse Transfer Function*, or by isolating the less dispersive and/or carrying the majority of the signal's energy modes with *Stacking*, which is discussed in the next section. These steps are necessary in regions with significant reverberation and ambient noise, which severely distort the propagating signal; however, they can be computationally intensive or require additional equipment not always available.

The concept of transfer functions was introduced in Chapter 3, where it is defined as the response of the transmission channel in the frequency domain for an impulse excitation. It was also stated that multiplication of the frequency spectrum of any signal with the transfer function provides the response of the channel to that particular signal,

while transformation back to the time domain provides the time history response. The main idea of this signal processing step is to reverse the effect of the channel on the propagating wave by applying the inverse of the transfer function representing the channel. According to the proposed method, the transfer function is estimated experimentally by the transmission of a trial signal, a priori known to the receiver. The receiver identifies the transfer function by comparing the recorded signal with the locally stored copy of the transmitted signal, and applies the inverse on every incoming signal to remove the channel distortion. In case the channel has time varying characteristics, retransmission of the same trial signal and re-estimation of the transfer function may be required at appropriate time intervals.

The transfer function can be modeled as a causal *Infinite Impulse Response* (IIR) filter, the coefficients of which can be found using an *Auto-Regressive Moving Average* (ARMA) method. Assuming that the output of the transmission channel $y[n]$ for an input signal $x[n]$ can be modeled as:

$$y[n] = x[n] * h[n] + e[n] \quad (5.1)$$

where $h[n]$ is the transfer function, $e[n]$ corresponds to the additive Gaussian white noise and the operator $*$ denotes convolution. The parameter n indicates the discrete time counter, appropriate for the computational implementation of the algorithm. Ignoring the noise term for the transfer function calculation, in the frequency domain equation (5.1), is written as

$$Y(\omega) = X(\omega) \cdot H(\omega) \quad (5.2)$$

In an infinite impulse response form the filter $H(\omega)$ can be expressed as

$$H(\omega) = \frac{A(\omega)}{B(\omega)} \quad (5.3)$$

and by substituting in equation (5.2)

$$B(\omega) \cdot Y(\omega) = A(\omega) \cdot X(\omega) \quad (5.4)$$

where A and B are filters with N and M number of coefficients respectively. Converting equation (5.4) back in the time domain gives

$$\sum_{k=0}^M b[k] \cdot y[n-k] = \sum_{k=0}^N a[k] \cdot x[n-k] \quad (5.5)$$

with a and b being the coefficients of filters A and B respectively. By selecting $b[0] = 1$, the output of the channel at the time instance n can be expressed as the weighted sum of the previous inputs x and preceding outputs as follows

$$y[n] = \sum_{k=0}^N a[k] \cdot x[n-k] - \sum_{k=1}^M b[k] \cdot y[n-k] \quad (5.6)$$

This equation corresponds to a set of equations equal to the number of discrete time inputs. Assuming that the channel input x and response y at negative time indexes correspond to zero, the above set of equations is written as

$$\begin{aligned} y[0] &= a[0] \cdot x[0] \\ y[1] &= a[0] \cdot x[1] + a[1] \cdot x[0] - b[1] \cdot y[0] \\ y[2] &= a[0] \cdot x[2] + a[1] \cdot x[1] + a[2] \cdot x[0] - b[1] \cdot y[1] - b[2] \cdot y[0] \\ &\vdots \end{aligned} \quad (5.7)$$

This set of equations can be expressed in a convenient matrix form as follows for a total number of $L + 1$ time steps

$$\begin{bmatrix} y[0] \\ y[1] \\ \vdots \\ y[L] \end{bmatrix} = \begin{bmatrix} x[0] & 0 & 0 & \dots & 0 & 0 & 0 & 0 & \dots & 0 \\ x[1] & x[0] & 0 & \dots & 0 & -y[0] & 0 & 0 & \dots & 0 \\ x[2] & x[1] & x[0] & \dots & 0 & -y[1] & -y[0] & 0 & \dots & 0 \\ \vdots & \vdots & \vdots & \ddots & \vdots & \vdots & \vdots & \vdots & \ddots & \vdots \\ x[N-1] & x[N-2] & x[N-3] & \dots & 0 & -y[M-2] & -y[M-3] & -y[M-4] & \dots & 0 \\ x[N] & x[N-1] & x[N-2] & \dots & x[0] & -y[M-1] & -y[M-2] & -y[M-3] & \dots & -y[0] \\ x[N+1] & x[N] & x[N-1] & \dots & x[1] & -y[M] & -y[M-1] & -y[M-2] & \dots & -y[1] \\ \vdots & \vdots & \vdots & \ddots & \vdots & \vdots & \vdots & \vdots & \ddots & \vdots \\ x[L] & x[L-1] & x[L-2] & \dots & x[L-N] & -y[L-1] & -y[L-2] & -y[L-3] & \dots & -y[L-M] \end{bmatrix} \begin{bmatrix} a[0] \\ a[1] \\ \vdots \\ a[N] \\ b[1] \\ b[2] \\ \vdots \\ b[M] \end{bmatrix} \quad (5.8)$$

or more compactly

$$\mathbf{y} = \underline{\mathbf{W}} \cdot \mathbf{u} \quad (5.9)$$

where \mathbf{y} is the $((L+1) \times 1)$ vector containing the response of the channel, $\underline{\mathbf{W}}$ is the $((L+1) \times (N+M+1))$ matrix containing the channel inputs and the preceding response values formatted as shown above, and \mathbf{u} is the $((N+M+1) \times 1)$ vector containing the coefficients of filters A and B . The system of equations described above is over-determinate, assuming that the used time steps $L + 1$ are more than the number of equations $N + M + 1$. Therefore, there is no unique solution satisfying all equations, and a

Least squares type approach is employed to identify a sufficient solution. Multiplying with the transpose of matrix \underline{W} on the left each side of equation (5.9) gives

$$\underline{W}^T \cdot \underline{y} = \underline{W}^T \cdot \underline{W} \cdot \underline{u} \quad (5.10)$$

Inversion of the resulting matrix $\underline{W}^T \underline{W}$ provides the coefficients of the transfer function

$$\underline{u} = (\underline{W}^T \cdot \underline{W})^{-1} \cdot \underline{W}^T \cdot \underline{y} \quad (5.11)$$

At this point, the importance of the selection of the number of coefficients of the numerator N and denominator M of the transfer function H should be emphasized. At first, it is suggested that N should be larger than M . The values of N and M should be large enough to describe adequately the transmission channel, but not excessive in order to preserve the computational cost at reasonable levels. If computational cost is not an issue, large values for N and M can be selected; however, following the calculation of the transfer function, the coefficients with small values can be ignored, since they most probably attempt to describe the ambient noise of the physical system, which was neglected from the mathematical model presented above. For the stability of the response of the transfer function, it is important to preserve the poles of B and the roots of A inside the unit circle. The accuracy of the solution can also be improved if the initial N , or M whichever is larger, rows of matrix \underline{W} are eliminated, since they contain zeros that do not contribute to the final solution.

5.3.6 Stacking

Staking is the second method included in the preconditioning block. The main idea is to isolate the orders of modes and preserve the ones that present the minimum dispersion and/or carry the majority of the signals energy. Caution is however required, since there may be cases, especially for high frequency signals, where the modes with low dispersion characteristics do not carry significant part of the signals energy.

In geophysics the term stacking refers to transmission of multiple copies of the same signal, which by superposition reduce the effect of white noise, since it is considered a random process, while at the same time increase the transmitted signal's magnitude. However, reverberation is the main source of signal distortion for the in-pipe acoustic channel, rather than ambient noise and therefore stacking aims to reduce this

effect. For the proposed system, Stacking refers to the addition or subtraction of signals simultaneously received at various locations at the pipe cross section to remove the effect of the odd or even modes or isolate any necessary mode. The main disadvantage of this method is the need to install more than one receiver around the cross section of the pipe, which is not always feasible.

Isolation of different orders of modes is made possible due to the phase changes within the cross section of the pipe, illustrated in Figure 5.6 for the first 4 modes. Odd numbered orders of modes present reverse phase sign at opposite locations of the cross section, while even numbered orders of modes preserve the same phase sign. Therefore, addition of the signals received at positions across a diameter of the pipe results in removing the effect of the odd numbered orders of modes and doubling the effect of the even numbered orders of modes. Alternatively, subtracting those two signals removes the effect of the even numbered orders and doubles the effect of the odd numbered orders of modes.

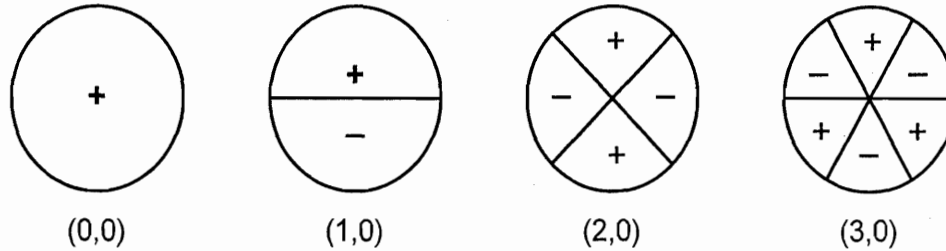


Figure 5.6: Azimuthally distributed modes of propagation
Regions of uniform phase along the cross section for the first mode of each of the first 4 orders

Further resolution in the isolation process can be achieved with the introduction of additional receivers. For example, if four receivers are installed at the internal periphery of a cross section the pipe at opposing locations separated by 90° , the effect of every fourth order of modes can be isolated. More explicitly, considering the modes presented in Figure 5.6, summation of the signals from all four receivers results in isolation of the zero numbered order. In such a case the next appearing order would be the fourth, then the eighth and so on, since summation of each pair of opposite located receivers cancels the odd numbered orders and then the summation of the horizontally and vertically positioned receivers cancels the second, sixth order and so forth. On the other hand

subtraction of the vertically and horizontally aligned receivers would eliminate the zero, fourth eighth and so on orders, preserving the second, sixth, and so forth order. By employing additional receivers and with the aforementioned pattern of summations and subtractions of the simultaneously received signals, it is possible to isolate the specific orders of interest, or eliminate modes that severely distort the propagating signal.

5.3.7 Bandpass Filtering

The frequency spectrum of the received signal may vary significantly from the corresponding spectrum of the transmitted signal due to channel dispersion, superposition with ambient noise and so on. Aforementioned techniques included in the preconditioning block are capable of reducing the signal distortion, but cannot control the magnitude of environmental noise. This noise is considered to be *white*, i.e. to have infinite bandwidth. Depending on the magnitude of this noise, its effect may be proven detrimental to the demodulation process, resulting in significant symbol detection errors. The scope of bandpass filtering is to remove the unwanted noise, outside the bandwidth of the transmitted signal. Even though noise within the frequency spectrum of the bandpass filter is still present in the received signal after the filtering process, it does not alter significantly the signature of the waveform, since it corresponds to a small fraction of the total noise energy. It becomes intuitively apparent that narrow bandwidth signals are affected less by white noise, since less noise energy overlaps with the frequency spectrum of the signal. Bandpass filtering is especially beneficial when the FSK modulation method is used, because it limits the frequency spectrum of the received signal to the bandwidth expected by the FSK demodulator.

Careful selection of the bandwidth of the applied filter is required in order not to annihilate useful data bearing signal along with the white noise. Recall, that the dispersive nature of the transmission channel may result in frequency shifts that may expand the bandwidth of the transmitted waveforms. In the proposed digital communication system, the bandwidth of the bandpass filter used is selected to be several kHz wider than the bandwidth of the transmitted signal, expanding proportionally for higher frequencies. The finite impulse response filter used is designed by employing a

Kaiser Window method [5], requiring the magnitude of the sidelobes to be at least 50 dB below the signal in the pass band.

5.3.8 Equalization

Equalization is the process of removing amplitude, phase and frequency distortion from waves propagating in dispersive transmission channels. When the equalizer employs algorithms that automatically adjust their properties to the response of the channel, the process is called adaptive equalization. Adaptive equalizers are required in channels with unknown characteristics, or which present time variability in their properties. In contrast with the proposed inverse transfer function technique, which corresponds to an infinite impulse response filter, the adaptive equalizer is essentially a finite impulse response filter with adaptive coefficients. The operation of adaptive equalizers, as well as the available adaptation methods of their coefficients are described in paragraph 4.5.4.

Within the scope of this research, the *Linear* and the *Decision Feedback Equalizers* (DFE) are examined, combined with the *Least Mean Squares* (LMS) and the *Recursive Least Squares* (RLS) as the adaptation algorithms. A large variety of adaptive equalizer structures are implemented, including transversal filters with 5 to 100 taps, or in other words delay elements. In general, the DFE requires lower number of taps with respect to the Linear equalizer to achieve the same level of performance, since the DFE benefits from the experience of past data while removes its effect from the current data. Signals with higher frequency spectra and channels with significant dispersion require larger equalizer structures, since finer resolution is required to describe the channel characteristics. In the current implementations, the step size parameter μ of the LMS algorithm varies from 0.001 to 0.1 depending on the size of the structure, the characteristics of the channel and their expected time variability. Larger μ results in larger steps in the adaptive algorithm, which consequently results in faster convergence to the region of the optimum solution. However, when the algorithm reaches the area of the optimum solution, a large step size parameter may prevent the algorithm from identifying the actual optimum solution. On the other hand, a small μ results in a slow convergence

to the optimal solution, or even worse, may trap the algorithm in the area of a local optimum. For this reason in most simulations a variation of the LMS algorithm is used, which allows to adjust the step size parameter μ between a high and low value, starting with the high value and decreasing it as it approaches the optimal solution.

The RLS algorithm requires specification of two adjustable parameters; the regularization parameter δ and the forgetting factor λ . The regularization parameter δ is given values between 0.5 and 0.004 with the high values corresponding to signals with low signal to noise ratio (SNR), and the low values corresponding to cases with high SNR, [6]. The forgetting factor λ is set equal to 0.95 for all adaptive equalizer implementations. The RLS algorithm converges faster than the LMS algorithm to the optimal solution. However, its stability is very sensitive to the selected parameters as well as to the dimensions of the equalizer. In general, the LMS algorithm is more suitable for equalizers with long filters.

5.4 *Hardware Implementation*

This section discusses the implementation the hardware components required to realize waveforms and execute the signal processing steps examined in the preceding paragraphs. Figure 5.2 illustrates the hardware layout of the transmitter and receiver. The blocks labeled *modulated signal* and *received signal* represent the integrated circuit processing units that execute all the required software operations for the transmitter and receiver respectively. A powering unit, essential for the operation of every block presented in this figure, is omitted but implied. Unfortunately, since the system has not yet been integrated for autonomous use in a pipeline network, some of the components' discussions remain at an abstract level, expressing the emerging trade-offs and issues that require attention, acting mostly as design guidelines rather than specifications. The hardware used for the experiments completed, will be presented in Chapter 7 along with the obtained results.

5.4.1 *Microprocessor*

All the aforementioned signal processing steps are implemented at the software level. The mathematical computations indicated by the software are executed in the proposed communication system by a micro-processing unit. This processing unit is a programmable microcontroller in which the developed software can be embedded. The selection of the microcontroller is mainly controlled by the computational demand of the transmission or reception algorithms. In an integrated wireless sensor node, the same processing unit may handle the computational load of the sensor data analysis and event recognition. Increased computational demand is translated in the selection of a more powerful microprocessor, which can handle more instructions per second. The computational capabilities of the microprocessor are controlled by its architecture and the frequency of its internal oscillator, or in other words, the internal clock. Higher oscillator frequency results into more data packets processed at a specific time frame. However, the increased calculation capabilities are provided at the expense of increased power demand. Since the power resources are limited for the in-pipe communication system, there exists a trade-off between processing time and power consumption. It should be noted that a microprocessor with low oscillator frequency would consume less power per unit time, but it would require more time to execute the prescribed calculations. Therefore, there exists an optimal solution which compromises the power consumption and the processing speed, and is heavily dependent on the microprocessor architecture and the amount of required calculations. The selection of the processing unit may also depend on the structure of the software code, and vice versa, indication that the software should be written in such a way to avoid expensive calculations, especially numbers with decimal points and matrix inversions.

In addition to the processing capabilities of the microprocessor, the available memory should also be considered. Memory is required for buffering the data to be processed, or temporary storage for further processing in the future, preserving an event logger, and so on. The trade-off between the power and the processing speed extends to the amount of memory as well, since increasing memory increases the power consumption of the system. Since most microcontrollers have sufficient memory only for the computational load they can handle, it may be required to include at the circuit board

some other form of data storage, such as flash memory chips, in order to preserve data for future processing.

5.4.2 Analog to Digital Converter

The signals prepared for transmission by the microprocessor are actually discrete in time points representing analog waveforms. Transmission of the waveform in a physical medium requires a real continuous analog signal. Therefore, the output of the microprocessor needs to be converted from discrete to continuous in time with the assistance of a *Digital to Analog Converter* (D/A). In turn, at the receiver side, the recorded signal is in the format of a continuous waveform. In order to process and extract the digital data for the incoming signal, it is necessary to convert it into a discrete time form, appropriate to be presented to the microprocessor. This operation is achieved with the assistance of an *Analog to Digital Converter* (A/D). The selection of these converter units are based on two parameters, namely the resolution and sampling rate. These two parameters are contradictory to each other, since increasing the resolution decreases the sampling rate capability and vice versa.

The sampling rate is the rate at which the converter is capable of converting the information from one form to the other. The sampling rate capability is controlled by the frequency spectrum of the data bearing signal. In order to convert the signal correctly, the sampling rate of the analog to digital converter needs to be at least twice than the highest frequency of the received signal, denoted as the Nyquist frequency. In the same context, the sampling rate of the digital to analog converter needs to be at least equal to the time step of the discrete signal generated at the transmitter microprocessor.

The resolution describes the accuracy with which conversion can be achieved. Higher resolution means that the converter is capable of representing smaller values. Therefore, the resolution of the converter must be high enough to avoid quantization errors, and be able to represent the signal as accurately as possible. However, increasing the resolution of the converter beyond a specific point is not beneficial due to signal magnitude and transducer sensitivity limitations. When the smallest quantity that can be represented by the converter is significantly smaller than the minimum value expected in

the data signal, or the sensitivity of the transducer, then the achieved accuracy is not useful, since these small quantities represent the ambient noise or the electrical noise of the transducer.

5.4.3 Signal Amplifier

The output of the digital to analog converter is a low power signal frequently normalized to a maximum value of one. Therefore, a power supply is required to provide the power required to drive the signal source. This power supply can be an amplifier, which will adjust the signal magnitude and power to the acoustic source, in order to generate an acoustic signal of sufficient intensity to reach the receiver. This amplifier is composed of either a single, or more frequently a collection of operational amplifiers, with appropriately adjusted gain to amplify the incoming signal, [7] and [8].

On the receiver side, an amplifier is required to adjust the unregulated output recorded from the transducer so as to fit the amplitude (or current depending on the transducer) range of the analog to digital converter. Adjusting the range of the incoming signal to the input range of the converter is necessary to utilize more efficiently the resolution of the converter. The digitization process, for signals with smaller amplitude range than that of the converter, utilizes only a part of the resolution of the A/D converter. On the other hand, signals beyond the range of the converter are represented by their maximum output value, resulting in significant errors. This amplifier is frequently denoted as *pre-amplifier*, since it regulates the input signal before any other processing operation.

5.4.4 Transducers

Underwater transducers are responsible for converting the acoustic pressure waves into electrical waves, usually in the form of a voltage signal, when they operate as receivers. On the other hand, used as sources of acoustic waves, underwater transducers convert energy provided by a power amplifier into an acoustic pressure output. An underwater transducer with the primary operation to receive acoustic signals is usually denoted as a *hydrophone*, while when it is used to transmit signals, it is named a

projector. The process of selecting an underwater transducer can be a painstaking and toilful procedure, since there exists a large number of parameters that must be specified, the most important of which are summarized next.

The most important attribute of a transducer used for an underwater acoustic communication system is its operating frequency range. Hydrophones have relatively flat receiving response with respect to input signal frequency, enabling them to be used over a large frequency range. On the other hand, projectors tend to have highly variable transmitting response with increasing frequency, limiting significantly the efficient transmitting frequency range for which they can be used. The transmitting frequency response of projectors typically presents a sharp peak at a specific narrow frequency range, and a highly decaying performance for all other frequencies. The operational frequency range of a projector is controlled mainly by its size and structure assembly. It should be understood that the smaller the transducer, the higher its efficient frequency range, due to improved generation of waves with smaller wavelength. The narrow operating frequency range of the projector may impose severe limitations to the bandwidth of the data bearing signal specified by the communication system. Moderate extension of the projector's operating bandwidth can be achieved, if high voltage power supplies are employed to drive it. This becomes possible since most underwater transducers are manufactured from piezoelectric materials, which can sustain and perform well under high voltage excitations. For this reason, many underwater transducers require high power sources with very high voltages; these are, however, unsuitable for the proposed in-pipe communication system due to limited power supply, as well as environmental concerns due to the presence of high voltage sources.

Aside from the frequency response, a very important property of an underwater transducer is the beam pattern of the waves that it generates. The beam pattern provides an indication of the relative amplitude of the transmitted or received acoustic wave as a function of the direction relative to the transducer. There exist several patterns such as omnidirectional, hemispherical, toroidal, conical, and so on, each one appropriate for a different class of applications. A collection of the aforementioned beam patterns are illustrated in Figure 5.7.

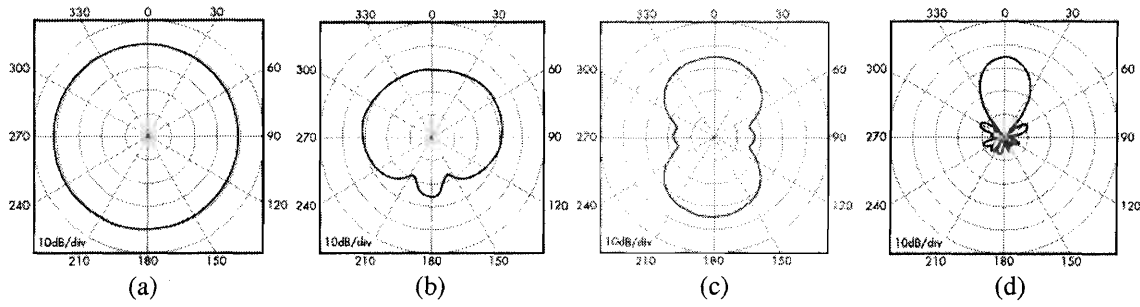


Figure 5.7: Beam Patterns (a) Omnidirectional, (b) Hemispherical, (c) Toroidal, and (d) Conical, [9]

It becomes apparent that for the in-pipe communication system a narrow beam transducer that would transmit along the length of the pipeline is desirable. A projector with a highly directional beam pattern would allow focusing the energy of the transmitted signal along the axis of the pipeline, reducing consequently the amount of multipath propagation and the energy of the reverberant signals. A highly directional hydrophone, on the other hand, is capable of collecting signals from specific directions, allowing to focus the energy of the received signal on the direction of the pipeline and hence to avoid multipath received signals. Along with the beam pattern, quantities such as the beam width and the directivity index must be specified. The beam width is the angle in degrees of the main lobe, usually defined between the half power points, i.e. where the amplitude has dropped by 3dB. The directivity index is a measure of the sound intensity of the transducer in the direction of the main lobe compared with the intensity generated from a point, and therefore omnidirectional, source. Unfortunately, high directionality and beam forming frequently requires large in size transducers, which may not be suitable for the in-pipe communication system.

Of critical importance for the successful implementation of the in-pipe communication system is the transmitting and receiving sensitivity of the transducers. A measure of the transmitting sensitivity is given by the *Transmitting Voltage Response* (TVR), which is calculated as the level of acoustic output referenced to one meter per one volt of input. The receiving sensitivity is provided by the *Open Circuit Voltage* (OCV), which is the level of electrical output for one micro-Pascal of acoustic input. It is understandable that the higher the sensitivity of the transducer the more the energy of the acoustic wave it generates. Therefore, a projector with high TVR is required for the proposed communication system in order to achieve the necessary magnitude of the

acoustic wave with lower voltage requirements. In the same context, the sensitivity of the hydrophone must be adequate to resolve the minimum pressure of the data bearing wave that arrives at the receiver. However, excessive receiver sensitivity would result in increase of the recorded noise levels, since even the smallest pressure disturbance is recorded and overlapped along with the data signal.

Secondary, but important, considerations include the mounting of the transducer at the internal surface of the pipeline, as well as its size and weight, the materials used, the service life and so forth. The mounting mechanism must provide a stable base in order to allow the efficient transmission and reception of acoustic waves. If the support of the transducer is not stable enough for the frequency range of the signals of interest, the operation of the transducer will not be efficient due to its relative motion with the support. The size of the transducer should be small enough to fit inside the pipeline from the insertion point, which may be an access point, a pumping station, and so on. However, recall that the transducer size affects the efficient operating frequency range, with smaller transducers operating at higher frequencies. This size restriction may impose significant limitations on the operation of the communication system, since higher frequency spectrum of the transmitted signal translates into increased reverberation. Special care is required for the materials in order to be safe for introduction inside a potable water pipeline. Further discussion of these issues is provided in paragraph 5.4.6. Design guidelines for the selection of available underwater transducers or the specification of their parameters are provided in literature, [10] and [11].

5.4.5 Power unit

All the aforementioned operations are feasible under one major, and frequently overlooked, condition; the availability of sufficient power supply. All the devices described above, along with the remaining components of the wireless sensor node as described in Chapter 1, require some amount of power to operate and implement the purpose for which they are employed. The uninterrupted operation of the wireless sensor network, for which this communication system is proposed, requires power sources capable of providing energy for a theoretically infinite amount of time, since the in-pipe

installation of these devices prohibits the use of batteries or any other form of power supply that requires replacement at frequent time intervals, due to access limitations. A potential solution for the required renewable energy source is provided from a system that harvests energy from the flow of water inside the pipeline. Such a system was created and is described in a subsequent paragraph.

First of all, it is necessary to identify the amount of power required for the operation of each wireless sensor node. The largest power consumer in each such node is the amplifier-projector combination of the communication system. The power required by the projector is controlled by the amplitude of the pressure wave necessary to transmit the data from the source to the receiver. An estimation of the required pressure wave amplitude is provided by calculating the signal attenuation due to spreading and absorption. The resulting amplitude of the wave at the location of the receiver should be at least equal to the minimum detectable pressure by the hydrophone. Considering that the sensitivity of a typical hydrophone, as expressed by the open circuit voltage, is in the order of -180 dB/Volt/mPa , the output of the receiver is 1 nVolt per $1 \mu\text{Pa}$ of pressure. In order to exceed the levels of the ambient noise of the water and the electrical noise of the circuit, the mean value of received pressure level is required to be around 0.5 Pa , which translates to a hydrophone response of 0.5 mVolts . The basic sonar equation relating the sound pressure level L_p at the location of the receiver with the energy of the signal L_w at the location of the transmitter in water is written as

$$L_p = L_w + 171 + DI - H \quad (5.12)$$

where DI is the directivity index and H is the transmission loss. All the quantities are expressed in dB for the default references values for water of 1 m distance, $1 \mu\text{Pa}$ pressure, and 1 Watt of power. If the transmitter and receiver are assumed conservatively to be omnidirectional, the directivity index is equal to zero. The transmission loss is calculated as the addition of the signal attenuation due to spreading and absorption. Even though signal spreading for the in-pipe waveguide matches better the cylindrical pattern, for simplification it is considered here spherical, which provides again conservative results. Thus the transmission loss is expressed as:

$$H = 10 \cdot \log \left(\frac{r^2}{r_{ref}^2} \right) + a \cdot r \quad (5.13)$$

where r is the propagation distance, r_{ref} is the reference distance for pressure waves in water, which is equal to 1m, and α is the sound absorption factor for water. The sound absorption factor is a function of the frequency spectrum of the wave as well as several environmental parameters such as temperature, pressure, salinity, and so on. For a water temperature between 10 and 20 degrees Celsius and for an approximately maximum signal frequency of 60 kHz, according to Figure 5.8 the absorption factor is equal to 0.4 dB/km. Assuming a propagation distance of 1km, which is within the objectives of this research, the transmission loss is found to be equal to $H = 54.4$ dB re. 1m. The only term missing in the above transmission loss equation is the signal attenuation due to fading, i.e. destructive overlap of multipath signals, which however cannot be easily predicted and modeled.

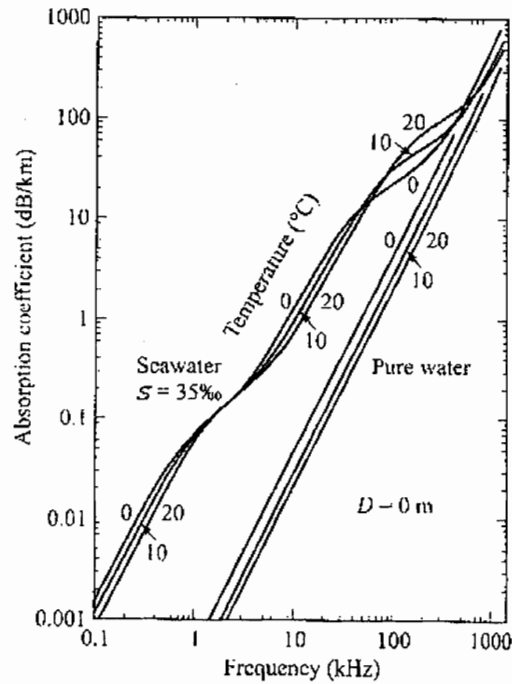


Figure 5.8: Volumetric absorption including all known relaxation processes, [12]

The objective sound pressure level is calculated from the desirable mean pressure of 0.5Pa as

$$L_p = 10 \log \left(\frac{P^2}{P_{ref}^2} \right) = 10 \log \left(\frac{0.5^2}{(1 \cdot 10^{-6})^2} \right) = 114 \text{ dB re } 1 \mu\text{Pa} \quad (5.14)$$

Substituting the above values in equation (5.12) the energy level of the wave at the location of the source is found to be

$$L_w = 114 - 171 + 54.4 = -2.6 \text{ dB re } 1 \text{ Watt} \quad (5.15)$$

The energy level is expressed in terms of watts as

$$L_w = 10 \log \left(\frac{W}{W_{ref}} \right) \quad (5.16)$$

where W is the power in Watts of the wave at the location of the transmitter. Therefore, from equations (5.15) and (5.16) the power of the wave is calculated to be equal to

$$W = 0.55 \text{ Watts} \quad (5.17)$$

It is important to note that the power demand increases exponentially with the input pressure requirement. Therefore, for a required pressure of 1Pa the power requirement would be in the order of 2 Watts, i.e. four times higher power for two times pressure increase. However, the projector operates only when a signal transmission is required. The power calculated above is the power consumed by the projector during signal transmission. Since the duty cycle of the transmitter is usually low, higher power surges may be available from the same energy source, which would allow generation of higher amplitude pressure signals.

The power consumption of each of the remaining components of the wireless sensor node, such as sensors, microprocessors, A/D converters, and so forth, lie in the order of mWatts. Summing typical values for the power consumption of each component requires approximately another 0.4 Watts raising the total power consumption of the system in the order of just less than 1 Watt.

At this point the energy demand has been specified and remains to identify the potential renewable energy source that can satisfy this demand. The most readily available source of energy at the pipeline environment is the flow of water inside the pipe. While the idea of harvesting energy from the flowing water is not new, it has only been applied at large and very large scale in water turbines used at hydroelectric power plants as well as lower intensity energy sources as harvesting energy from tides, waves

and so on. Several attempts for renewable energy have been presented for household use, [13], involving however, large rotating parts and requiring fast flowing streams. Most commercial power generators that use the water flow to extract energy employ a propeller as a turbine. The flowing water causes the propeller to rotate, which in turn is connected to a generator that produces electricity. However, the efficiency of the propeller as a generator is relatively low, in the order of 20%, [14]. A very promising energy harvester from tides and waves is the patented Gorlov's Helical Turbine, [15] and [16], which offers a higher efficiency than regular propellers with a claimed maximum efficiency of 35%, [14]. However, the efficiency of this turbine has only been verified for large scale generators, in the order of kW to MW. In general, there is a lack of small scale power generators in the order of 1 watt.

According to the proposed power harvesting system, the energy extracted from the water flow, with the assistance of the turbine, is converted to electrical energy with the use of a generator, as illustrated in Figure 5.9.

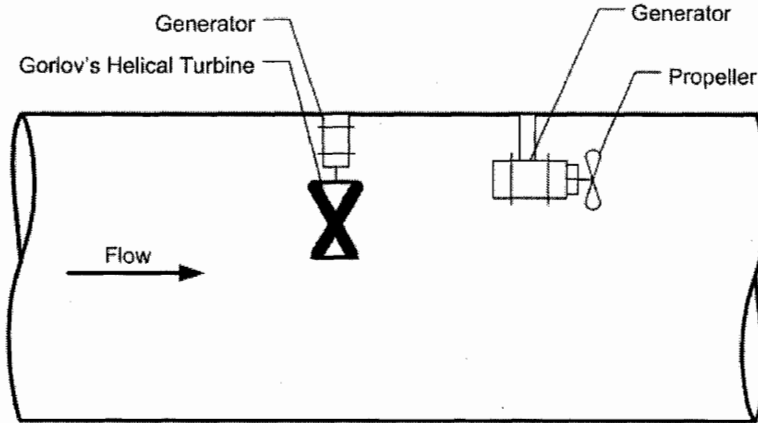


Figure 5.9: Power harvesting system from the flow of water inside the pipeline

The capacity of such a system is restricted to the energy potential of the flow. However, the undisturbed operation of the pipeline needs to be considered, and therefore the turbine needs to be as small as possible. The power extracted from a generator can be approximately calculated according to

$$P = \frac{1}{2} \rho A V^3 \eta \quad (5.18)$$

where P is the power, ρ is the fluid density, A is the area of the turbine perpendicular to the flow, V is the velocity of the water and η is the efficiency of the turbine. The dimensions of the turbine and its corresponding efficiency are the only variables on this equation. Considering that the density of the water is 1000kg/m^3 , the velocity of the water within a pipeline is often at most in the order of 1m/sec , the dimensions of a miniature turbine to be approximately 10cm tall by 10cm wide, and having efficiency of at most 35% , the maximum available power that the power harvesting system can generate lies in the order of 1 watt .

Due to the aforementioned necessity of using a small turbine, the helical turbine lacks the initial torque to startup easily for slow water velocities. For this reason, within the scope of this research, a hybrid scheme that encapsulates the high efficiency of the helical turbine with the high initial startup torque of a Savonius turbine was designed, with dimensions $2''$ in diameter by $9''$ tall and capable of generating energy up to 1 Watt for water flow velocity 1m/sec . The hybrid design along with illustrations of Gorlov's Helical Turbine and the Savonius turbine are presented in Figure 5.10.

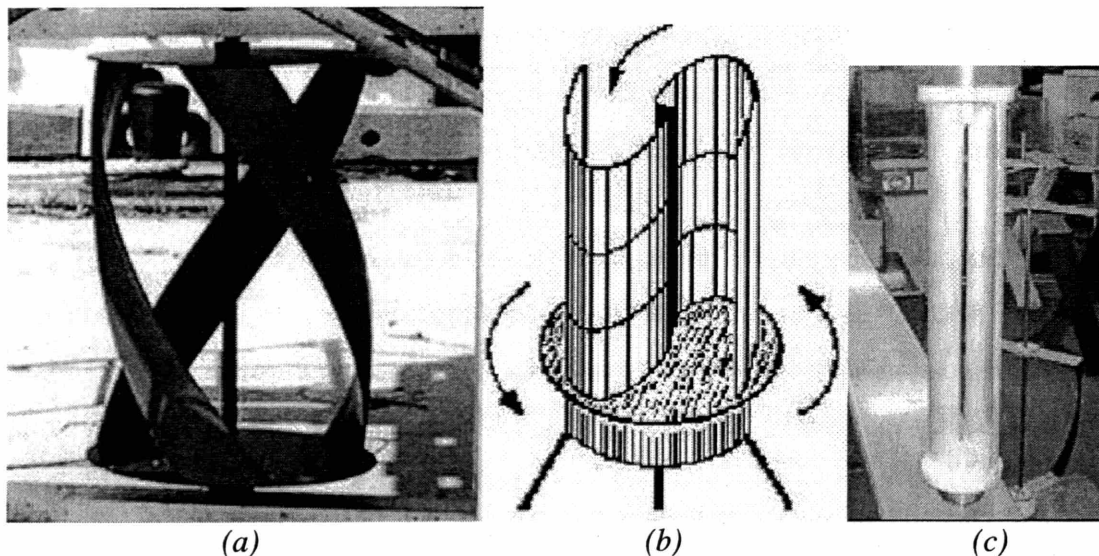


Figure 5.10: (a) Gorlov's Helical Turbine, (b) Savonius Turbine, [17], (c) Hybrid Design

Since the energy requirements of a wireless sensor network, due to processing and transmission of data, as well as the available energy, in terms of water flow, vary over time, it is required to employ an energy storage device. This storage device can be

realized with a rechargeable battery or a capacitor, which will be charged and discharged according to the needs of the system. According to the expected scenario, the power harvesting system will operate at all possible times, i.e. when the water flow is sufficient, and will charge the energy storage device, which in turn continuously supplies power to the sensor node.

5.4.6 *Installation*

One of the most troublesome parts of the in-pipe communication system implementation is its installation inside the pipeline. The communication system integrated with the sensors, CPU and the power unit, comprises an independent node of the wireless sensor network. Each node must be inserted in the pipe enclosed in a waterproof, insulated and compact package. Access points with sufficient clearance for the insertion of each package are required. Such access points may be in the form of pumping stations, or gate valves, located along the length of the pipe and usually installed for inspection purposes. However, gate valves are infrequent and of small size, thus restricting the number of available access points inside the pipeline as well as the maximum size of the wireless sensor node packaging. For this reason, large components such as the turbine may need to be deployed in a collapsible manner, i.e. implement a mechanism that would allow collapsing the turbine into a small tube for the installation phase, and expanding it when it is ready to be used. Pumping stations, as well as other points of complete exposure of the pipe on the surface, are points of potential access to the complete cross section of the pipe. This allows the use of robots, similar to Figure 5.11, which may carry several sensor nodes and install them as they crawl along the length of a pipeline segment.

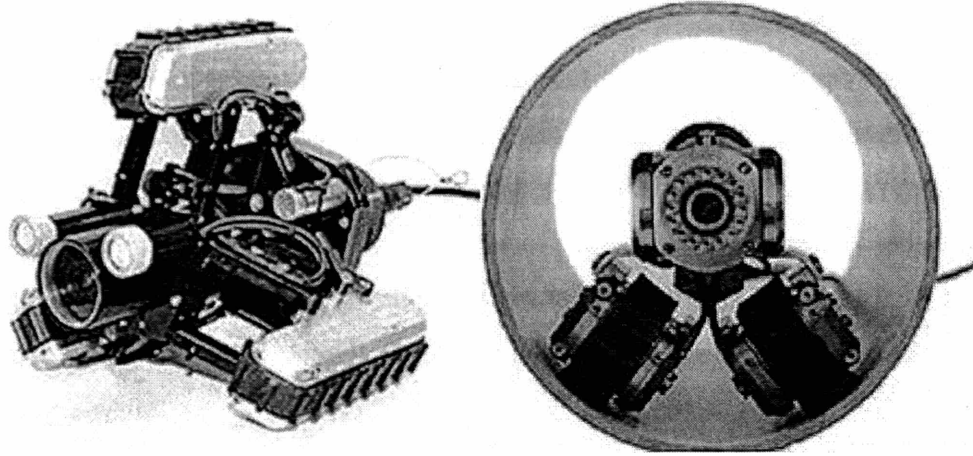


Figure 5.11: Examples of Pipeline Robot Configurations, [18]

The packaging of each sensor node, not only must be small, but also it should have a hydrodynamic shape, such that its presence generates the minimum possible disturbance of the water flow. It is desired to have minimal turbulence around the sensor node in order to avoid interaction with the acoustic communication system as well as minimal disturbance of the biofilm, a thin biological layer present on the inside of all fresh water pipelines.

Within the same context, the installation and the materials used for the sensor node, must be compatible with the pipeline environment and safe for long term exposure to underwater conditions. Special care should be taken for the safety of the system, which must comply with all water pipeline health regulations, since it is intended primarily for potable water pipelines. Therefore, to attach the sensor node at the pipe wall, special non-toxic and suitable for underwater use epoxy should be used. Alternatively, a magnetic connection may be feasible, provided that the pipe is made from a ferromagnetic material, such as steel or cast iron, and that it will not interfere with the electronics of the sensor node. In general, solutions such as attaching the sensor node with screws and drilling the pipe wall should be avoided, since it may create failure prone areas in terms of the structural integrity of the pipe as well as contamination of the water.

Finally, it should be noted that water pipelines usually operate under pressure, with typical values of 4atm and peaks up to 10atm. Therefore, the container of the sensor node must be insulated and capable of sustaining such high pressures. Alternatively, the whole system can be manufactured under the same pressure conditions existent in the

pipeline, such that the container is in equilibrium of pressures under normal operating conditions. Insulation is necessary, to protect the electronics from corrosion as well as leakage to and from the water. Special care is required for the insulation of the rotating shaft connecting the turbine with the generator. High pressure seals are required that would allow at the same time the rotation of the shaft with minimal friction. To remove this obstacle, magnetically driven shaft connections can be used instead of a solid axle. According to this system, the rotating turbine is connected with a transversally attached magnet, both located at the outside of the insulation shield. This magnet drives in sequence a magnet attached to the generator, installed inside the shield and facing the location of the turbine. This mechanism eliminates the use of specialized seals with solid axle shafts, which are failure prone areas, and completely isolates the electronics compartment inside the container from the flowing water.

5.5 References

- [1]. Sklar B., "Digital Communications: Fundamentals and Applications", *Prentice-Hall*, 2nd Edition, Upper Saddle River, NJ, 2001.
- [2]. Proakis J.G., "Digital Communications", *McGraw Hill*, 4th Edition, Boston, MA, 2001.
- [3]. Barker, R.H., "Group Synchronization of Binary Digital Systems", *Communication Theory*, W. Jackson ed., Academic Press Inc., New York, 1953.
- [4]. Fahy F., "Foundations of Engineering Acoustics", *Academic Press*, London, UK, 2001.
- [5]. Oppenheim A.V., and Schafer R.W., "Discrete Time Signal Processing", 2nd Edition, *Prentice Hall*, Upper Saddle River, NJ, 1999.
- [6]. Haykin S.S., "Adaptive Filter Theory", *Prentice-Hall*, 4th Edition, Upper Saddle River, NJ, 2002.
- [7]. Jung W.G., "IC Op-Amp Cookbook", *Prentice Hall*, 3rd Edition, Upper Saddle River, NJ, 1986.
- [8]. Mancini R., "Op Amps for Everyone", *Newnes*, 2nd Edition, 2003.
- [9]. International Transducer Corporation, Company Website, Electronic Reference Sept. 2005, <http://www.itc-transducers.com/>
- [10]. Kuntsal E, and Bunker W.A., "Guidelines for specifying underwater electroacoustic transducers", *Proceedings of UDT '92 Conference*, London, England, June 1992. (See also revised version at <http://www.itc-transducers.com/pdf/guidespec.pdf>).
- [11]. Coates R.F.W., "The design of transducers and arrays for underwater data transmission", *IEEE journal of Oceanic Engineering*, Vol. 16, No. 1, pp. 123-135, January, 1991.
- [12]. François R.E, and Garrison G.R., "Sound absorption based on ocean measurements: Part II. Boric acid contribution and equation for total absorption", *Journal of Acoustical Society of America*, Vol. 72, pp. 1879-1890, 1982.
- [13]. ABS Alaskan Inc. Website, Electronic Reference Sept. 2005, <http://www.absak.com/alternative-energy/hydro-power.html>

- [14]. Gorban A.N, Gorlov A.M., and Silantyev V.M, "Limits of the turbine efficiency for free fluid flow", *ASME Journal of Energy Resources Technology*, Vol. 123, pp. 311-317, December, 2001.
- [15]. Gorlov A. M., "The Helical Turbine: A New Idea for Low-Head Hydropower", *Hydro Review*, 14, No. 5, pp. 44–50, 1995.
- [16]. "Creating Electricity with undammed hydropower", *Environmental Science and Technology, American Chemical Society*, pp 55A-56A, February 1, 2004.
- [17]. "Solar Electric Basics", *ISEA Fact Sheet 6*, Illinois Solar Energy Association, Apr. 2004, Electronic Reference Aug. 2005, http://www.illinoissolar.org/fact_sheets/06%20ISEA%20Fact%20Sheet%20-%20Solar%20Electric%20Basics.pdf.
- [18]. Roboprobe Technologies Inc. Website, Versatrax pipeline inspection crawlers, Electronic Reference Aug. 2005, <http://www.roboprobe.com>

Chapter 6

Simulations

6.1 Introduction

This Chapter evaluates the performance of the proposed digital communication system, utilizing the signal processing techniques described in Chapter 5. For this purpose computerized simulations as well as scaled laboratory experiments are conducted, according to which the digital communication system attempts to transmit and receive digital data reliably through a pipeline waveguide. This Chapter presents the results from the data transmissions inside a simulated pipeline, while the actual lab experiments are presented in Chapter 7.

The main purpose of the computerized simulations is to evaluate the performance of every single component of the digital communication system, and the effectiveness of the available alternative methods. Parametric analyses are conducted, with respect to the signal processing techniques presented in the previous chapter, isolating as much as possible the effect of the controlled parameter. The aggregating improvement of the error performance of the system for each technique is estimated by adding constructively, one by one, the proposed signal processing components up to the implementation of the complete communication system. More explicitly, the effect of the selected modulation technique is initially examined, by transmitting signals modulated with the binary *Frequency Shift Keying* (FSK), binary *Amplitude Shift Keying* (ASK) or the equivalent *Phase Shift Keying* (PSK), and the *Quadrature Amplitude Modulation* (QAM). Transmission through the pipeline waveguide and demodulation of these signals provides an indication of the robustness of each modulation method, while the high error rates prove the necessity of the error and distortion correction steps. Thus, the Reed Solomon encoding step is added in sequence, followed by the preconditioning and the adaptive equalizer blocks. The effectiveness of adaptive equalizers is demonstrated by implementing both *Linear* and *Decision Feedback Equalizers* (DFE) of various lengths,

utilizing the *Least Mean Squares* (LMS) and the *Recursive Least Squares* (RLS) adaptation algorithms.

The effect of white noise on the reliability of the system is examined by adding Gaussian white noise onto signals. Received signals of various *signal to noise ratios* (SNR) are achieved by varying the power of the added noise. A direct comparison between the channel distortion due to the reverberation and the ambient noise is therefore accomplished. The performance of the Baker code is finally verified by the presented results, as well as an initial estimate for the appropriate silent time for each carrier frequency is justified.

In accordance with the results presented in Chapter 3, the digital communication system's parametric analyses also involve geometric parameters of the waveguide, such as the length and diameter of the pipeline. The reference case for the parametric analyses presented includes an FSK modulated signal with a carrier frequency of 3kHz transmitted through a 0.5m radius pipeline for a length of 10m, while both the transmitter and receiver are located at the internal periphery of the pipe. The messages used in the following simulations are packetized in blocks of 42 to 140 bits. The simulations are conducted with the rigid pipe approximation code described in Chapter 3, in order to limit the number of adjustable parameters related to the pipeline environment.

6.2 Modulation

This section examines the performance of the employed modulation method with respect to the integrity of the received signal. The results provided in the subsequent paragraphs illustrate the transmission of a modulated signal through the pipeline waveguide. In order to evaluate the performance of each modulation method, no error or distortion correction as well as no filtering is applied to the received signal, which is directly demodulated. The poor error performance in the attempt to detect the encapsulated bits proves the necessity of the error compensation signal processing steps.

Preceding the signal modulation the textual message to be transmitted must be converted into bits and formatted into an appropriate style for further processing. The data conversion to bits is achieved according to the 7-bit ASCII code, presented in

paragraph 5.3.1, which represents each character of the textual message with a string of 7 binary bits. For example if the message desired to be send is “George” the string of bits takes the form

G	1	1	1	0	0	0	1
e	1	0	1	0	0	1	1
o	1	1	1	1	0	1	1
r	0	1	0	0	1	1	1
g	1	1	1	0	0	1	1
e	1	0	1	0	0	1	1

with each one of the rows of the above steam of bits representing one of the letters of the textual message. In the above example the matrix representation is used for the reader’s convenience, while the message is actually processed in the transmitter in the form of a bit stream. The following paragraphs present results from messages modulated with the binary Frequency Shift Keying, binary Amplitude Shift Keying, and Quadrature Amplitude Modulation, respectively. The textual message at the simulations implemented is modulated at data rates ranging from 1 to 21 kbps. However, this section presents results in the 1 to 7 kbps range, for direct comparison with the scaled experiments introduced in Chapter 7. High data rate results are presented in paragraph 6.5.5 towards the end of the chapter.

6.2.1 Frequency Shift Keying

According to this modulation method the analog representation of the binary bits is implemented with frequency shifts upwards or downwards from the central frequency of the carrier signal. Examples of FSK modulated signals are illustrated in Figure 6.1, which presents the amplitude of the signals to be transmitted, normalized to unity, along with the resultant frequency responses. The three sets of plots correspond to signals modulated at 1, 4, and 7kbps data rates, respectively. The signal amplitude plots, along with the modulated signal, feature the Barker code and the appropriate silent time in between. The introduction of the Barker Code is required for the synchronization of the data bearing signal at the receiver side.

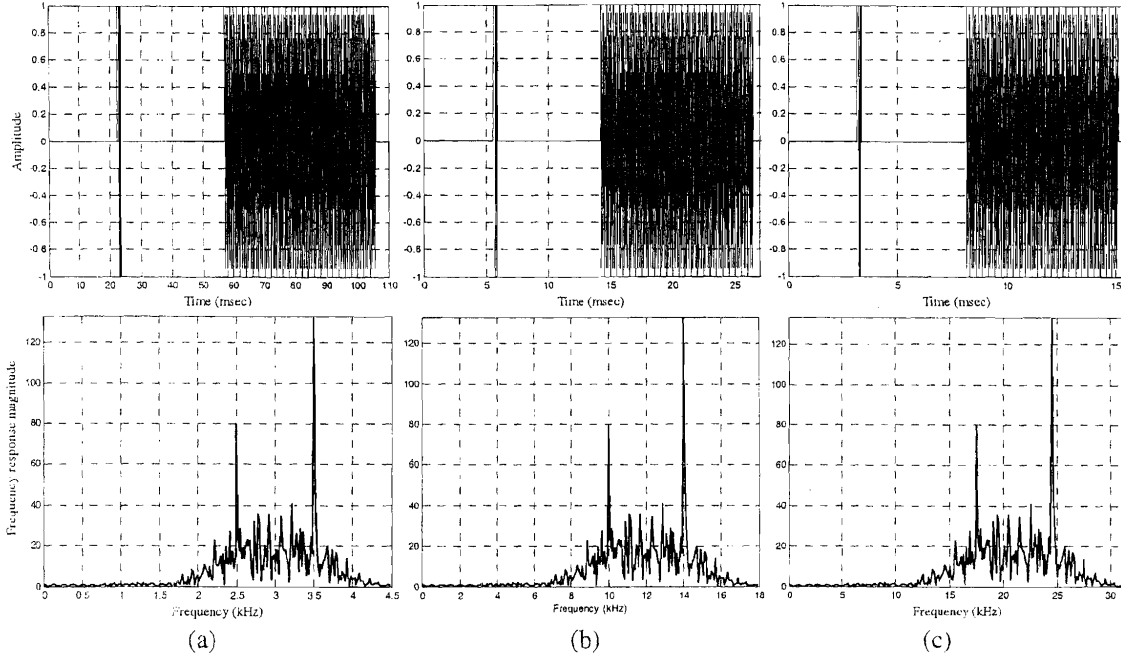


Figure 6.1: Amplitude and Frequency Response of Transmitted Signal for FSK modulation at data rates (a) 1kbps, (b) 4kbps and (c) 7kbps

Since in all three cases the textual message represented is the same, the resulting signal is essentially the same waveform, scaled in time to correspond to the shifted carrier frequency. In sequence, the frequency spectra of the signals generated are shifted versions of the leftmost spectrum to higher frequencies and wider bandwidths. The two distinctive peaks in each of the presented frequency spectra correspond to frequency shifts from the central frequency, often denoted as the *carrier frequency*, representing the 0 and 1 bits, respectively.

Figure 6.2 presents the pressure time histories, along with the frequency response, of the received signals corresponding to the transmission of the above waveforms through a $R = 0.5\text{m}$ radius pipeline for a propagation distance $z = 10\text{m}$. The transmitter and receiver of the communication system are located at the crown of the pipe. In accordance with the results presented in Chapter 3, the current pressure time histories reveal the lowpass character of the pipeline waveguide, since signals with a higher frequency spectrum present higher decay with distance, as observed from the smaller amplitude of the high frequency received signals. The dispersive nature of the channel results in received signals with time spreading and frequency shifts from the originally transmitted waveforms, as indicated by the presented plots. The decaying reverberations following

the initial signal arrival, observed at the pressure time histories, are the result of multipath propagation of the transmitted signal. These overlapping signals are the main cause of the demodulation errors, as will be presented in what follows. Moreover, the frequency spectrum response plots indicate the presence of several peaks within the bandwidth of the transmitted signal, which result in significant ambiguities at the detection of the encapsulated data bits.

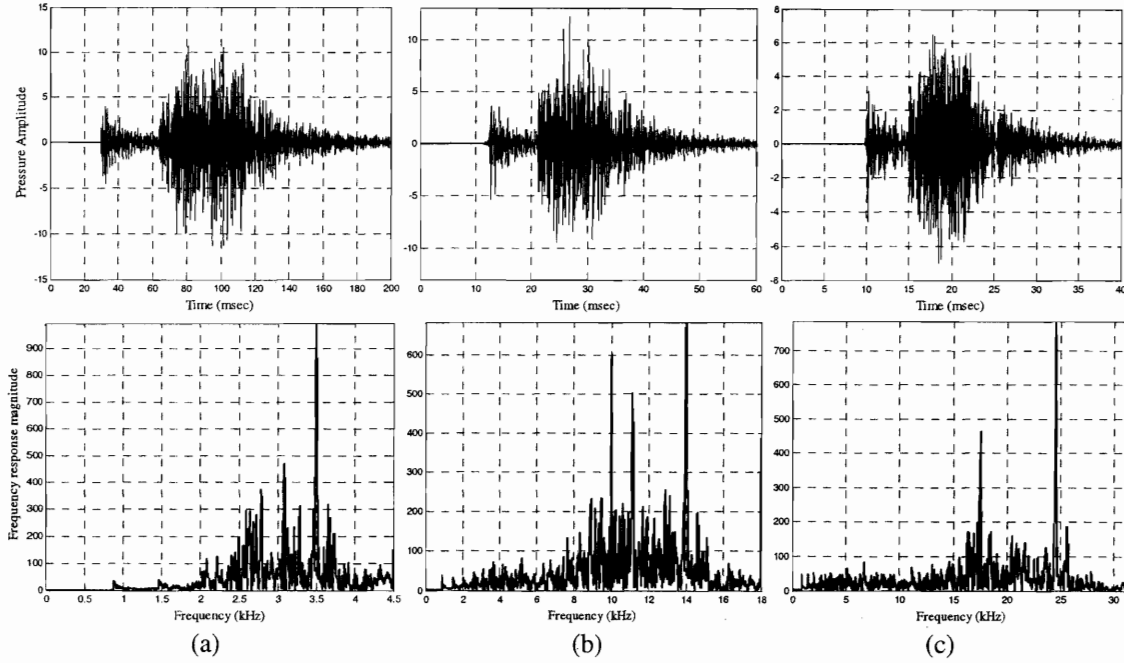


Figure 6.2: Pressure Time History and Frequency Response of Received Signal from a pipeline waveguide with $R = a = r = 0.5\text{m}$, $z = 10\text{m}$ for FSK modulation at data rates (a) 1kbps, (b) 4kbps and (c) 7kbps

The data bearing part of the received signal is identified with the assistance of the Barker Code, the exact time stamp of which is obtained from the correlation of the recorded signal with the original Barker Code. In the pressure time histories of Figure 6.2, the Barker Code corresponds to the first arriving signal, followed by some silent time in which its reverberations decay enough to avoid significant overlap with the subsequent modulated signal, hence justifying the selection of the silent time duration τ . Having identified the exact location of the Barker Code within the received signal, the data bearing signal can be isolated by extracting a block of length equal to duration of the original modulated waveform, allowing for exactly time τ following the Barker Code time stamp.

The correlation of the received signal with the original Barker Code is achieved with the use of a matched filter. The outcome of filtering the received signal reveals a sharp peak at the location of the Barker Code. This filter is called *matched* because their coefficients are matched to the elements of the Barker Code. Recall from Chapter 4 about the good autocorrelation properties of the Barker Code, which reveal a peak of magnitude equal to the length of the code at its location and unity elsewhere. Figure 6.3 illustrates the output of the matched filter for the transmitted and the received signal for the 4kbps data rate case, indicating also the silent time τ . Since no dispersion is introduced to the transmitted signal, the corresponding output of the matched filter is perfect, revealing excellent performance, as predicted in theory.

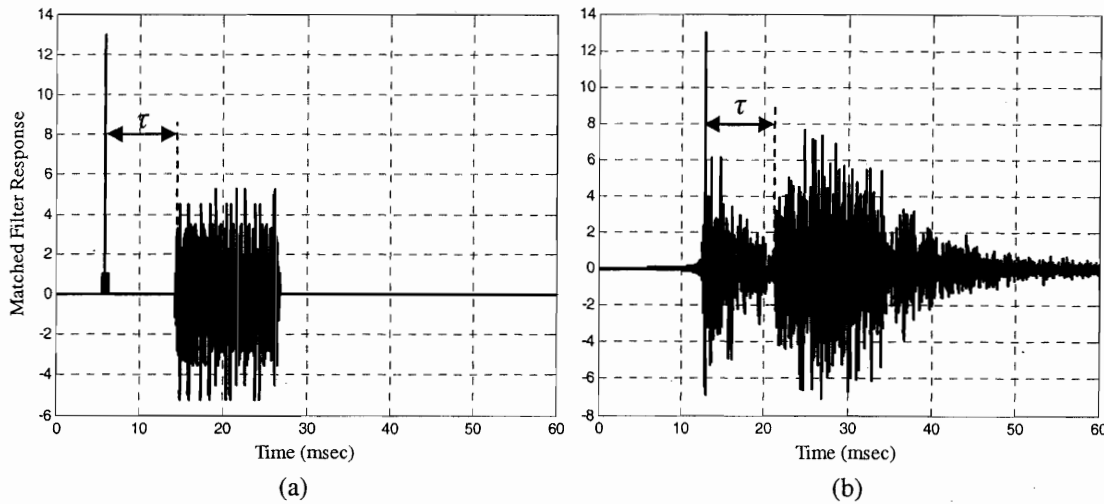


Figure 6.3: Synchronization with Barker Code, Matched Filter Response (a) Theoretical, and (b) Actual

The output of the matched filter for the received signal reveals successfully the exact location of the Barker Code, although the existence of several other peaks of significant magnitude may potentially affect the performance of the identification process. It is interesting to observe that the sidelobes of the main peak present magnitude larger than unity, mainly due to the presence of delayed multipath signals. It should be noted that the presented plot corresponds to scaling of the received signal to a maximum value of one, in order to evaluate the autocorrelation performance of the Barker Code. These plots are used only to identify the absolute time stamp of the Barker Code, while the data bearing signal is extracted directly from the recorded signal.

Demodulation of the extracted data bearing block of the signal provides the received message. Since in this section no error correction and distortion compensation is applied, it is expected that the reverberant nature of the received signal will result in high bit detection error rates. Indeed, the bit error rates are 32%, 30%, and 34% for the signals modulated at 1kbps, 4kbps and 7kbps, respectively. It should be noted that since the symbol alphabet contains only two values, 0 and 1, the maximum error rate is 50%. These significant error rates indicate the necessity of the error correction and distortion compensation signal processing steps. It is interesting to observe that the error rates do not monotonically increase or decrease with increasing frequency. This may be an indication of the existence of specific frequency regions corresponding to modes with significant magnitude and low dispersion characteristics throughout this range. Such regions can be identified with the assistance of the transfer functions, as it will be discussed in a subsequent section. However, the error rates are high enough that prohibit the extraction of a safe conclusion at this stage.

6.2.2 Amplitude Shift Keying

In Amplitude Shift Keying the data symbols are represented as variations of the amplitude of the transmitted signal. For the binary symbol case examined here, the symbol alphabet consists of only two elements, 0 and 1, resulting into only two required signal amplitude stages. Recall from Chapter 4, and [1], that the binary ASK is equivalent to the binary phase shift keying, and for this reason only one of the two methods needs to be examined.

The textual message to be transmitted is modulated at data rates from 1 to 21 kbps. Figure 6.4 presents the messages modulated at 1, 4, and 7 kbps, respectively, along with their corresponding frequency spectra. Similarly to the FSK, they are essentially the same waveform scaled appropriately in time to represent signals of different carrier frequency and bandwidth, and consequently different bit rate. Hence, the frequency response of these signals are shifted versions of the same signal corresponding to the appropriate bandwidths. Once again, the amplitude plots feature the introduction of the Barker Code followed by the silent time τ .

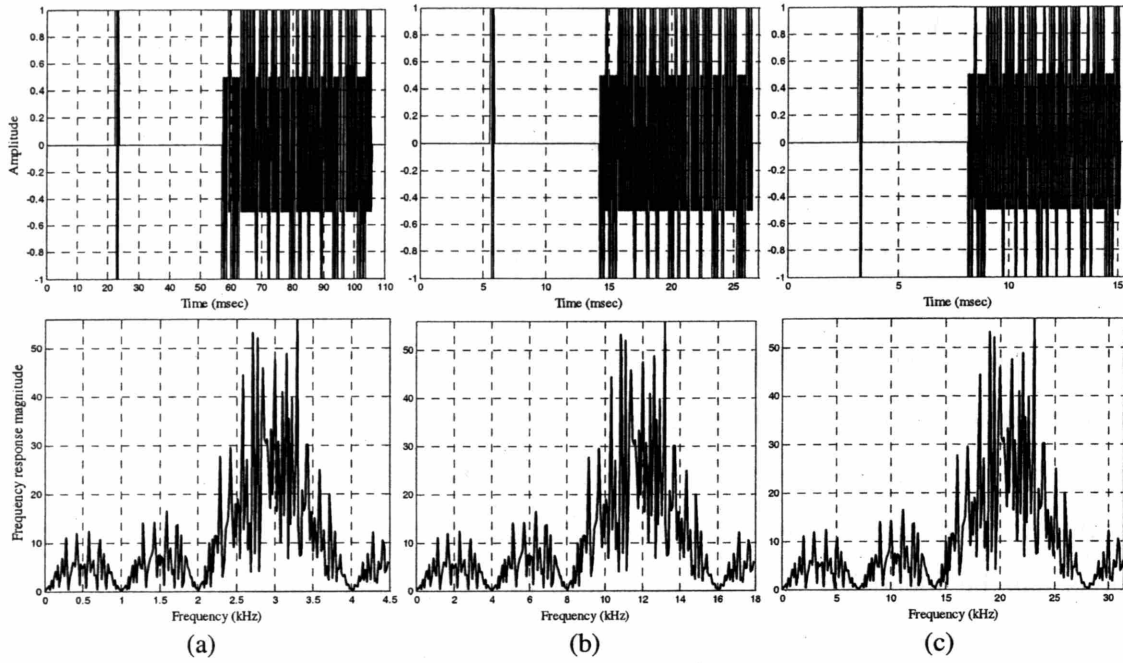


Figure 6.4: Amplitude and Frequency Response of Transmitted Signal for ASK modulation at data rates (a) 1kbps, (b) 4kbps and (c) 7kbps

The ASK signals described are introduced as excitations to a pipeline with the dimensions of the reference case, i.e. radius $R = 0.5\text{m}$, receiver and transmitter attached at the pipe wall separated by $z = 10\text{m}$ distance. The response of the transmission channel, along with the corresponding frequency spectrum is presented in Figure 6.5. These plots once more verify the lowpass character and the dispersive nature of the pipeline waveguide, presenting notable amplitude, frequency and time spreading. Moreover, it is interesting to observe that the resulting frequency response is in accordance with the transfer functions presented in Chapter 3, presenting high values at mid range frequencies from 1.5 to 30 kHz and low values elsewhere. The low response for values below 1.5kHz correspond to the excitation in the fundamental mode, while the decay for high frequencies is a result of the lowpass character of the transmission channel. In such a way, the usable frequency range for each pipeline waveguide can be determined. Further discussion on this topic is included in paragraph 6.4, along with the introduction of transfer functions.

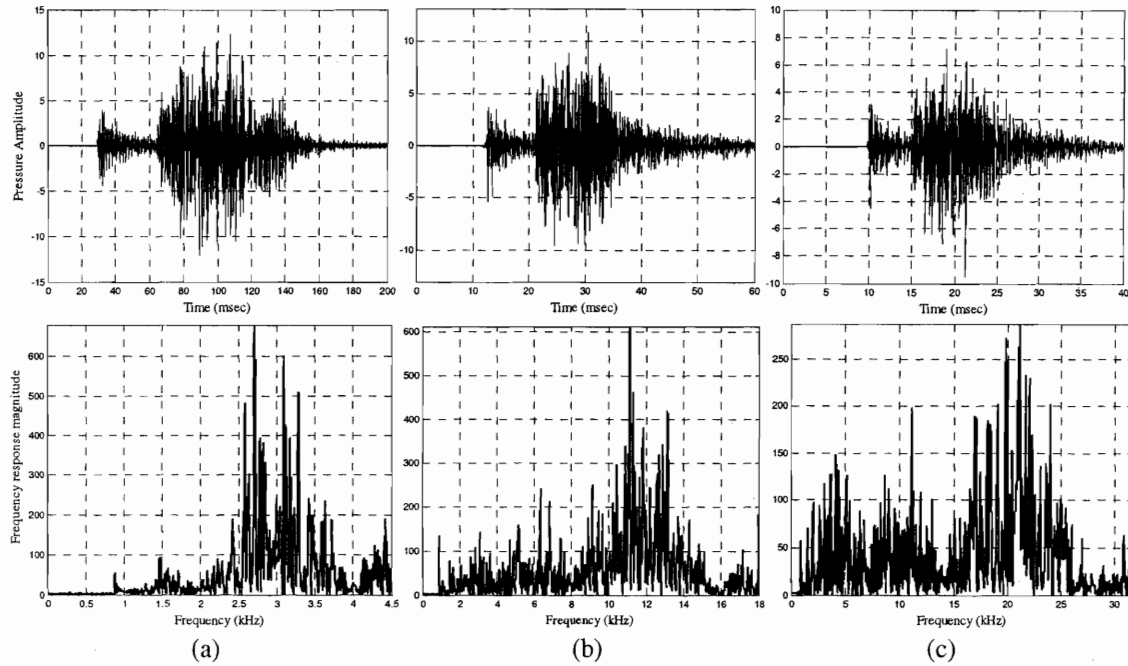


Figure 6.5: Pressure Time History and Frequency Response of Received Signal from a pipeline waveguide with $R = a = r = 0.5\text{m}$, $z = 10\text{m}$ for ASK modulation at data rates (a) 1kbps, (b) 4kbps and (c) 7kbps

Following the data extraction with the assistance of Barker Code synchronization, the demodulation step provides the corresponding error rates. The ASK modulated signals present slightly worse error performance than the FSK modulation. More explicitly, the demodulation of the data bearing signals provided error rates of 36%, 35%, and 38% for the 1kbps, 4kbps and 7kbps data rates, respectively. The frequency response of the received signals for ASK modulation does not provide clear indication of the performance of the algorithm, since the modulation method is based on adjustment of the amplitude of the carrier signal. To illustrate the error performance of demodulator for amplitude or phase modulation the signal constellation plot is usually presented. Such a plot presents the location of the detected symbols in the solution space. For reference the desirable solutions, as indicated at the modulation step, are also included. The corresponding signal constellation plots for the signals recorded in this section are provided in Figure 6.6, along with the desired solutions as described in Figure 5.12. In these plots the horizontal axis corresponds to the in-phase components of the solutions and the vertical to the out of phase components, often denoted as *quadrature*. For the ASK method all the solution points are expected to have the same phase, while their location on the horizontal axis indicates the corresponding amplitude. For the binary

ASK modulation only two points are prescribed as the desired solutions, corresponding to the 0 and 1 bits, as described in Chapter 4. Due to the channel imposed noise and reverberations, the detected solutions from the demodulator are expected to present some variance around the desired locations. The demodulator then matches the obtained point to the nearest desired solution, in order to regenerate the digital data. However, from the results obtained in this section, the significant spread on the horizontal axis of the detected points becomes apparent, indicating the ambiguity of the matching process, and thus the increased error rates. Following the appropriate filtering and dispersion compensation signal processing steps, the detected solutions will approach the neighborhood of the prescribed points.

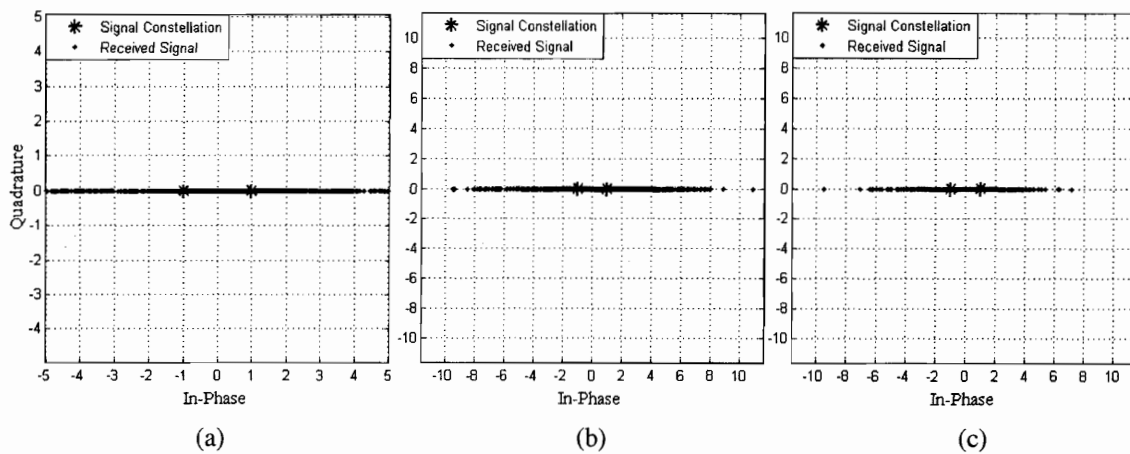


Figure 6.6: Signal Constellations for ASK modulated signals (a) 1kbps, (b) 4kbps, and (c) 7kbps.

6.2.3 Quadrature Amplitude Modulation

Quadrature Amplitude Modulation (QAM) is essentially the combination of two modulation methods, according to which both the amplitude and the phase are adjusted simultaneously, representing two symbols with every transmitted waveform. Therefore, even though binary representations are used in both amplitude and phase, the resulting modulation method presents significantly increased bandwidth efficiency, at the expense of required power as indicated in Chapters 4 and 5. The amplitude and the phase plots of the transmitted signals modulated at 1kbps, 4kbps and 7kbps data rates are presented in Figure 6.7.

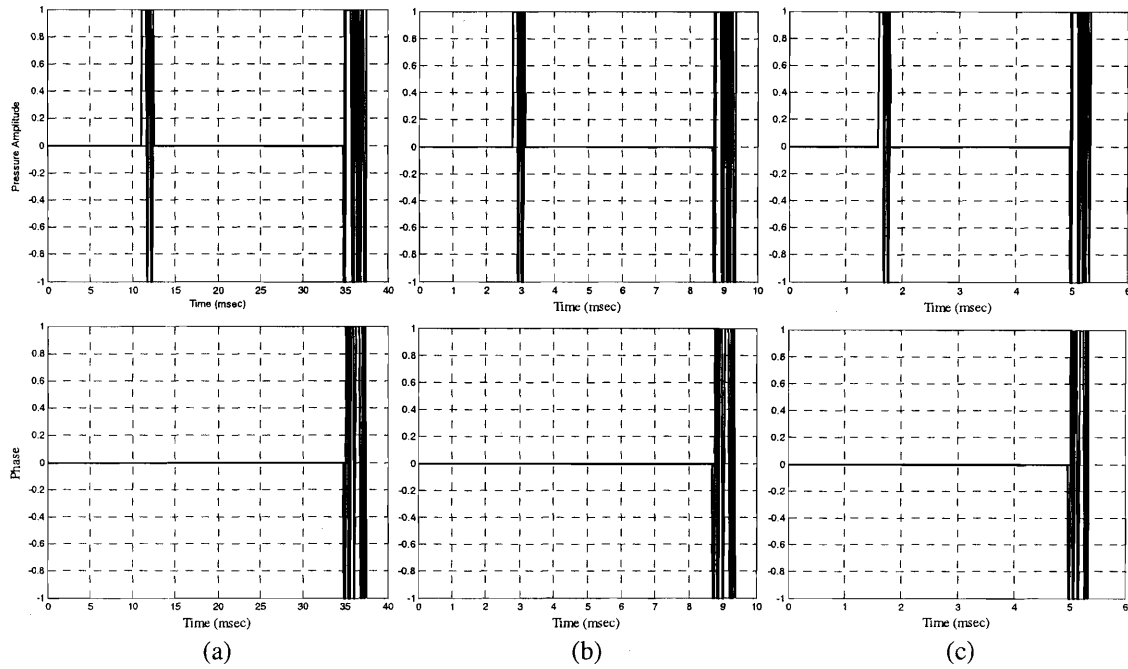


Figure 6.7: Amplitude and Phase of Transmitted Signal for QAM at data rates (a) 1kbps, (b) 4kbps, and (c) 7kbps

It is interesting to observe the significantly smaller duration of the transmitted signals, especially compared with the previously presented FSK and ASK modulated signals. The modulation in both amplitude and phase allows more efficient bandwidth usage and generates shorter signals, while preserves the similar detection ambiguity on the solution space with the binary methods presented in the preceding paragraphs. Due to the binary representation in amplitude and phase, the generated signal has two states with respect the amplitude and two states regarding phase changes. The combination of these states generates four distinct solutions each one of them representing two bits, as shown in Figure 4.16.

Figure 6.8 presents the response of the pipeline waveguide to the excitation presented above. The characteristics of the waveguide correspond to the reference case with radius $R = 0.5\text{m}$, propagation distance $z = 10\text{m}$, and with the transmitter and receiver located at the internal periphery of the pipe. Along with the pressure time histories, Figure 6.8 presents the constellation of the detected symbols from the received signal, whereas for reference the transmitted signal constellation is also provided.

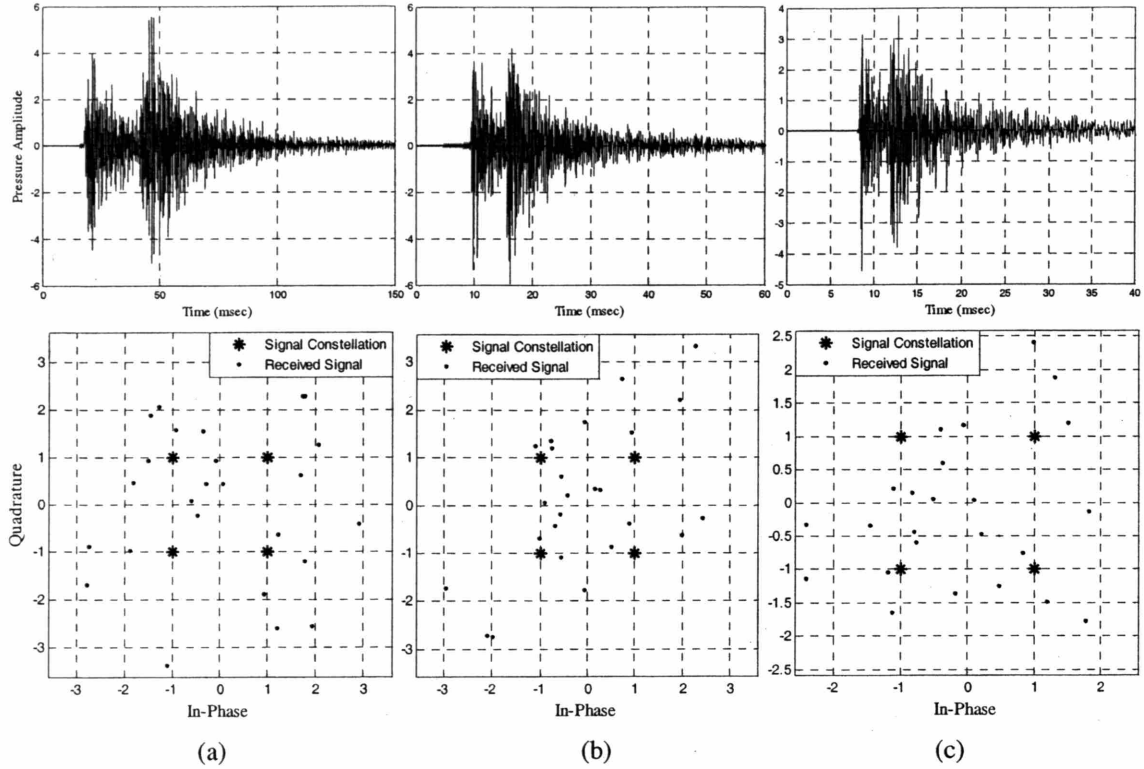


Figure 6.8: Pressure Time History and Signal Constellation of Received Signal from a pipeline waveguide with $R = a = r = 0.5\text{m}$, $z = 10\text{m}$ for QAM at data rates (a) 1kbps, (b) 4kbps, and (c) 7kbps

The received signal constellation plots reveal the magnitude of the dispersion of the detected symbol solutions with respect to the original signal's four points. The resulting error rates are 76%, 80%, and 68% for the 1kbps, 4kbps, and 7kbps QAM data rates, respectively. Unlike to the binary ASK and FSK methods, in QAM more than 50% error rates are realizable, since they correspond to errors both in phase and in amplitude. The ambiguity of the symbol detection, as illustrated by the signal constellation plots, and the high error rates confirm the severe dispersion of the transmitted signal, initially observed at the received pressure time history plots. It should be noted that these error rates are comparable with the error rates obtained from the binary FSK and ASK modulation methods, as a result of the similar ambiguity of the binary representation in the solution space.

The poor performance of the communication system regardless of the applied modulation method proves the necessity of the introduction of the filtering, the dispersion compensation and the error correction signal processing steps, in order to achieve reliable transmission inside the pipeline waveguide. On the other hand, due to the comparable

error rates, obtained by all modulation methods, the trade-off between bandwidth and power becomes the controlling parameter of the selection of the method used, as will be discussed in a subsequent section.

6.3 *Encoding*

To identify the sole effect of encoding on the error performance of the communication system, the encoding signal processing step is added next. Once again, no other form of distortion compensation or filtering is applied to the received signal, allowing to evaluate the error correction capabilities of the proposed method, as observed by the reduction of the obtained bit error rates. The encoding block employs the Reed-Solomon algorithm, as described in Chapter 4 and implemented in Chapter 5. According to the method, every 7 bits block is transformed into a 15 bits long codeword selected from a specific pool of previously generated codewords. The selected *code rate* enables the correction of 4 incorrectly detected bits in each codeword. It becomes apparent that the encoding procedure adds redundancy to the communication system, but on the other hand increases significantly the length, and consequently the duration, of the transmitted message, with significant effect on the effective data throughput and signal dispersion.

At this stage, an estimation of the error rate reduction achieved by the introduction of the encoding step can be provided. For simplicity, assume that the error rate is constant regardless of the length of the message, even though this is not true since longer messages result in longer reverberations, consequently degrading the quality of the received signal. Considering that the error rate is proportional to the number of incorrectly received bits with respect to the total number of bits of the message, and that the mean error rate achieved in the preceding section is in the order of 35%, the error improvement can be estimated as follows. As indicated by the code rate, the encoding algorithm can correct up to 4 incorrectly received bits in each code word. Then, assuming that the error rate is constant, every from 15 bits transmitted, which correspond to a single codeword, the $15 \times 35\% = 5.25$ bits will be received incorrectly. If the algorithm succeeds in correcting four bits, only 1.25 bits of the message will remain erroneous, resulting in an error rate of 8.3%. This oversimplified approach provides an upper limit of

the error rate reduction, since the algorithm may not be capable to correct four bits incorrectly received bits in case of severely distorted signals, according to the discussion of Chapter 4. In case of low SNR, the algorithm may be unable to match the received signal to one of the predefined codewords. However, the estimated error rate reduction from 35% to 8.3% is very significant, even though it is still not sufficient for the reliable operation of a digital communication system.

The encoding step is applied while the message is at a pure digital state, i.e. consisted of binary bits. At the proposed digital communication system the encoding block is located between the formatting and the modulation blocks. An example of the encoded message is provided below, where the textual message is going through a two step procedure before the modulation block.

G	1	1	1	0	0	0	1	1	0	0	1	0	1	0	1	1	1	0	0	0	1
e	1	0	1	0	0	1	1	0	0	0	1	1	0	1	0	1	0	1	0	0	1
o	1	1	1	1	0	1	1	1	0	1	1	1	0	0	0	1	1	1	1	0	1
r	0	1	0	0	1	1	1	1	1	1	1	1	0	1	1	0	1	0	0	1	1
g	1	1	1	0	0	1	1	0	1	0	0	0	0	1	0	1	1	1	0	0	1
e	1	0	1	0	0	1	1	0	0	0	1	1	0	1	0	1	0	1	0	0	1
Message \Rightarrow	Binary form							\Rightarrow	Encoded message												

The first step is the conversion in binary form with the use of the ASCII code, identical to what is presented in the preceding section. In sequence, the binary formatted message is encoded with the assistance of the Reed-Solomon code. The message is finally presented to the modulator which converts it into a waveform appropriate for transmission into physical media. The message is presented above in a matrix like form, in which each row corresponds to a different character of the textual message, for the reader's convenience; it is however processed at the transmitter in a sequential bit stream form.

In order to examine the single effect of the encoding on the error performance of the communication system, only the reference method of FSK will be presented in this section. Figure 6.9 presents the amplitude and frequency response of the signals generated from the modulation at data rates 1, 4, and 7kbps of the encoded signals. It is important to observe the increased duration of the generated signals, due to the added

redundant bits, with respect the modulated signals presented in Figure 6.1, in which the modulated signal is not encoded.

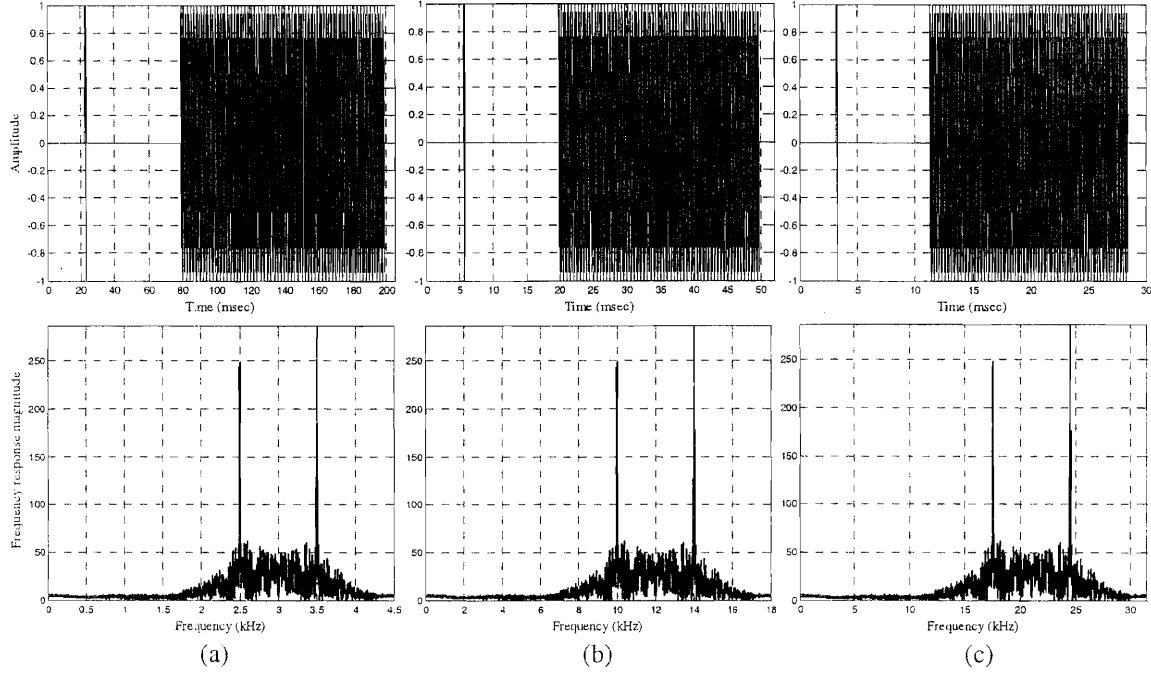


Figure 6.9: Amplitude and Frequency Spectrum of Transmitted signals for FSK modulation of encoded messages at data rates (a) 1kbps, (b) 4kbps, and (c) 7kbps.

The modulated signals presented above are introduced as excitation to the reference pipeline waveguide, with radius $R = 0.5\text{m}$, with the transmitter and receiver installed at the internal surface of the pipe wall at a distance $z = 10\text{m}$. The received pressure time histories and the corresponding frequency spectra are presented in Figure 6.10. From the received signals, the data bearing signal is extracted with the assistance of the Barker code synchronization. Thereafter, it is demodulated and decoded.

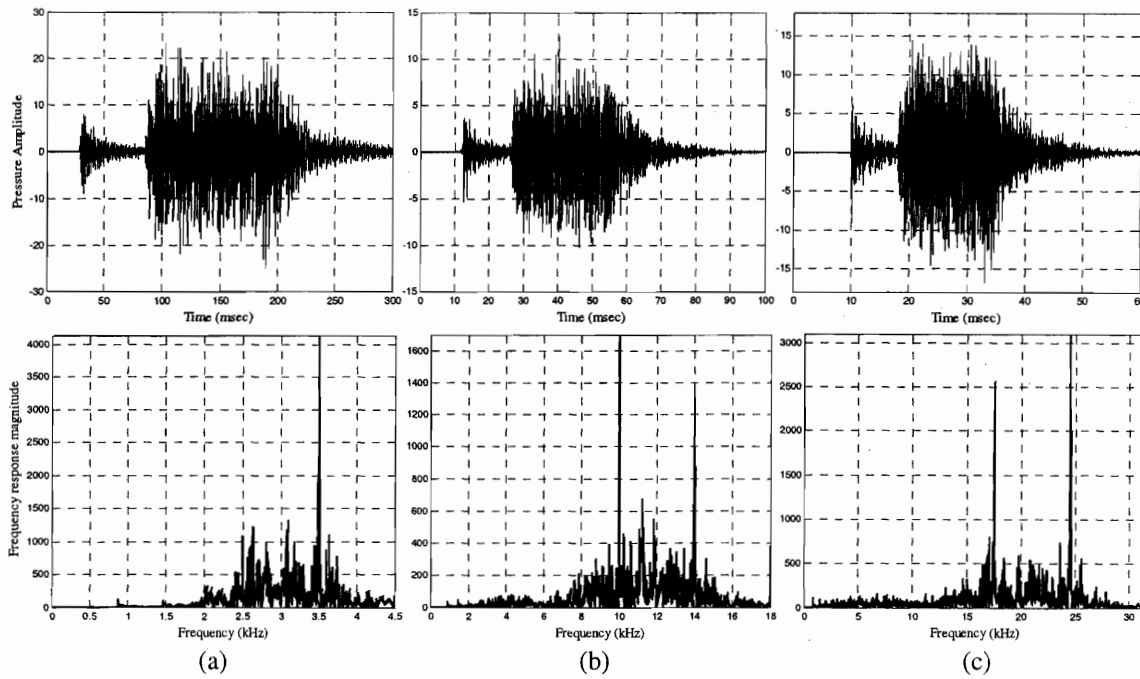


Figure 6.10: Pressure Time History and Frequency Response of Received Signal from a pipeline waveguide with $R = a = r = 0.5\text{m}$, $z = 10\text{m}$ for FSK modulation of encoded messages at data rates (a) 1kbps, (b) 4kbps, and (c) 7kbps

The bit error rates of the demodulated signal before application of the decoding are 33%, 32% and 36% for the 1kbps, 4kbps and 7kbps data rates, respectively. The increased data rates with respect to the previously received FSK signals presented in paragraph 6.2.1 can be attributed to the increased duration of the pulse, which causes significant overlaps of the main signal with the arrivals of the multipath propagating signals. However, following the decoding process of the detected message, the corresponding error rates drop at 12%, 10% and 16%, respectively. These error rates are close to the improvement estimated by the aforementioned simplified procedure. The lowest expected value is in the order of 8.3%. The actual improvement provides higher error rates due to the inability of the error correction algorithm to detect erroneous bits in low SNR signals. Recall that the examples presented in the current section do not include any filtering or dispersion compensation methods. Introduction of such techniques in advance of the decoding process increases the effective signal to noise ratio, by removing the signal dispersion and ambient noise, allowing the more efficient operation of the Reed-Solomon decoder.

6.4 *Stacking*

The stacking process belongs, along with the inverse transfer function method, to the preconditioning block of the receiver. These methods may be required only in case of extreme signal distortion and should be applied with caution, since they impose radical irreversible changes on the recorded signal. Such changes, if applied unwarily, may remove from the signal features necessary for the symbol detection process.

According to the stacking process, a synthetic received signal is generated by addition or subtraction of simultaneously received signals at several locations around a specific cross section of the pipeline. The purpose of stacking is to isolate or eliminate the effect of specific orders of modes. This process is made possible due to the phase changes of the various orders of modes throughout the cross section, as presented in Chapter 5. In the proposed system two receivers are installed at opposite locations across a diameter of the pipe, such as the crown and the bottom of the pipe, allowing to control over the odd or even numbered orders.

Considering initially the FSK modulation, for the signals presented in Figure 6.9, and a transmitter installed at the crown of the pipe, the received signals at the crown of the pipe are presented in Figure 6.10, while the signals received simultaneously at the bottom are presented in Figure 6.11. Observe that the response of the pipeline at the bottom, as indicated by the pressure time histories presented below, is significantly different from the response at the top, as a result of the superposition of the odd numbered orders of modes, which change phase at the bottom, with the even numbered orders of modes, which preserve the phase sign at the bottom.

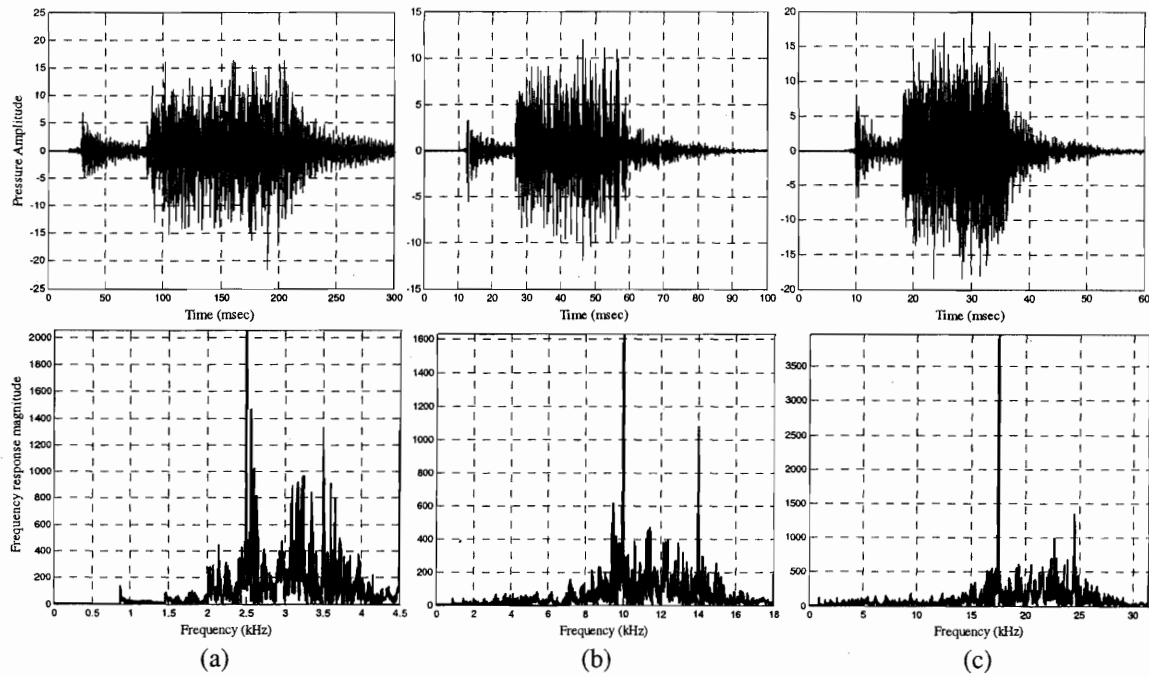


Figure 6.11: Pressure Time History and Frequency Response of Received Signal at the bottom of a pipeline waveguide with $R = a = r = 0.5\text{m}$, $z = 10\text{m}$ for FSK modulation of encoded messages at data rates (a) 1kbps, (b) 4kbps and (c) 7kbps

It is interesting to observe that the performance of the communication system based solely on the signals received at the bottom of the pipe, with the transmitter located at the crown, is degraded with respect to the error rates achieved from the signals received at the crown. The error rates of the received signals at the bottom are 39%, 40% and 40% for the 1kbps, 4kbps and 7kbps data rates, respectively. These error rates are improved after the Reed-Solomon decoding, by reducing to 20%, 22% and 23%, respectively.

Isolation of the odd or even numbered orders of modes is achieved by superposition of the pressure time histories received at the crown and the bottom of the pipe, presented in Figure 6.10 and Figure 6.11, respectively. Addition of these signals results in the elimination of the odd numbered modes, the result of which is presented in Figure 6.12. On the other hand, Figure 6.13 presents the outcome of the subtraction of the aforementioned signals, which results in elimination of the even numbered modes.

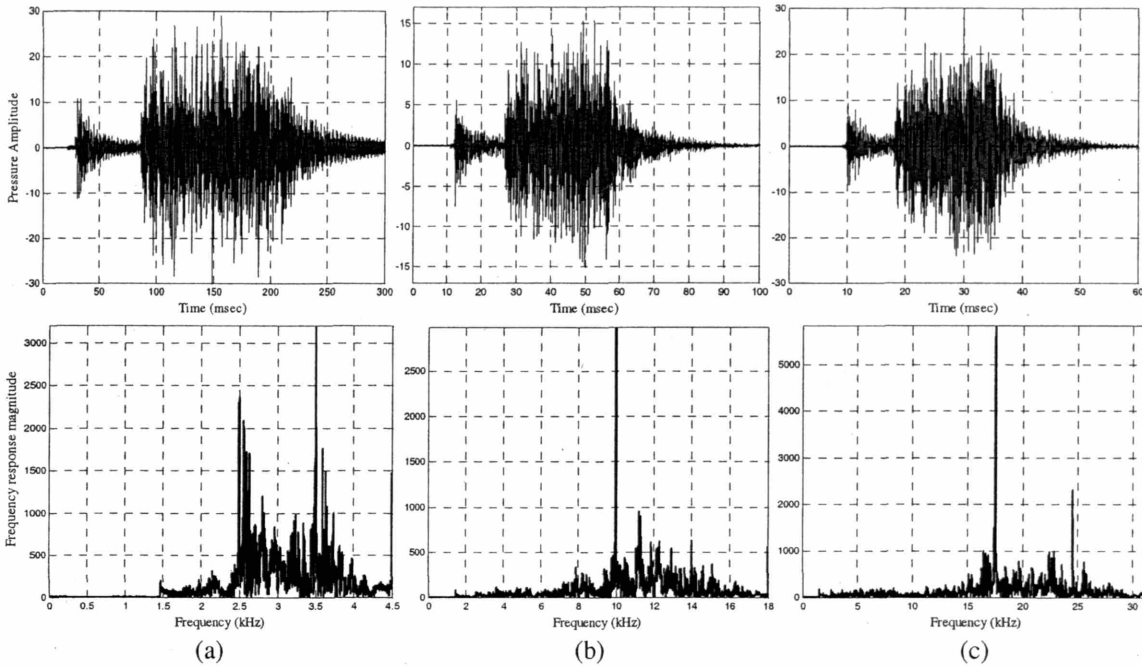


Figure 6.12: Stacked Signal by addition of received signals at crown and bottom of pipe. Pressure Time History and Frequency Response for FSK modulation at data rates (a) 1kbps, (b) 4kbps and (c) 7kbps

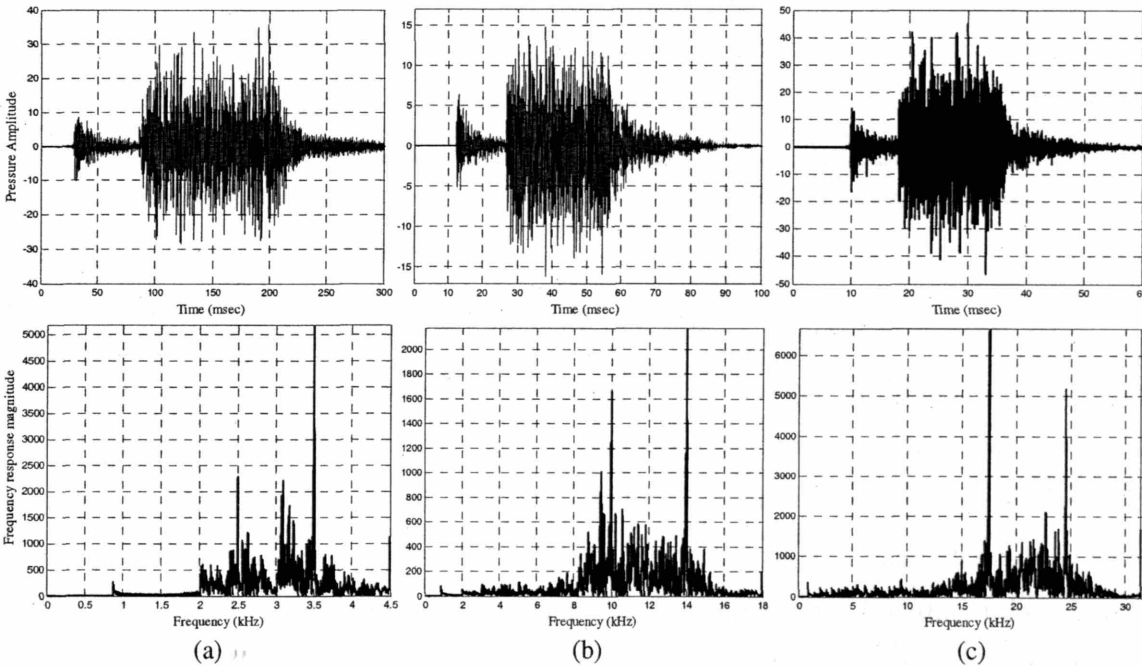


Figure 6.13: Stacked Signal by subtraction of received signals at crown and bottom of pipe. Pressure Time History and Frequency Response for FSK modulation at data rates (a) 1kbps, (b) 4kbps and (c) 7kbps

The error performance of the above generated stacked signals demonstrates the importance of understanding which modes carry the most energy of the propagating

signal. More explicitly, the error rates of the pressure time histories obtained by addition of the received signals at the crown and the bottom of the pipe are 27%, 40% and 39%, for the 1kbps, 4kbps and 7kbps data rates respectively. Following the decoding process, these error rates are improved to 9%, 30% and 28%, respectively. On the other hand, the corresponding error rates for the pressure time histories generated by the subtraction of the aforementioned signals are 41%, 37% and 25%, for the 1, 4 and 7kbps throughputs, respectively. Again, the decoding process improved these error rates to 32%, 19% and 8%, respectively. The error performance of the communication system, employing the stacking and decoding processes, is summarized in Table 6.1 for the crown and bottom received signals, as well as the signals generated by their addition or subtraction. Each cell presents the error rates before and after decoding, while the best performance is emphasized with bold letters.

	Crown	Bottom	Stacked = Crown + Bottom	Stacked = Crown – Bottom
1kbps	33% \Rightarrow 12%	39% \Rightarrow 20%	27% \Rightarrow 9%	41% \Rightarrow 32%
4kbps	32% \Rightarrow 10%	40% \Rightarrow 22%	40% \Rightarrow 30%	37% \Rightarrow 19%
7kbps	36% \Rightarrow 16%	40% \Rightarrow 23%	39% \Rightarrow 28%	25% \Rightarrow 8%

Table 6.1: Error Performance before and after decoding of Crown, Bottom and Stacked signals for FSK modulation

The error performance results presented above indicate that stacking can be beneficial, but should be applied with great caution. Indeed for the low and high data rates presented, stacking achieved reduction of the error rate by approximately 10%. However, for the 4kbps case stacking actually increased the error rate, indicating that the energy of the data bearing signal is spread along several orders of modes including both odd and even numbered ones. Moreover, it is interesting to observe that for low data rate signal the error performance is improved by addition of the top and bottom signals, while for the high data rate signal the error rate is improved from their subtraction, presenting also the overall best performance so far.

It can be intuitively understood that a significant part of the energy of the low data rate signal propagates with the zero ordered modes, due to its low frequency content.

Therefore, elimination of the odd numbered modes, by addition of the top and bottom signals, allows isolation of the even numbered modes including the zero order, which contains the fundamental mode that is non-dispersive. Recall that the effect of each mode on the propagating signal decreases with increasing modal order, so the effect of the second, fourth and so on orders, which remain on the stacked signal, is less important in the 1kbps example. On the contrary, the stacked signal, generated by the subtraction of the top and bottom received signals, presents significantly worse error performance, since only the highly dispersive modes remain present following the stacking process, while an important part of the signal's energy is lost.

An inverse analysis from the above can explain the behavior of stacking for the 7kbps signal, where subtraction of the crown and bottom signals provides the best results. The first and third orders modes have significant energy content in the frequency range of the 7kbps signals, making their presence imperative for the demodulation process. Stacking in this case removes as many modes as possible, reducing consequently the level of signal distortion. On the other hand, the error performance degrades for the stacked signals generated by the subtraction of the crown and the bottom recordings.

Similar conclusions can be extracted from the analysis of examples introducing QAM and ASK modulated signals. Signals modulated at 1kbps benefit from addition of crown and bottom recordings, whereas signals modulated at 7kbps benefit from subtraction of these recordings. Stacking proves harmful for signals with 4kbps data rates for the current pipeline waveguide configuration. The consistency of these results, regardless of the modulation method used, indicates the importance of identifying the orders of modes excited for each frequency band used, since the only common parameter of the above signals with uniform data rate is the carrier frequency. The distortion imposed by the modes of propagation affects not only the frequency of the signal but also its phase and amplitude. However, the selective correction, with respect to the carrier frequency achieved with stacking, regardless of the modulation method, is a strong indicator that certain modes are predominant in certain frequency ranges. When a signal of some bandwidth is presented to the pipeline waveguide, these modes carry the majority of the energy and therefore it is essential to preserve them. Estimation of the transfer function separately for each mode can reveal such zones of high energy. For

reference, the transfer functions for the first four modal orders for a pipeline waveguide, with radius $R = 0.5\text{m}$ and length $z = 10\text{m}$, are calculated with the assistance of the rigid pipe simulation code and presented in Figure 6.14. Even though these plots seem complicated, careful examination reveals frequency bands where one set of modes predominates. For example, there exists a frequency band around 17kHz , where the magnitude of the $n = 1$ modal order dominates over all other modes. Similar, but less pronounced, effect can be identified in the region of 21kHz , which coincides with the 7kbps data rate signals used in the above examples, explaining the effect of stacking on the error performance, since subtraction of the top and bottom recordings removed the effect of even modes, allowing the $n = 1$ modes to carry the majority of the signal's energy content with minimal distortion. A more apparent demonstration of the frequency band identification with the assistance of the transfer function plot is provided in Chapter 7.

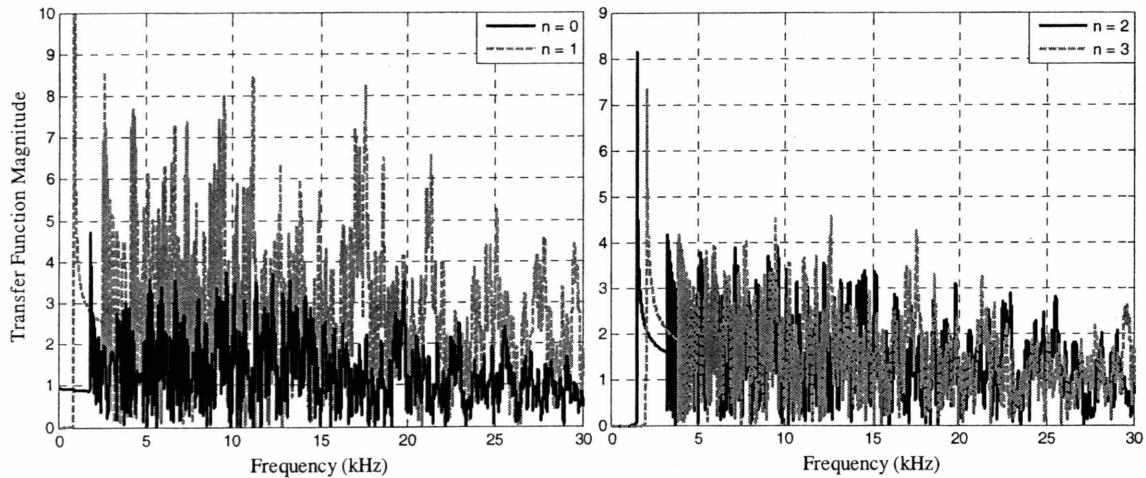


Figure 6.14: Transfer Functions of the first four orders of modes for a pipeline waveguide with $R = 0.5\text{m}$ and $z = 10\text{m}$

Alternatively, the modes of propagation that get excited can be identified with the assistance of the dispersion curves, presented in Chapter 3, see Figures 3.13 and 3.14. When the frequency spectrum of the signal is matched to a frequency band in the horizontal axis of the dispersion curve plots, the region above the specified band contains the modes that get excited by the signal. By selecting the modes that present the minimum curvature, i.e. the minimum dispersion, the set of modes that must be preserved

from stacking can be identified. On the other hand, the dispersion curves can provide useful insight during the design phase of the communication system, to avoid excitation of highly dispersive modes. This can be achieved by generating signals with a frequency spectrum below the cut off frequency of the specific modes.

An interesting application of the aforementioned guideline is the transmission of signals below the cut off frequency of the first mode, leaving only the fundamental mode being excited by the signal. For this reason an FSK modulated signal is generated with data rate 0.4kbps, which generates waveforms with frequency content at the limit of the first cut off frequencies. Figure 6.15 presents the amplitude and frequency response of the transmitted signal as well as the pressure time history of the received signal at the top of the pipe and the result of the stacking process, for a signal that propagates inside the reference pipeline. In the frequency response plots of the received and stacked signals, the effect of the propagating modes becomes apparent along with their cut off frequencies. Addition of the top and bottom recorded signals removes the effect of the first modal order, leaving the zero order as the predominant one. The first cut off frequency of the first mode of zero order is 1.5kHz approximately, as it is clearly indicated in the frequency response of the stacked signal. This mode is dispersive and its effect can be removed with filtering, allowing perfect reconstruction of the initially transmitted signal, thus resulting in zero error rate.

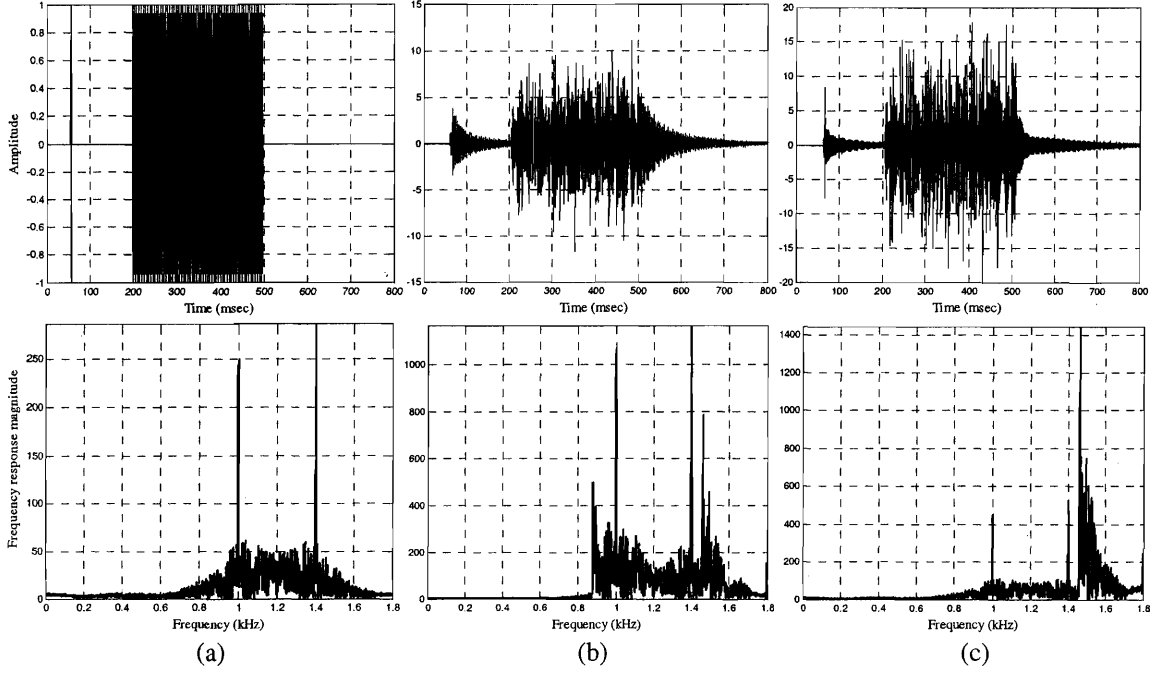


Figure 6.15: Pressure Time Histories and Frequency Response of FSK modulated signal at 0.4kbps data rate for a pipeline waveguide with $R = a = r = 0.5\text{m}$, $z = 10\text{m}$ (a) Transmitted signal, (b) Received signal at the crown, and (c) Stacked signal generated by addition of top and bottom recorded signals

6.5 Adaptive Equalizer

Even though the application of stacking improves significantly the error performance of the in-pipe acoustic communication system, the error rates achieved are not sufficient for reliable operation. Moreover, stacking presents selective performance improvement, and since its effect is irreversible, it should be applied with caution only in case of extreme signal distortion. A reliable and robust dispersion compensation technique is required that is capable of dropping the error rate to acceptable values for a digital communication system. A very powerful dispersion compensation technique is the adaptive equalization, as presented in Chapter 4, the results of which are presented in what follows. The inverse transfer function method, described in Chapter 5, is an alternative method to reverse the distortion effect of the transmission channel. However, it is computationally expensive and will not be applied at this stage. Moreover, its effect is similar to the linear adaptive equalizer, since the inverse transfer function implements an infinite impulse response filter with constant coefficients, while the linear adaptive

equalizer realizes a finite impulse response filter with adjustable coefficients, thus achieving more efficiently a comparable distortion compensation performance.

The error performance objective for the digital communication system is to achieve a bit error probability of less than 10^{-3} . This performance criterion is achieved with the introduction of the adaptive equalizer block, as will be shown in what follows. Initially, the performance of various adaptive equalizer structures is examined by further processing the FSK modulated signals presented in the preceding paragraphs. Two forms of adaptive equalizers are considered, the linear equalizer and the decision feedback equalizer. For each form both the Least Mean Squares (LMS) and Recursive Least Squares (RLS) adaptation methods are implemented and evaluated. The main performance parameters considered for adaptive equalizers are the length of the filter required to achieve the objective error rate, as well as the training cycles required for the algorithm to converge. In sequence, the performance of adaptive equalization is verified with the introduction of QAM and ASK modulated signals, as well as signals modulated at higher data rates, such as 12kbps and 21kbps. Finally, parametric analyses with respect to the pipeline waveguide characteristics are implemented, such as the radius and propagation distance. While the reference case corresponds to a pipeline with radius $R = 0.5\text{m}$ and propagation distance $z = 10\text{m}$, the parametric analyses include pipeline radii of 0.15m and 1m and propagation distances of 100m and 500m. To evaluate the sole effect of the equalizer, the stacking process is not applied in any of the aforementioned examples, due to its selective performance with respect to frequency content of the signal.

6.5.1 Linear Equalizer

This section utilizes a linear adaptive equalizer, which is essentially a transversal feedforward filter with an adaptation algorithm that adjusts the tap weights in each cycle, as described in Chapters 4 and 5. The equalizer is initially trained with a test message until a desirable performance is achieved. As indicated in paragraph 4.5.4, during the training stage the equalizer is provided with both the recorded signal and the desirable equalizer response. During normal operation the equalizer is fed with the received signal

and the potential detection error of the demodulator. In what follows plots of the equalizer output are presented for FSK modulated signals propagating in a 0.5m radius pipeline for a distance of 10m, with the transmitter and receiver located at the internal periphery of the pipe. The plots display the pressure time history and frequency response of the data bearing signal only, i.e. after the barker code synchronization, since only this part of the signal is presented to the equalizer in the proposed digital communication system.

The filter length of the adaptive equalizer must be sufficient to reverse the signal dispersion imposed by the channel. Also the training sequence must be long enough and representative of all channel characteristics to allow the convergence of the adaptation algorithm to the optimal solution, or in other words, to the desirable equalizer behavior. In case of poor training or inadequate filter length, the performance of the equalizer may be compromised and reliable transmission may not be feasible under variable channel conditions. In general, the more severe the signal dispersion, the longer the training sequence and equalizer structure needs to be. Figure 6.16 presents examples of poorly trained and insufficient structure adaptive equalizer cases.

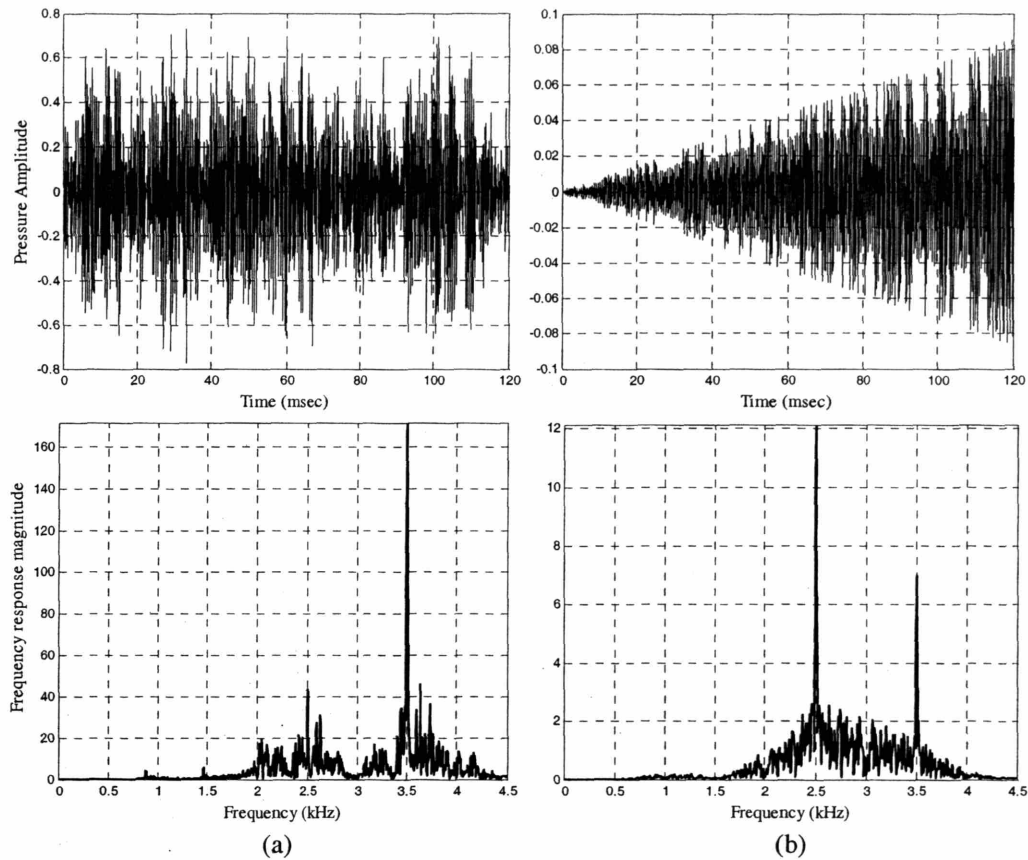


Figure 6.16: Example Pressure time history and Frequency response of (a) inadequate length and (b) poorly trained Linear Adaptive Equalizer using the LMS filter tap weight adaptation algorithm for FSK modulated signals at 1kbps data rate

The irregular pressure time histories and the corresponding frequency responses presented above illustrate the effect of inadequate equalizer structures as well as the effect of poor training. The inadequate length equalizer is incapable of achieving zero error rates, regardless of the training time. However, it removes a considerable amount of signal distortion with respect to frequency, as indicated from the frequency response plot, which consequently significantly reduces the bit error rate to 4%. On the other hand, the poorly trained equalizer is repeatedly attempting to correct its response by adjusting the filter tap weights, as indicated by the large variations in amplitude and frequency. It finally achieves zero error rate following application of the Reed-Solomon error control algorithm. However, the behavior of a particular equalizer is prone to errors, since it is trained mostly to the characteristics of the particular signal and not the nature of the transmission channel. The signal-specific training may lead to detection errors, in case of variation of the characteristics of the channel simultaneously with the transmission of a

significantly different waveform, due to the inability of the equalizer to adjust to both the signal and channel changes.

Figure 6.17 and Figure 6.18 present the response of linear adaptive equalizers for FSK modulated signals at 1kbps, 4kbps and 7kbps data rates propagating in a 0.5m radius pipeline at a distance of $z = 10\text{m}$. The adaptation algorithms used are the Least Mean Squares (LMS) and the Recursive Least Squares (RLS), respectively. The plots illustrate the amplitude and the corresponding frequency response of each equalized data bearing message, which resembles as much possible to the original modulated message. The originally received signal was presented in Figure 6.10.

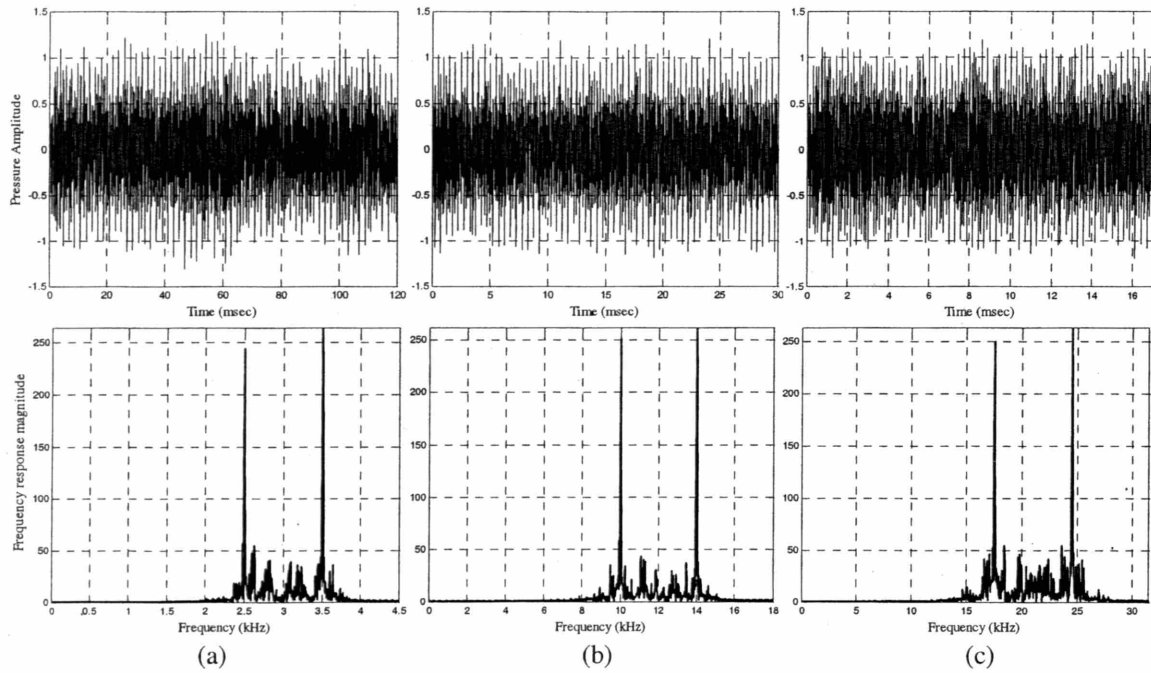


Figure 6.17: Pressure time history and Frequency response of Linear Equalizer using the LMS filter tap weight adaptation algorithm for FSK modulated at data rates (a) 1kbps, (b) 4kbps and (c) 7kbps

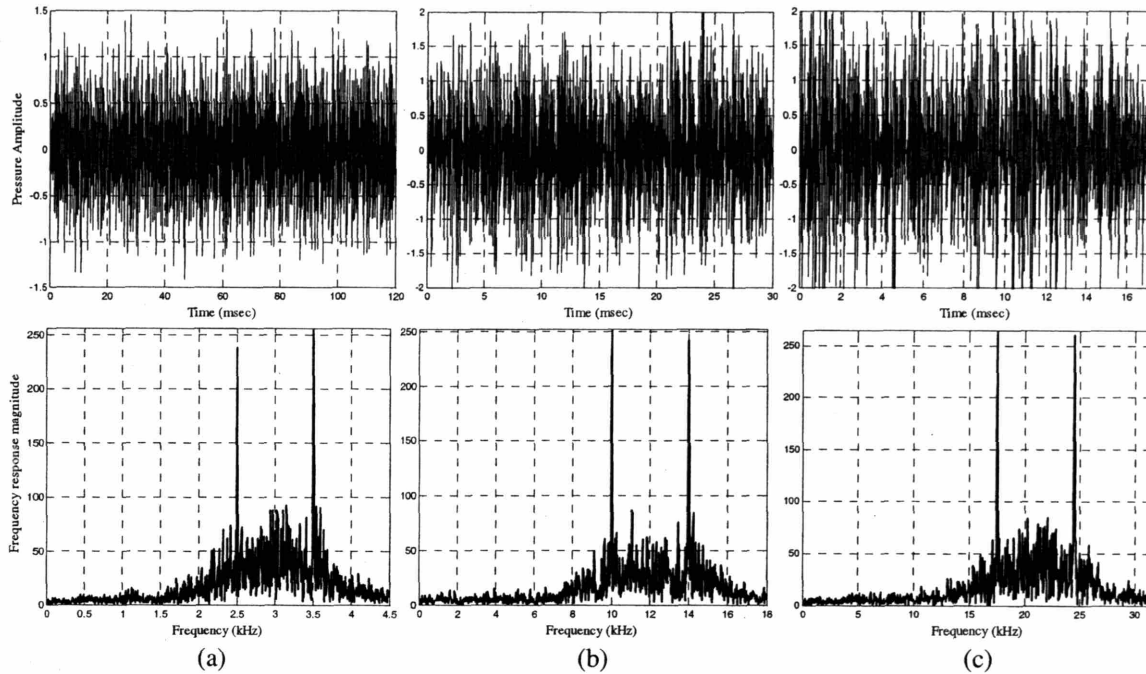


Figure 6.18: Pressure time history and Frequency response of Linear Equalizer using the RLS filter tap weight adaptation algorithm for FSK modulated signals at data rates (a) 1kbps, (b) 4kbps and (c) 7kbps

The equalizers employing both the LMS and RLS adaptation algorithms achieved perfect error performance, reducing the detection bit error level to zero. The equalizer structures used vary from 40 to 100 filter elements depending on the data rate, and consequently the dispersion level, as well as the adaptation algorithm. Generally, the RLS algorithm converges to the optimum tap weights in fewer training cycles than the LMS. However, it is computationally intensive, requiring therefore significantly higher total training time than the LMS. Moreover, the exponential growth of the complexity of the RLS algorithm with increasing length of the filter prevents the use of long equalizer structures. Such long equalizers, allowed by the LMS algorithm, present noticeable performance improvement with respect to RLS, as indicated by the smooth output of the LMS equalizer and the clean corresponding frequency response plots. On the other hand, the shorter equalizers used in the RLS case, result in more abrupt equalizer outputs. The frequency response plots of the output of the RLS equalizers present clear frequency peaks, of similar magnitude with the corresponding LMS response, enabling reliable detection of the zero and one bits. However, this output signal presents more ambiguity than the LMS output, since it is richer in intermediate frequencies.

In general, the linear equalizer requires long filters that need many training cycles, especially with respect to the decision feedback equalizer that is presented in the next section. Moreover, it is observed that the length of the filter is controlled by the complexity of the channel distortion mechanism, with highly dispersive channels requiring longer equalizer structures. The accurate description of the channel behavior requires a sufficient number of taps at the transversal filter. Recall the inability of the equalizer presented in Figure 6.16 to describe the pipeline waveguide due to the inadequate filter length. With the introduction of appropriate stacking, shorter equalizer structures are required, due to the reduced levels of signal dispersion. However, as it has been mentioned before, stacking should be applied with caution, since it may remove from the signal features necessary for the correct detection of the encapsulated symbols.

6.5.2 Decision Feedback Equalizer

The decision feedback equalizer (DFE) is comprised of a pair of filters, similar to the transversal filter of the linear equalizer. The main difference is that one of the filters is used to feedback information from the detector output to the input of the equalizer, while the second filter retains its traditional feedforward operation. Therefore, the equalizer's response is dependent on both the current block of inputs as well as some subset of the previous, already equalized, outputs. The feedback filter allows the DFE to remove the reverberant effect of past inputs from the current input signal. The response of the DFE thus takes advantage of previously received information, and more importantly, of the outcome of this information, resulting in more efficient dispersion compensation with shorter equalizer structures. Detailed description of the DFE's operation is included in Chapter 4. Figure 6.19 and Figure 6.20 illustrate the response of the DFE utilizing the LMS and RLS adaptation algorithms respectively. The signals presented correspond to FSK modulation at 1kbps, 4kbps and 7kbps data rates propagating in the reference pipeline with radius $R = 0.5\text{m}$ at a distance of $z = 10\text{m}$.

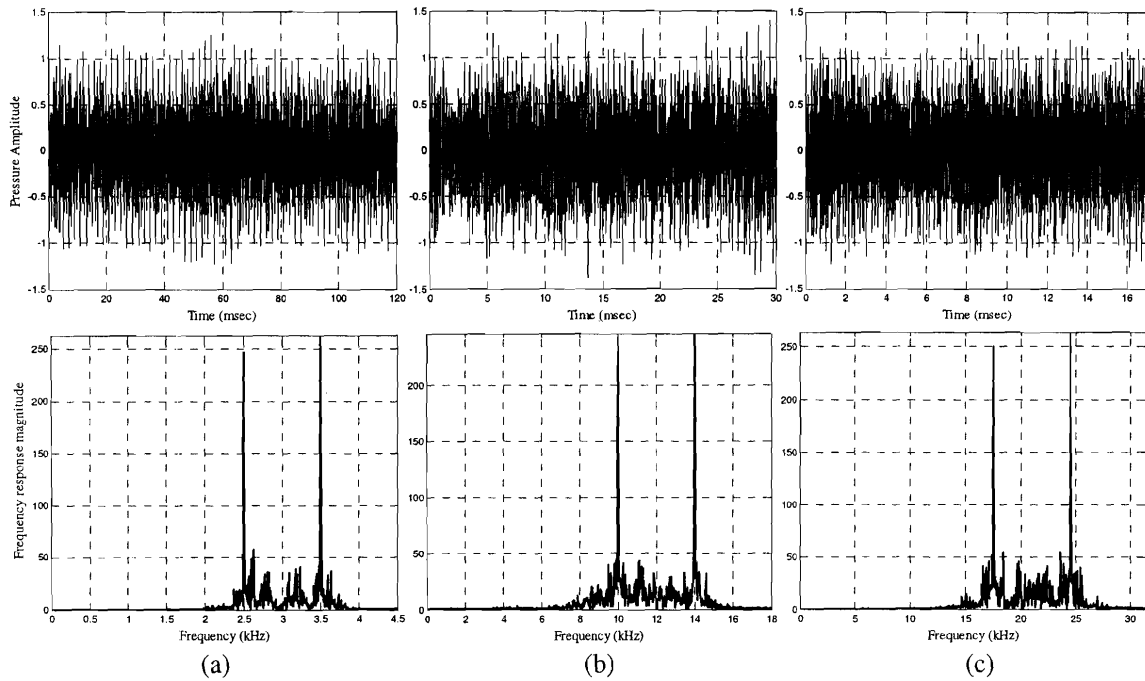


Figure 6.19: Pressure time history and Frequency response of DFE using the LMS filter tap weight adaptation algorithm for FSK modulated signals at data rates (a) 1kbps, (b) 4kbps and (c) 7kbps

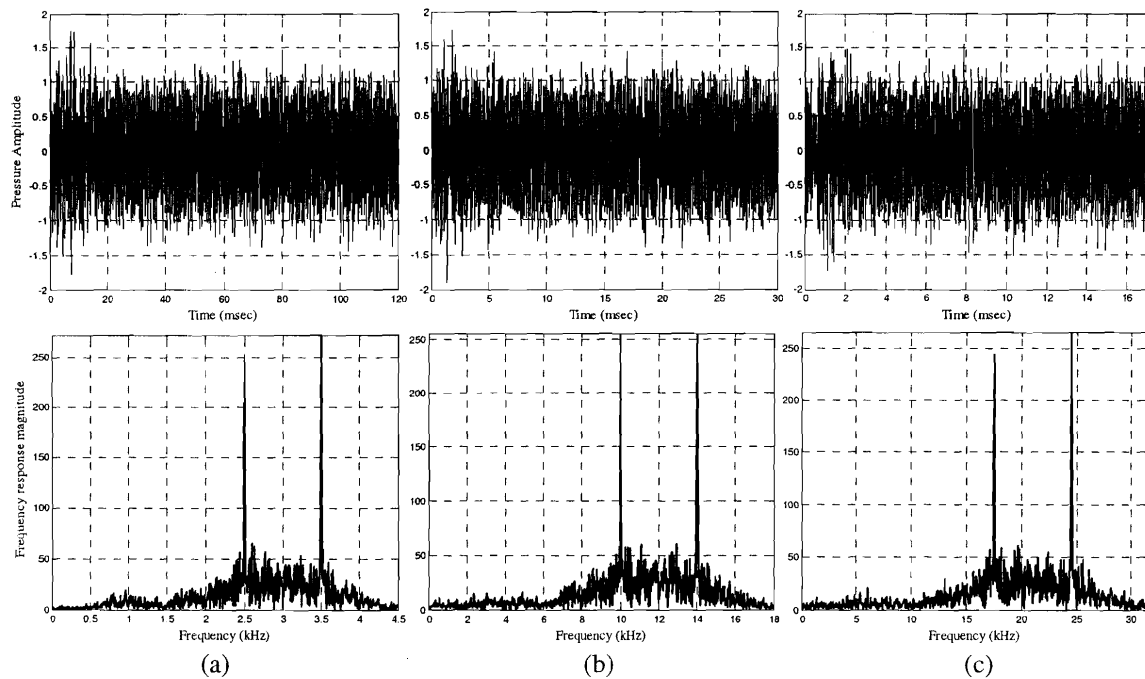


Figure 6.20: Pressure time history and Frequency response of DFE using the RLS filter tap weight adaptation algorithm for FSK modulated signals at data rates (a) 1kbps, (b) 4kbps and (c) 7kbps

The DFE was capable of removing from the signal most of the channel imposed distortion, allowing the communication system to achieve perfect error performance in all

cases. The similarity of frequency response plots among the Linear Equalizer and DFE for each of the adaptation algorithms indicates that the LMS and RLS arrived at similar solution spaces regardless of the structure of the equalizer. The solution identified by LMS minimizes the frequency everywhere except for the frequencies corresponding to the symbols, while the RLS solution attempts to reconstruct the original signal's spectrum. The observed equalizer response may be an indication that the LMS algorithm arrives at an excessive dispersion correcting solution, due to the longer training cycles as well as the increased filter length.

In general, the DFE requires smaller equalizer structures to achieve similar distortion compensation performance as the Linear Equalizer. The equalizer structures used varied from 20 to 40 elements for the feedforward filter and from 10 to 20 elements for the feedback filter, depending on the signal distortion. The more efficient organization of the DFE allows the RLS adaptation algorithm to present excellent behavior, since it required significantly smaller training times and reached the optimum solution in very few cycles, due to the shorter implemented filters.

6.5.3 Equalization of ASK and QAM signals

For completeness, equalization examples of signals modulated with the ASK and QAM methods, at 1, 4 and 7kbps data rates, are presented in Figure 6.21 and Figure 6.22, respectively. Figure 6.21 presents the response of the DFE for an ASK modulated signal, using the LMS adaptation algorithm. The plots present the pressure time history of the equalized data bearing signal, and the corresponding frequency response, along with the resulting signal constellation.

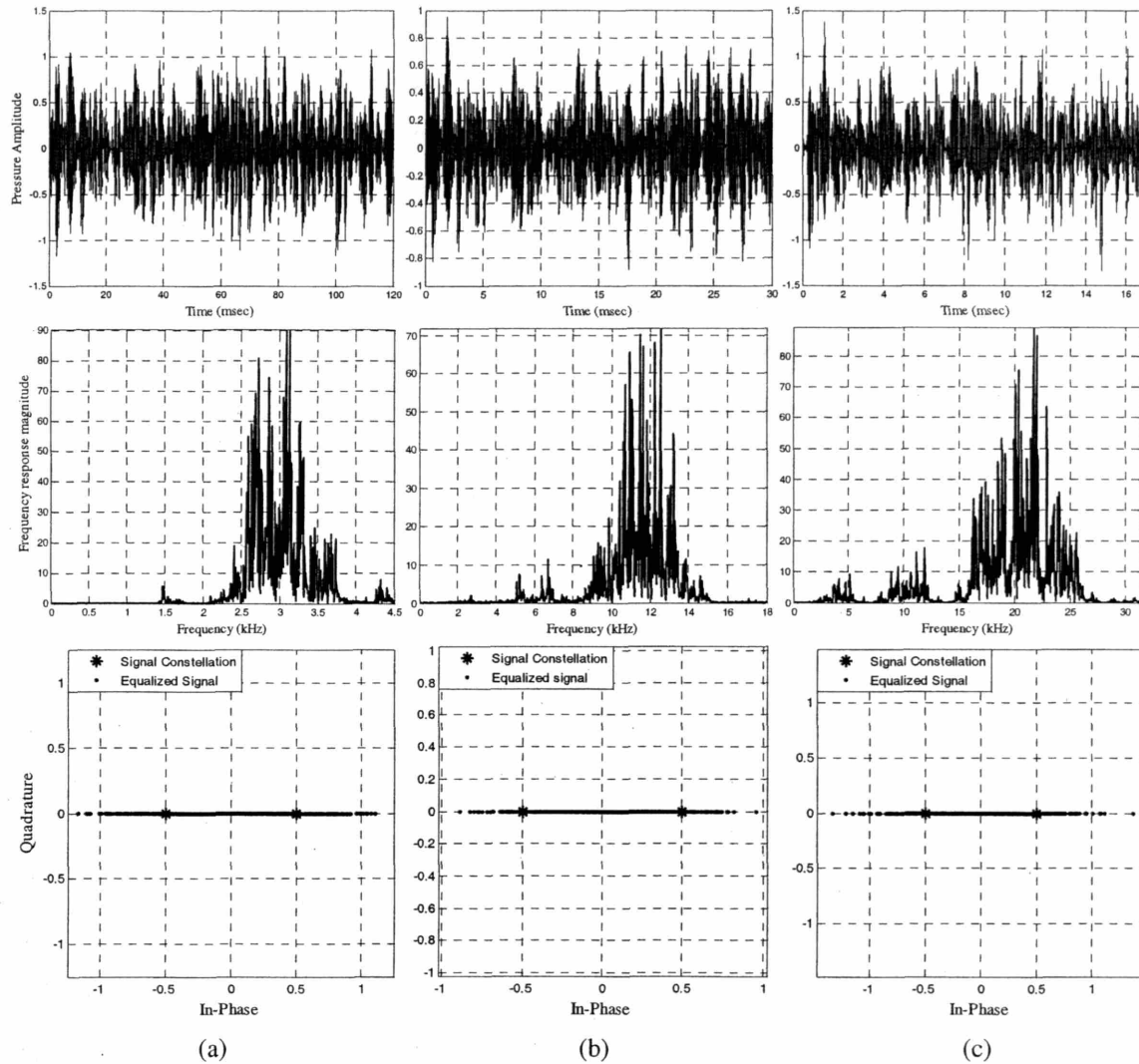


Figure 6.21: Pressure time history, Frequency Response, and Signal Constellation of DFE using the LMS filter tap weight adaptation algorithm for ASK modulated signals at data rates (a) 1kbps, (b) 4kbps, and (c) 7kbps

The absolute nature of the solution provided by the LMS adapted equalizer is apparent in the ASK case from the frequency response plots, where, similarly to the FSK examples, it leaves only the signal corresponding to the usable bandwidth while it diminishes the sidelobes, explaining the abrupt variations observed at the amplitude of the equalized signal. Recall that the frequency response of the initial signal indicates the presence of several sidelobes, similar to the ones observed in Figure 6.4. The DFE is always successful in removing the signal distortion and achieving the objective error performance. The signal constellation of resulting signal, also presented in the above plots, indicates the reduction of ambiguity of symbol detection since it distributes them

closely around the transmitted signal constellation points. For comparison, even though it does not represent the same textual message, review the great ambiguity in the ASK signal observed without dispersion compensation, presented in Figure 6.6. The remaining detection errors are corrected with the implementation of the Reed-Solomon decoding, in order to achieve perfect bit error performance.

Figure 6.22 presents the response of the DFE for a QAM modulated message. Each column of plots corresponds to the 1, 4, and 7kbps data rate signals, while the rows represent the pressure time history of the received signal, as well as the signal constellation before and after equalization, respectively. The signal is transmitted in a 0.5m radius pipeline across a distance of 10m. The transmitter and receiver are located at the reference positions at the crown of the pipe.

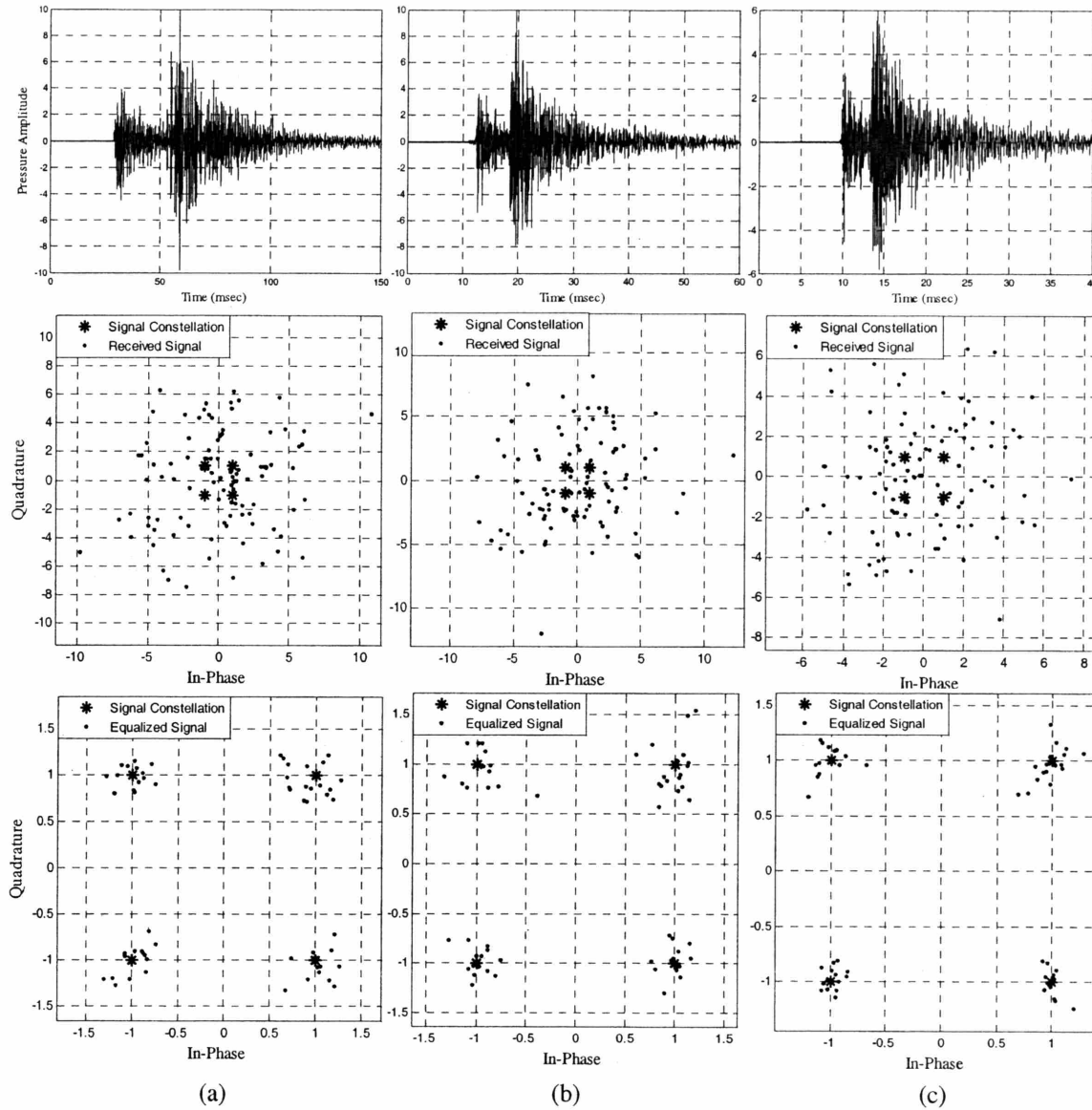


Figure 6.22: Pressure Time History and Signal Constellation of received and equalized signals with DFE using the LMS filter tap weight adaptation algorithm for QAM modulated signals at data rates (a) 1kbps, (b) 4kbps, and (c) 7kbps

The high signal dispersion of the received signal is not only apparent in the recorded waveform, but also in the received signal's constellation, indicating the excessive ambiguity of the detected symbols. The even distribution of the detected symbols across the scatter plot explain the inability of the detector to identify the underlying symbols, which in sequence result in very high error rates from 75 to 80%. However, the introduction of the DFE compensates for most of the signal distortion, concentrating the detected symbol representations very close to the transmitted signal

constellations, essentially eliminating any ambiguity in symbol detection. Therefore, the bit error rate of the communication system following the equalization process is zero as a result of the perfect bit representation. The ASK and QAM examples verified the increased efficiency of the DFE with respect to the filter length. The equalizer structures used are similar to the ones identified for the FSK signals presented above and thus the feedforward and feedback filters are composed from 20 to 40 elements and 10 to 20 elements, respectively, depending on the signal distortion.

6.5.4 Effect of pipeline waveguide on equalization process

This section examines the effect of the pipeline waveguide geometry on the equalization process. The filter length and dispersion compensation efficiency of the equalizer is studied with respect to the pipeline diameter and the propagation distance. It is expected that the parameters affecting the signal reverberation level will also affect accordingly the required equalizer structure. The effect of each parameter is studied separately. Initially, the radius of the pipe is varied from the reference value of $R = 0.5\text{m}$ studied above to a small pipeline with $R = 0.15$ and a large pipeline with radius $R = 1\text{m}$, which correspond to the values used in the waveguide parametric analyses of Chapter 3, while the distance of transmitter and receiver is preserved at the reference value of $z = 10\text{m}$. In sequence, the radius of the pipe is constant and equal to the reference case of $R = 0.5\text{m}$, while the propagation distance is set to $z = 100\text{m}$ and $z = 500\text{m}$.

According to the above, the effect of the pipeline radius on the equalization process is initially examined. Figure 6.23 presents the pressure time histories and the corresponding frequency spectra of the received signals for a propagation distance of $z = 10\text{m}$ inside a pipeline with radius $R = 0.15\text{m}$ and 1m , respectively. The transmitted signal is modulated at a data rate of 4kbps using the FSK method, illustrated in Figure 6.9b. In accordance with the findings of Chapter 3, the larger pipeline increases the reverberations on the propagating signal, due to the increased number of modes excited for a specific frequency spectrum. The resulting bit error rates for signal demodulation, without any error correction or signal compensation, is 30% and 40% for the $R = 0.15\text{m}$ and 1m respectively.

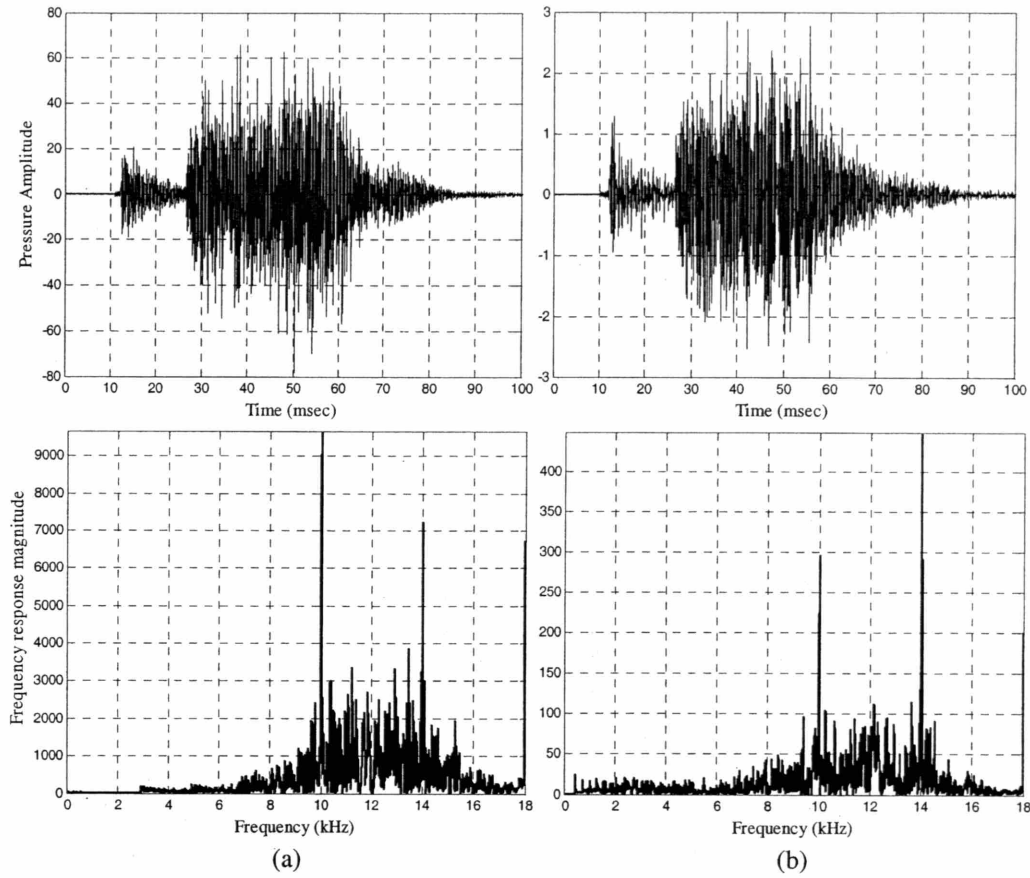


Figure 6.23: Pressure Time History and Frequency Response of Received Signal for FSK modulation at 4kbps data rate for propagation distance $z = 10\text{m}$ and pipeline radius (a) $R = 0.15\text{m}$, and (b) $R = 1\text{m}$

Figure 6.24 presents the result of a decision feedback equalizer using the LMS adaptation algorithm on the data bearing part of the recorded signals. In both cases the equalizer removed the majority of the signal dispersion and achieved perfect message reproduction, i.e. zero symbol detection errors. However, the larger pipe required longer filters at the DFE, with the feedforward and the feedback filter consisting of 50 and 20 elements, respectively. At the same time, the $R = 0.15\text{m}$ case required an equalizer with 20 elements in each of the feedforward and feedback filters. Moreover, the excitation of additional modes at the $R = 1\text{m}$ case, resulted in an increase of the required training cycles to allow the LMS algorithm to identify the optimal solution. It is interesting to observe, however, that the increased equalizer structure length for the large pipe resulted in complete elimination of the frequencies not representing transmitted bits, as illustrated in the frequency response plot of Figure 6.24b.

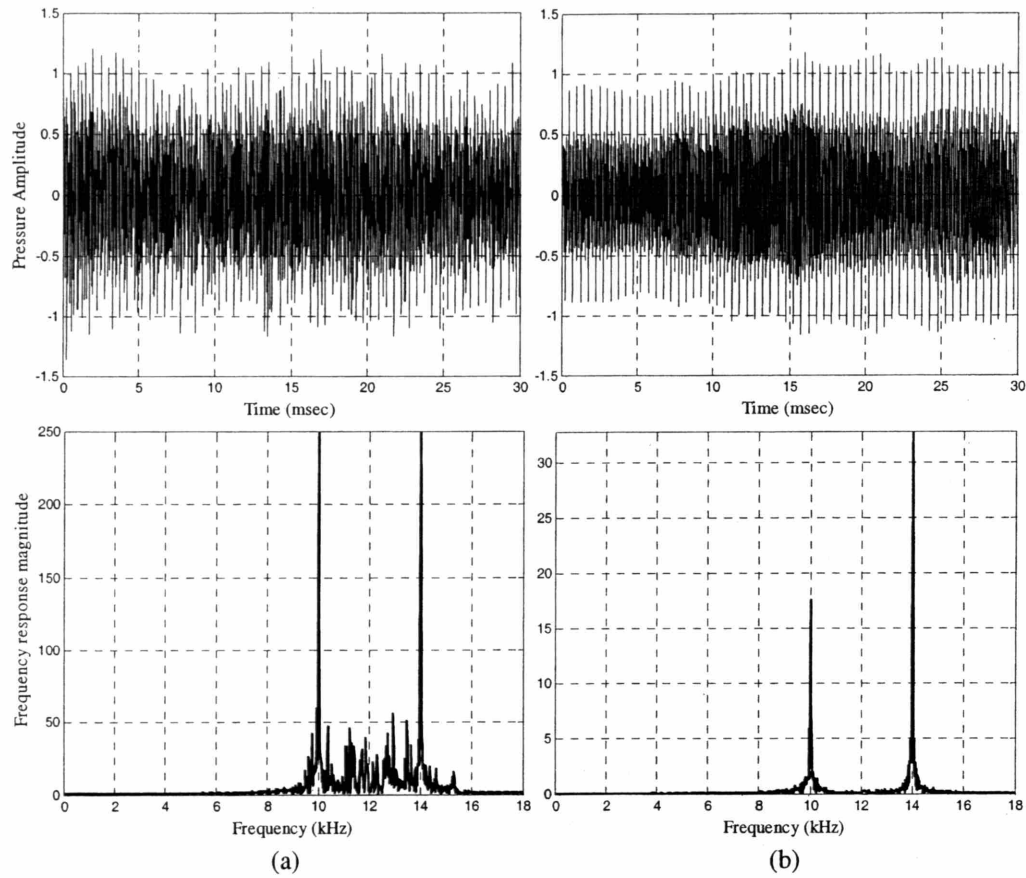


Figure 6.24: Pressure time history and Frequency response of DFE using the LMS filter tap weight adaptation algorithm for FSK modulated signals at 4kbps data rate, for a propagation distance of $z = 10\text{m}$ in a pipe with radius (a) $R = 0.15\text{m}$ and (b) $R = 1\text{m}$

In what follows the effect of propagation distance on the equalization structure is examined. Preserving the pipeline radius at 0.5m , the transmitted signal is recorded at 100m and 500m distance. Figure 6.25 presents the pressure time histories and frequency contents of the recorded signals in the aforementioned locations. The significant shift of the received signals towards lower frequencies indicates once again the lowpass character of the propagation channel, which becomes more pronounced with increasing distance. The signal dispersion is so severe that the Barker code is almost indistinguishable from the modulated signal, while the amplitude and frequency content of the signal is highly distorted. The resulting bit error rates before any error correction or dispersion compensation is applied are 42% and 49% for $z = 100\text{m}$ and 500m , respectively. The extraordinarily high error rate for the 500m propagation distance indicates that the

demodulator is essentially randomly selecting bits, due to the ambiguity of the received waveforms.

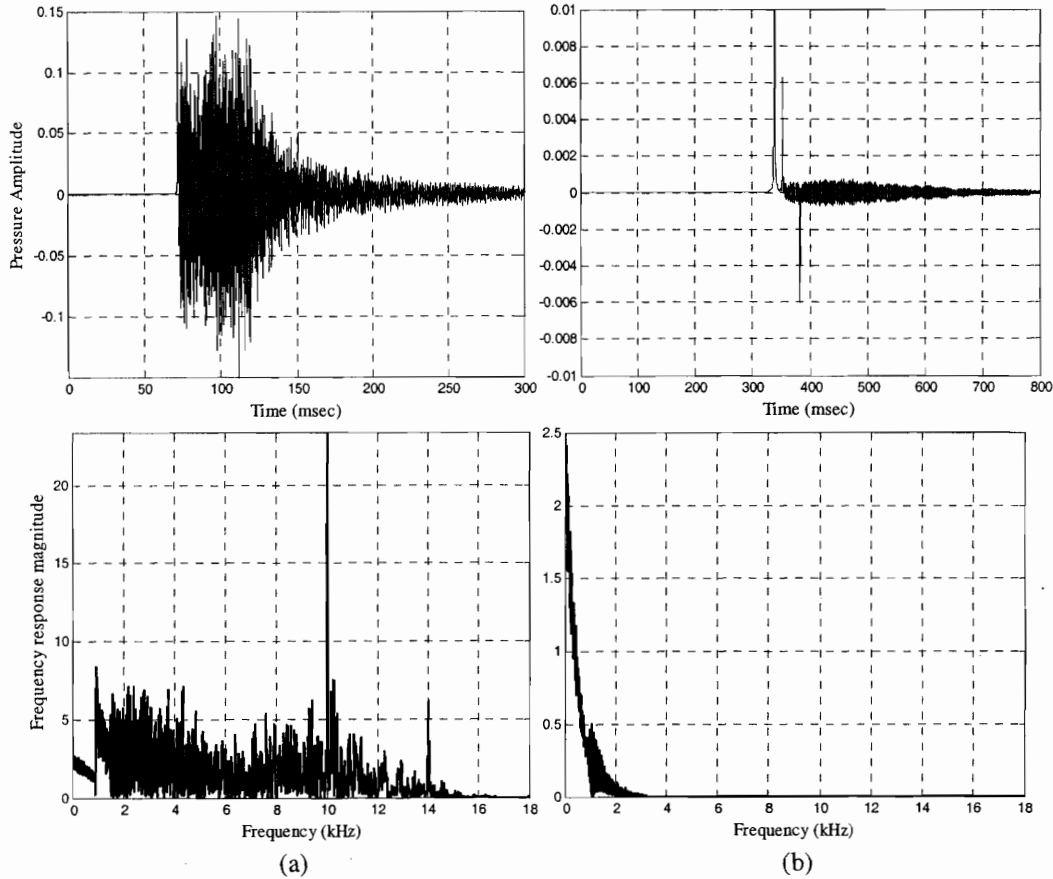


Figure 6.25: Pressure Time History and Frequency Response of Received Signal for FSK modulation at 4kbps data rate for pipeline radius $R = 0.5\text{m}$ and propagation distance (a) $z = 100\text{m}$, and (b) $z = 500\text{m}$

Despite of the high error rates before any dispersion compensation, the received waveform encapsulates the required information, which can be extracted with the use of the receiver signal processing blocks of the proposed communication system. Figure 6.26 presents the pressure time histories and frequency content of the equalized signals produced by a DFE. However, the required equalizer structure is rather large, with 60 and 30 elements at the feedforward and feedback filters respectively. The receiver achieved perfect reconstruction of the transmitted message in both cases. However, the extended equalizer structure removed all the frequencies that do not correspond to transmitted bits, as illustrated by the frequency response plots. The DFE utilized the LMS adaptation

algorithm, which in order to identify the optimal solution required extensive training time, with several training sequences through many cycles.

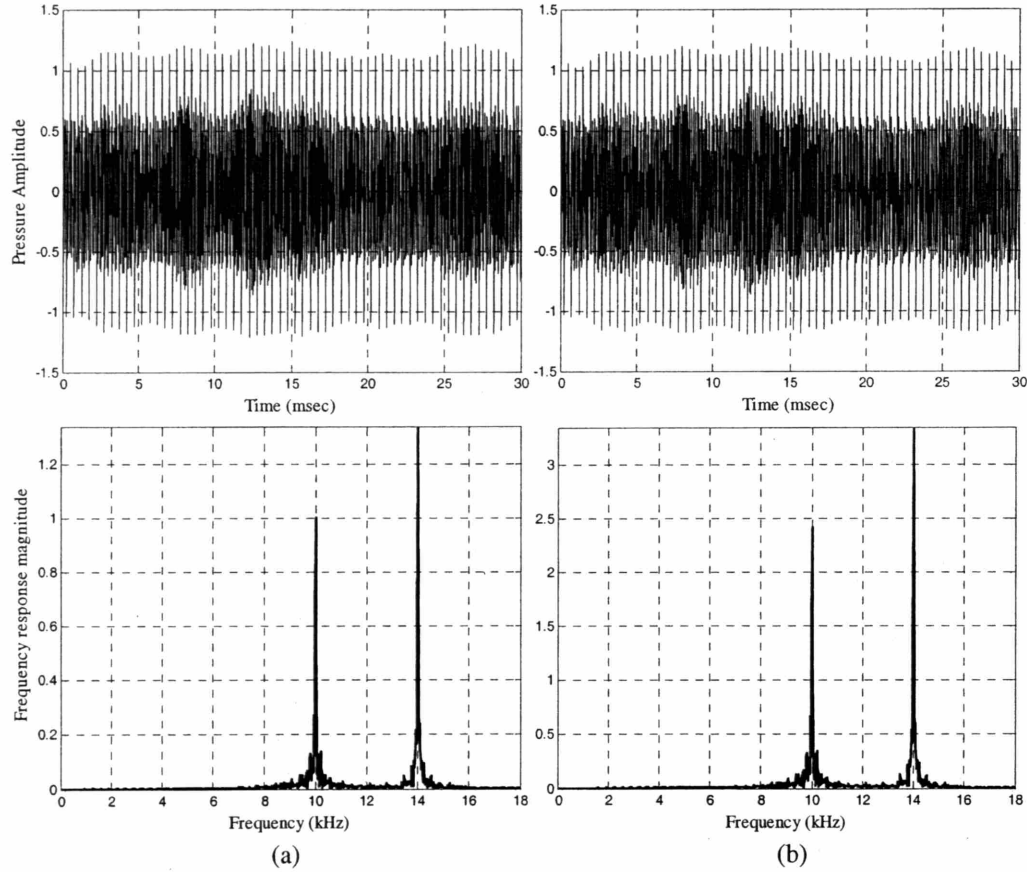


Figure 6.26: Pressure time history and Frequency response of DFE using the LMS filter tap weight adaptation algorithm for FSK modulated signals at 4kbps data rate inside a $R = 0.5\text{m}$ pipeline for a propagation distance of (a) $z = 100\text{m}$, and (b) $z = 500\text{m}$

6.5.5 Equalization of higher data rate signals

The final paragraph regarding adaptive equalization is concerned with the transmission of high throughput signals. For reference purposes, the pipeline waveguide used corresponds to the reference case, with radius 0.5m, and propagation distance 10m between the transmitter and receiver, which are installed at the crown of the pipe. In order to amplify the effect of reverberation a longer transmitted signal is selected, which will result in increased overlap among the delayed multipath arrivals. However, the results presented in the current section correspond to signals modulated with the

bandwidth efficient Quadrature Amplitude Modulation technique at 12 and 21kbps data rates, which generates complicated but relatively short waveforms. Figure 6.27 presents the formatting and encoding of the textual message selected, or in other words the conversion of the alphanumeric message into a stream of bits and the redundancy introduction by the Reed-Solomon error correction code.

G	1 1 1 0 0 0 1	1 0 0 1 0 1 0 1 1 1 1 0 0 0 1
e	1 0 1 0 0 1 1	0 0 0 1 1 0 1 0 1 0 1 0 0 1 1
o	1 1 1 1 0 1 1	1 0 1 1 1 0 0 0 1 1 1 1 0 1 1
r	0 1 0 0 1 1 1	1 1 1 1 1 0 1 1 0 1 0 0 1 1 1
g	1 1 1 0 0 1 1	0 1 0 0 0 0 1 0 1 1 1 0 0 1 1
e	1 0 1 0 0 1 1	0 0 0 1 1 0 1 0 1 0 1 0 0 1 1
	0 0 0 0 0 1 0	0 1 1 0 0 0 0 0 0 0 0 0 0 1 0
K	1 1 0 1 0 0 1	0 1 1 1 0 1 1 0 1 1 0 1 0 0 1
o	1 1 1 1 0 1 1	1 1 0 1 0 0 1 1 1 1 1 1 0 1 1
k ⇒	1 1 0 1 0 1 1 ⇒	0 0 1 1 0 1 1 0 1 1 0 1 0 1 1
o	1 1 1 1 0 1 1	1 1 0 1 0 0 1 1 1 1 1 1 0 1 1
s	1 1 0 0 1 1 1	1 0 0 0 1 1 0 0 1 1 0 0 1 1 1
s	1 1 0 0 1 1 1	1 0 0 0 1 1 0 0 1 1 0 0 1 1 1
a	1 0 0 0 0 1 1	1 1 1 0 0 0 1 1 1 0 0 0 0 1 1
l	0 0 1 1 0 1 1	1 0 0 0 1 1 1 0 0 0 1 1 0 1 1
a	1 0 0 0 0 1 1	1 1 1 0 0 0 1 1 1 0 0 0 0 1 1
k	1 1 0 1 0 1 1	0 0 1 1 0 1 1 0 1 1 0 1 0 1 1
i	1 0 0 1 0 1 1	1 1 0 1 0 1 0 1 1 0 0 1 0 1 1
s	1 1 0 0 1 1 1	1 0 0 0 1 1 0 0 1 1 0 0 1 1 1

Figure 6.27: Formatting and encoding of textual message

Figure 6.28 presents the amplitude and phase time histories of the modulated signals at 12 and 21kbps data rates preceded by the Barker code.

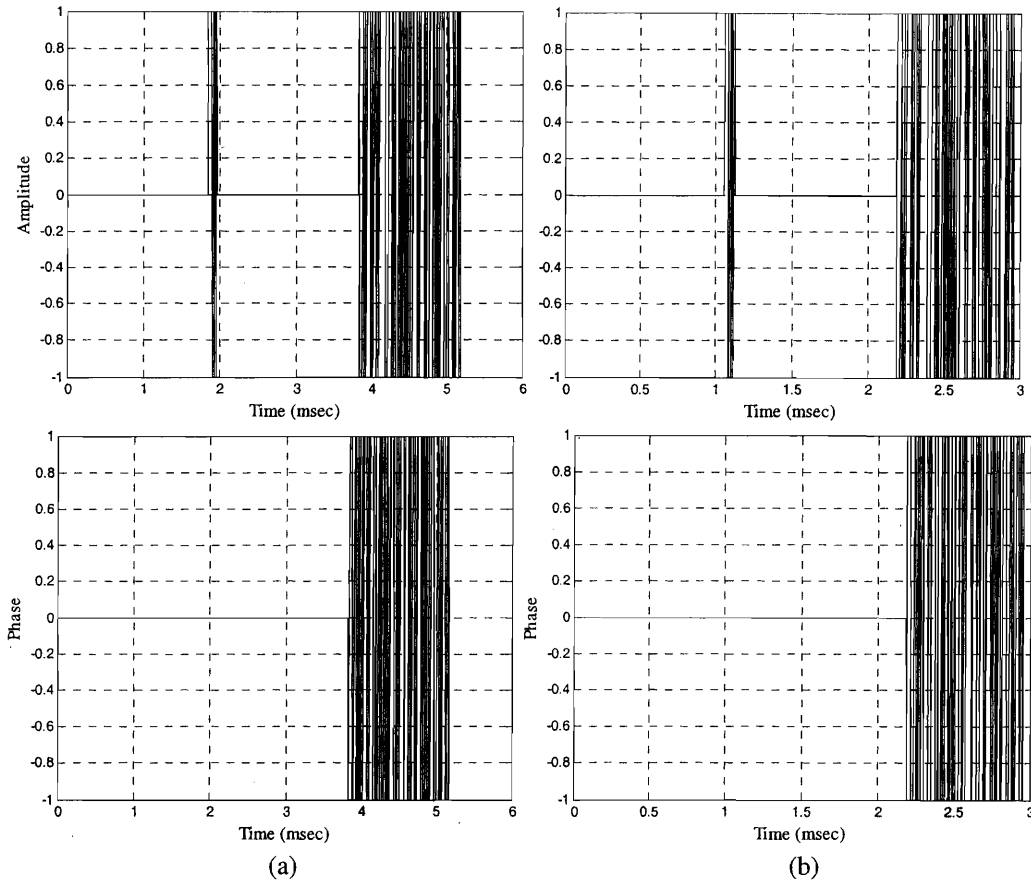


Figure 6.28: Amplitude and Phase of Transmitted Signal for QAM at data rates (a) 12kbps, and (b) 21kbps

The pressure time histories of the received signals are presented in Figure 6.29, illustrating the increased reverberations with respect to lower frequency content signals. The silent time between the barker code and the modulated signal is proven sufficient for the synchronization purposes; however, its reverberations significantly overlap with the data bearing signal. The severity of the received signal distortion is also illustrated by its signal constellation, presented in the second row of plots in Figure 6.29. These scatter plots demonstrate the ambiguity of the detected symbols directly from the received signal, due to their uniform distribution across the solutions space, indicating no apparent correlation to the four original signal constellation points. The aforementioned ambiguity of symbol detection is responsible for the 82% and 85% bit error rates of the demodulator without any dispersion compensation.

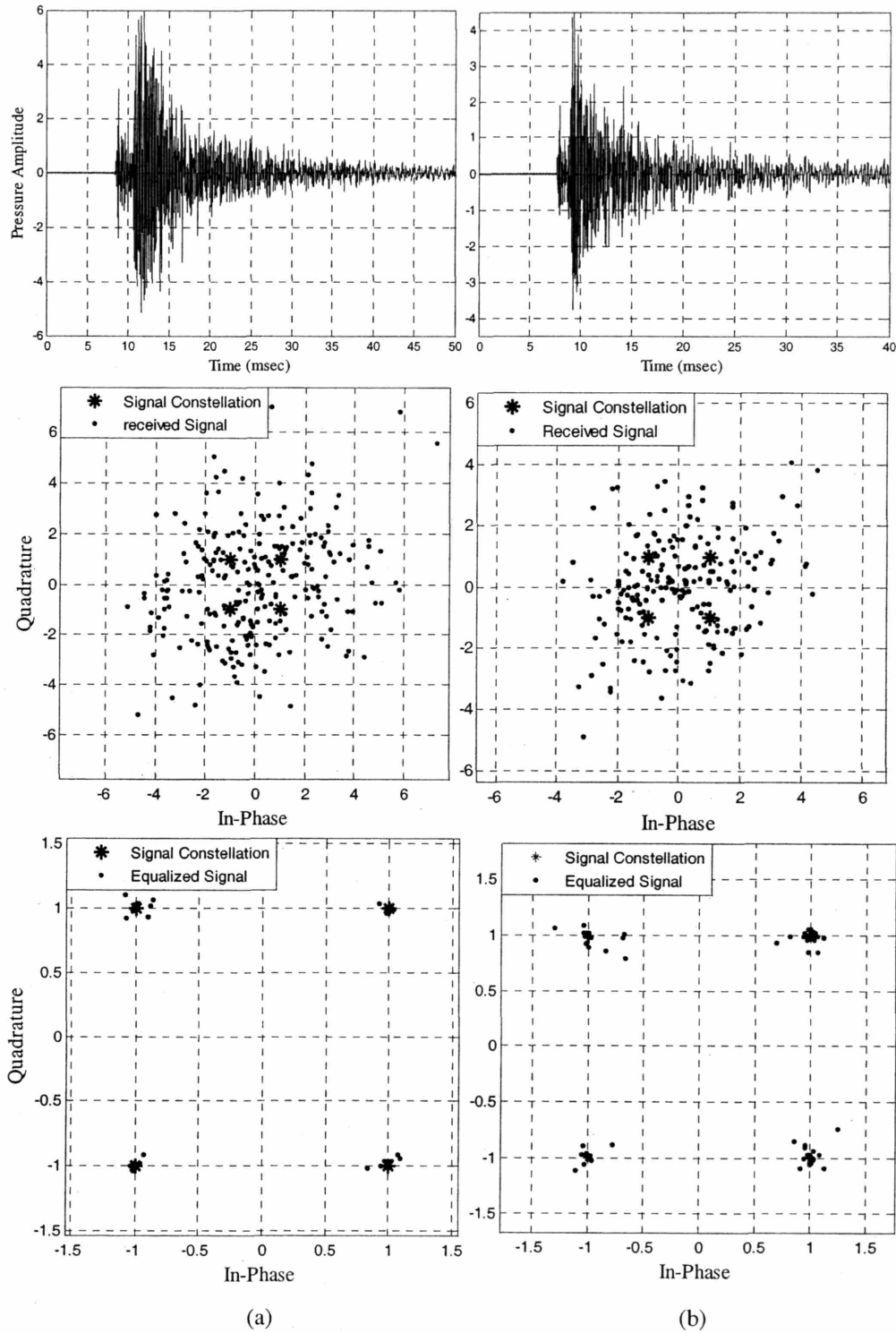


Figure 6.29: Pressure Time History and Signal Constellation of Received Signal and equalized signals with DFE using the RLS adaptation algorithm for QAM at data rates (a) 12kbps, and (b) 21kbps inside a pipeline waveguide with $R = a = r = 0.5\text{m}$, $z = 10\text{m}$

The final row of plots in Figure 6.29 presents the constellation of the equalized signal, when a DFE is employed. The signal distortion is almost completely removed as indicated by the perfect alignment of the detected symbols with the transmitted constellation points. The required equalizer structure is composed by 50 feedforward and 20 feedback filter elements, while the RLS adaptation algorithm is employed. The RLS algorithm performed exceptionally in identifying the optimal solution, since it required very few training cycles for the two data rates considered here.

In general, the adaptive equalizer proves to be an invaluable tool for removing the signal dispersion imposed by the channel. Its stability and robustness, along with the “real time” adjustability of its response, provide the necessary confidence and reliability for the proposed in-pipe acoustic digital communication system. The decision feedback equalizer is established as more efficient than the linear equalizer in terms of required filter length. The LMS adaptation algorithm is relatively fast, but requires many training cycles, while the RLS requires significantly lower number of training cycles, but its computational complexity prohibits its use for long equalization filters.

6.6 *Effect of Ambient Noise*

The simulations executed and presented up to this point considered the dispersion from the transmission channel as the only signal distortion mechanism. However, apart from dispersion, the signal distortion is also a result of the ambient noise. Thus, this section is concerned with the effect of environmental noise on the integrity of the received signal. According to the discussion in paragraph 4.4.1, the environmental noise is considered Gaussian and White, or in other words it follows the Gaussian distribution with a certain mean amplitude value that remains constant throughout a theoretically infinite frequency spectrum. The effect of such a noise source is additive to the propagating signal, i.e. the received signal is the result of superposition of the transmitted signal and the ambient noise level.

For the simulations presented in this section, the additive Gaussian white noise model presented in Chapter 4 is used. The received signal is considered to be simply the addition of the transmitted waveform and a random signal with mean value equal to zero

and variance appropriate to generate the required signal to noise ratio. No other channel effect is introduced, such as reverberation, in order to identify the sole effect of environmental noise in the propagation signal and to enable a direct comparison between dispersion and ambient noise. Bandpass filtering is introduced to the communication system as remedy for the noise effect, according to the discussion of paragraph 5.3.7. A Kaiser Window filter is implemented with a length appropriate to eliminate any signal outside a prespecified frequency band, which is essentially an extended range of the used bandwidth. The signal reduction achieved by the used Kaiser filters for the signal outside the desired frequency range is of the order of 50dB. Figure 6.30 and Figure 6.31 present the effect of ambient noise on the pressure time history and frequency response of FSK and ASK modulated signals at 4kbps data rates respectively, for an increasing noise level.

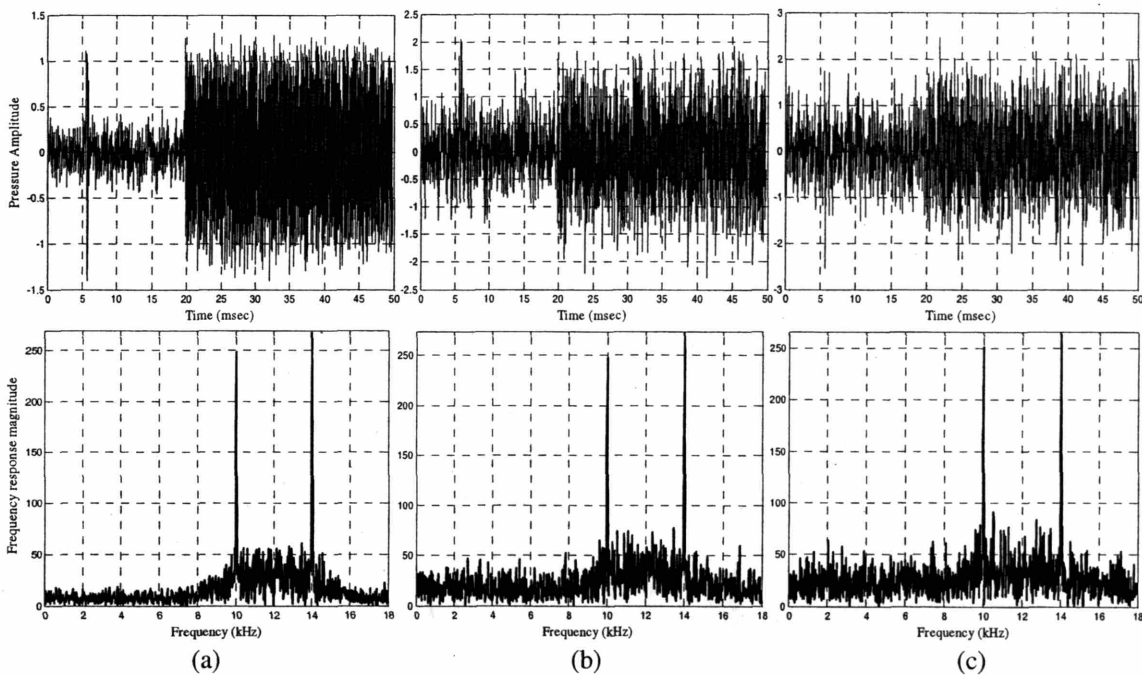


Figure 6.30: Effect of Ambient noise on transmitted signal; Pressure Time History and Frequency response for FSK modulated signal at 4kbps data rate for SNR equal to (a) 10dB, (b) 2dB, and (c) 0dB

The plots presented above illustrate the effect of ambient noise on an FSK modulated signal from an intermediate to extreme noise levels, corresponding to SNR = 10dB, 2dB, and 0dB, respectively. The latter case indicates that the amplitude of the noise added is of the same order of magnitude as the transmitted signal. The frequency

response plots indicate that the FSK modulated signals are little affected by the ambient noise introduction, since the frequencies representing the encapsulated bits are easily identifiable. The bit error level for the 10dB SNR is zero even without filtering, while the bit error rates for the 2dB and 0dB cases are in the order of 5% and 8% respectively. The communication system achieves perfect message reconstruction in all cases following the bandpass filtering. The low error rate of the received signal can be explained from the fact that the FSK demodulator depends on frequency detection, which remains essentially unaffected even when noise levels are very high. It is important to observe that the bit error rates imposed by ambient noise are significantly smaller than the corresponding error levels due to reverberation, before dispersion compensation and error correction, indicating that reverberation is the main cause of signal distortion for the in-pipe waveguide.

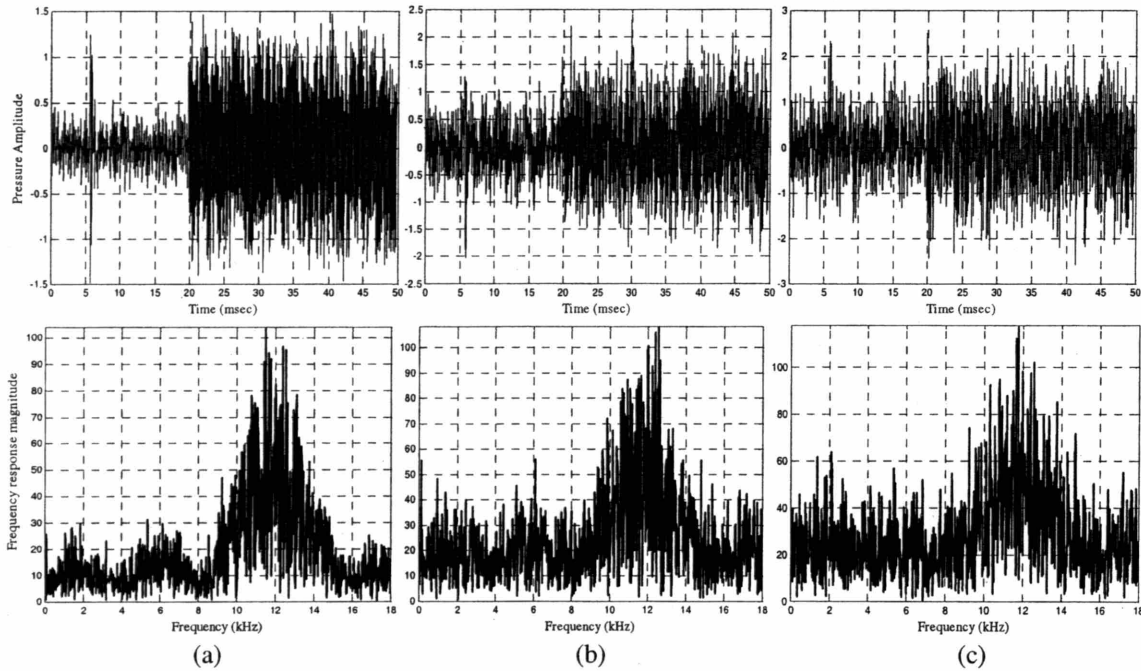


Figure 6.31: Effect of Ambient noise on transmitted signal; Pressure Time History and Frequency response for FSK modulated signal at 4kbps data rate for SNR equal to (a) 10dB, (b) 2dB, and (c) 0dB

Figure 6.31 presents the result of additive Gaussian white noise on ASK modulated signals. This time the error rates before filtering are higher than the FSK case, on the order of 2%, 9% and 16% for the 10dB, 2dB and 0dB SNR, respectively, while

bandpass filtering reduces these error levels to zero, 3% and 5%. The digital communication system achieves perfect message reconstruction with the assistance of the Reed-Solomon decoding. The ASK demodulators seem more prone to errors by the introduction of ambient noise with respect to FSK modulation, since according to ASK symbol detection depends on amplitude variations, which are significantly affected by the noise random amplitude, explaining the increased error levels. However, the error rates of the received signal are once again significantly lower than the error rates associated with channel imposed reverberation, confirming the aforementioned conclusion that dispersion is the main source of signal distortion for the pipeline waveguide. It is therefore shown that under any noise conditions the introduction of simple filtering and error correction processes ensure reliable transmission with the proposed digital communication system. For very long propagation distances, where attenuation, absorption, and spreading have reduced significantly the amplitude of the propagating wave, or in case of even more extreme noise levels, it may be required to increase the power and consequently the amplitude of the transmitted signal. Evaluation of the communication system including the effect of both ambient noise and reverberation is implemented in the scaled experiments presented in Chapter 7.

6.7 Conclusions

This Chapter essentially demonstrated the use, and justified the selection, of each signal processing block proposed for the in-pipe communication system. The effectiveness of each method is verified, identifying at the same time the advantages and disadvantages. The effect of the environmental parameters, as well as the characteristics of the transmitted signal, on the fidelity of the communication system are also examined.

Each of the various signal processing blocks serves a different purpose and enables a feature of the digital communication system. For example the formatting and packetizing block is necessary to convert the textual message to blocks of binary streams appropriate for further processing. The encoding step adds redundancy to the binary stream in order to recover potential errors at the receiver, since complete removal of dispersion or ambient noise related distortion is not always feasible. Modulation is

required to map the binary streams in a set of waveforms appropriate for transmission in physical media. The Barker code enables accurate synchronization of the transmitted blocks. The preconditioning block, which includes the stacking and inverse transfer function processes, is necessary in case of severe signal distortion, since it can enhance the original features of the signal and decreases significantly the signal dispersion and noise. The combination of bandpass filtering and adaptive equalizer is necessary for the compensation of the channel imposed signal distortion, since the first is responsible for reducing the ambient noise level in the recorded signal, while the second removes the dispersion.

The pipeline waveguide characteristics, initially identified in Chapter 3, are present in the simulations completed in this chapter. The pipeline acoustic channel behaves like a lowpass filter, presenting increasing signal decay with propagation distance and frequency content. The higher frequency signals also exhibit increased levels of reverberation, since they correspond to propagation of higher and therefore more dispersive modes. Moreover, larger pipes present increased levels of channel imposed signal dispersion, due to the increased number of modes excited, or in other words due to the drop of the cut off frequencies of each mode. Therefore, signals containing higher frequencies and/or propagating inside larger pipes may potentially require extensive dispersion compensation and noise cancellation processing, since they present higher dispersion and their corresponding amplitude is smaller than lower frequency signals propagating in smaller radius pipes.

The computerized simulations indicate that the proposed communication system design allows reliable data transmission under a wide range of circumstances, with appropriate adjustment of its parameters. The received signal is generally severely distorted by the propagation within the pipeline waveguide and, therefore, direct detection of the encapsulated symbols usually results in very high error rates. Each of the signal processing steps implemented at the receiver is responsible for some reduction of the error rate, since it removes part of the channel imposed signal distortion. The error rate reduction for each receiver signal processing block, including all alternative proposed techniques, is summarized in Table 6.2 for a wide range of parameters, such as the achieved data rates from 1 to 21kbps, message lengths from 42 to 140 bits,

propagation distances from 10 to 500m, pipeline radii from 0.15 to 1m, and ambient noise levels from 0 to 10dB. The error rates presented in the following table are corresponding to the complete set of the conducted simulations, whether or not presented in the preceding paragraphs.

	Received signal	Stacking	Bandpass Filtering	Adaptive Equalization	Reed Solomon Decoding
FSK	30 – 49%	8 – 45%	8 – 36%	0 – 2%	0%
ASK	35 – 50%	14 – 50%	12 – 40%	0 – 3%	0%
QAM	68 – 85%	42 – 80%	35 – 70%	0 – 4%	0%

Table 6.2: Bit error rates following the signal processing blocks of the receiver

The error rates presented above indicate that the greatest error reduction is achieved with the introduction of the adaptive equalizer. Similar error reduction can be potentially achieved with the implementation of the inverse transfer function. The top error rates following the stacking process correspond to cases where stacking has not effect or is even harmful to the detection process. However, the low values indicate that careful application of stacking can be very beneficial for the communication system, especially for severely distorted signals.

It is very important to notice that for the in-pipe acoustic communication the maximum error rate of the received signal corresponding only to ambient noise distortion is 18%, while the error rate due to reverberation can be up to the maximum error rate, i.e. 50% for the binary symbols presented or 100% for the four bit symbols in QAM. Moreover, the noisy message can be completely restored with relatively simple processes such as bandpass filtering and decoding. These facts indicate that reverberation is the main source of signal distortion for the in-pipe transmission channel, justifying the focus of this research study on dispersion compensation.

Alternative techniques are considered for several signal processing blocks, such as the modulation and adaptive equalization. The selection of one for the implementation of the digital communication system is usually controlled by several parameters, such as computational complexity, available power, available bandwidth, required data rate, and so forth. Three methods are considered for the modulation process, the Frequency Shift

Keying, the Amplitude Shift Keying and the Quadrature Amplitude Modulation. All modulation methods provided comparable bit error rates, which are always completely eliminated with the introduction of the appropriate signal processing steps. Therefore, the selection of the modulation method will be decided on the basis of the bandwidth vs. power requirement and/or availability trade-off. According to the discussion of Chapter 4, the FSK modulation is more appropriate for power limited transmission channels, since it has low power requirements at the expense of used bandwidth. On the other hand, methods such as ASK and QAM are suitable for bandwidth limited channels, since they can be very bandwidth efficient at the expense of excessive power requirement. However, for the in-pipe acoustic communication system, the transmission channel is bandwidth limited while the device is power limited, as has been discussed in Chapter 5. The selection of one modulation method will, therefore, be specific to the application of the communication system, and more explicitly will be controlled by the data throughput requirement as well as the bandwidth and renewable power availability.

With respect to adaptive equalizer structures the Decision Feedback Equalizer turned out to be the most efficient, since it requires significantly shorter filters than the Linear Equalizer. The Recursive Least Squares adaptation algorithm is potentially preferable, due to its fast convergence with respect to training cycles to the optimal solution. However, when long equalizer filters are required, the Least Mean Squares should be used, due to the exponentially increasing computational complexity of the RLS algorithm with filter length. In any case, both adaptation algorithms achieved similar dispersion compensation performance, leaving the selection only to computational restrictions.

The findings of this Chapter will be compared and verified with the corresponding results in Chapter 7, where the communication system is tested in laboratory experiments.

6.8 *References*

- [1]. Proakis J.G., "Digital Communications", *McGraw Hill*, 4th Edition, Boston, MA, 2001.

Chapter 7

Laboratory Experiments

7.1 *Introduction*

To verify the results of the communication system performance evaluation conducted with the assistance of the computerized simulations presented in Chapter 6, it is necessary to implement real pipeline experiments. However, since no water pipeline was readily available within the time frame of this research, this Chapter presents results from pipeline experiments executed in a laboratory environment. Space and equipment limitations restricted the length, diameter and materials of the pipes used. The experiments are conducted in an appropriate fashion scaling all the parameters by a certain factor in order the results to correspond to larger pipes and longer distances. More explicitly, a 4" diameter PVC pipe is used, with length varying from 10 to 30 feet, while the acoustic transmission medium is air at atmospheric pressure. The scaling factor achieved with this arrangement is in the order of 10, as explained in the subsequent paragraph. The laboratory experiments allow examination of the combined effect of reverberation and ambient noise on the propagating signal. In addition, the cumulative effect of scatterers at the signal reverberation is also studied. Such scatterers are present at frequent locations along the pipeline in the form of joints. Finally, bends and branches are added in the experimental pipeline configuration, resulting in an aggravated factor of signal distortion and attenuation. Water pipelines are assembled into a network with numerous curves, merges and divisions, all of which have potentially detrimental effects on the propagation of a transmitted signal. It is necessary to examine such disturbances, while the design of the in-pipe communication system should compensate for their effect.

In what follows, a detailed description of the experimental layout is provided, along with the hardware used. The scaling factor of the experiment is also determined and justified. Furthermore, the limitations of this experimental configuration in comparison to a real water pipeline network are discussed. Thereafter, the results

obtained from the three pipeline configurations, straight, bend, and branch, are provided, along with a comparison to the corresponding computerized simulations of Chapter 6. Finally, general conclusions from the research work, as a feasibility study of the in-pipe acoustic communication system, along with potential future work that would establish and extend the use of such a system, are discussed.

7.2 *Experimental Layout*

Three main experimental layouts are selected for laboratory testing of the in-pipe acoustic communication system, namely straight, bent and branch pipe sections. All the computerized simulations, presented up to this point, involved straight pipeline segments from 10m to 500m. However, pipelines in real water transmission and distribution systems are arranged in a network manner, and they must conform to landscape restrictions, such as roads, bridges, and hills, turn around buildings, and so forth. Therefore, the presence of pipe bends as well as other pipes branching on the pipe of interest is inevitable. Such deviations from a straight pipeline affect the propagation of the transmitted waves, necessitating investigation of not only of straight waveguides, but also of curved and branched ones, justifying the selection of the experimental layouts. Figure 7.1 presents the three main pipeline configurations tested. The experiments are conducted with 4" diameter, 10 feet long PVC pipe segments. These sections are connected with sleeve type joints that generate a 0.5" to 1" long, and 0.3" deep, indentations around the internal circumference of the pipe, which act as scatterers. In the case of bent pipe configuration one of the joints is replaced with a 90° curved connection. While the angle of this turn is considered excessive for actual water pipeline networks, to avoid hydraulic hammers, it provides an upper limit on signal distortion effect that can be encountered in real pipes. For the branched pipe configuration, one of the joints is replaced with a T-shaped connector on the side of which a 10 feet long, 1.5" in diameter pipe is connected. This configuration attempts to simulate the connection of a distribution, i.e. a local and small diameter, pipe onto a transmission main pipeline. Due to laboratory space restrictions, only up to three 10 feet segments are used, resulting in a

total of 30 feet long pipeline. Experiments are conducted employing one, two or all three segments, so as to identify the effect of propagation distance.

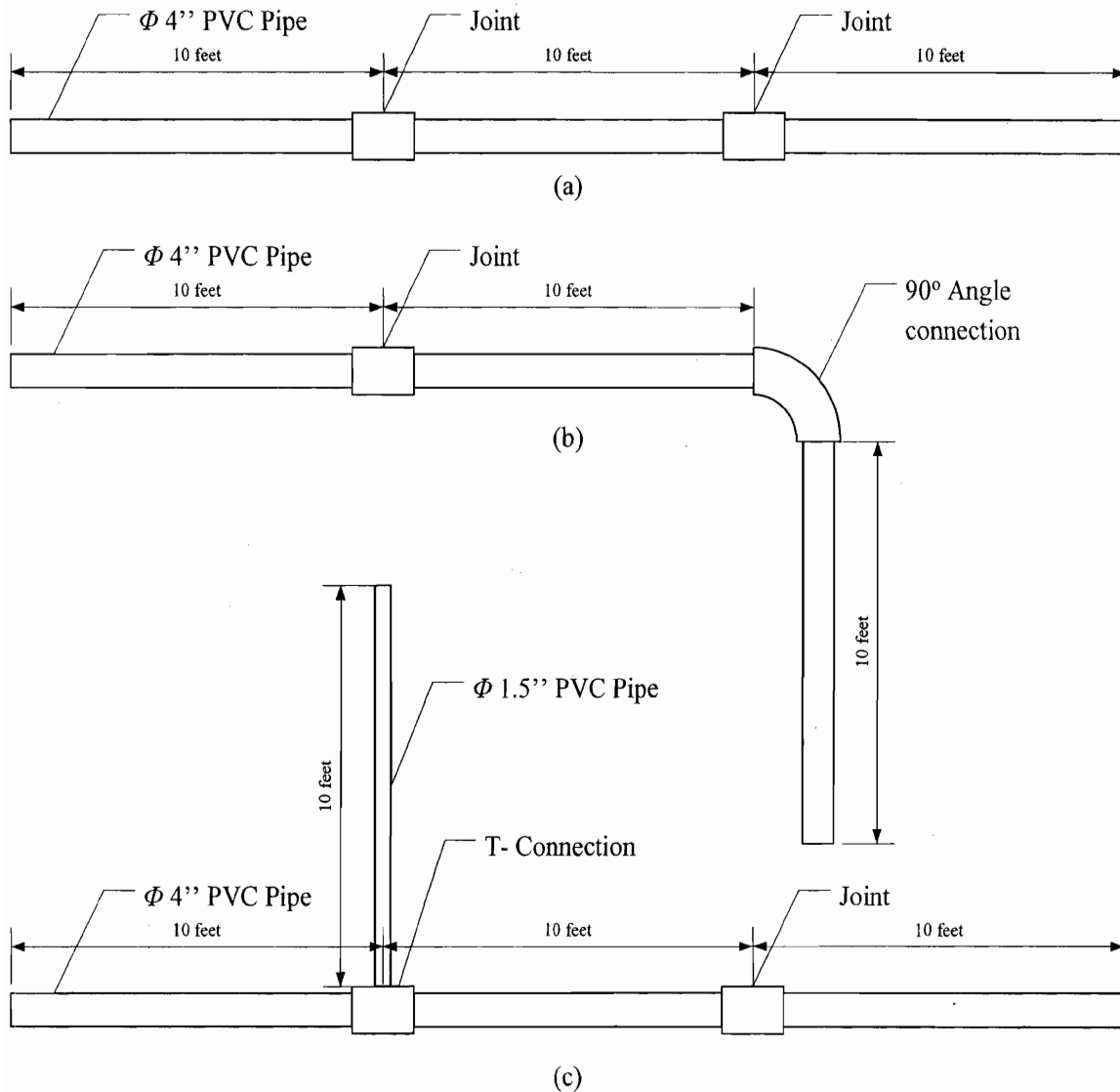


Figure 7.1: Laboratory Experiment Pipeline layout (a) Straight, (b) Bend, (c) Branch

It is necessary to identify the correlation, or in other words what is the distance correspondence, between the laboratory experiment and the actual pipeline, usually denoted as *scaling factor* of the experiment. An estimation of the scaling factor can be obtained by equating the pressure fields generated by both configurations. A first approximation can be obtained by the theoretical development of the rigid pipe case presented in Chapter 3. Considering equation 3.66, provided below for convenience, it

can be observed that the response of the waveguide is controlled mainly by the summation term while the remaining part outside is just an amplitude scaling factor.

$$p(r, \theta, z, \omega) = \frac{\rho}{2\pi R^2} \omega f(\omega) e^{i\omega t} \sum_{j=1}^{\infty} \frac{e^{-i|z|\sqrt{k_0^2 - k_{nj}^2}}}{\sqrt{k_0^2 - k_{nj}^2}} \frac{J_0(k_{0j}r)}{J_0^2(k_{0j}R)} \quad (0.1)$$

Reformulating the above formula in order to collect the constant terms provides

$$p(r, \theta, z, \omega) = \frac{\rho}{2\pi R} \omega f(\omega) e^{ia\tau} \sum_{j=1}^{\infty} \frac{e^{-i\left|\frac{z}{R}\right|\sqrt{(k_0 R)^2 - (k_{nj} R)^2}}}{\sqrt{(k_0 R)^2 - (k_{nj} R)^2}} \frac{J_0(k_{0j}r)}{J_0^2(k_{0j}R)} \quad (0.2)$$

where $a = k_0 R = \frac{\omega R}{c}$ is the dimensionless frequency and $\tau = \frac{tc}{R}$ is the dimensionless

time. Both dimensionless quantities must be preserved constant in each pipeline case to maintain consistency of the resulting pressure fields. From the above equation it becomes

apparent that the summation part is controlled only by the $\left|\frac{z}{R}\right|$ term with respect to the

comparison of the actual and laboratory pipeline pressure fields, since every other term cancels out for equivalent radial distances. Considering that the radius of the actual pipeline considered is 0.5m while the radius of the PVC pipe is 0.05m, a distance of 10m in the laboratory corresponds to 100m in the field by equating the above ratio for both pipes.

A simplified procedure similar to the above is the estimation of the effective scaling factor by a direct comparison of the impedance contrast of the water and cast iron pipe combination with the air and PVC pipe. The absolute acoustic impedance of a material is defined as the product of the density and acoustic wave velocity over the cross sectional area of the material in which the wave propagates. The impedance contrast of two materials provides a measure of the reflection intensity when the propagating wave reaches their interface, which in the pipeline waveguide case controls the amount of reverberation. Considering the acoustic wave velocities and densities of water, cast iron, air and PVC, provided for convenience in Table 7.1, as well as a water pipeline of 1m diameter and approximate wall thickness 2cm, while the PVC pipe is 4" in diameter, i.e. 0.10m, and has approximate thickness of 5mm, the ratio of acoustic impedance contrasts is calculated to be approximately equal to 10, agreeing with the aforementioned factor.

	Acoustic Wave Velocity (m/sec)	Density (kg/m ³)
Water	1500	1000
Cast Iron	5100	7874
Air	343	1400
PVC	1580	1.25

Table 7.1: Acoustic wave velocity and density of Water, Cast Iron, Air, and PVC

It is also important to preserve the ratio of the wavelength over the pipe diameter in both configurations, in order to achieve similar channel imposed distortion characteristics. This ratio is equivalent to the aforementioned ratio of dimensionless frequency a . Thus, considering the properties of the two systems and that $\frac{d}{\lambda} = \frac{d \times f}{c}$, where d is the diameter of the pipe, λ is the wavelength, f is the frequency and c is the acoustic wave velocity we get

$$\frac{d_{iron} \times f_{water}}{c_{water}} = \frac{d_{PVC} \times f_{air}}{c_{air}} \Rightarrow f_{air} = 2.3 \times f_{water} \quad (0.3)$$

where f_{water} is the frequency of the acoustic wave in the water filled iron pipeline, and f_{air} is the frequency of the acoustic wave in the air filled PVC pipeline. The above equation indicates that the frequency content of the signal in the actual water pipe corresponds to 2.3 times the frequency content of the signal in the scaled experiment. For example, transmission of a signal with carrier frequency of 21kHz over 10m length in the laboratory experiment corresponds to a 130m of propagation distance in an actual water pipeline of a 9.1kHz carrier frequency signal.

A first proof of compatibility of the laboratory experiment with the actual water pipeline can be obtained from computerized simulations of both systems. Figure 7.2 presents the pressure time histories of the laboratory and the actual pipeline systems for a single pulse excitation. The actual pipeline result corresponds to propagation of a single pulse with 2kHz central frequency over a distance of 100m. The laboratory experiment result corresponds to a propagation of a single pulse with central frequency 4.6kHz over a

distance of 10m, following approximately the scaling factor for both frequency and distance.

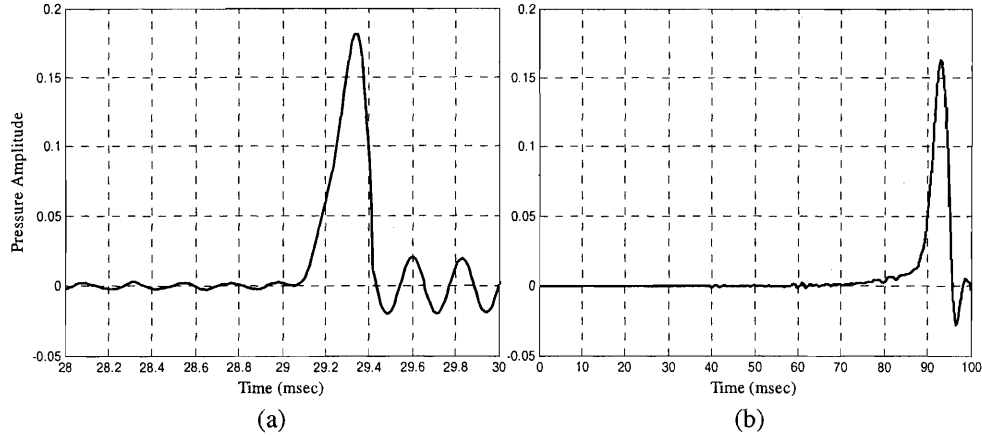


Figure 7.2: Simulated Pressure Time Histories single pulse transmitted inside a (a) 4" diameter, 10m long PVC pipe, and (b) 1m diameter, 100m long cast iron pipe.

The above plots reveal the similarity in attenuation characteristics and energy distribution among the main received pulse and the dispersive part of the signal in the two acoustic channels. The energy distribution is illustrated by the area, magnitude, and duration of the main and the subsequent pulses. The shorter duration of the pulses illustrated at laboratory experiment plot are explained from their higher frequency correspondence. However, the number and strength of modes that get excited in both examples remain the same as indicated by the similar dispersion patterns. Recall from Chapter 3, that pipes of smaller diameter excite fewer modes for the same frequency content, thus justifying the necessity for increased frequency spectrum in the laboratory experiments to achieve the same results with the large water pipes. Finally, it is interesting to notice the essentially identical magnitude of the main pulse received in both examples presented above, indicating the similar levels of signal decay from parameters such as attenuation, absorption, and radiation damping.

7.3 Hardware

Within the scope of the laboratory experiments, essentially all the components of the proposed digital communication system, presented in Chapter 5, are implemented. A schematic diagram of the hardware configuration used for the experiment is presented in Figure 7.3. All the software signal processing steps of both the transmitter and receiver are realized with the assistance of a portable personal computer equipped with the MS Windows operating system. The projector – hydrophone pair of underwater transducers, required for an actual pipeline implementation, is replaced in the laboratory experiment by a speaker – microphone set. The remaining hardware components are the data acquisition board that serves as analog to digital converter and vice versa, as well as the necessary amplifiers that drive the transmitter and receiver.

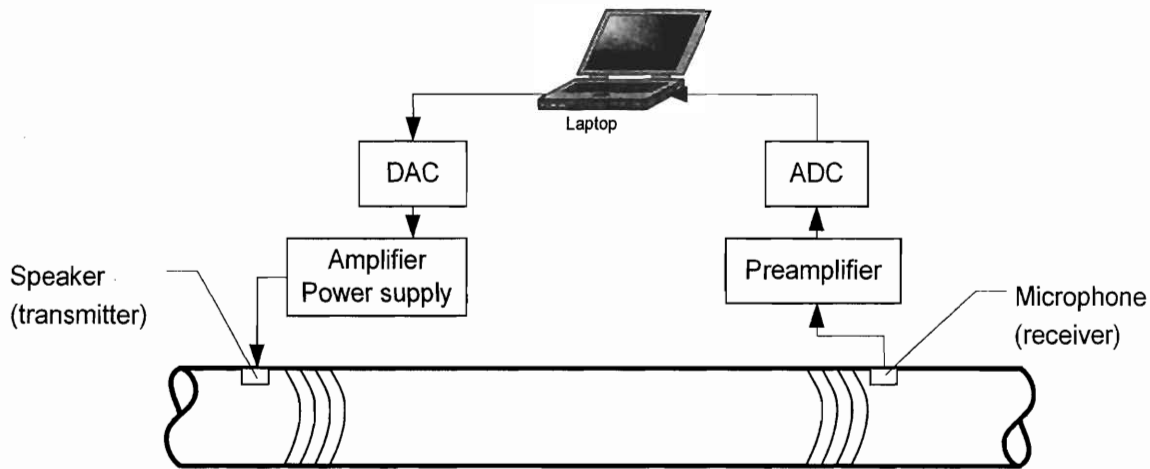


Figure 7.3: Schematic Diagram of Laboratory Experiment Hardware Configuration

More explicitly, the experiment progresses as follows. The portable computer is programmed to implement all the signal processing blocks of the transmitter and receiver, from the textual message formatting of the transmitter, to the symbol detection and conversion back to text of the receiver. The transmitter code executes all the necessary calculations and generates a waveform as described in Chapter 5. This waveform is converted into a continuous voltage varying signal with the assistance of the digital to analog converter. This signal is in turn amplified appropriately and fed, with the assistance of a power supply, to the speaker, which acts as an acoustic source. The

speaker under the electrical excitation generates pressure pulses that propagate along the pipeline waveguide. These pulses are recorded at the receiver with the assistance of a microphone, and converted into an electric signal. This signal following a pre-amplification stage, which adjusts its amplitude into an appropriate range, is converted into a discrete time waveform with the assistance of the analog to digital converter. This discrete time signal is presented to the portable computer, which recovers the transmitted message by executing software implementing the signal processing steps of the receiver.

The immediate availability of speakers and microphones lead to their selection as transmitter and receiver units. However, this selection limits the usable transmitted signal bandwidth in the audible frequency range. Unfortunately, there is a shortage of commercially available microphones capable of receiving ultrasonic range acoustic signals in the air. The speaker used is the “WM-R30B Panasonic Card Type Speaker”, with transmitting frequency range from 400Hz to 100kHz and sound pressure level 70dB referenced at 0.3m distance with 3V RMS input. The microphone used is the “WM-61A Panasonic Omnidirectional Back Electret Condenser Microphone Cartridge”, with receiving frequency range 20Hz to 20kHz and sensitivity -35 ± 4 dB at 1kHz. The speaker and microphone along with their transmitting and receiving frequency responses respectively are illustrated in Figure 7.4.

The digital to analog and analog to digital conversion of the signal at the transmitter and receiver respectively is achieved with the assistance of a “6062E National Instruments Data Acquisition Card”. This data acquisition card (DAC) is capable of receiving 16 analog inputs and transmitting 2 digital outputs at a combined sampling rate of 500 thousand samples per second with 12-bit resolution. The high sampling rate of the DAC is important in order to maintain accurate representation of the signal with high frequency content and avoid effects such as aliasing. The resolution of the selected card is considered adequate due to the high levels of ambient noise present during the experiments, while higher resolution would just represent accurately the noise part of the signal. Finally, this DAC uses the PCMCIA interface, making it ideal for use with portable computers, especially during field experiments, since it requires no external power supply.

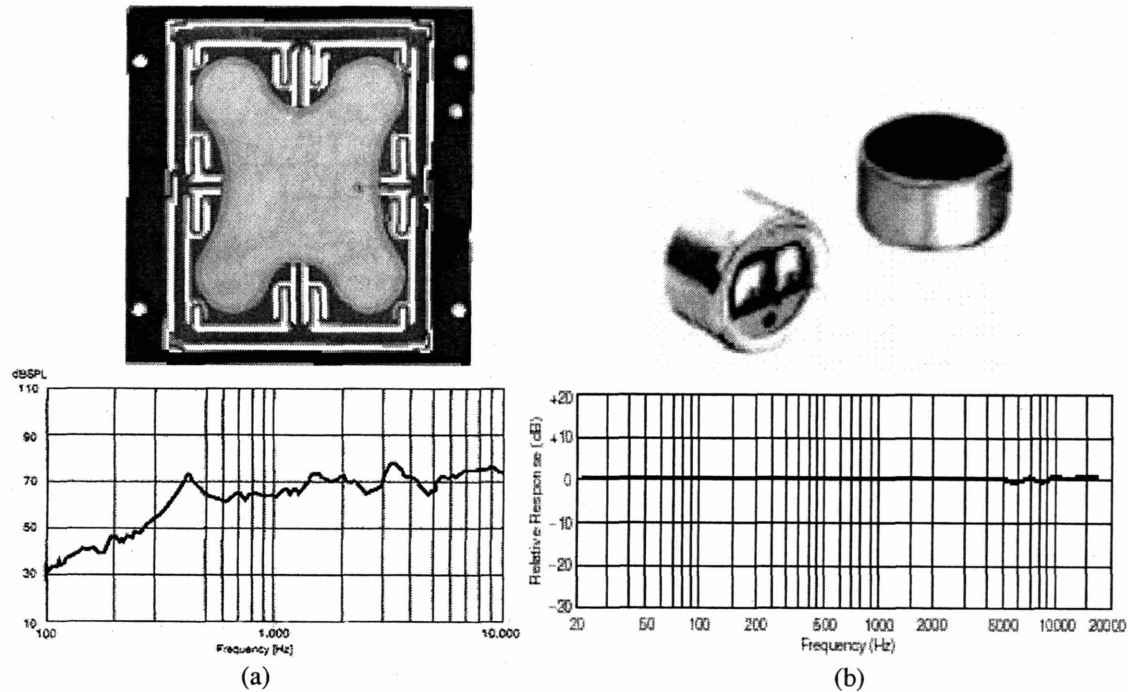


Figure 7.4: (a) Speaker and (b) Microphone used as transmitter and receiver and corresponding frequency response, [1]

According to the aforementioned experimental procedure, the signal prepared by the transmitter is converted into a continuous form with the assistance of a digital to analog converter (D/A) and presented to the speaker through an amplifier. The electronic circuit driving the speaker is presented in Figure 7.5, and consists essentially in the D/A converter, an operational amplifier, and several resistors and capacitors. The design of the driving amplifier is selected to be as simple as possible so as to reduce sources of potential failures and easily control the amplification parameters. The selected operational amplifier is the “OPA2350PA Burr-Brown Texas Instruments High Speed Low noise Operational Amplifier”, which is optimized for low voltage, single-supply operation, with wide range of input and output voltages, low noise ($5\text{nV}/\sqrt{\text{Hz}}$), and high speed operation (38MHz, $22\text{V}/\mu\text{s}$). The input voltage of the amplifier is biased at +2.5V, while the gain is controlled by the ratio of the negative feedback resistances, and currently set at 10. Capacitive coupling is used at both the amplifier input and output to block the low frequencies and mainly the dc level. The reference voltage V_+ from the external power supply is set at 5Volts.

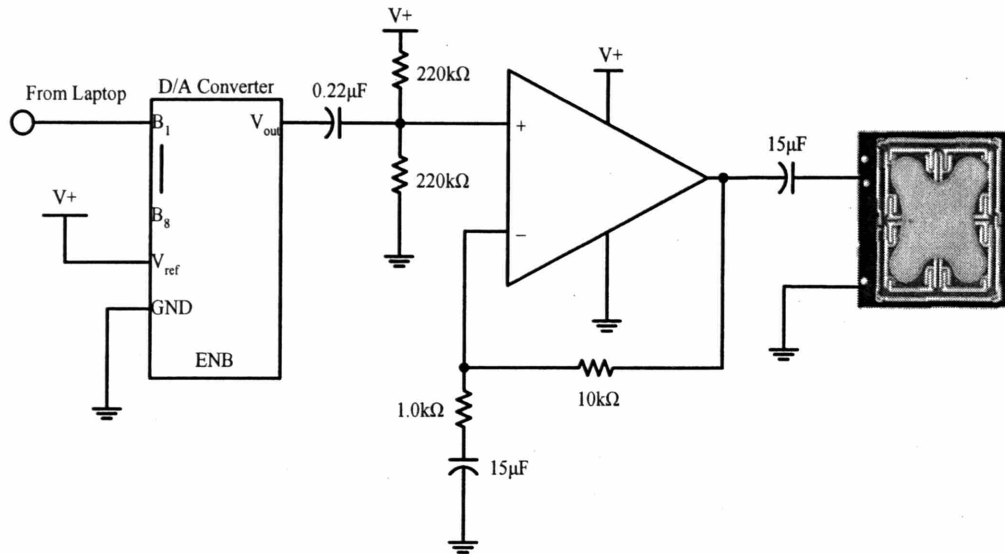


Figure 7.5: Speaker Amplifier

A similar amplification structure is also implemented at the receiver side to pre-amplify appropriately the recorded signal for use in the analog to digital (A/D) converter. The microphone used is essentially a variable capacitor which adjusts its value according to the input pressure level. Changes at the input pressure level correspond to variations of the capacitance and consequently its effective resistance. The capacitive nature of the microphone requires a resistance and capacitor bridge, which allows acquiring its pressure recording as variations of the voltage drop across its electrodes due to the varying electric charge. The circuit diagram of the receiver hardware configuration is presented in Figure 7.6. The operational amplifier used is identical to the one employed at the transmitter, with a gain of 4.5 at this time. The estimated microphone output voltage level is in the range $\pm 200\text{mV}$, corresponding to the expected input pressure level. The selected gain scales the maximum expected value to the unit range, in order to utilize the complete resolution of the A/D converter. Once again, a simple circuit structure is implemented in order to easily identify potential sources of problems. Future implementations will incorporate multistage amplification for precision and stability, along with analog filters, in the form of resistance and capacitor combinations around the operational amplifiers, for noise elimination outside the bandwidth of the transmitted signal.

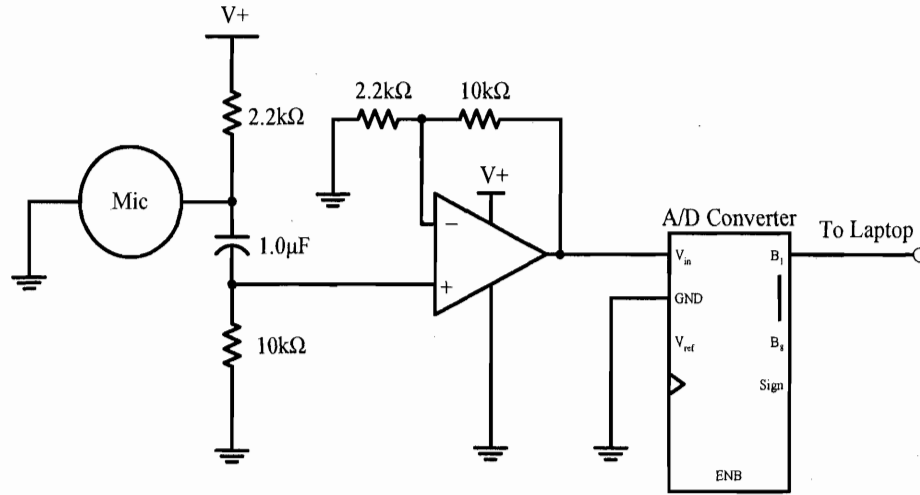


Figure 7.6: Microphone supporting circuit and preamplifier

A piece of acoustic Styrofoam is used at both free endpoints of the pipeline serving as a cushion for the speaker and microphone, as a damper for the reflected waves, and as an absorber of ambient noise. The speaker and microphone are both installed at opposite ends of the pipeline embedded in the cushioning sponge, which isolates potential vibrations from the laboratory environment. The cell structure of the Styrofoam covering the complete cross section of the pipeline endpoints acts as a damper, eliminating the corresponding reflections, and therefore transforming the finite length pipe into an infinite length pipeline. This model is closer theoretically to the actual pipeline network configuration, where no reflections from the pipe endpoints are expected, due to their substantial distance from the communication system. Finally, the foam acts as a filter of the environmental noise that inserts the pipe from the free endpoints. Ambient noise enters the in-pipe waveguide penetrating the pipe wall, similarly to the expected behavior encountered in actual water pipelines in the field.

However, ambient noise is not only existent in the form of acoustic waves, but also in the form of electromagnetic interference. When electric current is passing through any piece of equipment, an electromagnetic field is formulated around it, radiating energy to the environment. Therefore live wires, monitors, motors, power supplies, and so forth, present in any laboratory environment, act as sources of electromagnetic noise. This kind of noise is present but less apparent in the open field. It is very important to protect the communication system components from such noise sources, since they account for a

significant part of the total signal noise as it will be shown in what follows. In order to limit the electromagnetic noise pickup from the electrical components of the system coaxial connection cables and grounded shield cages, enclosing all the circuits, are used. The shield of the cage and coaxial cable captures the electromagnetic noise and drives it directly to the ground, i.e. to the point with zero voltage potential, protecting the circuits and the live wires used. It is interesting to observe that some of this noise is systematic, i.e. corresponds to sources with specific frequency spectrum such as the 60Hz of the AC domestic electrical circuit, and therefore can be easily filtered out.

Noise measurements are conducted by recording for some period of time without any signal transmission. The magnitude of the received signal without any electromagnetic shield protection was in the order of 20mV, while it dropped to 3mV following the grounded shield activation. This drop corresponds to elimination of electromagnetic noise, while the remaining noise is attributed to acoustic noise as well as electrical noise from the components used. It becomes apparent that 85% of the initially received noise corresponds to electromagnetic interference. The electrical noise from the components used is also known as *Johnson* or *Thermal noise* and can be calculated on the resistors by the following equation:

$$V_{noise} = \sqrt{4 \cdot K \cdot T \cdot R \cdot \Delta f} \quad (0.4)$$

where K is the Boltzman constant equal to $1.38 \cdot 10^{-23}$ Joules/K, T is the temperature in Kelvin considered equal to 300K (26°C) for the laboratory environment, R is the resistance of the component, and Δf is the frequency of the electrical signal passing through the resistor. The maximum resistor used in the implemented circuits is 220kΩ and the maximum frequency is in the order of 21kHz, leading to Johnson noise level of 8.54μV. The noise corresponding to the operational amplifier is 5nV/√Hz leading to 0.7μV for the aforementioned frequency. It becomes obvious that the electrical noise of the components is on the order of μV, orders of magnitude less than the recorded 3mV, which consequently can be safely assumed that corresponds to the ambient acoustic noise.

The complete pipe configuration is supported on top of several sawhorses with the assistance of Styrofoam padded restraints, in order to avoid propagation of vibrations on the pipe wall from the laboratory floor. Vibrations existent in any building, caused from

off balanced machines and people walking to nearby passing cars and trucks, can excite the pipe wall and add a constant ringing to the in-pipe acoustic waveguide. The results presented in the subsequent paragraphs correspond to the system utilizing all the noise protection components described.

7.4 Results

The effect of the pipeline waveguide on the transmitted signal for three pipe configurations is presented in this section. The subsequent paragraphs provide results from the straight, bent, and branched pipe configurations, respectively, identifying the effect of different geometries. The transmitted signals are the FSK, ASK and QAM modulated signals, identical to the signals presented in Chapter 6.

7.4.1 Straight Pipe

The straight pipeline configuration is first examined in the laboratory environment, with lengths varying from 10 to 30 feet. This corresponds to the simplest and most common waveguide geometry, with no special features such as bends or branches which generate strong localized signal distortion areas.

Considering the 30 feet pipeline a collection of FSK modulated signals at 1kbps, 4kbps and 7kbps data rates are initially transmitted. The original waveforms are identical with the signals used in the computerized simulations and are presented in Figure 6.9. The pressure time histories and the corresponding frequency spectrum of the recorded signals at the receiver side of the pipeline are presented in Figure 7.7. It is important to realize that these plots represent the pre-amplified electrical response of the microphone to the pressure wave that arrives at the receiver location, which consequently explains the amplitude discrepancy between the current and the Chapter 6 corresponding plots. Due to the pre-amplification stage the maximum pressure representing voltage level is on the order of 1.

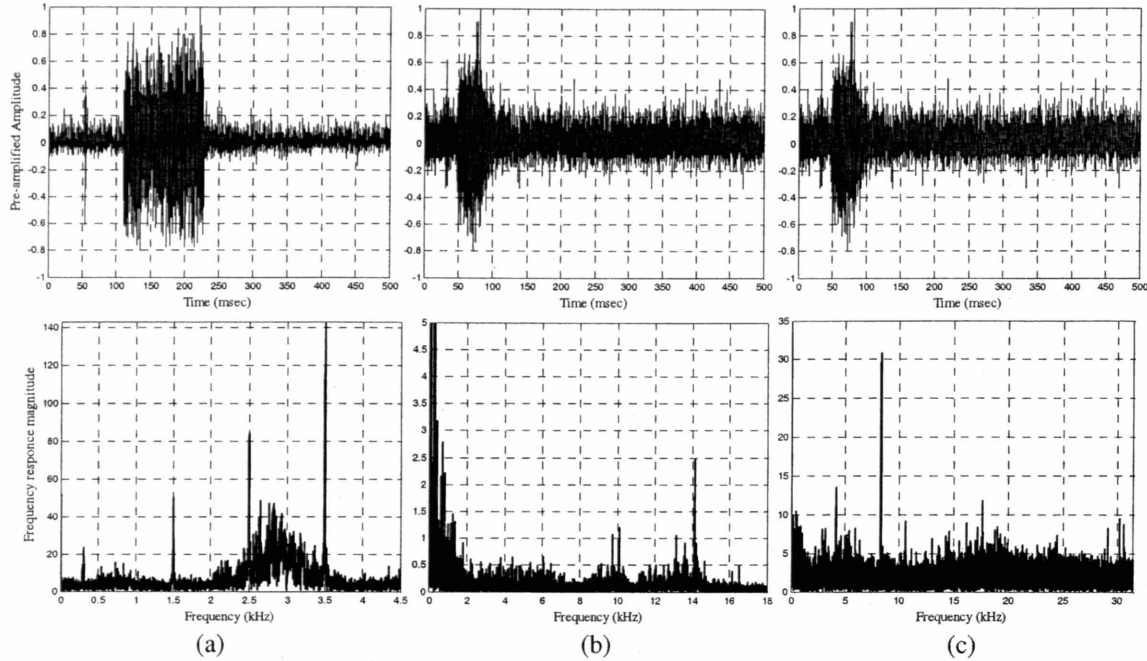


Figure 7.7: Pressure Time History and Frequency Response of Laboratory Experiment for 30 ft propagation distance in straight pipe of FSK modulated signals at data rates (a) 1kbps, (b) 4kbps, and (c) 7kbps

The signal distortion presented in the above plots is the result of the simultaneous effect of channel imposed dispersion and ambient noise. Considering the level of signal dispersion it can be observed that it is significantly lower than the dispersion of same data rate signals obtained from the computerized simulations, as shown in Figure 6.10. In order to preserve the consistency of the simulated and experimental results, it is important to realize the effect of the aforementioned frequency scaling factor imposed on this experiment. The frequencies of the signals presented in this Chapter correspond to signals with frequency contents 2.3 lower in reality. For example the 7kbps signal presented above has 21kHz carrier frequency which corresponds to 9.1kHz frequency in the actual water pipe. The significantly reduced signal dispersion of the above signals is, therefore, an indication that fewer modes are excited, as it is expected for smaller pipes, see Chapter 3. Figure 7.8 illustrates the transfer functions estimated for the first 9 orders of modes of the air filled PVC pipeline configuration for 30 feet length and 0.05m radius. The transfer function plots can provide very useful insight on the behavior of the pipeline waveguide. Considering the 1kbps data rate signal, which its bandwidth extends from 2.5 to 3.5kHz, it can be found that only the first 3 orders of modes are getting excited. More importantly the frequency content of the 1kbps signal is below the cut-off frequencies of the highly

dispersive modes, thus presenting minor reverberation mainly due to the slightly delayed arrivals of the first three orders of modes excited and their variation in magnitude. This analysis approach can be extended to the remaining signals, while comparison with the transfer function of the actual pipeline would indicate the required frequency shift by 2.3 to correspond to similar regions of excited modes and dispersion levels.

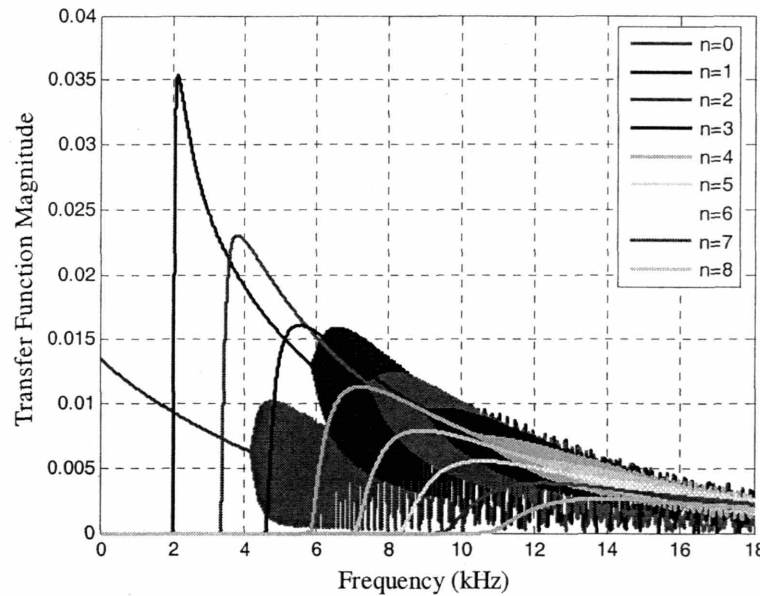


Figure 7.8: Transfer Functions of the 30 feet straight pipe laboratory experiment for the first 9 orders of modes

The above time histories reveal the effect of ambient noise level on the integrity of the received signal. Signal attenuation, which is not important for the dispersion analysis presented in the preceding chapters, becomes here imperative, since it becomes the controlling factor of the signal to noise ratio for severely attenuated signals. Factors that affect the level of signal attenuation such as the frequency content and the propagation distance may impose restrictions on the capabilities of the communication system. It becomes apparent that the 7kbps signal is severely attenuated, due to its high frequency content, resulting in very low signal to noise ratio levels. Aside from the frequency related attenuation, the 7kbps signal has a carrier frequency of 21kHz, which is at the limit of the receiving frequency spectrum of the microphone resulting in lower sensitivities and therefore lower amplitudes of the recorded signal. However, the remedy for the ambient noise effect can be found in very simple techniques such as bandpass

filtering and increase of the transmitted signal's power. Aside from the signal to noise ratio, the effect of ambient noise becomes apparent from the frequency response plots, where the noise level affects the frequency distribution, since it generates a level of response at all frequencies. Therefore, similarly to the amplitude, low levels of signal frequency response may become indistinguishable from the noise, since it dominates over the complete frequency spectrum.

The resulting bit error levels for the 1kbps, 4kbps and 7kbps signals before any distortion compensation or error correction are 10%, 21%, and 32%, respectively, which are significantly lower than the corresponding data rate signals of Chapter 6, but comparable considering the frequency scaling of the experiment. Due to the increased error levels of the 7kbps signal, stacking is applied as a preliminary measure of distortion compensation. Figure 7.9 presents the pressure time history and frequency response of the stacked signal generated by subtraction of the recordings at the crown and bottom of the pipe. Recall that subtraction of opposite received signals eliminates the even numbered orders of modes, while it enhances the effect of odd orders of modes.

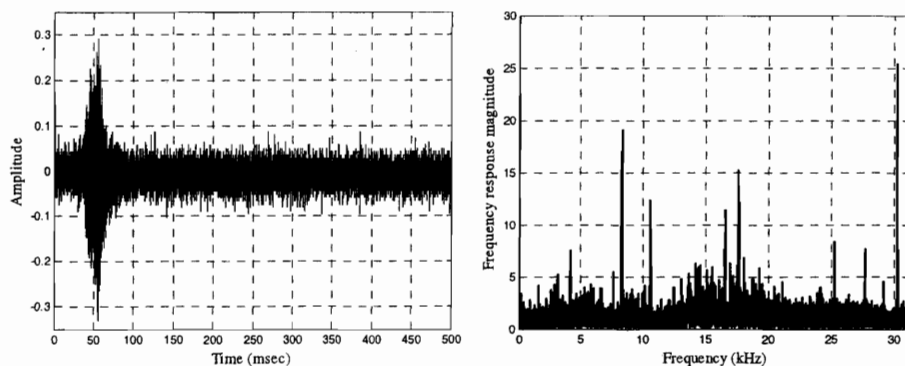


Figure 7.9: Pressure Time History and Frequency Response of Stacked signal generated by subtraction of the crown and bottom recordings for the 7kbps FSK modulated signal in a 30ft straight pipe

The resulting stacked signal presents significantly reduced dispersion and noise levels, while the frequencies of interest are emerging in the frequency response plot. The dispersion level is reduced, due to the fewer number of modes contributing to the received signal, while the noise level drops due to the addition, or subtraction in this case, of two zero mean random processes, which cancels out some part of the received noise. However, in this case these noise random processes are correlated, since they correspond

to noise recorded at two points simultaneously. The reduced dispersion and noise level is responsible for the appearance of various peaks in the frequency response plots; however the presence of several peaks within the region of interest indicates the ambiguity in the signal detection. The bit error rate following the stacking process dropped to 24%.

Figure 7.10 presents the data bearing part of the signal following the bandpass filtering and adaptive equalization processes of the receiver. The bandpass filter is responsible for removing the noise outside the bandwidth of the transmitted signal in order to improve the signal to noise ratio, while the adaptive equalizer removes the channel imposed signal distortion. The decision feedback equalizer is used in these examples, employing 30 elements for the feedforward filter and 10 elements for the feedback filter, while utilizes the recursive least squares tap weight adaptation algorithm.

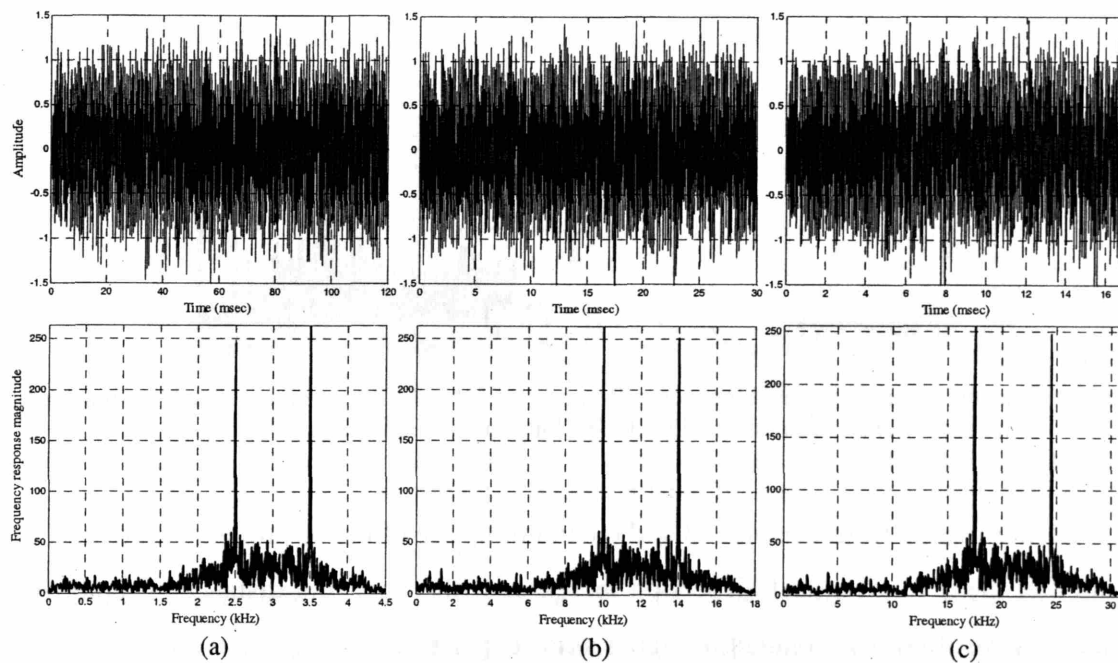


Figure 7.10: Pressure Time History and Frequency Response of equalized signal with a DFE utilizing the RLS adaptation algorithm for FSK modulated signals at data rates (a) 1kbps, (b) 4kbps, and (c) 7kbps

Following the DFE the detector achieves perfect reconstruction of the original signal, reducing the bit error level to zero. The similarity of the current frequency response of the equalized signal with the solution identified during the simulated results of Chapter 6 indicates that the RLS algorithm arrived at a comparable “optimal”

configuration, allowing frequencies present across the spectrum and representing accurately the transmitted waveform.

The consistency of the results obtained from the computerized simulations is validated by Figure 7.11, which presents the pressure time history and frequency response of a 7kbps FSK signal transmitted inside a simulated air filled PVC pipeline waveguide. The simulation code used in Chapter 6 is employed here to reproduce the behavior of the laboratory experiment pipeline for a propagation distance of 30 feet and a pipe radius of 0.05m. Close inspection reveals that the resulting waveform has similar dispersion characteristics in terms of amplitude and frequency distortion with the 7kbps signal presented in Figure 7.7. Of course in this case the ambient noise is not present in the received signal.

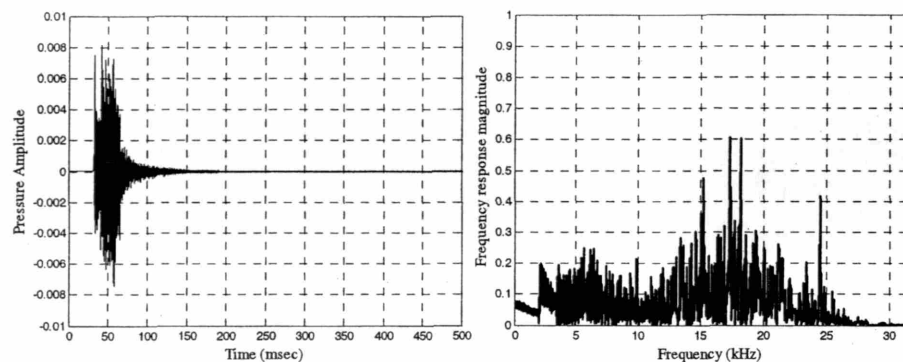


Figure 7.11: Pressure Time History and Frequency Response of 7kbps FSK transmitted signal for simulated laboratory experiment of air filled 30 feet long and 0.05m in radius PVC pipe

Earlier results from Chapters 3 and 6 examining the effect of propagation distance indicate that the level of signal dispersion increases with increasing distance. The above statement is verified by conducting laboratory experiments at 10 and 20 feet. For reference, Figure 7.12 presents the received signal from a laboratory experiment identical to the preceding, with the exception of the propagation distance that is now reduced to 10 feet. More explicitly, Figure 7.12 presents the received pressure time history and frequency response for the transmission of a 7kbps FSK modulated signal. The resulting signal following the equalization process with a DFE utilizing the RLS adaptation algorithm is also presented. The received pressure time history and the corresponding frequency response indicate the reduced dispersion levels with respect to the 30 feet

propagation distance case. Moreover, the signal to noise ratio is significantly improved due to the notably higher signal amplitude. As a consequence of the low reverberation and attenuation, the bit error level for the received signal is 17%, significantly improved with respect to the 30 feet case, while the application of the DFE results again in perfect reconstruction of the original signal.

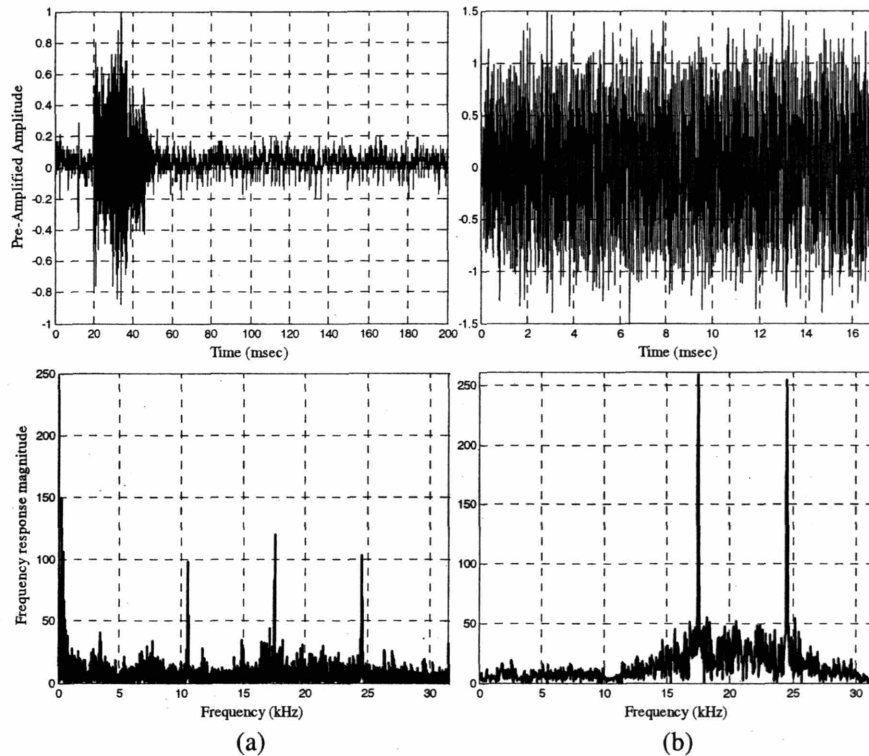


Figure 7.12: Pressure Time History and Frequency Response of received and DFE equalized FSK 7kbps signal for propagation distance 10 feet

For completeness Figure 7.13 and Figure 7.14 present the response of the laboratory experiment waveguide for a propagation distance of 30 feet and for the transmission of 7kbps ASK and QAM signals respectively. The included plots correspond to the pressure time history and frequency response or signal constellation of the received, stacked, and equalized signal for the ASK or QAM case, respectively. Once again the received signal is severely dispersed and attenuated, resulting in high initial bit error rates of 32% for the ASK and 76% for the QAM case. The stacked signal generated by the subtraction of the crown and bottom received signals presents lower noise and dispersion levels, as indicated by the emerging of the frequencies of interest or the even

distribution of detected symbols in the constellation space for the ASK and QAM signals, respectively. The achieved error rates following the stacking process dropped to 25% and 49%, while the application of the DFE resulted in elimination of all erroneously detected bits.

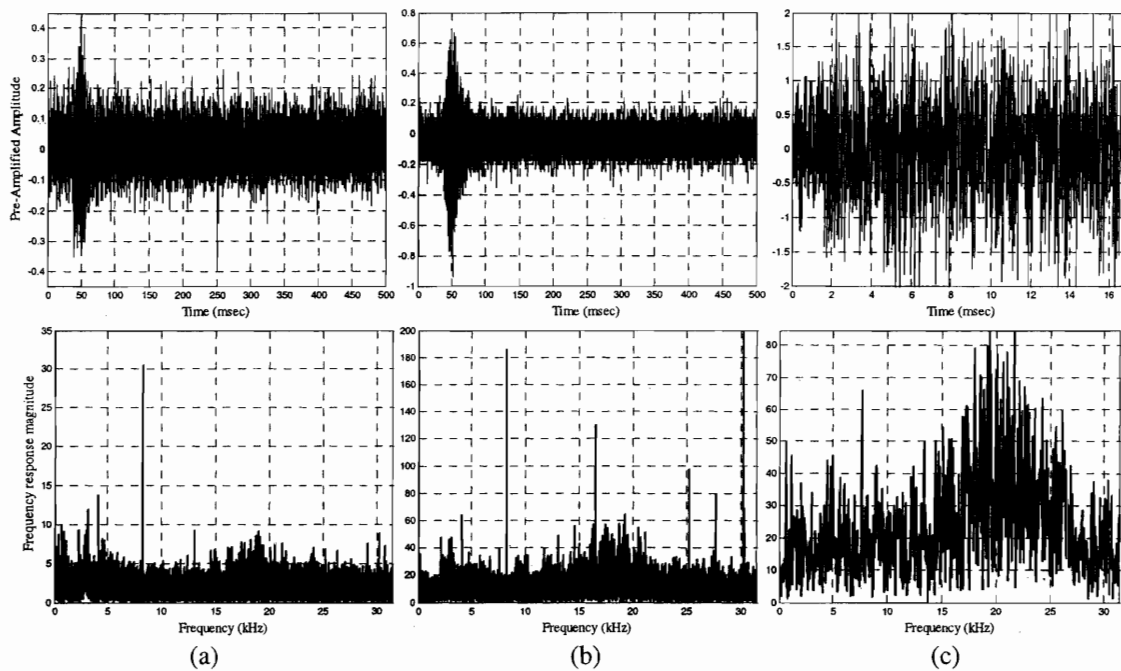


Figure 7.13: Pressure Time History and Frequency Response of (a) received, (b) stacked by subtraction, and (c) DFE equalized, 7kbps ASK modulated signal for 30 ft propagation distance in straight pipe

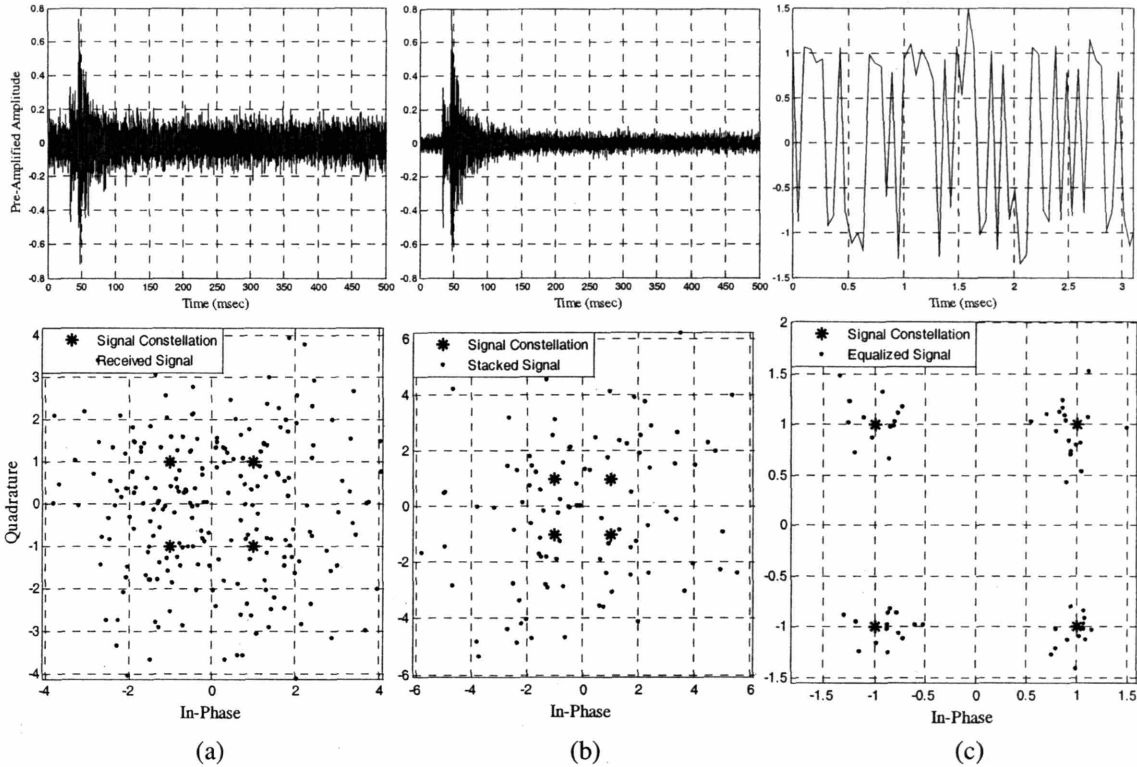


Figure 7.14: Pressure Time History and Signal Constellation of (a) received, (b) stacked by subtraction, and (c) DFE equalized, 7kbps QAM modulated signal for 30 ft propagation distance in straight pipe

7.4.2 Bent Pipe

The effect of pipe bends on the propagating wave is the main focus of this paragraph. Landscape restrictions constitute inevitable the presence of bends at the pipeline network. The bend location flexures the trajectory of the transmitted wave's propagation path, resulting in generation of multiple reflections and distortion of the signal characteristics. It is intuitively understandable that the sharper the change of direction, the more the generated reflections. In order to study the effect of pipe bends on the reverberation level of the signal and consequently on the integrity of the transmission, a 90 degree turn is introduced to the pipe in the laboratory experiments. Transmitting signals of various carrier frequencies allows identifying how the signal distortion is affected with respect to its frequency content. Figure 7.15 demonstrates the received signals from a 30 feet air filled PVC pipe with a 90 degree turn at one third of the total distance from the receiver, for the transmission of the 1kbps, 4kbps, and 7kbps data rate FSK modulated messages presented in Figure 6.9.

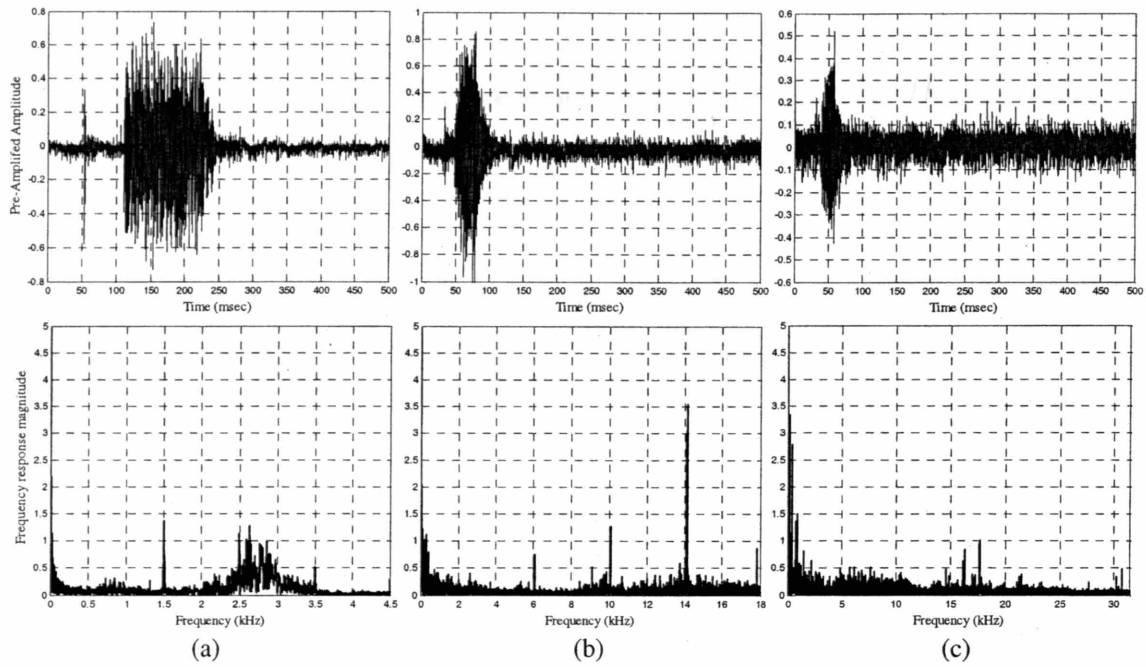


Figure 7.15: Pressure Time History and Frequency Response of a 30ft bent pipe Laboratory Experiment for FSK modulated signals at data rates (a) 1kbps, (b) 4kbps, and (c) 7kbps

Due to the reciprocity theorem experiments with the same feature, such as a bend, a scatterer or a branch, located at equal distances from the transmitter or the receiver produce identical results, constituting the above experiment equivalent to having the location of the bend at distance 10 feet from the transmitter.

The pressure time histories presented above illustrate the increased level of reverberation with respect to the straight pipe case. The received waveform not only is more distorted, but also is significantly attenuated, revealing that the presence of the pipe bend redistributes, or in other words reflects, the signal energy in trajectories away from the receiver. It is very interesting to notice that the 1kbps signal, which for the straight pipeline case presented almost no dispersion, is severely distorted, while the frequency peaks representing the zero and one bits are absent from the frequency response of the received signal. The radical change of behavior can be explained by the spatial phase change of the wave before and after the bend location. A qualitative explanation can be provided with the assistance of Figure 7.16. Consider the reflection of a uniform phase incident wave approaching the bend location. It is important to notice that even though the phase is uniform along the cross section, the wave has varying phase along the axis of

propagation. The spatial phase gradient of the pressure field produced by interference between the incident wave and that reflected from the bend wall increases with frequency. The phase distribution of the wave downstream becomes increasingly mismatched with the corresponding incident wave with increasing frequency. The mismatch reaches a maximum when the pipeline diameter equals half the wavelength.

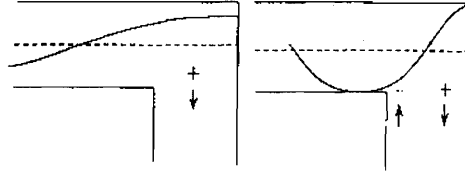


Figure 7.16: Qualitative explanation of transmission loss near to the frequency at which the wavelength equals twice the pipe diameter, [2]

For the case of the PVC pipe with 0.10m diameter, the frequency corresponding to the maximum loss of energy due to reflection and phase change is

$$f = \frac{c}{\lambda} = \frac{343 \text{ m/sec}}{0.20 \text{ m}} = 1715 \text{ Hz}, \text{ very close to the bandwidth of the 1kbps signal. The}$$

resulting bit error rates at this stage, with no distortion compensation or error correction, are 40%, 32%, and 38% for the 1, 4, and 7kbps data rates, respectively, significantly increased, as expected, from the straight pipeline. It is interesting to notice that the ambient noise level presented in the above pressure time histories is significantly lower in comparison with the straight pipeline case. A possible explanation can be that the bend pipe experiment was conducted at a time with lower environmental noise levels, such as late evening or night, while the straight was conducted during daytime.

The stacking process, successfully applied at the 7kbps case at the straight pipe case, provides no particular benefit in any of the received signals during the bend pipe experiment. For reference the stacked pressure time history and frequency response of the 7kbps signal is presented in Figure 7.17, which is generated by the subtraction of the crown and bottom received signals. The resulting bit error rate of the stacked signal is 39%, which is considered randomly varying around the error rate of directly received signal, indicating the inability of stacking to separate the orders of modes. The stacking process is not necessarily inappropriate for bend pipelines, and the results may be

representative only for the audible frequency spectrum. However, there is a strong indication that the modes of propagation are severely differentiated from the straight pipeline, with the aforementioned phase change downstream of the bend, incapacitating the stacked signal's advantage.

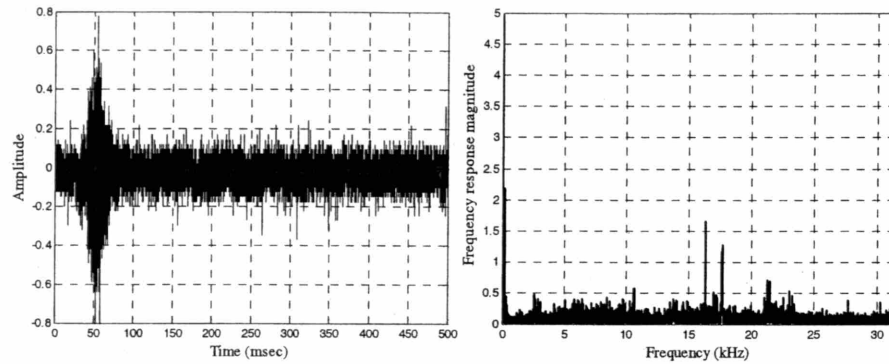


Figure 7.17: Pressure Time History and Frequency Response of Stacked signal generated by subtraction of the crown and bottom recordings for the 7kbps FSK modulated signal propagating inside a 30ft bend pipe

It becomes clear that the whole burden of dispersion compensation is carried out by the adaptive equalizer. Figure 7.18 presents the amplitude and frequency response of the data bearing signal following the bandpass filtering and adaptive equalization processes. The DFE adaptive equalizer is used with 40 elements at the feedforward and 20 elements at the feedback filter. The RLS filter tap weight adaptation algorithm is used, providing fast convergence to a robust solution, or in other words the optimal set of filter coefficients. The produced waveforms allow the detector to perfectly reconstruct the transmitted signal, providing once more error free reliable communication.

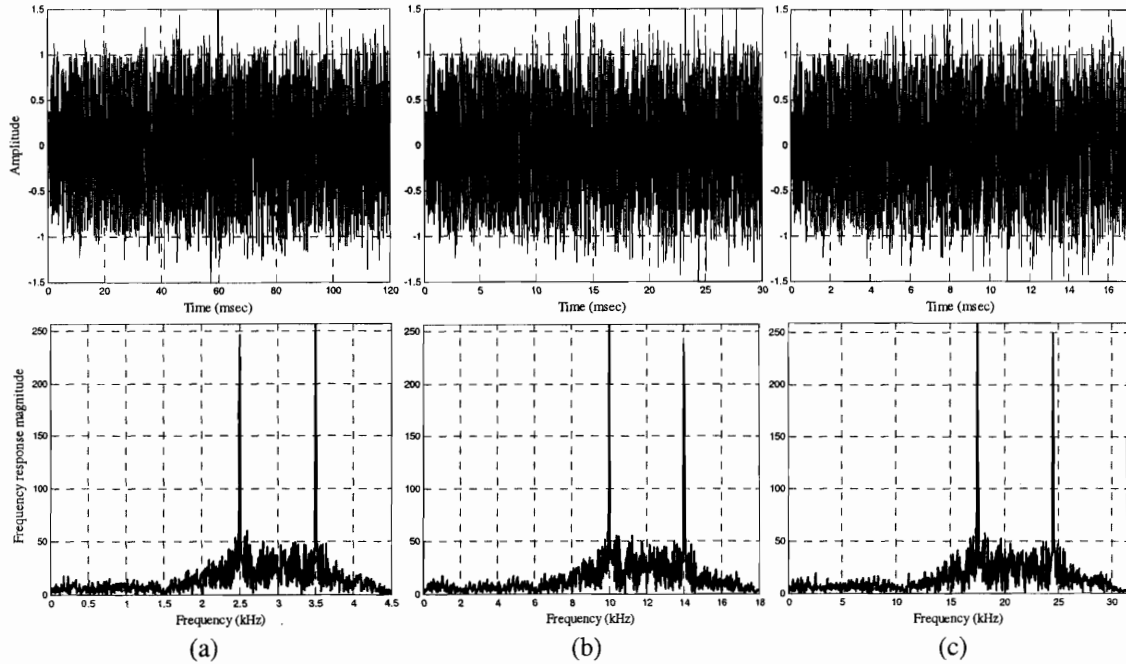


Figure 7.18: Pressure Time History and Frequency Response of equalized signal with a DFE utilizing the RLS adaptation algorithm for FSK modulated signals at data rates (a) 1kbps, (b) 4kbps, and (c) 7kbps

Figure 7.19 and Figure 7.20 present the received and equalized pressure time history and frequency response or signal constellation of 7kbps ASK and QAM transmitted signals, respectively. The received signals present significantly increased dispersion with respect to results corresponding to the straight pipe. However, reliable error free transmission is achieved with the application of bandpass filtering, decision feedback equalizer and Reed-Solomon error control, as illustrated by the plots of the equalized data bearing waveforms indicating perfect amplitude and frequency response for the ASK signal and close to the original solution signal constellation for the QAM signal, eliminating essentially the detection ambiguity.

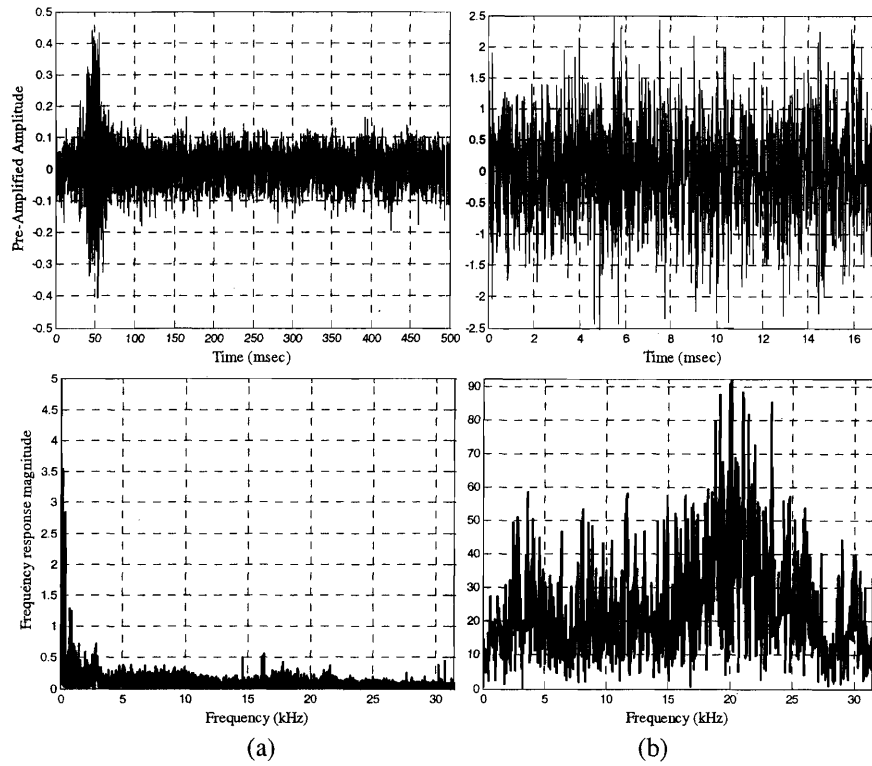


Figure 7.19: Pressure Time History and Frequency Response of (a) received, and (b) DFE equalized, 7kbps ASK modulated signal for 30 ft propagation distance in a bent pipe

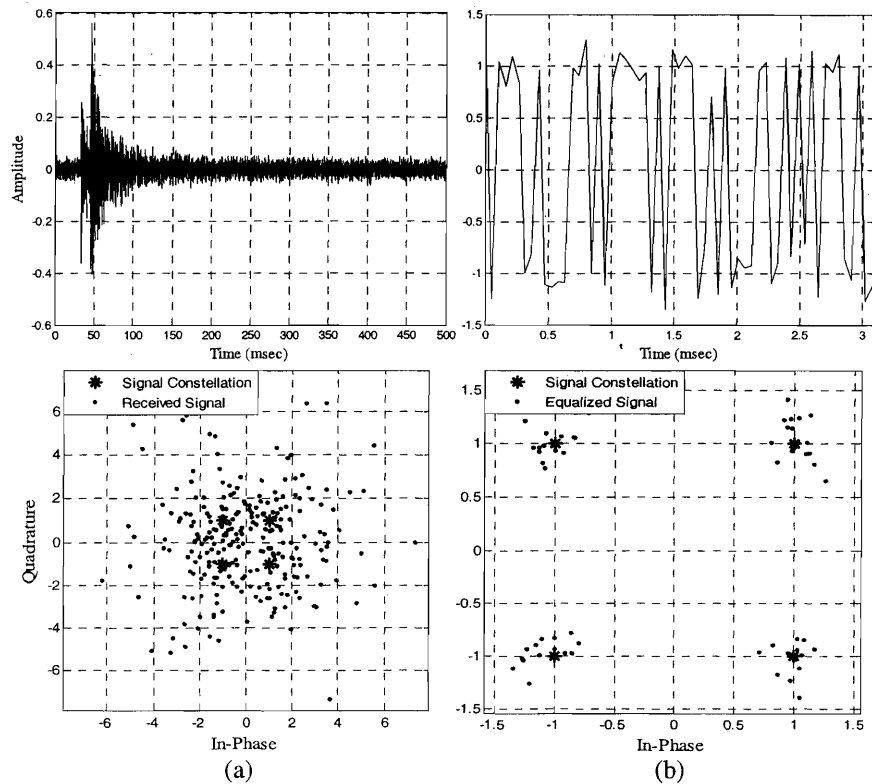


Figure 7.20: Pressure Time History and Signal Constellation of (a) received, and (b) DFE equalized, 7kbps QAM modulated signal for 30 ft propagation distance in a bent pipe

7.4.3 Branch Pipe

In an attempt to simulate the effect of network layout of the water transmission system the final configuration examined in the laboratory environment employs a pipeline system formed into a “T” shaped arrangement. The straight pipe section examined initially is modified including at this stage a transversely connected pipe of smaller diameter. The original straight pipe segment is 4” in diameter and 30ft long, while the branch is 1.5” in diameter and 10ft long, both made from PVC. The modulated signal is transmitted at the one end of the main pipe and received at the far end of both the main and branched pipelines. The connection location generates a local zone of reduced stiffness, where the propagating wave is not sufficiently supported by the pipe wall. As a consequence, there is leakage of signal energy from the main to the branching pipe. The connection area also resembles the interface of two different acoustic media, where portion of the propagating wave gets transmitted through the second medium, while the remaining wave gets reflected back into the original medium. As a result of the aforementioned mechanisms, a pictorial representation of which is provided in Figure 7.21, the recorded signal at the receiver is severely attenuated with respect to the simple straight pipe case.

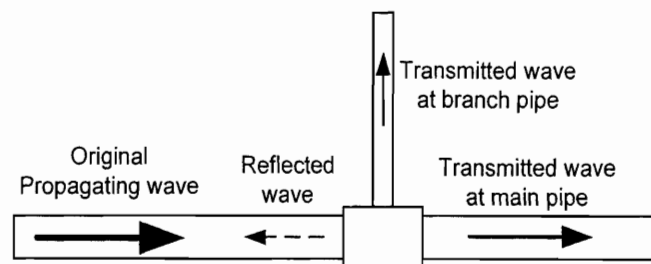


Figure 7.21: Signal energy distribution at branch location

The existence of the above mechanisms can be identified and verified from the signal recordings at the far end of the main pipe. Figure 7.22 presents the pressure time histories and the corresponding frequency response plots for the FSK modulated at 1kbps, 4kbps, and 7kbps signals, presented in Figure 6.9, transmitted across the 30ft main pipeline. A direct comparison of the provided pressure time history plots with the corresponding results presented in Figure 7.7, which includes the pressure time history

plots for the 30ft long simple straight pipeline, illustrates the significant signal decay of the received signal. Despite the significantly reduced amplitude, it is important to notice that the dispersion level in both cases remains the same, since both signals present similar time spreading and frequency shift characteristics. The attenuation level presents a strong positive correlation with the frequency content, disproportional to what is predicted by the lowpass behavior of the transmission channel, indicating that either the reflection or the energy redistribution increases with frequency. The relative effect of these two attenuation parameters with respect to frequency is examined with the assistance of the signal received at the end of the branched pipe, presented in Figure 7.23.

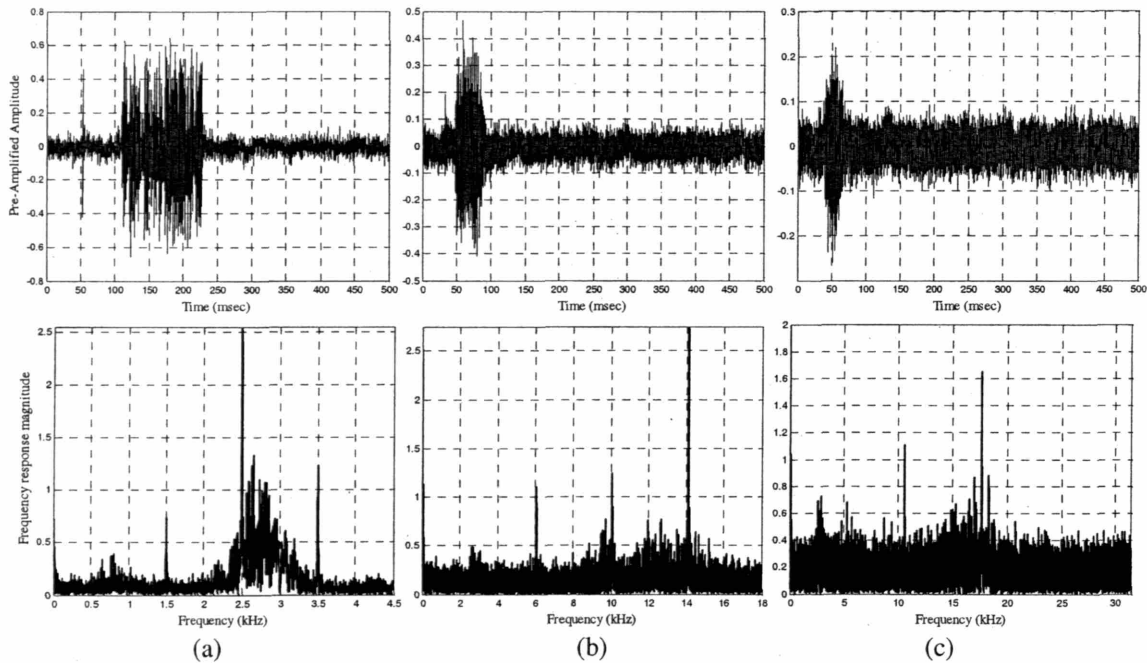


Figure 7.22: Pressure Time History and Frequency Response of Laboratory Experiment for 30 ft propagation distance in branched pipe of FSK modulated signals at data rates (a) 1kbps, (b) 4kbps, and (c) 7kbps

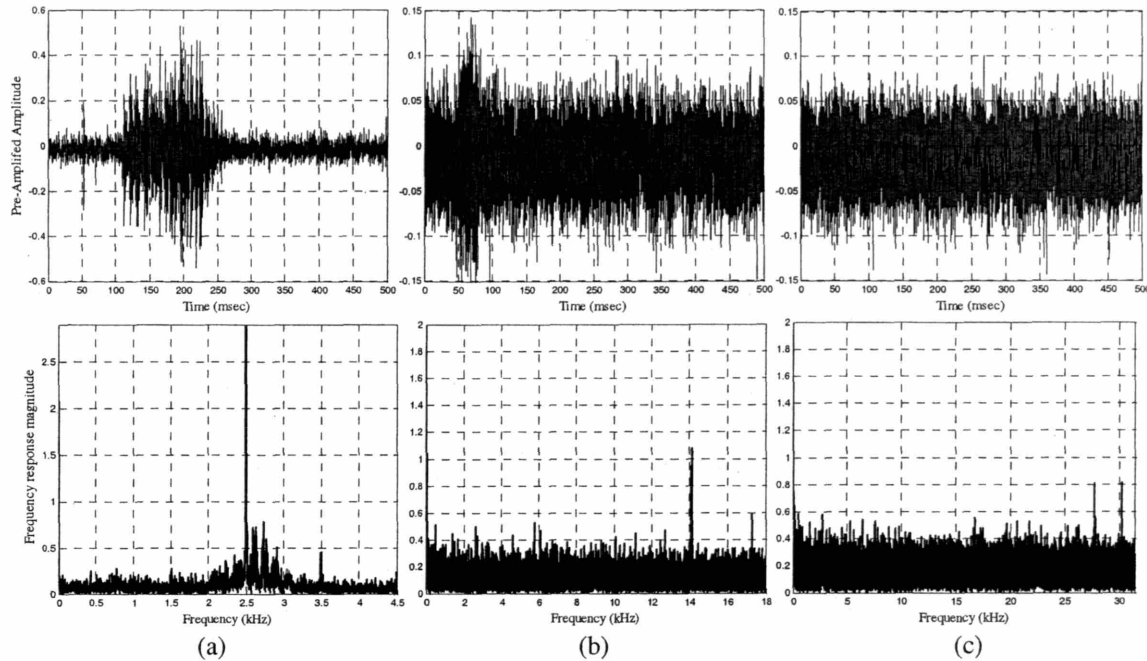


Figure 7.23: Pressure Time History and Frequency Response of branch pipe received signal from 30ft branched pipe Laboratory Experiment for FSK modulated signals at data rates (a) 1kbps, (b) 4kbps, and (c) 7kbps

The above pressure time histories indicate a decreasing level of signal amplitude diverted into the branched pipeline with increasing frequency. The received signal corresponding to the 1kbps data rate presents a very strong energy signal within the same order of magnitude as the signal propagating inside the main pipeline. On the other hand, the higher data rate plots present minimal received signal, which for the 7kbps case is diffused within the ambient noise level. Consequently, it can be safely assumed that the observed signal attenuation in the main pipe is a result of energy redistribution between the main and the branched pipe for the low frequency signals, while it is a result of strong reflections at the connection interface for high frequency signals. Such behavior is consistent with the results obtained by the bent pipeline experiments. More explicitly the wavelength of the 1kbps signal, which corresponds to carrier frequency of 3kHz, is 11.4cm, much larger than the diameter of the branched pipe, which is 3.81cm, while the 4 and 7kbps signals correspond to wavelengths of 2.86cm and 1.63cm, respectively, smaller than the pipe diameter. The long wavelength of the 1kbps signal allows the propagating wave to maintain uniform phase across the branched pipe diameter, resulting in significant energy transfer inside it. On the other hand, the short wavelength of the

high data rate signal results in multiple simultaneous phase changes across the branched pipe cross section, which add destructively inside it explaining the absence of identifiable data bearing signal for the 7kbps case.

In contrast with the main pipeline, the signal received at the branched segment presents significant dispersion. The frequency characteristics of the recorded signal are severely distorted with respect to the original waveform, while the pressure time history presents significant time spreading. The 90 degree turn that the propagating signal has to take in order to propagate inside the branch pipe can account for these severe dispersion levels, which result in large bit error levels before any distortion compensation and error correction, i.e. 40%, 45%, and 49% for the 1kbps, 4kbps and 7kbps data rate FSK modulated signals, respectively. The corresponding bit error rates for the signals received in the main pipe, and for the same propagation distance, are 13%, 27%, and 34%, for the 1, 4 and 7kbps data rate signals, respectively. These bit error rates are slightly higher than the corresponding error rates obtained from the straight pipe laboratory experiment, but significantly lower than the bend pipe and the branched pipe results.

As expected from the straight pipe experiment, application of the stacking process improves the fidelity of the 7kbps signal received in the main pipe. Figure 7.24 presents the pressure time history and frequency response of the signal generated by the subtraction of the crown and bottom recordings in the main pipe. The stacked signal presents increased amplitude and slightly reduced noise levels with respect to the single point reception, while frequency peaks of interest, representing the binary bits, are emerging. The application of the stacking process drops the bit error rate to 27%, achieving similar rate of improvement with the straight pipeline case.

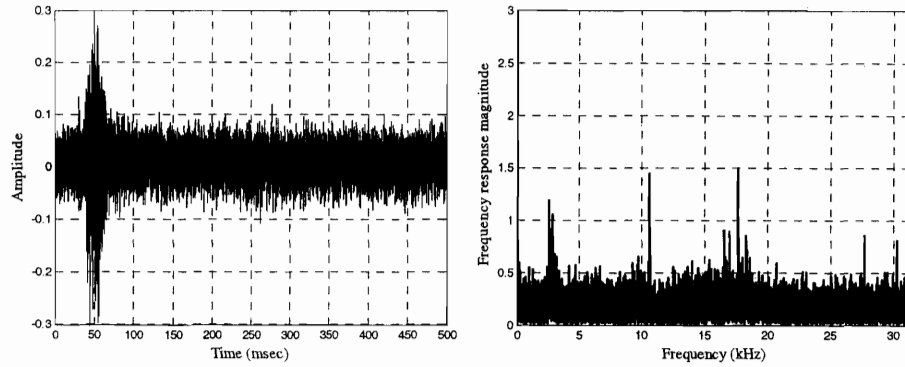


Figure 7.24: Pressure Time History and Frequency Response of Stacked signal generated by subtraction of the crown and bottom recordings for the 7kbps FSK modulated signal in a 30ft branched pipe

In order to achieve perfect reconstruction of the original transmitted signal the combination of the adaptive equalizer and Reed-Solomon error correction algorithm can be applied. A decision feedback equalizer with 40 feedforward and 20 feedback filter elements, using the recursive least squares adaptation algorithm, is employed for the equalization process. Figure 7.25 presents the pressure time histories and corresponding frequency responses of the data bearing part of the signal following the bandpass filtering and equalization processes for signals with 1kbps, 4kbps and 7kbps data rates respectively.

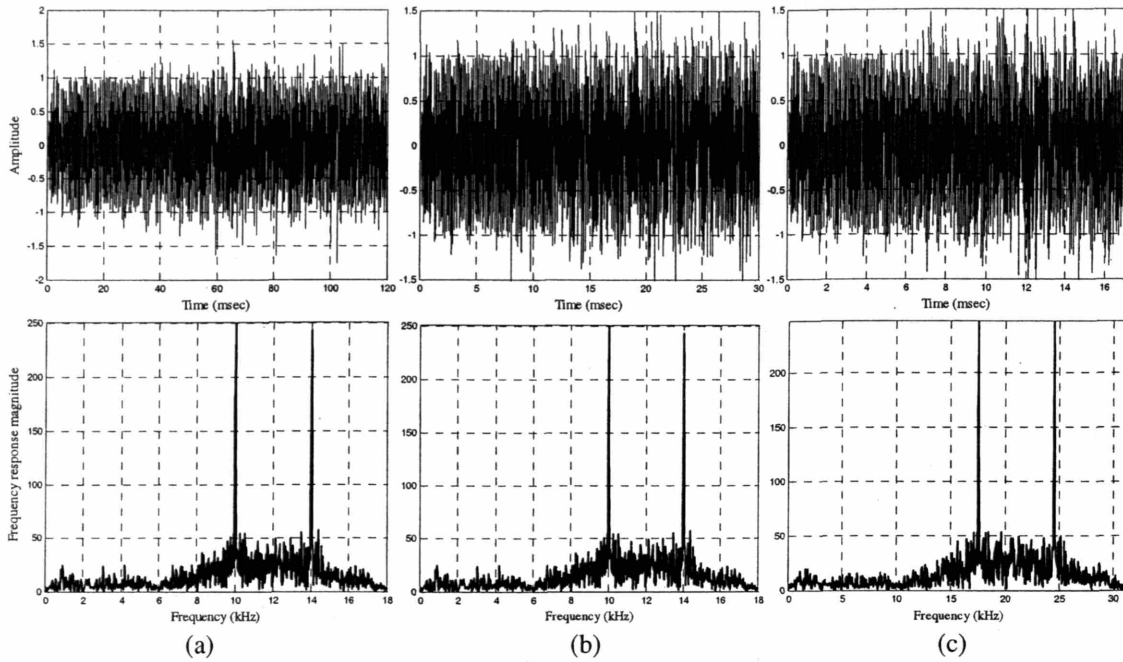


Figure 7.25: Pressure Time History and Frequency Response of equalized signal with a DFE utilizing the RLS adaptation algorithm for FSK modulated signals at data rates (a) 1kbps, (b) 4kbps, and (c) 7kbps

For reference, Figure 7.26 and Figure 7.27 present the results at various incremental signal processing stages at the receiver, for the transmission of a 7kbps signal modulated with ASK and QAM methods, respectively.

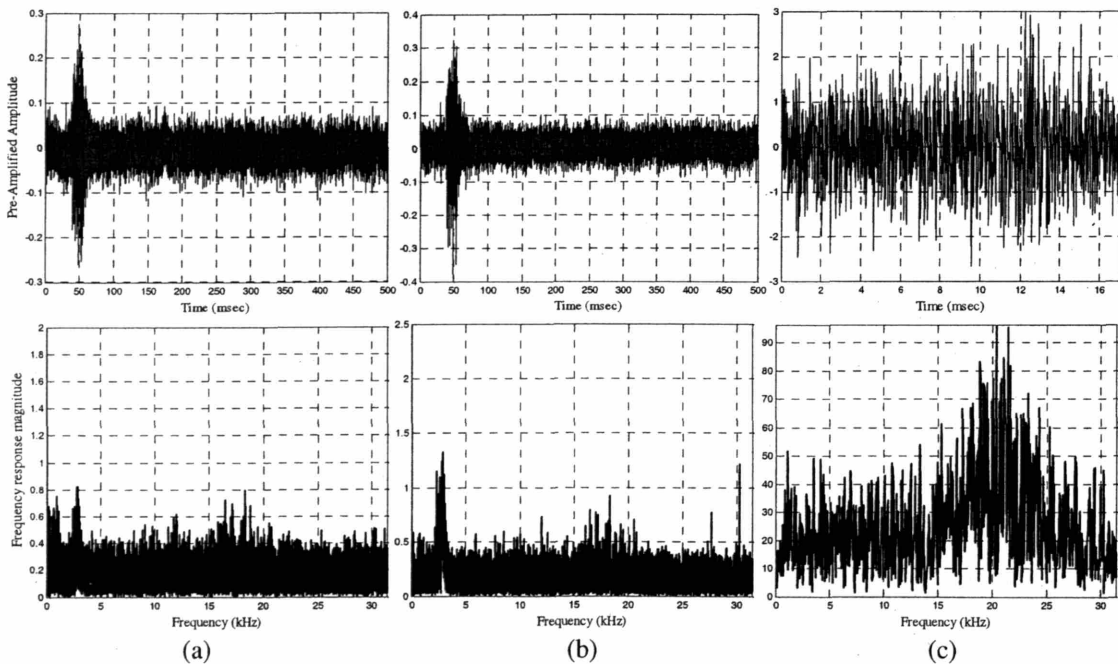


Figure 7.26: Pressure Time History and Frequency Response of (a) received, (b) stacked by subtraction, and (c) DFE equalized, 7kbps ASK modulated signal for 30 ft propagation distance in a branched pipe

The recorded signal for both the ASK and QAM cases presents similar distortion behavior with the previously observed at the 7kbps FSK signal, presenting similar attenuation and time spreading. Consequently, the bit error rates achieved, 34% and 76% for the ASK and QAM methods respectively, are close to the previously presented 7kbps received signals. The stacked signal, generated by the subtraction of the crown and bottom received signals, improves these error rates to 27% and 50%, respectively. The application of bandpass filtering and the combination of the aforementioned adaptive equalizer and Reed-Solomon decoding, reduces the bit error level to zero.

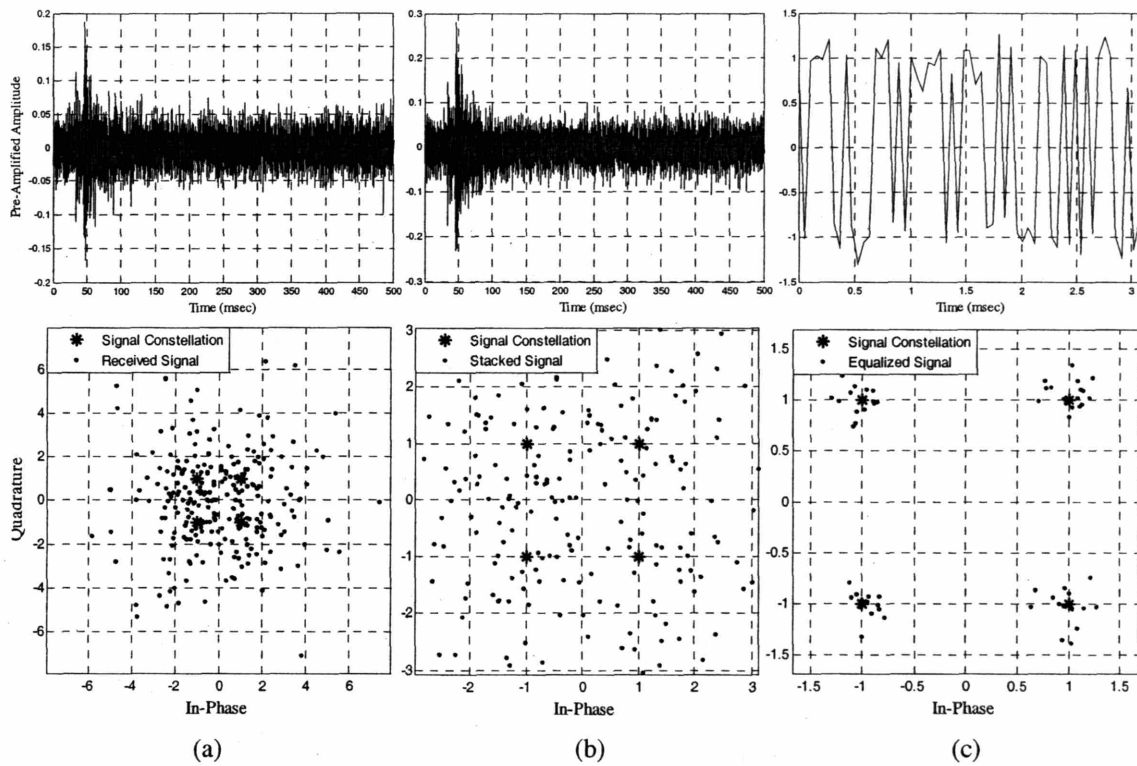


Figure 7.27: Pressure Time History and Signal Constellation of (a) received, (b) stacked by subtraction, and (c) DFE equalized, 7kbps QAM modulated signal for 30 ft propagation distance in a branched pipe

7.5 *References*

- [1]. Panasonic Corporation, Industrial Components Website, Electronic Reference Aug. 2005, <http://www.panasonic.com/industrial/components/components.html>.
- [2]. Fahy F., “Foundations of Engineering Acoustics”, *Academic Press*, London, UK, 2001.

Chapter 8

Conclusions

8.1 *Conclusions*

The first and foremost conclusion is that the proposed digital communication system is capable of achieving reliable transmission under all the studied circumstances. Perfect reconstruction of the original transmitted signal is feasible in both simulated and experimental results, under a number of varying parameters including from the waveguide geometry to environmental factors to signal characteristics. The contribution of the adaptive equalizer and the Reed-Solomon encoding algorithms are indispensable for the performance of the communication system.

The laboratory experiments examined the performance of the digital communication system under the presence of both ambient noise and the dispersive nature of the pipeline waveguide. During the computerized simulations the effect of only one of the two distortion parameters was taken into account, while the level of ambient noise was unknown and estimated. However, there is a strong agreement of the simulated and experimental results, in terms of signal distortion and resulting bit error levels, validating the mathematical models used in the computerized simulations. The behavior of the transmission channel introduced in Chapter 3 and examined with respect to the digital communication system in Chapter 6 was verified from the results of Chapter 7. The channel was characterized as highly dispersive, the level of which is mainly controlled by the frequency content of the propagating wave, the radius of the pipeline, and the propagation distance, presenting positive correlation for all of the aforementioned parameters. Other factors affecting the dispersion level is the impedance contrast between the fluid and the pipe wall, examined by varying the pipe material, as well as the stiffness of the acoustic waveguide, studied by controlling the acoustic wave velocity of the surrounding soil, and the pipe wall thickness.

The observed performance of the digital communication system was essentially identical during both the simulations and laboratory experiments, since similar bit error rates were obtained following the introduction of each of the receiver's signal processing steps, for the various modulation methods at the corresponding data rates. Recall that the laboratory experiment imposes a frequency scaling factor of 2.3, which consequently also scales the data throughput. According to the results, all modulation methods provided similar bit error performance, with the FSK having usually a slight advantage under severe signal distortion conditions. Therefore the selection of the modulation method used for the digital communication system will be decided with respect to the available power and bandwidth, as well as the data throughput mandated by the application, as discussed in Chapter 6. The two sources of signal distortion, ambient noise and multipath propagation, were attacked by employing the bandpass filtering and adaptive equalization processes. In case of severe distortion, a signal preconditioning block was introduced including the inverse transfer function and the stacking methods. While an algorithm for estimating the inverse transfer function was provided, the technique was not used during the computerized simulations, since the transfer function was calculated by the simulation code analytically, whereas there was no need for it during the laboratory experiments since no extraordinarily high dispersion level was developed. The stacking process was proven very useful in both the dispersion compensation and noise reduction; however its application requires caution due to the selective correction behavior, as discussed in Chapter 6. Finally, the Reed-Solomon decoding process corrects any potentially remaining erroneously detected bits, ensuring the high reliability of the digital communication system.

Concerning the laboratory experiment implementation two scaling factors are identified with respect to distance and with respect to frequency. The first one provides the correspondence between the length of the scaled experiment and the propagation distance in an actual pipeline. The second scaling factor indicates the frequency range that must be used in the laboratory experiment in order to preserve the same dispersion characteristics between the scaled and the actual transmission channel. Therefore, the first scaling factor is desirable, since it allows conducting experiments in shorter distances and projecting the results to longer ones, while the second factor is restrictive,

since it increases the frequency of the signal used in the laboratory experiment in order to preserve the consistency of the produced results.

It should be noted that the laboratory hardware implementation was proven invaluable, since it revealed several potential sources of problems in the communication system, such as the electromagnetic interference, recognized the importance of several parameters and identified its restrictions. Even though the implementation of the laboratory experiment was extremely beneficial for the evaluation of the in-pipe acoustic communication system, there exist several limitations that restrict its simulative capabilities. The most significant limitation relates to the restriction of the frequency content of the propagating signal in the audible range, imposed by the microphone used as receiver. The frequency scaling factor of 2.3, used for consistency of the dispersion characteristics of the laboratory experiment with the actual pipeline, emphasizes more the significance of this restriction. More explicitly, not only the frequency range of the signals tested in the laboratory environment is restricted to approximately 20kHz, but also this signal corresponds to 8.7kHz in the actual water pipeline. The current laboratory layout is unable to experiment with higher frequencies and therefore evaluate the communication systems performance at high frequencies and consequently high data rates. Moreover, space limitations restricted the length of the experimental pipeline configuration to 30ft, confining the maximum transmission distance that was examined. Finally, the laboratory experiment is limited in the level of representation of the channel imposed dispersion and energy distribution among the multipath propagating signals, since the experimental pipe is supported in mid air in contrast with the actual water pipeline that is buried underground. According to Chapter 6, the surrounding soil affects the ambient noise level and the stiffness provided to the pipe wall, diversifying the sources of signal distortion with respect to the implemented experiment. However, as it was mentioned above the effect of the surrounding soil on the signal dispersion is less pronounced than other geometric and signal specific parameters. Moreover, the agreement with the computerized simulations supports the validity of the experimental results.

8.2 *Future Work*

As an extension of the present work a full scale experiment implemented in an actual water pipeline is necessary to further validate the simulated and experimental results. The produced communication and power harvesting systems should be integrated with the wireless sensor node and deployed for a long term monitoring project, in order to reveal potential problems in sustaining reliable communication and sufficient power for an extended period of time. Potential issues related to the integration of the system as well as its deployment inside the pipeline were discussed briefly within the context of this dissertation, but by no means were resolved. Following the field trial, several features should be introduced to the communication system, such as a robust communication protocol that will allow the co-existence of multiple simultaneous users within the same transmission channel, as well as encryption methods for increased security from data retrieval or malevolent infiltration. Finally, it would be very interesting to introduce the acoustic data communication system in other types of pipelines and underground infrastructure, such as oil and gas pipes, and so forth. It is very appealing to identify novel applications in which a generic communication system similar to the one proposed in this research study would be of essence. The acoustic communication system enables reliable data transmission where radio frequency communication is not feasible, providing a robust solution to applications requiring data exchange underground, underwater, or in environments presenting severe electromagnetic interference. Therefore, the proposed communication system can be invaluable for certain applications, for instance monitoring of critical infrastructure, dealing with emerging vital issues of the current society such as infrastructure sustainability and homeland security.